



**SYNTHESIS AND CHARACTERIZATION OF LONG
CHAINED ALKANE PORPHYRINS AND
THEIR DERIVATIVES FOR ALCOHOL SENSOR AND
ANTIBACTERIAL PROPERTIES APPLICATIONS**

BY

MISS MONTA MALAITHONG

**A THESIS SUBMITTED IN PARTIAL FULFILLMENT OF
THE REQUIREMENTS FOR THE DEGREE OF
MASTER OF SCIENCE (CHEMISTRY)
DEPARTMENT OF CHEMISTRY
FACULTY OF SCIENCE AND TECHNOLOGY
THAMMASAT UNIVERSITY
ACADEMIC YEAR 2016
COPYRIGHT OF THAMMASAT UNIVERSITY**

**SYNTHESIS AND CHARACTERIZATION OF LONG
CHAINED ALKANE PORPHYRINS AND
THEIR DERIVATIVES FOR ALCOHOL SENSOR AND
ANTIBACTERIAL PROPERTIES APPLICATIONS**

BY

MISS MONTA MALAITHONG

**A THESIS SUBMITTED IN PARTIAL FULFILLMENT OF THE
REQUIREMENTS FOR THE DEGREE OF
MASTER OF SCIENCE (CHEMISTRY)
DEPARTMENT OF CHEMISTRY
FACULTY OF SCIENCE AND TECHNOLOGY
THAMMASAT UNIVERSITY
ACADEMIC YEAR 2016
COPYRIGHT OF THAMMASAT UNIVERSITY**

THAMMASAT UNIVERSITY
FACULTY OF SCIENCE AND TECHNOLOGY

THESIS

BY

MISS MONTA MALAITHONG

ENTITLED

SYNTHESIS AND CHARACTERIZATION OF LONG CHAINED ALKANE
PORPHYRINS AND THEIR DERIVATIVES FOR ALCOHOL SENSOR AND
ANTIBACTERIAL PROPERTIES APPLICATIONS

was approved as partial fulfillment of the requirements for
the degree of master of science (chemistry)

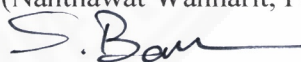
on July 7, 2017

Chairman



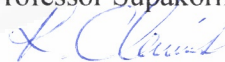
(Nanthawat Wannarit, Ph.D.)

Member and Advisor



(Assistant Professor Supakorn Boonyuen, Ph.D.)

Member and Co-advisor



(Assistant Professor Kittipong Chainok, Ph.D.)

Member



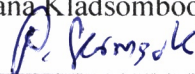
(Assistant Professor Pariya Na Nakorn, Ph.D.)

Member



(Sumana Kladsomboon, Ph.D.)

Dean



(Associate Professor Pakorn Sermsuk, M.Sc.)

Thesis Title	SYNTHESIS AND CHARACTERIZATION OF LONG CHAINED ALKANE PORPHYRINS AND THEIR DERIVATIVES FOR ALCOHOL SENSOR AND ANTIBACTERIAL PROPERTIES APPLICATIONS
Author	Miss Monta Malaithong
Degree	Master of Science (CHEMISTRY)
Major Field/Faculty/University	Chemistry Science and Technology Thammasat University
Thesis Advisor	Assistant Professor Supakorn Boonyuen, Ph.D.
Thesis Co-Advisor (If any)	Assistant Professor Kittipong Chainok, Ph.D.
Academic Years	2016

ABSTRACT

Porphyrins are aromatic heterocyclic compounds and they are also important in biomimetic chemistry. Porphyrins and their metal complexes have been widely studied with interesting spectroscopic and chemical properties. They have attracted considerable attention for many applications such as dye-sensitized solar cell, antibacterial activity, and sensor device.

In the present work focus on the synthesis, properties and applications, which including the antibacterial activity and alcohol sensing applications of a series of symmetric *meso*-alkoxy long chain substituents on *para*-position of the phenyl ring in porphyrin and their silver(II) complexes. The free base porphyrin and their derivatives were prepared by a modification of Adler-Longo method, namely tetrakis(4-phenyl) porphyrin (TPP **4**), tetrakis(4-methoxyphenyl) porphyrin (TOMPP **5**), tetrakis(4-butyloxyphenyl) porphyrin (TOBPP **6**), tetrakis(4-octyloxyphenyl) porphyrin (TOOPP **7**) and tetrakis(4-decyloxyphenyl) porphyrin (TODPP **8**). Furthermore, synthesized porphyrins were added silver(II) ion into the central hole of porphyrin ring to give Ag-TPP **9**, Ag-TOMPP **10**, Ag-TOBPP **11**,

Ag-TOOPP **12** and Ag-TODPP **13**, which were prepared by refluxing each long chained porphyrin and silver(I) nitrate in DMF.

The nuclear magnetic resonance (^1H and ^{13}C NMR), elemental analysis (CHN), mass spectrometry (MS), Infrared spectroscopy (IR), UV-Vis and fluorescence spectroscopy were characterized the structure of all synthesized porphyrins. The ^1H - and ^{13}C -NMR for Ag-TPP and their derivatives gave a silence signal due to the paramagnetic properties of Ag(II)-complexes.

Furthermore, the porphyrins were also tested for antibacterial activity using disc diffusion, minimum inhibitory concentration (MIC) and minimum bactericidal concentration (MBC) method, which were founded to be an effective compound against *Staphylococcus aureus* and *Escherichia coli*. For the test of alcohol sensing, the silver(II) porphyrins were fabricated as porphyrin film for detection of alcohol vapors (methanol, ethanol and iso-propanol) in an electronic nose device (E-nose). The data were collected and analyzed by using principal component analysis (PCA). Thus, the result shows that all silver(II) porphyrin complexes have high potential to modify as the alcohol vapors sensor with a good sensitivity.

Keywords: Silver(II) porphyrins, Alcohol sensing, Antibacterial activity

“Hark, ô Goddess! Anyone who knows for sure that his activities will not meet with success, can be deemed to be doomed; if that one desists from perseverance in that way, he will surely receive the consequence of his indolence. Hark, ô Goddess! Some people in this world strive to get results for their endeavours even if they don't succeed. Hark, ô Goddess! You do see clearly the results of actions, don't you? All the others have drowned in the ocean; we alone, are still swimming and have seen you hovering near us. As for us, we are going to endeavour further to the utmost of our ability; we are going to strive like a man should to reach the shores of the ocean.

His Majesty King Bhumibol Adulyadej
The Story of Mahajanaka

ACKNOWLEDGEMENTS

This thesis would not have been possible without the support of many people. I take this opportunity to express my gratitude to the people who helped me in the successful completion of this project.

My special thanks go to Assoc. Prof. Dr. Somluck Ruangsuttinarupap for who is an inspiration to me.

First and foremost, I would like to thank my supervisor, Asst. Prof. Dr. Supakorn Boonyuen for his continued support, guidance, and encouragement. Without his encouragement and guidance this project would not have materialized. Thank you for providing me with opportunities to grow and experiences I would not have had elsewhere.

I would like to thanks to my co-supervisor, Asst. Prof. Dr.Kittipong Chainok and my committee member, Dr.Nanthawat Wannarit for profitable suggestion and collaboration.

I am very grateful to Dr. Sumana Kladsomboon for their constant support and help in test the gas sensing application and Asst. Prof. Dr. Pariya Na Nakorn for support the instrument and chemical substance in the test the antibacterial activity.

My thanks also to my scholarship, The National Research Council of Thailand (NRCT) for supporting “FY2017 Thesis Grant for Master Degree Student”

The authors gratefully acknowledge the financial support provided by Thammasat University Research Fund under the TU Research Scholar (2017) and Scholarship for Talent Student to study graduate program in Faculty of Science and Technology, Thammasat University (2015-2016).

Most importantly, I need to thank my family. Without their love support, I would have never made it this far. They always encourage and believe in me that I can do it!

Finally, I would like to thank the authors acknowledge the Department of Chemistry, Faculty of Science and Technology, Thammasat University.

Miss Monta Malaithong

TABLE OF CONTENTS

	Page
ABSTRACT	(1)
ACKNOWLEDGEMENTS	(4)
LIST OF TABLES	(8)
LIST OF FIGURES	(9)
LIST OF ABBREVIATIONS	(13)
CHAPTER 1 INTRODUCTION	1
1.1 Porphrins and metalloporphyrin	1
1.2 Natural Porphyrins	3
1.2.1 Hemoglobin and Myoglobin	4
1.2.2 Chlorophyll	4
1.2.3 Vitamin B12	5
1.2.4 Cytochromes	5
1.2.5 Enzyme	6
1.3 Synthetic porphyrin	6
1.4 Application of porphyrins	8
1.5 Research objectives	10
1.6 Scope and limitations of study	10
1.7 Expected results	11
CHAPTER 2 REVIEW OF LITERATURE	12
2.1 The <i>meso</i> -substituted porphyrins and matalloporphyrins	12
2.2 Porphyrins and metalloporphyrins substituted with long chains	16

2.3 Applications of porphyrins and long chain substituted metalloporphyrins	33
2.4 Porphyrins in sensing applications	42
CHAPTER 3 RESEARCH METHODOLOGY	51
3.1 Materials	51
3.1.1 Reagents	51
3.1.2 Apparatus	52
3.2 Methods	53
3.2.1 Synthesis of alkyloxybenzaldehydes	54
3.2.2 Synthesis of porphyrin and its derivatives	56
3.2.3 Synthesis of metalloporphyrins	60
3.1 Biological activity	63
3.4 Gases sensing application	64
3.4.1 Preparation of silver(II) porphyrin molecular films	64
3.4.2 E-nose measurement	64
CHAPTER 4 RESULTS AND DISCUSSION	66
4.1 Synthesis and characterization of various aldehydes	66
4.1.1 Aldehyde synthesis	66
4.1.2 Aldehyde characteristic	67
4.1.2.1 Mass spectrometry	67
4.1.2.2 NMR spectroscopy	68
4.1.2.3 Infrared spectroscopy	71
4.2 Synthesis and characterization of porphyrins and silver(II) porphyrins	73
4.2.1 synthesis of porphyrins and silver(II) porphyrins	73
4.2.2 Porphyrins and silver(II) porphyrins characterization	74
4.2.2.1 CHN elemental analysis	74
4.2.2.2 Mass spectrometry	76
4.2.2.3 NMR spectroscopy	78

4.2.2.4 Infrared spectroscopy	82
4.2.2.5 UV-Vis spectroscopy	85
4.2.2.6 Fluorescence spectroscopy	88
4.3 Biological activity of porphyrins and silver(II) porphyrins	91
4.3.1 Disc diffusion method	91
4.3.2 MIC/MBC method	93
4.4 Alcohol vapor sensing application of silver(II) porphyrins film	94
4.4.1 Optical sensing characteristic	94
4.4.2 Principal component analysis (PCA)	100
CHAPTER 5 CONCLUSIONS AND RECOMMENDATIONS	104
REFERENCES	106
APPENDICES	
APPENDIX A MASS SPECTRA	121
APPENDIX B NMR SPECTRA	126
APPENDIX C IR SPECTRA	132
APPENDIX D UV-VIS ABSORPTION SPECTRA	137
APPENDIX E FLUORESCENCE SPECTRA	143
APPENDIX F THE DYNAMIC RESPONSE	149
APPENDIX G PUBLICATIONS	163
BIOGRAPHY	174

LIST OF TABLES

Tables	Page
1 The structures of the <i>meso</i> -tetraphenylporphyrins with long chain alkoxy substituents	19
2 The structures of the porphyrins and metalloporphyrins	22
3 Characteristic data of aldehydes 1-3	66
4 ^1H and ^{13}C NMR spectroscopic data for aldehydes 1-3	70
5 The IR data of aldehydes 1-3	72
6 The characteristic data for free base porphyrins, and silver(II) porphyrins	75
7 ^1H and ^{13}C NMR spectroscopic data for free base porphyrins	81
8 The IR spectroscopic data of free base porphyrins	83
9 The absorption data of all compounds	87
10 The absorption-emission wavelength and the estimated energy gap of free base porphyrins in dichloromethane	90
11 Antibacterial screening data for the synthesized porphyrins 9 – 13	92
12 The MIC and MBC value of silver(II) porphyrin complexes 9 – 13	93
13 The LED light sources used in this test	94
14 Summarized result of PCA data based on PC1 and PC2 axis	103

LIST OF FIGURES

Figures	Page
1 The structure and the numbering system for porphyrins	1
2 Delocalization pathway in porphyrin structure according to [18] annulene model	2
3 Structure of metalloporphyrin cycle; M is the incorporated metal atom	2
4 Structure of (a) heme [8], (b) chlorophyll (c) vitamin B12 and (d) coenzyme B12	3
5 Example of applications of porphyrin and metalloporphyrins	9
6 Tetrakis(2-hydroxy-5-nitrophenyl)porphyrin 1a	13
7 Synthesis of tetrakis(4-nitrophenyl)porphyrin 2a	14
8 The structure of <i>meso</i> -tetrakis(10-alkyl-phenothiazin-3yl)porphyrins 3a-4a	14
9 Structure of Co(II)-5,10,15,20-meso-tetra(3-hydroxyphenyl) porphyrin (Co-3OHPP) 5a	15
10 The structure zinc porphyrin dyes	15
11 The molecular structure of 12a and 13a	16
12 The structure of palladium porphyrin 14a	17
13 Synthesis of <i>meso</i> -aryl-substituted porphyrins 19-22a	18
14 The structure of novel <i>meso</i> -substituted porphyrins 23a and 24a	20
15 The structure of <i>meso</i> -tetra (4-alkylamidophenyl)porphyrin ligands	21
16 Synthesis of porphyrins 25a,b - 31a,b	23
17 Structure of mixed <i>meso</i> -substituted Zn(II) porphyrins	24
18 The structure of porphyrins, Cu(II) and Ni(II) complexes	25
19 The structures of the porphyrin 36a and silver complex 37a	26
20 The structures of the porphyrin 38-41a and Zn(II) complex 39-41b	27
21 Synthesis of tetra (Schiff-base substituted phenyl) porphyrins and their metal (Zn ²⁺) complexes	27
22 Synthesis of porphyrin 50-52a and Zn(II) complexes 53-55a	28
23 The structure of carboxylic porphyrin 56a and 57a	29
24 The structure of porphyrin 58a , 59a , and zinc complex 60a	30
25 The structures of the manganese (III) porphyrin 61-63a	30

26 The structures of the two porphyrin dyes 64-65a	31
27 Synthetic method for metalloporphyrins	32
28 Peripherally substituted porphyrin arrays combined with a flexible cyanuric chloride bridge	33
29 Molecular structure of the three meso- π -A-porphyrins	34
30 The structure of synthesized three new donor- π -acceptor porphyrins.	35
31 Structure of 74a and 75a	35
32 Molecular structure of 76a-79a	36
33 Structure of investigated compounds	38
34 Chemical structures of porphyrins 97a and Ag(II) complex 98a	39
35 The structure of amphiphilic porphyrin 99a and hydrophilic porphyrin 100a	40
36 The structure of 5,10,15,20-tetrakis-{4-[2-(3-pentadecyl)phenoxy]-ethoxy} phenylporphyrin	41
37 Structures of porphyrin catalysts 101-107a	41
38 Macromolecule structures of the ZnPc and CuP used as sensing layers	42
39 (a) Diagram of the optical electronic nose system in experiment (b) Principal component analysis plot of the MgTPP thin film to alcohol vapors	45
40 The structure of 5,10,15,20-tetrakis[3,4-bis(2ethylhexyloxy)phenyl] 21H,23H-porphine (EHO, left) and p-tert-butylcalix[8]arene (C8A, right)	45
41 Two-step reaction mechanism of ZnTPP to NO ₂	47
42 The 5-(4-carboxy-phenyl)-10,15,20-triphenyl-porphyrin and the silver(I) ion with 5-(4-carboxy-phenyl)-10,15,20-triphenyl-porphyrin at carboxylic group	47
43 Schematic view of the e-nose measuring system	48
44 The chemical structure of 5,10,15,20-tetrakis[3,4-bis(2-ethylhexyloxy)phenyl]-21H,23H-porphyrinato magnesium(II) (MgEHO)	49
45 Trends of published paper for porphyrin-based sensor application	50
46 Synthesis of aldehydes	54
47 The structure of various alkyloxybenzaldehyde (1-3)	55
48 Synthesis of free base porphyrins	56
49 The expected structure of TPP 4 and TOMPP 5	58

50 The expected structure of TOBPP 6 , TOOPP 7 and TODPP 8	59
51 Synthesis of silver(II) porphyrins	60
52 The expected structure of AgTPP 9 , AgTOMPP 10 and AgTOBPP 11	62
53 The expected structure of AgTOOPP 12 and AgTODPP 13	63
54 Electronic nose (E-nose) instrument in this experiment and the diagram of the electronic nose system set up	65
55 Synthesis of butyloxybenzaldehyde 1	66
56 The mass spectrum of butyloxybenzaldehyde 1 in CH ₂ Cl ₂	67
57 The ¹ H NMR spectrum of butyloxybenzaldehyde 1 in chloroform-d	69
58 The ¹³ C NMR spectrum of butyloxybenzaldehyde 1 in chloroform-d	69
59 The IR spectrum of butyloxybenzaldehyde 1 in NaCl	72
60 The route synthesis of silver(II) porphyrins	74
61 The mass spectrum of TOBPP 6 in CH ₂ Cl ₂	76
62 The mass spectrum of Ag-TOBPP 11 in CH ₂ Cl ₂	77
63 The ¹ H NMR spectrum of TOBPP 6 in chloroform-d (CDCl ₃)	79
64 The ¹³ C NMR spectrum of TOBPP 6 in chloroform-d (CDCl ₃)	80
65 IR spectrum of TOBPP 6 and Ag-TOBPP 11 in KBr	84
66 UV-Vis spectra of free base porphyrins in dichloromethane	85
67 UV-Vis spectra of silver(II) porphyrins in dichloromethane	86
68 UV-Vis spectra of TOBPP 6 and Ag-TOBPP 11 in dichloromethane	86
69 The emission spectra of the free base porphyrins in dichloromethane	88
70 The emission spectra of the silver(II) porphyrins in dichloromethane	89
71 The texture thin film of Ag-TPP and its derivatives.	94
72 The dynamic response of Ag-TOBPP film in the presence of methanol vapor	96
73 The dynamic response of Ag-TOBPP film in the presence of ethanol vapor	97
74 The dynamic response of Ag-TOBPP film in the presence of <i>iso</i> -propanol vapor	98
75 The UV-Vis spectra of Ag-TOBPP in various alcohol solvent	99
76 The UV-Vis spectra of Ag-TOBPP film	99

77 PCA plot of the optical response of the a) Ag-TPP b) Ag-TOMPP c) Ag-TOBPP to alcohol vapors (methanol, ethanol and <i>iso</i> -propanol)	101
78 PCA plot of the optical response of the d) Ag-TOOPP and e) Ag-TODPP to alcohol vapors (methanol, ethanol and <i>iso</i> -propanol)	102



LIST OF ABBREVIATIONS

Symbols/Abbreviations Terms

1a	Tetrakis(2-hydroxy-5-nitrophenyl) porphyrin
2a	5, 10, 15, 20-tetrakis (<i>p</i> -nitrophenyl)-21H, 23H-porphyrin
3a	Meso-tetrakis(10-methyl-phenothiazin-3yl)porphyrins
4a	Meso-tetrakis(10-ethyl-phenothiazin-3yl)porphyrins
5a	Co(II)-5,10,15,20-meso-tetra(3-hydroxyphenyl)porphyrin
6a	5,10,15,20-tetra(3-cyanophenyl) porphyrin
7a	5,10,15,20-tetra[3-(2,3,4,5-tetrazolyl)phenyl] porphyrin
8a	5,10,15,20-tetra(2-cyanophenyl) porphyrin
9a	5,10,15,20-tetra-kis(23-carboxyphenyl)porphyrin
10a	5,10,15,20-tetra-kis(2-carboxyphenyl)porphyrin
11a	Zn-5,10,15,20-tetra[3-(2,3,4,5-tetrazolyl)phenyl] porphyrin
12a	Tetrekis(4'-carboxamidophenyl) porphyrin
13a	Tetrakis(3',5'-dicarboxamidophenyl)porphyrin
14a	Palladium porphyrin
15a	4-tetradecyloxybenzaldehyde
16a	Tetrakis(3',5'-dicarboxamidophenyl)porphyrin
17a	<i>meso</i> -tetradecyloxyphenyl)dipyrromethane
18a	<i>meso</i> -tetradecanoyloxyphenyl)dipyrromethane
19a	5,15-bis(4-tetradecyloxyphenyl)-10,20-diphenylporphyrin
20a	5,15-bis(4-tetradecyloxyphenyl)-10,20-diphenylporphyrin
21a	5,10,15,20-tetra(4-tetradecyloxyphenyl)porphyrin
22a	5,10,15,20-tetra(4-tetradecanoyloxyphenyl)porphyrin
23a	5,10,15,20-tetra[4-(3-phenoxy)-propoxy] phenyl porphyrin
24a	5,10,15,20-tetra[2-(3-phenoxy) propoxybenzaldehyde
25a	4-(5-methoxycarbonylpentyloxy)benzaldehyde
25b	4-(10-methoxycarbonyldecyloxy)benzaldehyde

- 26a 5,10,15,20-tetrakis[4-(5-methoxycarbonylpentyloxy) phenyl]porphyrin
- 26b 5,10,15,20-tetrakis[4-(10-methoxycarbonyldecyloxy) phenyl]porphyrin
- 27a 5,10,15,20-tetrakis[4-(5-carboxypentyloxy) phenyl] porphyrin
- 27b 5,10,15,20-tetrakis[4-(10-carboxydecyloxyphenyl)] porphyrin
- 28a 5,10,15,20-tetrakis[4-(6-hydroxyhexyloxy)phenyl] porphyrin
- 28b 5,10,15,20-tetrakis[4-(6-hydroxydecyloxy)phenyl] porphyrin
- 29a M(II)-5,10,15,20-tetrakis[4-(5-methoxycarbonyl pentyloxy)phenyl]porphyrin
- 29b Zn(II)-5,10,15,20-tetrakis[4-(10-methoxycarbonyldecyloxy) phenyl] porphyrin
- 30a Zn(II)-5,10,15,20-tetrakis[4-(5-carboxypentyloxy) phenyl]porphyrin
- 30b Zn(II)-5,10,15,20-tetrakis[4-(10-carboxydecyloxyphenyl)] porphyrin
- 31a Zn(II)-5,10,15,20-tetrakis[4-(6-hydroxyhexyloxy)phenyl] porphyrin
- 31b Zn(II)-5,10,15,20-tetrakis[4-(6-hydroxydecyloxy)phenyl]porphyrin
- 32a Nickel-2-formyl-5,10,15,20-tetra(4-decyloxyphenyl) porphyrin-fullerene
- 33a Copper-2-formyl-5,10,15,20-tetra(4-decyloxyphenyl) porphyrin-fullerene
- 34a Nickel-2-formyl-5,10,15,20-tetra(4-tetradecyloxyphenyl) porphyrin-fullerene
- 35a Copper-2-formyl-5,10,15,20-tetra(4-tetradecyloxyphenyl) porphyrin-fullerene
- 36a *meso*-tetrakis[4-(heptyloxy) phenyl]porphyrin
- 37a { *meso*-tetrakis[p-(heptyloxy)phenyl]porphyrinato } silver(II)
- 38a 5,10,15,20-tetrakis(4-hydroxyphenyl)porphyrin
- 39a 5,10,15,20-tetrakis(4-octanolyoxyphenyl)porphyrin
- 39b Zn(II)- 5,10,15,20-tetrakis(4-octanolyoxyphenyl) porphyrin
- 40a 5,10,15,20-tetrakis(4-decanolyoxyphenyl)porphyrin

40b	Zn(II)-5,10,15,20-tetrakis(4-decanolyoxyphenyl) porphyrin
41a	5,10,15,20-tetrakis(4-dodecanolyoxyphenyl)porphyrin
41b	Zn(II)-5,10,15,20-tetrakis(4-dodecanolyoxyphenyl) porphyrin
42a	<i>meso</i> -tetra (p-benzylideneamino) phenyl porphyrin
43a	<i>meso</i> -tetra [p-(p-benzylideneamino)] phenyl porphyrin
44a	<i>meso</i> -tetra [p-(p-carboxy benzylideneamino)] phenyl porphyrin
45a	<i>meso</i> -tetra [p-(p-methoxy benzylideneamino)] phenyl porphyrin
46a	Zn(II)- <i>meso</i> -tetra (p-benzylideneamino) phenyl porphyrin
47a	Zn(II)- <i>meso</i> -tetra [p-(p-benzylideneamino)] phenyl porphyrin
48a	Zn(II)- <i>meso</i> -tetra [p-(p-carboxy benzylideneamino)]phenyl porphyrin
49a	Zn(II)- <i>meso</i> -tetra [p-(p-methoxy benzylideneamino)]phenyl porphyrin
50a	5,10-bis (4-pyridyl)-15,20-bis (4-octadecyloxyphenyl) porphyrin
51a	5,10-bis (4-pyridyl)-15,20-bis (4-hexyloxyphenyl) porphyrin
52a	5,10-bis (4-pyridyl)-15,20-bis (4-methoxyphenyl) porphyrin
53a	Zinc 5,10-bis (4-pyridyl)-15,20-bis (4-octadecyloxy phenyl) porphyrin
54a	Zinc 5,10-bis (4-pyridyl)-15,20-bis (4-hexyloxyphenyl) porphyrin
55a	Zinc 5,10-bis (4-pyridyl)-15,20-bis (4-methoxyphenyl) porphyrin
56a	carboxylic porphyrin I
57a	carboxylic porphyrin II
58a	5,10,15,20-tetrakis(4-ferrocenylethynylphenyl)porphyrin
59a	5,10,15,20-tetrakis(3-ferrocenylethynylphenyl) porphyrin
60a	5,10,15,20-tetrakis(3-ferrocenylethynylphenyl) porphyrinatozinc(II)
61a	(5,10,15,20-tetrakis(3,5-di- tert-butyl-4-hydroxyphenyl) porphynato)manganese(iii)chloride
62a	(5-(4-hydroxyphenyl)-10,15,20- tris(3,5-di-tert-butyl-4-hydroxyphenyl)porphynato)manganese(iii)chloride
63a	(5-(4-palmitoy- loxyphenyl)-10,15,20-tris(3,5-di-tert-butyl-4-hydroxyphenyl)porphynato) manganese(III) chloride

- 64a Porphyrin dyes with long alkoxy chain LP-11
- 65a Porphyrin dyes with long alkoxy chain LP-12
- 66a Free-base porphyrin (H_2P) ($M= 2H$, $R= Cl$)
- 66b Free-base porphyrin (H_2P) ($M= 2H$, $R= C_{60}-X-NH$)
- 67a Zinc porphyrin (ZnP) ($M= Zn$, $R= Cl$)
- 67b Zinc porphyrin (ZnP) ($M= Zn$, $R= C_{60}-X-NH$)
- 68a Zn(II)-5,15-bis(2,6-dihexoxyphenyl)-10-(4-carbonylphenyl)-porphyrin
- 69a Zn(II)-5,15-bis(2,6-dihexoxyphenyl)-10,20-bis(4-carbonylphenyl)-porphyrin
- 70a Zn(II)-5,15-bis(2,6-dihexoxyphenyl)-10-(4-carbonylethenyl)-porphyrin
- 71a [5,15-bis(2,6-dioctoxyphenyl)-10-(4-(di-p-tolylamino) phenyl)- 20-(5-carboxythiophene-2-yl-ethynyl) porphyrinato]zinc(II)
- 72a [5,15-bis(2,6-dioctoxyphenyl)-10-(4-(di-p-tolylamino) phenyl)- 20-(5-carboxy-6-methylthieno[3,2-b]thiophene-2-ylethynyl) porphyrinato] zinc(II)
- 73a [5,15-bis(2,6-dioctoxyphenyl)-10-((4-n,n-dimethylaminophenyl) ethynyl)-20-(5-carboxy-6-methylthieno[3,2-b]thiophene-2-yl-ethynyl) porphyrinato] zinc(II)
- 74a Porphyrin based sensitizers DHC-1
- 75a Porphyrin based sensitizers DHC-2
- 76a Zn-porphyrin XW18 contain linear octyloxy chains
- 77a Zn-porphyrin XW19 contain branched 2-ethylhexyloxy chains
- 78a Zn-porphyrin XW20 contain linear octyloxy chains
- 79a Zn-porphyrin XW21 contain branched 2-ethylhexyloxy chains
- 80a Tetrakis-5,10,15,20-(3-hydroxyphenyl)porphyrine
- 81a 5-(4-hexadecyloxyphenyl)-10,15,20-tris(3-hydroxyphenyl) porphyrine
- 82a Tetrakis-5,10,15,20-(4-hydroxyphenyl)porphyrine
- 83a Tetrakis-5,10,15,20-(4-hydroxy-3-methoxyphenyl) porphyrine

- 84a Tetrakis-(4-hydroxy-3,5-dimethoxyphenylene)porphyrine
- 85a 5-(4-hexadecyloxyphenyl)-10,15,20-tris(4-hydroxyphenyl) porphyrine
- 86a 5-(3-hexadecyloxyphenyl)-10,15,20-tris(3-hydroxyphenyl) porphyrine
- 87a [5-(4-oxyphenyl)-10,15,20-tris(4-hydroxyphenyl)porphyrine] palmitate
- 88a [5-(3-oxyphenyl)-10,15,20-tris(3-hydroxyphenyl) porphyrine]palmitate
- 89a 5-(4-hexadecyloxy-3-methoxyphenyl)-10,15,20-tris(4-hydroxy-3-methoxyphenyl)porphyrine
- 90a [5-(3-methoxy-4-oxyphenyl)-10,15,20-tris(4-hydroxy-3-methoxy phenyl)porphyrine] palmitate
- 91a 5-(4-hexadecyloxy-3,5-dimethoxyphenyl)-10,15,20-tris(4-hydroxy-3,5-dimethoxyphenyl) porphyrine
- 92a [5-(3,5-dimethoxy-4-oxyphenyl)-10,15,20-tris(4-hydroxy-3,5-dimethoxyphenyl)porphyrine] palmitate
- 93a 5-(4-acetylaminophenyl)-10,15,20-tris(4-methoxyphenyl) porphyrine
- 94a 5-(4-aminophenyl)-10,15,20-tris(4-methoxyphenyl) porphyrine
- 95a *N*-[5-(para-phenylene)-10,15,20-tris(4-methoxyphenyl) porphyrine] palmitylamide
- 96a *N*-[5-(para-phenylene)-10,15,20-tris(4-hydroxyphenyl) porphyrine] palmitylamide
- 97a 5-mono(3'-methoxy-4'-hexadecyloxyphenyl)-10,15,20-tri(4'-nallyl pyridyl)porphine tribromide
- 98a 5-mono(3'-methoxy-4'-hexadecyloxyphenyl)-10,15,20-tri(4'-nallyl pyridyl)Porphinato Ag(II) trinitrate
- 99a 5-(4-octadecanamidophenyl)-10,15,20-tris(n-methylpyridinium-3-yl)porphyrin trichloride

100a	5-(4-acetamidophenyl)-10,15,20-tris(n-methyl pyridinium-3-yl)porphyrin trichloride
101a	5,15-di[4-(4-tributylammoniobutoxy)phenyl]porphyrin zinc(II) difluoride
102a	5,15-di[4-(4-tributylammoniobutoxy)phenyl]porphyrin zinc(II) dichloride
103a	5,15-di[4-(4-tributylammoniobutoxy)phenyl]porphyrin zinc(II) dibromide
104a	5,15-di[4-(4-tributylammoniobutoxy)phenyl]porphyrin zinc(II) diiodide
105a	5,15-di[3-(4-tributylammoniobutoxy)phenyl]porphyrin zinc(II) dibromide
106a	5,15-di[2-(4-tributylammoniobutoxy)phenyl]porphyrin zinc(II) dibromide
107a	5,15-diphenylporphyrin-zinc complex
¹ H NMR	Proton Nuclear Magnetic Resonance Spectroscopy
¹³ C NMR	Carbon Nuclear Magnetic Resonance Spectroscopy
δ	Chemical shift
Ag-TOBPP	Silver-butyloxyphenyl porphyrin
Ag-TODPP	Silver-decyloxyphenyl porphyrin
Ag-TOMPP	Silver-methoxyphenyl porphyrin
Ag-TOOPP	Silver-octyloxyphenyl porphyrin
Ag-TPP	Silver-phenyl porphyrin
E-nose	Electronic nose
TOBPP	Tetrakis(4-butyloxyphenyl)porphyrin
TODPP	Tetrakis(4-decyloxyphenyl)porphyrin
TOMPP	Tetrakis(4-methoxyphenyl)porphyrin
TOOPP	Tetrakis(4-octyloxyphenyl)porphyrin
TPP	Tetrakis(4-phenyl)porphyrin

CHAPTER 1

INTRODUCTION

1.1 Porphyrins and metalloporphyrin

Porphyrins are a large class of aromatic organic compounds of natural or synthetic origin, they are heterocyclic macrocycles consisting of four pyrroles connected by four methine bridges. In 1912, Kuster first proposes the correct structure of porphyrin and confirmed by Hans Fischer, the father of modern porphyrin chemistry, when he successfully synthesize the first porphyrin protoheme in 1929 [1].

The term porphyrin is derived from the Greek word *porphura*, meaning the purple color and implying their deep purple [2]. The porphyrin skeleton consists of twenty carbon atoms, which in the IUPAC system numbering of every carbon atom in the porphyrin follows number 1-20 with the integral nitrogen atoms numbered 21-24 shown in Figure 1.

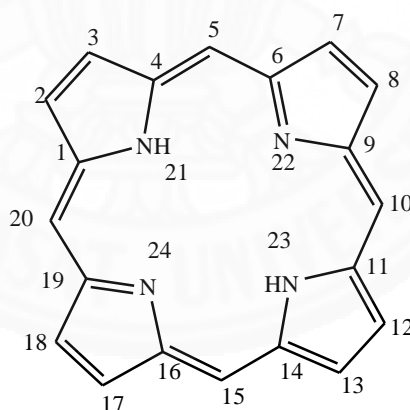


Figure 1. The structure and the numbering system for porphyrins.

The carbon atoms of porphyrin are labeled depending on their positions :

- a) α - positions, next to nitrogen which are labeled 1, 4, 6, 9, 11, 14, 16 and 19 ,
- b) β - positions, opposite to nitrogen in the pyrroles which are labeled 2, 3, 7, 8, 12, 13, 17 and 18 ,
- c) *meso*-carbon, in the bridging methane which are labeled 5,10,15 and 20 [3].

Porphyrin aromaticity is most regularly described in delocalization pathway is prominent in the macrocyclic compound; whereas aromatic according to the

traditional Hückel $[4n+2]$ rule. Porphyrins are aromatic compounds with 22- π conjugated electrons; however, only 18 participate in the π -electron of which is in anyone delocalization pathway [4].

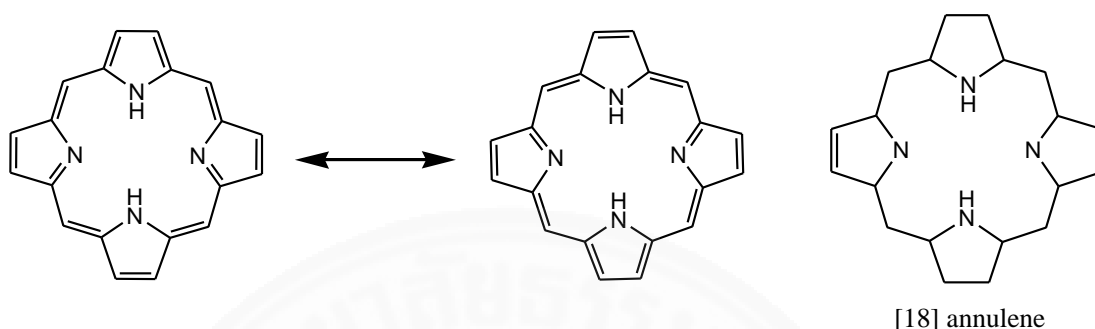


Figure 2. Delocalization pathway in porphyrin structure according to [18] annulene model.

The size of the central hole of porphyrin macrocyclic compound makes it easy to accommodate different metal ions (M^{n+}), such as Cu, Fe, Co, Ni, etc. The two diagonal nitrogen donor atoms were deprotonated and bound with the transition metal ion forming a dianionic ligand (Figure 2). Due to the size of the incorporated metal cause, the molecule might not remain planar (Figure 3), but can be distorted. Although the color of the porphyrin mainly comes from $\pi^* - \pi$ electron transition of porphyrin ring orbitals, the bounded metal's d orbitals do interact with π orbitals which it affects their energies; thence the metalloporphyrins have differences color [5].

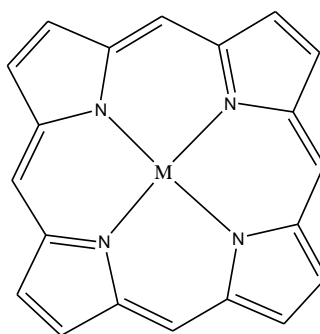


Figure 3. Structure of metalloporphyrin cycle; M is the incorporated metal ion.

1.2 Natural Porphyrins

Porphyrin derivatives, especially metal complexes, play an important role in the natural biological systems such as respiration, photosynthesis and solving transport and other problems in living systems [6-7]. They are ubiquitous class of compounds with many important biological representatives including heme, chlorophyll, vitamin B12, coenzyme B12 and several others (Figure 4).

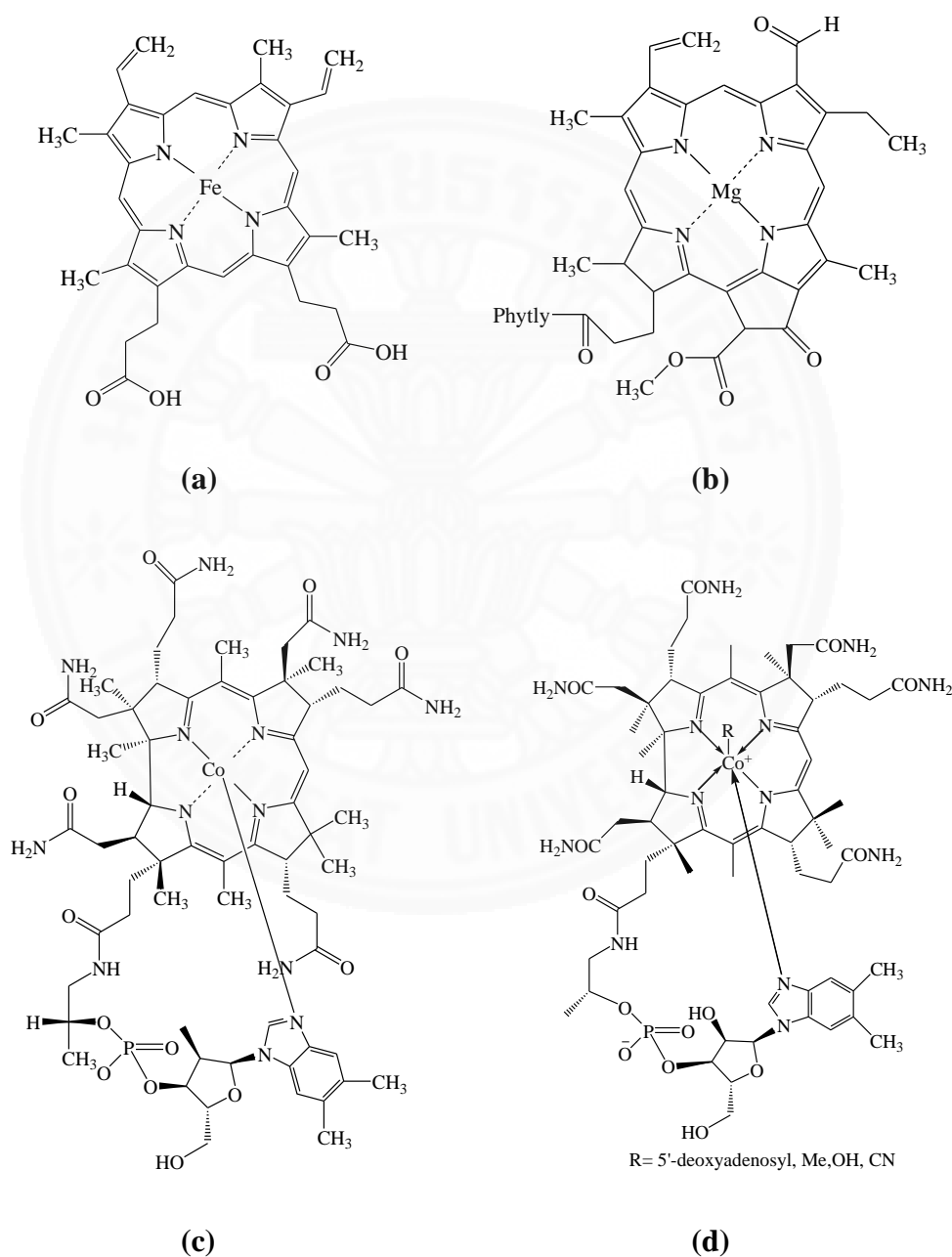


Figure 4. Structure of (a) heme [8], (b) chlorophyll, [12] (c) vitamin B12 [16] and (d) coenzyme B12 [21].

1.2.1 Hemoglobin and Myoglobin

Hemoglobin and myoglobin molecule are two of the most important proteins in the body. They are high molecular weight protein systems containing a positive-charged iron(II) protoporphyrin IX units [8]. They are responsible for transport and storage of molecular oxygen in animals. Hemoglobin transports dioxygen from its the lungs, to the muscle cells. Then, it transfers O₂ to myoglobin for respiration use. Myoglobin has higher affinity for O₂ than does hemoglobin. By itself, heme is not a good oxygen carrier. It must be part of a larger prevent oxidation of the Fe²⁺ to Fe³⁺ in the porphyrin core [9].

The iron(II) in hemoglobin and myoglobin is in the ferrous state and has to have an N-base (histidine) coordinated to the metal from one of the sides of the plane to have dioxygen bound at the vacant sixth coordination site [10]. The oxidized form of iron, ie. ferric state, called metmyoglobin and methemoglobin will not bind oxygen. The free heme is immediately oxidized in the presence of oxygen and water and thus renders useless for O₂ transport.

1.2.2 Chlorophyll

Chlorophyll is used in photosynthesis, which allows plants and cyanobacteria absorb the light energy and convert it into chemical energy. Chlorophylls are mainly found in chloroplasts of plants and cyanobacteria [11]. Most of the chlorophylls are basically magnesium derivative of porphyrins and some slightly structural changes in porphyrin moiety results in different classes of chlorophyll such as chlorophyll a, b, c or bacteriochlorophyll etc with slightly difference in photocatalytic properties. Chlorophylls contain the isocyclic β -keto ester ring that is biosynthetically derived from the C13 propionic acid side chain protoporphyrin IX [12]. Peripheral substituents in chlorophylls vary widely. There are more than 50 derivatives that have been isolated and identified from photosynthetic organisms. All of the chlorophylls strongly absorb in the blue (mostly at 430 nm) and red (mostly at 660 nm) regions of the electromagnetic spectrum [13]. Thus, their absorption bands significantly overlap with the emission spectrum of the solar

radiation reaching the biosphere, resulting in efficient tools for conversion of radiation into chemical energy.

1.2.3 Vitamin B12

Vitamin B12, also called cobalamin, is the largest and a water-soluble vitamin which has a key role in the normal functioning of the brain and nervous system, and for the red blood cell formation [14]. It is involved in the metabolism of the human body cell, especially affecting DNA synthesis, fatty acid, and amino acid metabolism. The source of B12 can only be found naturally in animal products and supplements.

The structure of vitamin B12 is based on a corrin ring, which is similar to the porphyrin ring found in heme, chlorophyll, and cytochrome [15]. The central metal ion of a planar tetra-pyrrole ring is cobalt (Co^{2+}). Four of the six coordination sites are provided by the corrin ring, and a fifth by a dimethylbenzimidazole group. The sixth coordination site, the center of reactivity, is variable being a cyano group ($-\text{CN}$), a hydroxyl group ($-\text{OH}$), a methyl group ($-\text{CH}_3$) or a 5'-deoxyadenosyl group, respectively, which was aligned in axial position. The four form of vitamin B12 are all deeply red colored crystals and water solution due to the color of the cobalt-corrin complex [16].

1.2.4 Cytochromes

The cytochromes are electrons transferring proteins, containing iron porphyrin group [17]. They are found only in aerobic cells. In the past, these pigments were classified into groups, based on the position of the lowest energy absorption band in the reduced state. For example cytochrome-a (605 nm), cytochrome-b (565 nm) and cytochrome-c (550 nm) [18]. But nowadays cytochromes are subdivided into four classes depending on the nature and the mode of binding of the heme prosthetic groups to the protein.

1.2.5 Enzyme

Enzymes are organic biological catalysts that govern, initiate and control biological reactivity important for the life processes [19]. They are produced by the living organism and are usually present in only very small amounts in the various cells. All known enzyme are proteins, and some contain non-protein moieties termed prosthetic groups that are essential for the manifestation of catalytic activities. In a variety of natural enzymes, metalloporphyrins constitute these prosthetic group such as Oxygenases and Peroxidases etc [20].

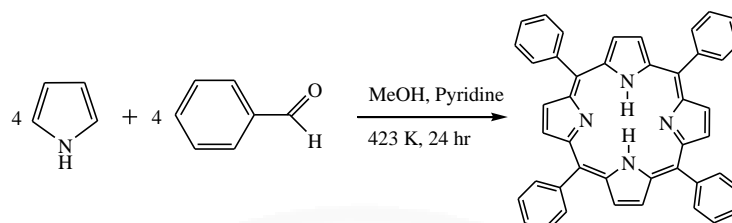
1.3 Synthetic porphyrin

In recent past, the synthesis of porphyrins provides the foundation for studies across a broad spectrum of scientific disciplines. A recurring theme in the synthesis of porphyrins involves the arrangement of the diverse substituent in specific patterns about the periphery of the macrocycle. Two distinct patterns of substituted are β -substituted porphyrins and *meso*-substituted porphyrins [22]. The β -substituted porphyrins closely resemble naturally occurring porphyrins. The porphyrins were substituted at *meso* position have no direct biological counterparts but have found wide applications such as biomimetic models and as useful components in material chemistry [23]. The substituents at the *meso*-positions can including alkyl, aryl heterocyclic or organometallic groups, as well as other porphyrins.

The chemistry of *meso*-substituted porphyrins had its foundation in the work of Rothmund in 1935 [24-25]. Rothmund performed the synthesis of *meso*-tetramethylporphyrin by the condensation reaction of acetaldehyde and pyrrole in methanol at various temperatures. Sealed vessels were employed to avoid the loss of volatile acetaldehyde. However, careful examination of each reaction product showed the presence of the second porphyrinic substance at the 10-25%. This contaminant was later isolated using chromatography and shown the consistent of various chlorins. The chlorin can be easily converted by oxidation to the corresponding porphyrin. Rothmund employed various synthetic modifications in order to optimize the

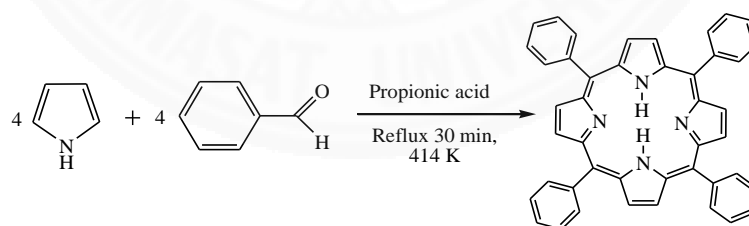
reaction conditions and finally settling on high concentration and high temperature in sealed vessel in the absence of an added oxidant.

Rothmund conditions



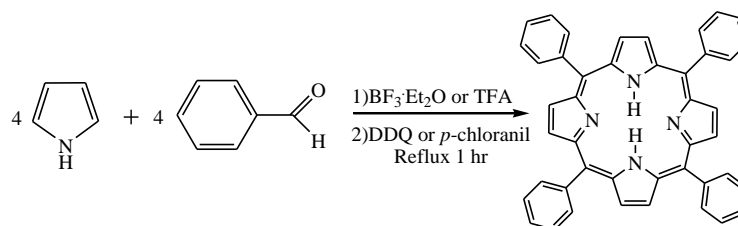
In the mid 1960's, Adler Longo and coworkers modified the syntheses of *meso*-substituted porphyrins by performing the condensations of benzaldehyde and pyrrole in a variety of acidic solvents, eq. HNO₃, H₂SO₄, propionic acid and acetic acid, under refluxing conditions in open an atmosphere [26]. Further study of these reaction conditions led to the use of propionic acid in place of acetic acid as the solvent. After a short reflux of the higher concentrations of aldehydes and pyrrole. This modified synthesis is known as the Adler-Longo method. The contaminated with chlorins of the final porphyrin product were removed using oxidizing agent known as DDQ [27].

Adler-Longo conditions



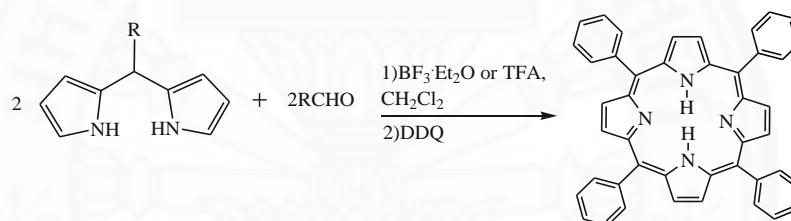
In 1980's, a new approach for the syntheses of *meso*-substituted porphyrins under gentle conditions was developed namely, the Lindsey method [28]. This synthetic methodology involved a condensation reaction of aldehyde and pyrrole to form porphyrinogen. Then, the reaction followed by the oxidation step sequentially. The compound was purified by column chromatography to afford the desired product in 35-40 % yield.

Lindsey conditions



In order to synthesize the less symmetrical, *trans*- or *cis*- substituted porphyrins, synthetic pathway based on the MacDonald [2+2] condensation between a dipyrromethane and an aldehyde in acid catalyst [29]. The synthesis of *trans*-meso-substituted porphyrins is important as model systems in the material application.

MacDonald [2+2] condensation



1.4 Application of porphyrins

Porphyrins and their metal complexes have been widely studied with interesting spectroscopic and chemical properties. They have attracted considerable attention for dye-sensitized solar cell (DSSCs) [30-32], organic photo-electronics [33] such as organic light emitting diodes (OLEDs) and organic field-effect transistors (OFETs) due to they possess great conjugation of π electrons in macrocycles unique electronic properties and tenability by chemical derivation. For the applications of porphyrin in DSSCs have been interested continuous attention due to the advantages of low-cost, relatively high efficiency and simplified production processes that properties of porphyrins were suitable to exploit their applications in DSSC devices. In addition, porphyrins can be modified in many applications such as catalysis [34], anticancer [35], antimicrobial agent [36], molecular sensor [37] and applications for the photosensitizing drug in photodynamic therapy (PDT) [38] etc. For the application of porphyrins, PDT has been usefulness in anticancer photodynamic therapy. The

photosensitization can represent approach to destroy the tumor tissue with light applications. Porphyrins and metalloporphyrins are one class of molecules under intense investigation due to their photosensitizing ability, which is based on rich π electron conjugation of heterocyclic rings [39]. For another application, Metalloporphyrins are a natural choices for the optical detection of volatile organic as a result of it unique large π -conjugated system as well as electrical and optical properties of interaction between the metal central of porphyrin and the gas sensitivity [40].

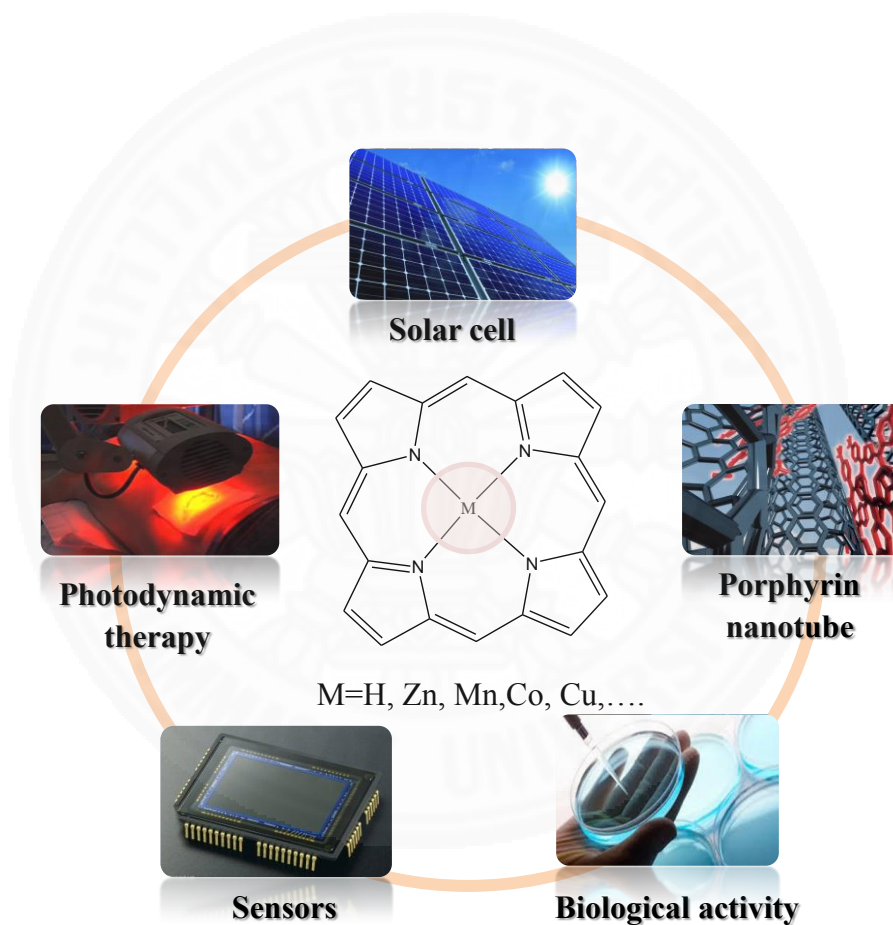


Figure 5. Example of applications of porphyrin and metalloporphyrins.

1.5 Research objectives

1.5.1 To synthesize and characterize various aldehydes with long chain alkane, including butyloxybenzaldehyde **1**, octyloxybenzaldehyde **2** and decyloxybenzaldehyde **3**.

1.5.2 To synthesize and characterize the free based porphyrins from various aldehydes such as benzaldehyde, *p*-anisaldehyde, butyloxybenzaldehyde, octyloxybenzaldehyde and decyloxybenzaldehyde, following the modification of Adler-Longo method.

1.5.3 To synthesize and characterize the silver porphyrins by adding silver ion, into the center hole of free base porphyrin structure.

1.5.4 To study and compare the chemical and physical properties of each porphyrins long chain and metalloporphyrins, along with investigating the effects of peripheral substitutions to the macrocycle which can be confirmed by using spectroscopy techniques.

1.5.5 To study the biological activity against *Staphylococcus aureus* (*S. aureus*) and *Escherichia coli* (*E.coli*) of all synthesized compounds.

1.5.6 To modify silver porphyrins for alcohol sensor applications.

1.6 Scope and limitations of study

1.6.1 The various aldehyde were prepared by refluxing a solution of 4-hydroxybenzaldehyde with alkyl bromides such as 1-bromobutane, 1-bromooctane and 1-bromodecane.

1.6.2 The long chains porphyrins and their derivatives with different peripheral substitutions ligands were prepared by refluxing pyrrole with the various aldehyde such as *p*-anisaldehyde, butyloxybenzaldehyde, octyloxybenzaldehyde and decyloxybenzaldehyde, with the modification of Alder-Longo method.

1.6.3 The metalloporphyrins with various porphyrin were prepared by adding silver(II) ion (Ag^{2+}) in the center hole of long chain free base porphyrin.

1.6.4 The NMR, IR spectroscopy, mass spectrometry and elemental analysis technique were applied to confirm the synthesized structure of porphyrins and their derivatives.

1.6.5 The effects of macrocyclic structures with different peripheral substitutions, a group of long chains porphyrins and metalloporphyrins, were characterized by UV-Vis spectroscopy and fluorescence.

1.6.6 The biological activity of each compound was tested by using disc diffusion technique and the active compounds were selected for MIC and MBC test.

1.6.7 The sensor applications were employed by E-nose and estimate by PCA (principal component analysis) for detection and separation of methanol, ethanol, and *iso*-propanol.

1.7 Expected results

1.7.1 The synthesized and characterized aldehydes, free base porphyrins, silver porphyrin were achieved with high yield with an expected structure.

1.7.2 Porphyrins and metalloporphyrins optical properties can be compared by using UV-Vis spectroscopy and fluorescence spectroscopy.

1.7.3 Porphyrins long chain and metal complexes give a high potential for several applications such as the coating on ITO glass and other fields.

1.7.4 All compounds have the positive biological activity.

1.7.5 Silver porphyrins can be successfully developed to use in alcohol sensor applications for the detection and separation of methanol, ethanol, and *iso*-propanol.

CHAPTER 2

REVIEW OF LITERATURE

2.1 The *meso*-substituted porphyrins and metalloporphyrins

The structure of a porphyrin can be classified into two main categories base on the pattern of substituents attached to the porphyrin ring such as *meso*-substituted and β -substituted porphyrin. The syntheses of *meso*-substituted porphyrin offer a great advantage to study the physical and chemical properties of the substituents that may be attached on the periphery. In addition, syntheses of *meso*-substituted porphyrin can be prepared by simple synthetic methodology by substitution of alkyl, aryl, heterocyclic or organometallic group as other porphyrins. [41]

In 2002, Yuichi T. *et al.* prepared Zinc(II) complexes of antipodal β -tetrasubstituted *meso*-tetraphenylporphyrin with trifluoromethyl [$\text{Zn}(\text{TPP}(\text{CF}_3)_4)$], bromine [$\text{Zn}(\text{TPPBr}_4)$], and methyl groups [$\text{Zn}(\text{TPP}(\text{CH}_3)_4)$]. Prepared porphyrins were characterized by UV-Vis, NMR spectroscopy and cyclic voltammetric. The analysis of X-ray crystal structures of the five-coordinate complexes revealed distorted macrocyclic cores where significant differences in the Zn-N distance between the β -substituted and the non- β -substituted side were observed. [42]

In 2004, Ana PJ. *et al.* synthesized the hydroxyl nitrophenylporphyrins by Adler's method. The synthesis of tetrakis(2-hydroxy-5-nitrophenyl) porphyrin **1a** is prepared by the condensation reaction of pyrrole and 2-hydroxy-5-nitrobenzaldehyde in propionic acid, at 414 K. The synthesized product yield was obtained 72 % yield. The structure was shown in Figure 6. These porphyrins were characterized by ^1H NMR, UV-Vis and fluorescence spectroscopy. The results presented these hydroxyl nitrophenyl porphyrins can be considered as promising photosensitizers in PDT. [43]

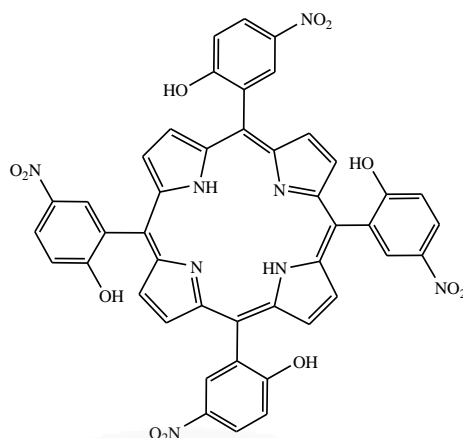


Figure 6. Tetrakis(2-hydroxy-5-nitrophenyl)porphyrin **1a**.

In 2009, Baris T. and Canan U. reported the new route synthesis of 5,10,15,20-tetraphenylporphyrins (H_2TPP). These porphyrins and derivatives have been prepared by the condensation reaction of dipyrromethanes and *N*-tosyl imines by using metal triflate catalyst such as $Gd(OTf)_3$, $Yd(OTf)_3$, $Y(OTf)_3$, $La(OTf)_3$, $Zn(OTf)_2$, $Nd(OTf)_3$ and $Cu(OTf)_2$. The synthesized reaction of H_2TPP required two steps. Firstly, the synthesis of porphyrinogen intermediate was prepared by condensation of diyrromethanes and *N*-tosyl imines. Secondly, the porphyrinogen was oxidized to H_2TPP . This synthesis method can be applied to synthesize *trans*- A_2B_2 -tetraarylporphyrins by mild reaction and give a high yield. [44]

In 2011, Zhi X. *et al.* synthesized nitro-porphyrin based on the condensation of nitrobenzaldehyde with pyrrole according to the modification method (e.g. Rothmund and Lindsey's method). The synthesis of 5, 10, 15, 20-tetrakis (*p*-nitrophenyl)-21H, 23H-porphyrin **2a** by using chloroform solution of H_2TPP was reacted with red fuming HNO_3 under an argon atmosphere at 273.18 K as shown in Figure 7. The product can be isolated with a good yield of nearly 90 % based on a solid phase extraction techniques. The substantial characterizations of synthesized porphyrin were evaluated by 1H -NMR, LR and HR-mass spectrometry, UV-Vis and fluorescence spectroscopy. [45]

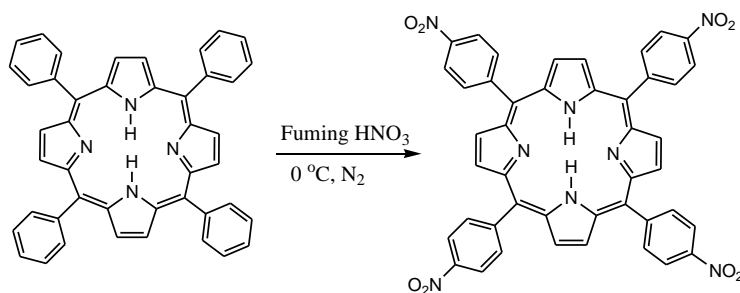


Figure 7. Synthesis of tetrakis(4-nitrophenyl)porphyrin **2a**.

In 2013, Emese G. *et al.* synthesized meso-tetrakis(10-alkyl-phenothiazin-3yl)porphyrins **3a** and **4a** as shown in Figure 8. The both compounds were prepared by modified Lindsey and Adler-Longo method. The structures have been assigned based on HRMS and NMR spectra. The optical properties and electron transfer properties were investigated by UV-Vis spectroscopy and cyclic voltammetry, respectively. [46]

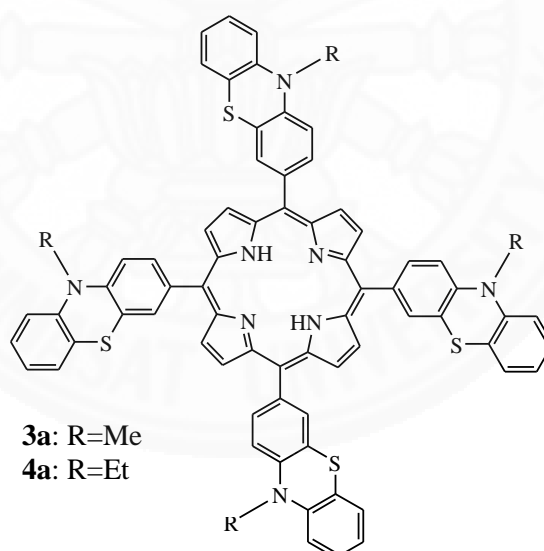


Figure 8. The structure of meso-tetrakis(10-alkyl-phenothiazin-3yl)porphyrins **3a-4a**.

In 2016, Eugenia F-C. *et al.* synthesized Co(II)-5, 10, 15, 20-meso-tetra(3-hydroxyphenyl)porphyrin (Co-3OHPP) **5a** (Figure 9.) by using tetra(3-hydroxyphenyl)porphyrin in THF were reacted in refluxing and stirring with $\text{CoCl}_2 \cdot 6\text{H}_2\text{O}$ dissolved in CH_3OH for 45 min and then recrystallized with CHCl_3 . The Uv-Vis spectroscopy

showed the only one Q band absorption spectrum of metalloporphyrin to confirm the increase in symmetry because the metal insertion in the porphyrin core. [47]

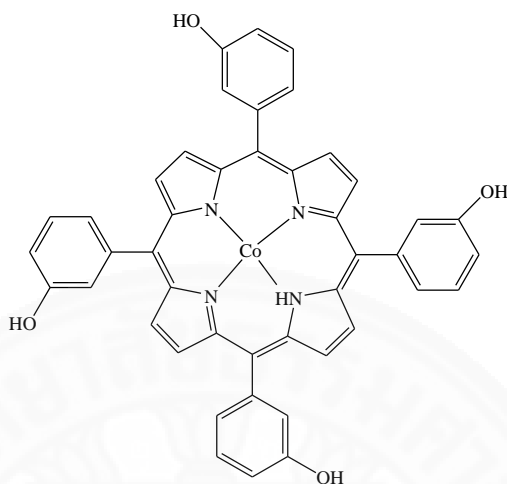


Figure 9. Structure of Co(II)-5,10,15,20-meso-tetra(3-hydroxyphenyl) porphyrin (Co-3OHPP) **5a**.

In 2016, Yu W. *et al.* synthesized ZnPA porphyrin dyes by the modified Lindsey method. The free based porphyrin **6a**, **7a**, and **8a** were added in the $\text{Zn}(\text{OAc})_2 \cdot 2\text{H}_2\text{O}$ in DMF, then the mixture was heated at reflux for 4-5 h to obtain the products were o-ZnPA **9a**, o-ZnPA **10a** and m-ZnPTz **11a**, respectively. The products were confirmed by ^1H -NMR, FT-IR, Mass spectrometry, UV-Vis and Fluorescence spectroscopy. [48]

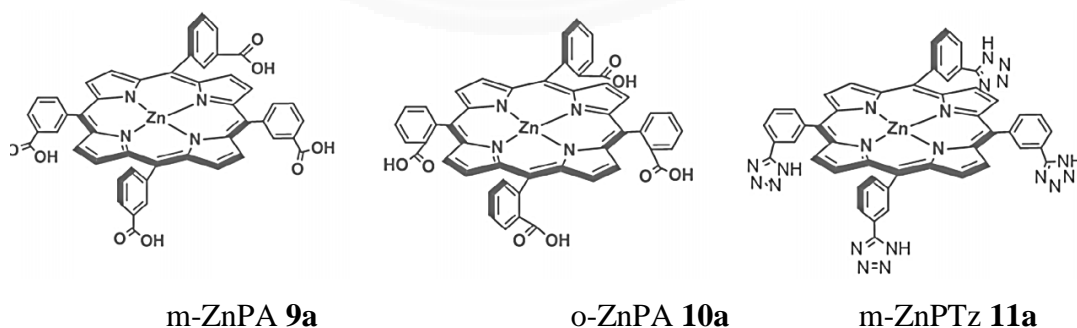


Figure 10. The structure zinc porphyrin dyes.

In 2017, Pinky Y. *et al.* synthesized the tetrakis(4'-carboxamidophenyl)porphyrin **12a** and tetrakis(3',5'-dicarboxamidophenyl)porphyrin **13a**. These compounds were characterized by various spectroscopic techniques. Both compounds showed planar conformation of porphyrin ring and displayed a marginal red-shift in Soret band at 419 nm of the electronic spectral feature as compared to H₂TPP (417 nm). [49]

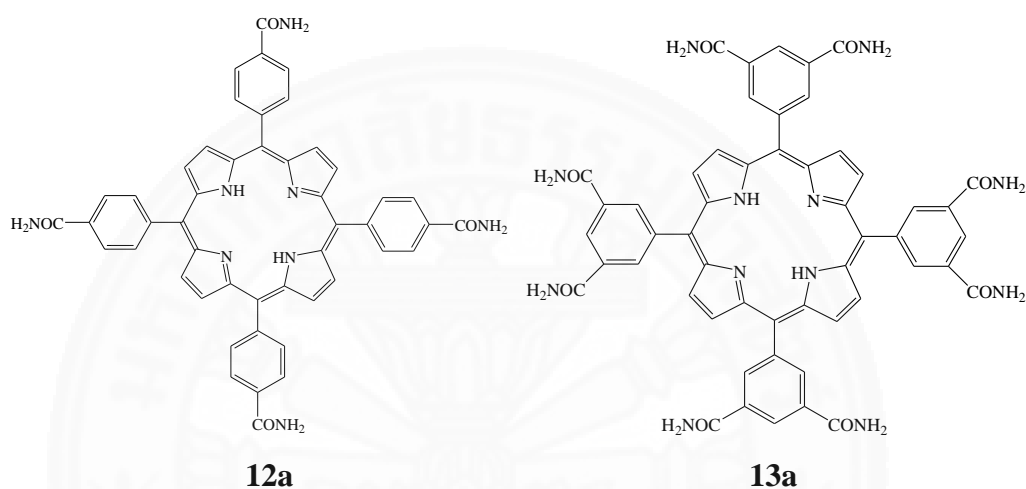


Figure 11. The molecular structure of **12a** and **13a**.

2.2 Porphyrins and metalloporphyrins substituted with long chains

Furthermore, the synthetic porphyrins and metalloporphyrins substituted with long chains have been interested due to substitute long chain in porphyrin ring can enhance the performance of physical and chemical properties of porphyrin.

In 2007, Ioannis D.K. *et al.* synthesized the water-soluble palladium porphyrin as shown in Figure 12. Synthesized aldehyde was obtained yield in 95 % by refluxing of the 4-hydroxybenzaldehyde with ethyl 4-bromobutyrate in the presence of K₂CO₃, in DMF at 353 K. The long chained porphyrin was synthesized by the Adler and Longo method. Palladium(II) porphyrin was carried out by using palladium chloride refluxed with the free base porphyrin in benzonitrile solvent. The desired solid porphyrin was obtained in 90% yield. Then, Pd(II) porphyrin **14a** was dissolved in different solvents (THF, methanol, and KOH) to prepare water soluble potassium

carboxylate salt. Palladium complex with a porphyrin ligand was used as a catalyst precursor for cross-coupling reactions as shown in Figure 12. [50]

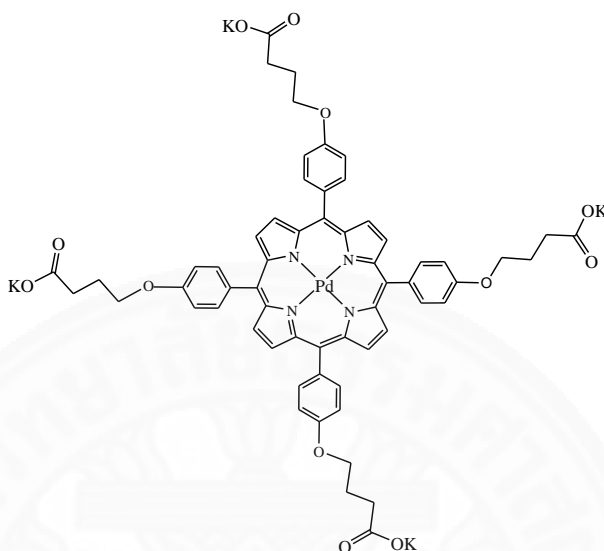


Figure 12. The structure of palladium porphyrin **14a**.

In the same years, Fedulova I.N *et al.* (2007) reported symmetrical *meso*-aryl substituted porphyrins with hydrophobic long chain, as shown in Figure 13. The lipoporphyrins can be designed as supramolecular lipid ensembles of nanometer size. The *meso*-aryl substituted dipyrrolylmetanes **17a** and **18a** by the condensation of substituted benzaldehydes and were obtained in 75 and 55 % yield, respectively. The substituted benzaldehydes **15a** and **16a** by acylation or alkylation of *p*-hydroxy benzaldehyde with tetradecyl bromide and myristic acid chloride and were obtained in 71 and 82 % yield, respectively. For the synthesis of all porphyrins, optimal routes were illustrated in Figure 13. However, the concentration of both benzaldehyde and pyrrole are given optimal yields, which the porphyrins long chain was obtained from the substituted benzaldehydes in 33 to 54 % yields. These porphyrins were characterized by IR, MS, ^1H -NMR spectroscopy, and CHN elemental analysis. [51]

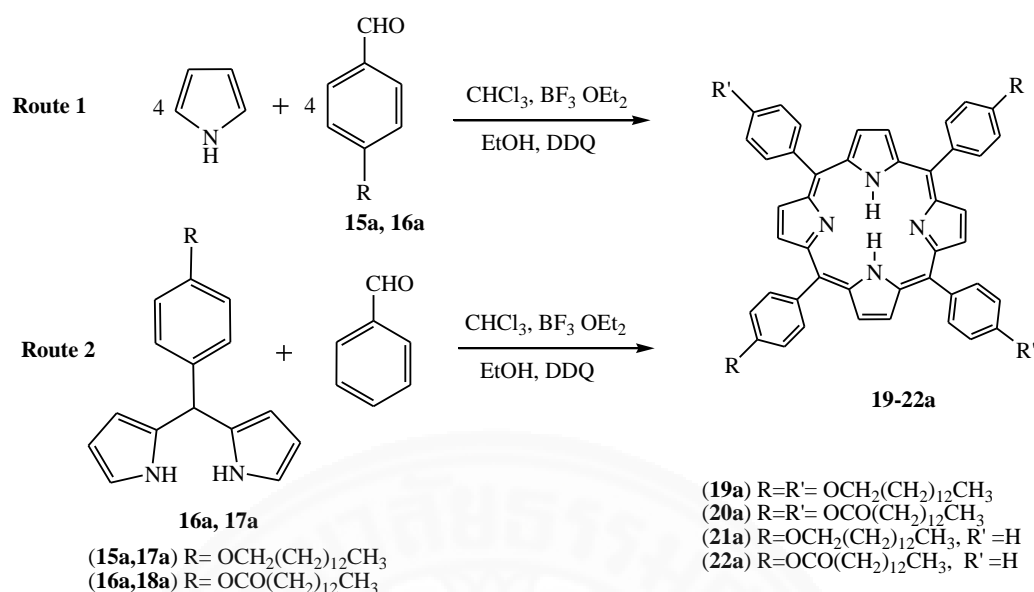
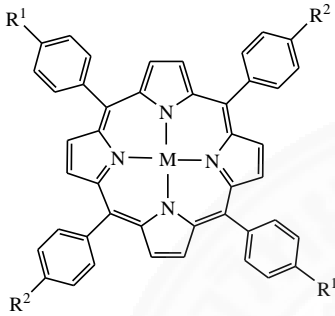


Figure 13. Synthesis of *meso*-aryl-substituted porphyrins **19-22a**.

The year later, Irina N.F. *et al.* (2008) successfully synthesized *meso*-tetraphenylporphyrins with long chain alkoxy substituents at *para*-positions of 5,15- or 5,10,15,20-phenyl groups and their Zn(II) and Co(II) complexes (as shown in Table 1). The synthesis of porphyrins with long chain prepared by the reaction of hydroxybenzaldehyde with alkyl bromides and condensation of pyrrole with various synthesized aldehydes. Porphyrins of two structure types were synthesized by monopyrrole condensation (Route 1) and using dipyrromethane (Route 2) in 36 to 44 % yields. Zn(II) and Co(II) complexes were prepared by refluxing porphyrin ligand with metal acetate and were obtained in 90 to 95 % yields. The synthesized porphyrins have been determined by UV-Vis spectroscopy, ^1H NMR spectroscopy, and CHN elemental analysis. [52]

Table 1 The structures of the *meso*-tetraphenylporphyrins with long chain alkoxy substituents.

Structural formula	Compound	R ¹	R ²	M
	1	O(CH ₂) ₇ Me	H	2H
	2	O(CH ₂) ₁₃ Me	H	2H
	3	O(CH ₂) ₁₅ Me	H	2H
	4	O(CH ₂) ₇ Me	H	Zn
	5	O(CH ₂) ₇ Me	H	Co
	6	O(CH ₂) ₇ Me	O(CH ₂) ₇ Me	2H
	7	O(CH ₂) ₁₃ Me	O(CH ₂) ₁₃ Me	2H
	8	O(CH ₂) ₁₅ Me	O(CH ₂) ₁₅ Me	2H
	9	O(CH ₂) ₇ Me	O(CH ₂) ₇ Me	Zn
	10	O(CH ₂) ₇ Me	O(CH ₂) ₇ Me	Co
	11	O(CH ₂) ₁₃ Me	O(CH ₂) ₁₃ Me	Zn

Ref: Irina N. F. *et al.* (2008). *Mendeleev Commun.*, 18, 324–326.

In 2008, Hua C. *et al.* synthesized *meso*-tetrakis[4-(pentyloxy)phenyl] porphyrin by the reaction of 4-pentyloxylbenzaldehyde with pyrrole, refluxing in propionic acid for 1 hour at 383 K. The product was obtained 12 % yield. The crystal structure of the compound was determined by single crystal X-ray diffraction methods. [53]

In 2009, Chen W. *et al.* reported two series of novel *meso*-substituted porphyrins contain 5,10,15,20-tetra[4-(3-phenoxy)-propoxy] phenyl porphyrin **23a**, and 5,10,15,20-tetra[2-(3-phenoxy) propoxybenzaldehyde **24a**, respectively (as shown in Figure 14). Both porphyrins were observed less than 15 % yield. Moreover, their metal (Co(II), Cu(II), and Zn(II)) complexes have been synthesized with 90 % yield. The structures of all compounds were characterized by the CHN elemental analysis, FT-IR, ¹H NMR, mass, and UV-Vis spectroscopy. Furthermore, the photocatalytic activities in degradation of 4-nitrophenol have been studied by using

polycrystalline TiO_2 impregnated with the synthesized porphyrins and metalloporphyrins. [54]

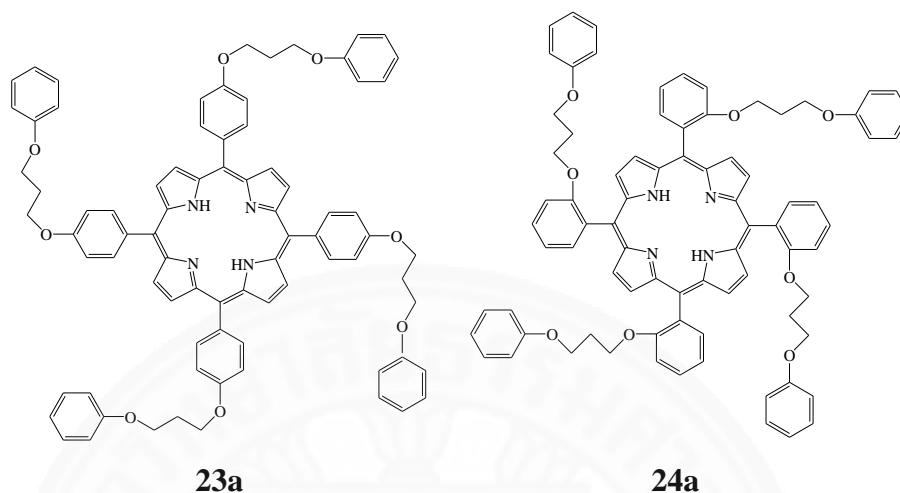


Figure 14. The structure of novel *meso*-substituted porphyrins **23a** and **24a**.

In 2009, Er-Jun S. *et al.* reported a series of novel porphyrin derivatives with long-chain-substituted. The *meso*-tetra (4-alkylamidophenyl)porphyrin ligands and their Zn complexes (alkyl = 8, 10, 12, 14, 16,18) were shown in Figure 15, which they were prepared by acylation reaction of the amino group of *meso*-tetra(4-aminophenyl)porphyrin with alkyl chloride. These porphyrin products have been characterized by using elemental analysis, ^1H NMR, IR, UV-vis spectroscopy, fluorescence spectroscopy and cyclic voltammetry. Moreover, the mesomorphism properties were studied by DSC, POM, XRD, SPS, and EFISPS. The results found that the ligand containing long chain carbon substituted (more than 12 atoms) exhibited liquid crystalline behavior, while Zn complexes are not. [55]

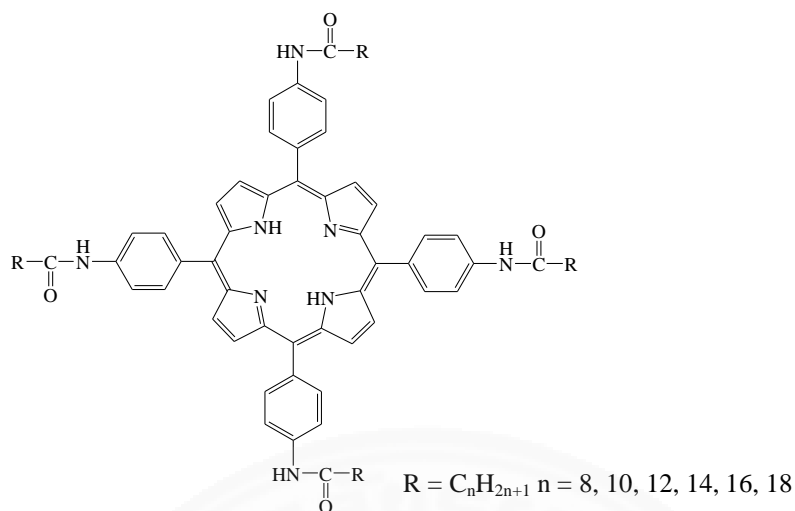
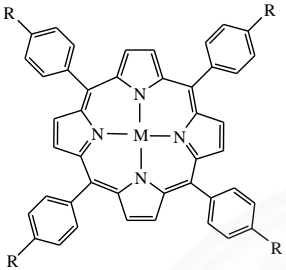


Figure 15. The structure of *meso*-tetra (4-alkylamidophenyl)porphyrin ligands.

In 2010, Nikita V.N. *et al.* synthesized porphyrins with substituents at the aromatic rings by using condensation according to Lindsey method. *meso*-Tetrakis[4-(6-bromohexanoyloxyphenyl)] porphyrins and *meso*-tetrakis[4-(11-bromo undecanoyloxyphenyl)]porphyrins were prepared from pyrrole and the respective substituted 4-hydroxybenzaldehydes to give 35 to 40 % yields. Synthesis of lipophilic porphyrins of metalloporphyrins (Zinc, cobalt, nickel and copper metal complexes) used as the precursors. These metalloporphyrins were obtained by standard techniques to gain 93 to 95 % yields. [56]

In 2011, Formirovsky K.A. *et al.* reported the novel amphiphilic alkoxyaryl porphyrins bearing long chain substituents terminated with carboxy and carboxymethyl groups. Their Zn(II) and Cu(II) complexes were shown in Table 2. The *meso*-tetra substituted porphyrins were obtained by using condensation reaction of monopyrrole in which the maximum yields of porphyrins were achieved at the concentrations of benzaldehyde and pyrrole equal to 10^{-2} M. The synthesis of symmetrical *meso*-tetrakis [4-(methoxycarbonylalkyloxyphenyl porphyrins)] and metal complexes were obtained yield in 35 to 40 % and 75 to 90 %, respectively. The structure of these compounds has been confirmed by TLC, UV-Vis, ^1H -NMR and mass spectrometry. Their mesomorphic properties were studied by optical polarizing microscopy. [57]

Table 2 The structures of the porphyrins and metalloporphyrins.

Structural formula	Compounds	M	R
	1	2H ⁺	-O(CH ₂) ₁₀ COOH
	2	2H ⁺	-O(CH ₂) ₅ COOMe
	3	2H ⁺	-O(CH ₂) ₁₀ COOMe
	4	Zn	-O(CH ₂) ₁₀ COOMe
	5	Cu	-O(CH ₂) ₁₀ COOMe

Ref: Formirovsky K.A. *et al.* (2011). *Macroheterocycles*, 4(2), 127-129.

The year later, Kirill A.F. *et al.* (2012) synthesized new amphiphilic alkoxyarylporphyrins with long-chain substituents containing carboxy, methoxycarbonyl and hydroxy groups, and their metal (Zn²⁺) complexes as shown in Figure 16. Mesogenic properties and liquid-crystal properties of all compounds were investigated by using optical polarization microscopy for identification. [58]

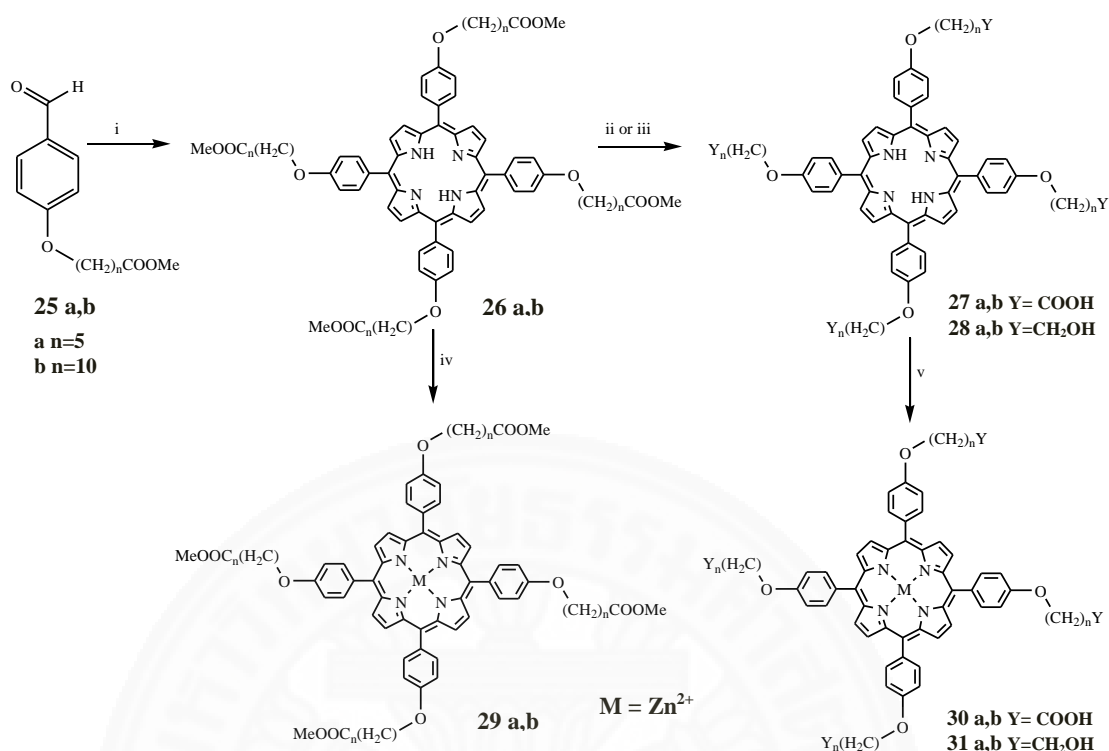


Figure 16. Synthesis of porphyrins **25a,b** - **31a,b**. (Reagents and conditions: i, pyrrole, Et₂O·BF₃, CH₂Cl₂, DDQ; ii, 50% NaOH, heating; iii, LiAlH₄, THF; iv, M(OAc)₂, CH₂Cl₂, MeOH; v, M(OAc)₂, DMF, heating. [58])

In 2011, Preecha M. *et al.* presented the simple method for identification of a series of six *meso*-substituted porphyrin derivatives by using ¹H NMR spectroscopy. The series of six porphyrins have been prepared by refluxing of mixed two aldehydes contain 3,5-di-*tert*-butylstyrylbenzaldehyde (**A**) and 4-iodobenzaldehyde (**B**) in 1:1 ratio, pyrrole, and zinc acetate in propionic acid for 3 hours. The crude mixed porphyrins were purified by column chromatography on silica gel and then eluted with mixed hexane and dichloromethane. The structures of these porphyrins are shown in Figure 17. The signal pattern of ¹H NMR of β-pyrrolic proton was used for identification of the mixed porphyrin structures. [59]

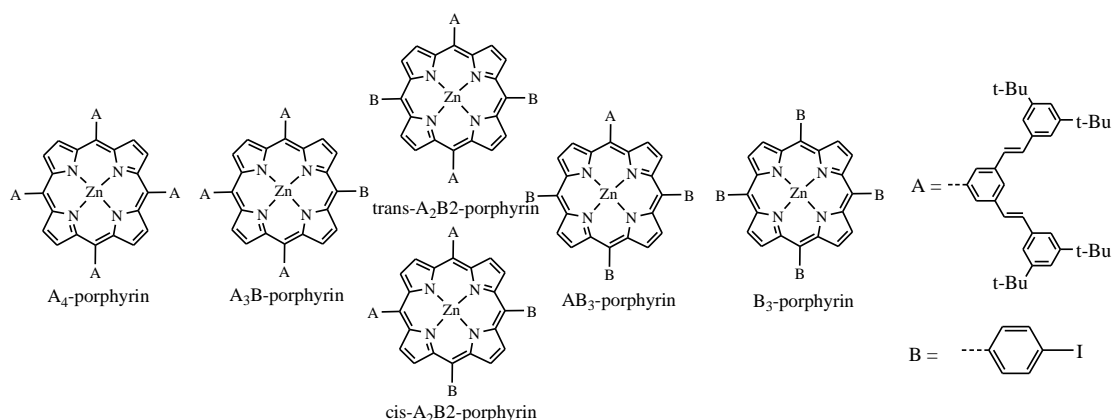


Figure 17. Structure of mixed *meso*-substituted Zn(II) porphyrins.

In 2012, Ekaterina S.Z. *et al.* reported the synthesis of covalent-bound porphyrin-fullerene conjugates based on fullerene C₆₀ and *meso*-aryl-substituted porphyrins with long chain substituents by using the Prato reaction. The starting *meso*-aryl-substituted porphyrins were gained in 40 % yield by the condensation reaction of pyrrole and the corresponding 4-alkoxybenzaldehydes. The copper(II) porphyrins were obtained with yields of 95 %, but nickel(II) porphyrins gave lower yield only 70%. These metalloporphyrins were performed in CH₂Cl₂ by refluxing for 5 to 6 hours. The yields of synthesized formylporphyrins were 55 to 60 %. The addition of fullerene C₆₀ to formylporphyrins was prepared by refluxing with *N*-methylglycine in anhydrous toluene under argon for 20 hours; the resulting conjugates were brown solid. Figure 18 shown structures of these porphyrin products. The products have been confirmed by nuclear magnetic resonance (¹H- and ¹³C- NMR), IR, UV-Vis, and mass spectrometry. [60]

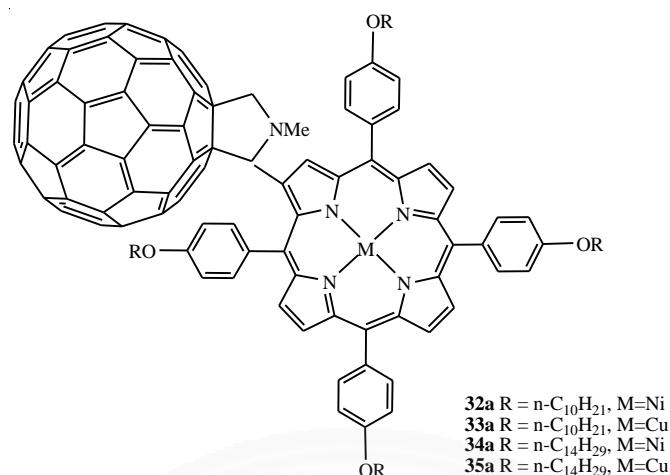
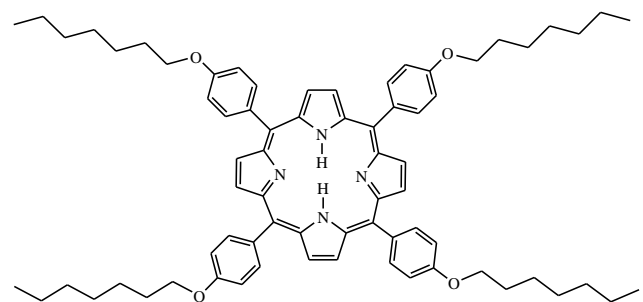


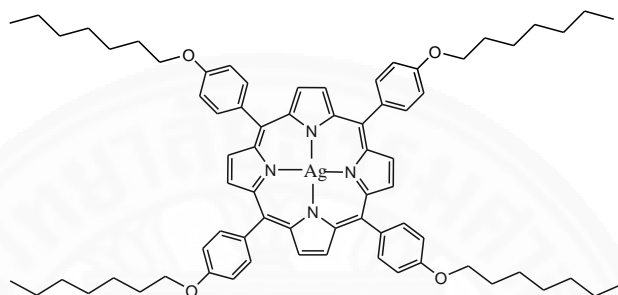
Figure 18. The structure of porphyrins, Cu(II) and Ni(II) complexes.

In 2013, Hong-Bin Z. *et al.* prepared the novel of *meso*-tetrakis[4-(heptyloxy) phenyl]porphyrin **36a**. The mixture was refluxed of 4-(heptyloxy) benzaldehyde and pyrrole in propionic at 298 K for 1 hour. The porphyrin product was obtained in 12 % yield (m.p.527-528 K) as shown Figure 19. Single crystals of *meso*-tetrakis[4-(heptyloxy)phenyl] porphyrin suitable for X-ray diffraction were obtained by vapor diffusion of hexane into a dichloromethane solution at room temperature. [61]

The previous year, Jun-Xu L. *et al.* (2011) reported the crystallographic data of {*meso*-tetrakis[*p*-(heptyloxy)phenyl]porphyrinato}silver(II) **37a** (Figure 19), where the Ag(II) cation are located on a center of porphyrin hole. The synthesis of this compound was prepared by the condensation reaction of *meso*-tetrakis[*p*-(heptyloxy)phenyl]porphyrin and AgNO₃ in chloroform, refluxed for 6 hours. The crystal product was obtained in 23 % yield as purple solid. The structure of this compound was confirmed by X-ray diffraction. Single crystals were obtained from recrystallization with a dichloromethane solution at room temperature. [62]



meso-Tetrakis[4-(heptyloxy)phenyl]porphyrin **36a**



{*meso*-Tetrakis[*p*-(heptyloxy)phenyl]porphyrinato}silver(II) **37a**

Figure 19. The structures of the porphyrin **36a** and silver complex **37a**.

In 2013, Wei L. *et al.* presented the synthesis liquid crystalline tetraalkanoxy phenylporphyrins, free base on tetrakis(4-hydroxyphenyl)porphyrin and Zn(II) complexes. Tetrakis(4-hydroxyphenyl)porphyrin **38a** has been synthesized by reacting 4-hydroxybenzaldehyde with pyrrole in propionic acid. Then, compound **38a** was further esterified with the appropriate acyl chloride in benzene and triethylamine solvent. The synthesized products were obtained in ranged from 86 to 88% (Figure 20). The metalloporphyrin complex was prepared by using free base porphyrin and zinc acetate, refluxed in chloroform and *N,N*-dimethylformamide. Zn(II) complexes were obtained 82 to 84 % yield. The compounds have been investigated their liquid crystalline behavior and structure. [63]

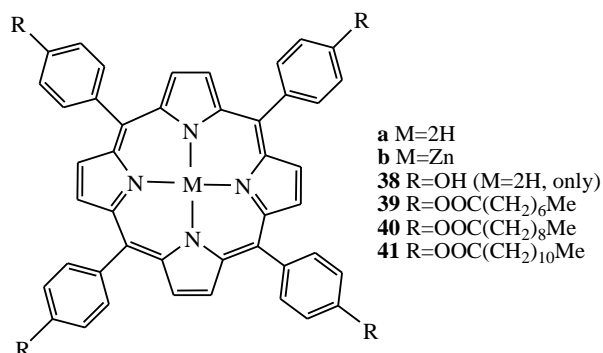


Figure 20. The structures of the porphyrin **38-41a** and Zn(II) complex **39-41b**.

In 2013, Ya-hong W. *et al.* synthesized a series of novel *meso*-tetra (Schiff-base substituted phenyl) porphyrin and their Zn(II) complexes. The Schiff-base porphyrins were synthesized by condensation reaction of porphyrin **42a** with various substituted benzaldehyde. Moreover, the Zn(II) porphyrin complexes were synthesized as shown in Figure 21. These compounds have been successfully characterized by UV-Vis and fluorescence spectroscopy, FT-IR, and EPR technique. [64]

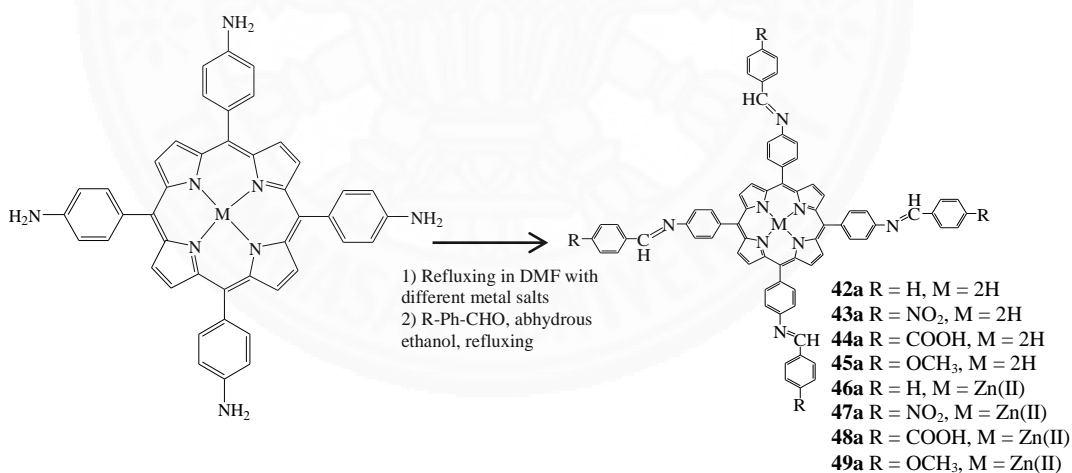


Figure 21. Synthesis of tetra (Schiff-base substituted phenyl) porphyrins and their metal (Zn²⁺) complexes.

In 2013, Yu Jing Z. *et al.* reported the novel *meso*-tetra[n-C_nH_{2n+1}-alkyl (n=12,14,16) Aarbazole] porphyrin and their lanthanide complexes (Dy, Hs, Er, and Gd). All synthesized porphyrins were characterized by ¹H-NMR, IR, UV-Vis spectroscopy and TGA-DTA. The synthetic ligand was obtained in low % yield as

18%. Moreover, the luminescence and electrochemical properties of these porphyrins have been investigated. The intensity of fluorescence emission spectra and the quantum yield were increased when the alkyl chain was longer. The Gd porphyrins complexes gave the strongest intensity fluorescence than other lanthanide complexes. [65]

In 2014, Renu G. and S.M.S. Chauhan prepared *cis*-A₂B₂ porphyrins, which carried out by the reaction of tripyrrane with pyrrole dicarbinol. The statistical condensation reaction of corresponding *p*-(alkoxy) benzaldehyde, 4-pyridine carboxaldehyde and pyrrole in refluxing with propionic acid gave the corresponding porphyrins. The porphyrin products contain different side chain lengths **50-52a** with minor modification in literature method. The desired *cis*-porphyrins were separated by using extensive column chromatography. The Zn(II) derivatives were gained by refluxing of the zinc acetate together with the corresponding porphyrin in DMF as shown in Figure 22. The porphyrin products were precipitated on cold water and vacuum. The structure of the compound has been characterized by NMR and UV-Vis spectroscopy. [66]

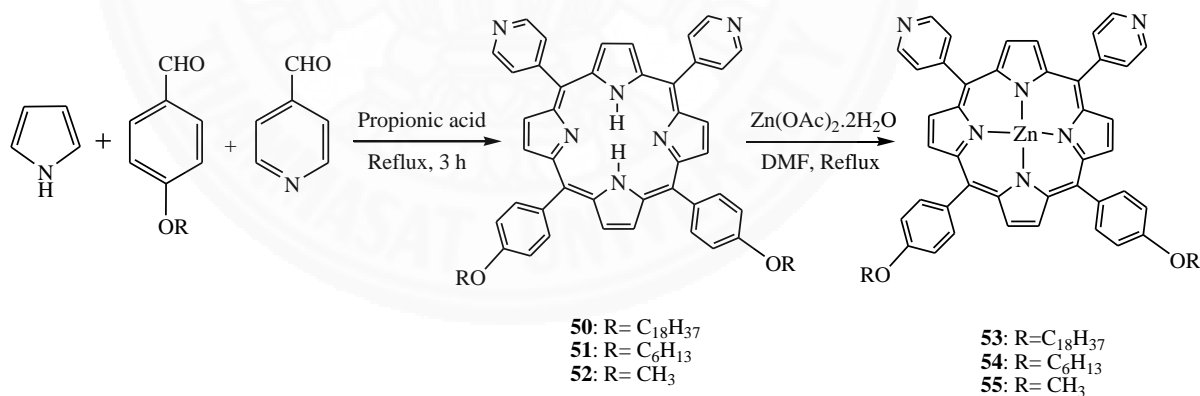


Figure 22. Synthesis of porphyrin **50-52a** and Zn(II) complexes **53-55a**.

In 2015, Ahmad J. *et al.* presented two new polycarboxylic photosensitizer. The 2,4,5-tris(tert-butoxycarbonylmethoxy)benzaldehyde and two derivatives of *meso*-dipyrromethane were synthesized, then both compounds were used in the synthesize porphyrin under Lindsey's method and obtained porphyrin in 20 % and 10 % yield, respectively. The desired product was reacted with the formic acid to give the carboxylic

porphyrin **56a** and **57a** as shown in Figure 23. All structure of compounds was confirmed by using the ^1H NMR and ^{13}C NMR spectroscopy and mass spectrometry (MALDI-TOF). The photophysical properties were investigated by UV-Vis spectroscopy. Both compounds were tested for photo-antimicrobial agents against *S. aureus* and *B. cereus*. The result shows the porphyrin **56a** give a significant antimicrobial activity than **57a** for tested bacteria at 50 μM or higher. [67]

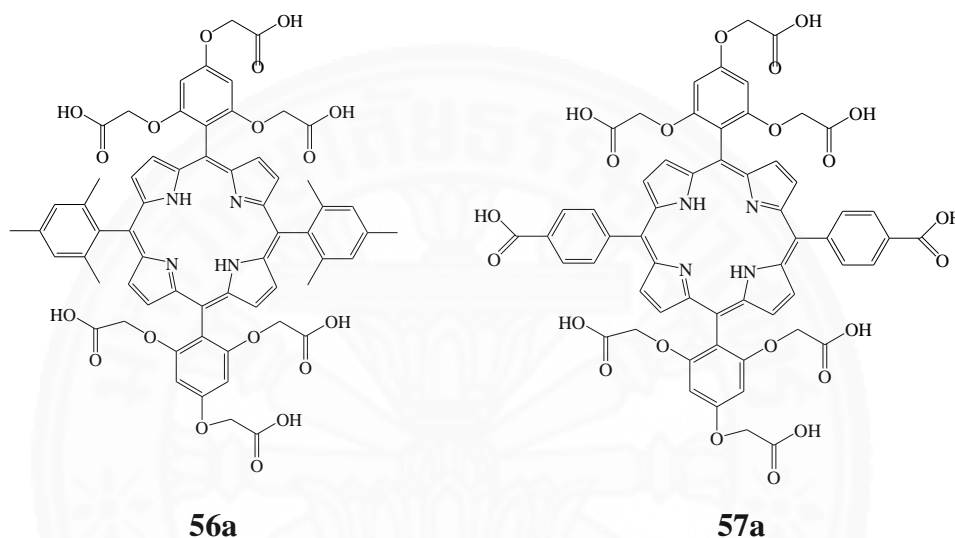


Figure 23. The structure of carboxylic porphyrin **56a** and **57a**.

In 2015, Rajneesh M. and Prabhat G. synthesized the *meso*-tetrakis (ferrocenyl ethynylphenyl)porphyrin **58a**, **59a** and zinc derivative **60a** as shown in Figure 24. The **58a** and **59a** have been synthesized by using ferrocenylethynylphenyl substituted aldehyde and pyrrole in dry CH_2Cl_2 under Linsey's method. TGA, photophysical and electrochemical properties have been investigated. The **59a** and ZnP2 **60a** exhibited better thermal stability than **58a**. [68]

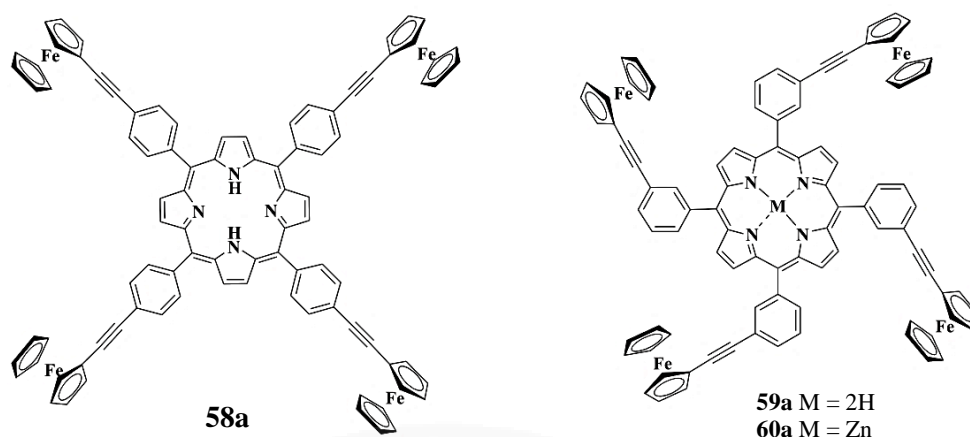


Figure 24. The structure of porphyrin **58a**, **59a**, and zinc complex **60a**.

In 2016, Korolev VV. *et al.* synthesized manganese(III) porphyrins, bearing 3,5-di-tert-butyl-4-hydroxyphenyl, 4-hydroxyphenyl, and 3,5-di-tert-butyl-4-palmitoyloxy groups in meso-positions **61-63a** as shown in Figure 25, reveal the paramagnetic properties. Furthermore, the magnetocaloric effect and heat capacity of 3 manganese(III) porphyrins were investigated. [69]

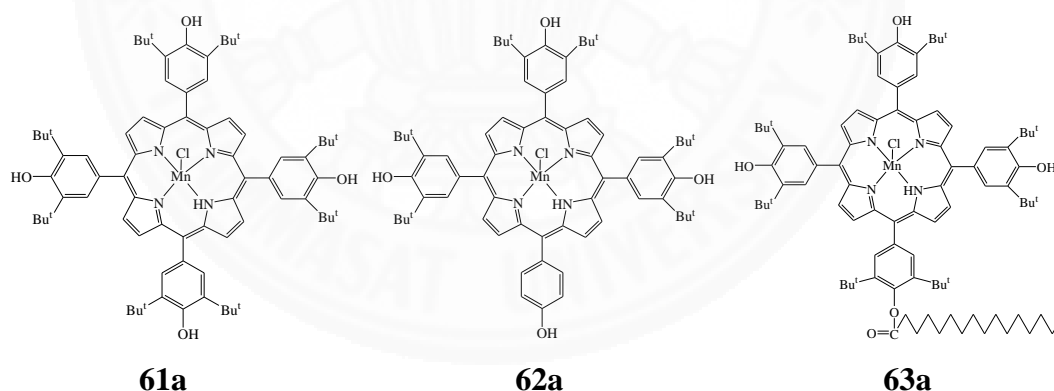


Figure 25. The structures of the manganese (III) porphyrin **61-63a**.

In 2016, Futai L. *et al.* reported the synthetic routes of the two porphyrin dyes with long alkoxyl chain LP-11 **64a** and LP-12 **65a**. The compound **64a** and **65a** as shown in Figure 26. The **64a** and **65a** product as a brown solid and were obtained in 78 % and 81 % yield, respectively. Both compounds have been characterized by using ^1H , ^{13}C -NMR and mass spectroscopy. The photophysical and electrochemical properties were investigated by UV-Vis spectroscopy and cyclic voltammetry. The

absorption spectrum of **64a** exhibits two absorption at 463 and 682 nm, while **65a** was slightly red-shifted and two absorption intensity were increased because of electron withdrawing between the porphyrin core and the anchoring group effect. [70]

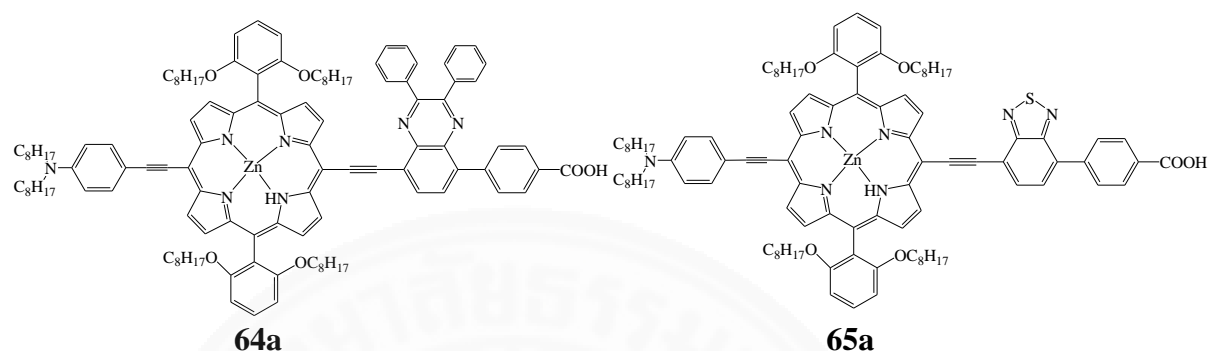


Figure 26. The structures of the two porphyrin dyes **64-65a**.

In 2017, Deyab M.A. *et al.* reported M-Porphyrins (Zn-Pp, Cu-Pp, and Co-Pp) with alkyd resin for the development of novel nanocomposite anticorrosive coatings. The porphyrin and metalloporphyrins have been synthesized as shown in Figure 27. The structure of the compound was confirmed by the analytical and spectral data. The impact of nanocomposite coatings containing the synthesized M-Porphyrins on the anticorrosive performance and mechanical properties of alkyd resin was investigated by electrochemical and mechanical analysis. The metal ion (Zn, Cu, Co) in the hole of porphyrin ring structure shows the main role for explaining the difference in the protection efficiency, which the protection efficiency increases in following the order: CoPp > Cu-Pp > Zn-Pp. [71]

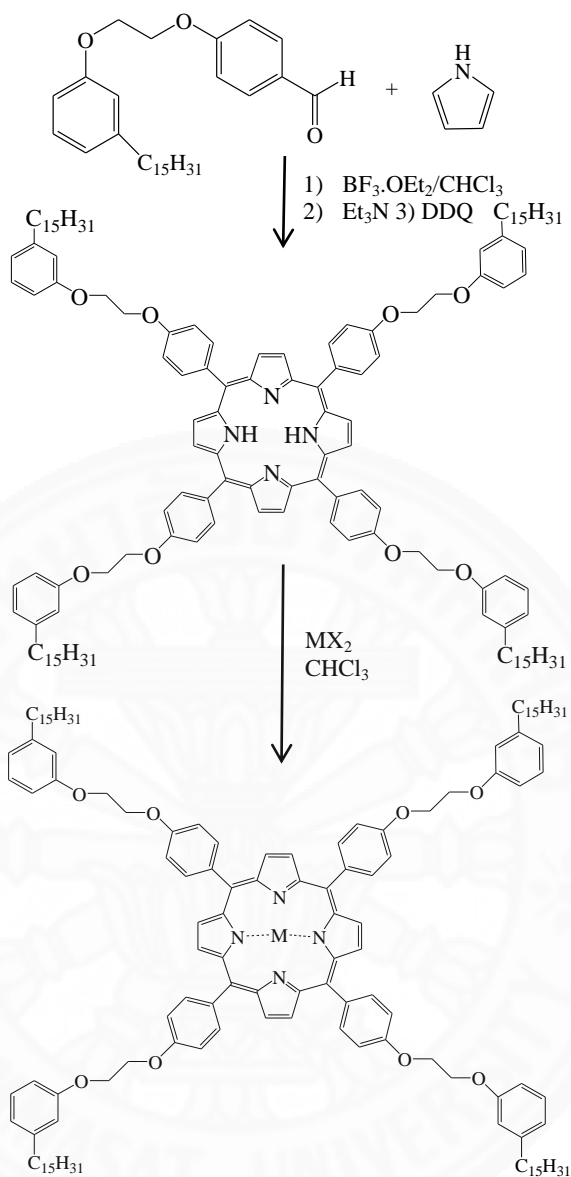


Figure 27. Synthetic method for metalloporphyrins.

2.3 Applications of porphyrins and long chain substituted metalloporphyrins

Porphyrins and metalloporphyrins have been interested in various applications such as dye-sensitized solar cell, photo-sensitizing drugs in medicine, and chemical sensors etc. Due to their thermal stability, non-linear optical effects from their extended π -conjugated macrocyclic ring, and the variation in their physical properties, that can be caused by chemical modification of their periphery.

For dye-sensitized solar cells (DSSCs) based on porphyrin derivatives as DSSC sensitizers have attracted attention because of their stable, low-cost, and high power conversion efficiency.

In 2014, Panagiotis A.A. *et al.* synthesized porphyrin **66a** and **67a**, in which a BDP chromophore is combined with a flexible cyanuric chloride bridge to either a free-base porphyrin (H_2P) or a Zinc porphyrin (ZnP). Then, both compounds were further functionalized with an electron accepting fulleropyrrolidine unit by an amino substituted aliphatic chain to give electron donor/acceptor conjugates **66b** and **67b**, respectively. The result observes that BDP chromophore increases significantly the light absorption capability of porphyrins. Moreover, functionalization of the arrays with redox active groups as fullerenes provides increasing of electron transfer dynamics in the excited state. [72]

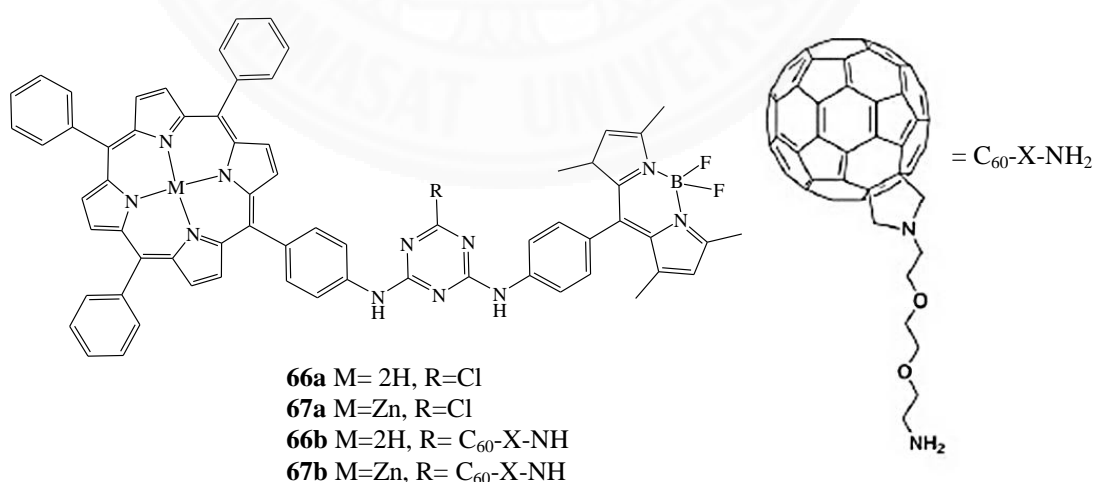


Figure 28. Peripherally substituted porphyrin arrays combined with a flexible cyanuric chloride bridge.

In 2015, Nuonuo Z. *et al.* synthesized three *meso*- π -A-porphyrins bearing long alkoxy chains were substituted at the ortho position of the phenyl ring and a phenyl carboxylate acid or acrylic acid at the meso position of porphyrin **68a**, **69a** and **70a**. All compound structures were confirmed by ^1H -NMR and mass spectrometry. Optical and electrochemical properties have also been investigated. The UV-Vis and emission spectra of the different porphyrin sensitizers show that the increasing of conjugation could affect their optical properties. Moreover, the photovoltaic properties of these porphyrins were determined for the efficiency in DSSC, resulting exhibits the sensitizers **68a** and **70a** achieved comparable light to electricity conversion efficiencies. [73]

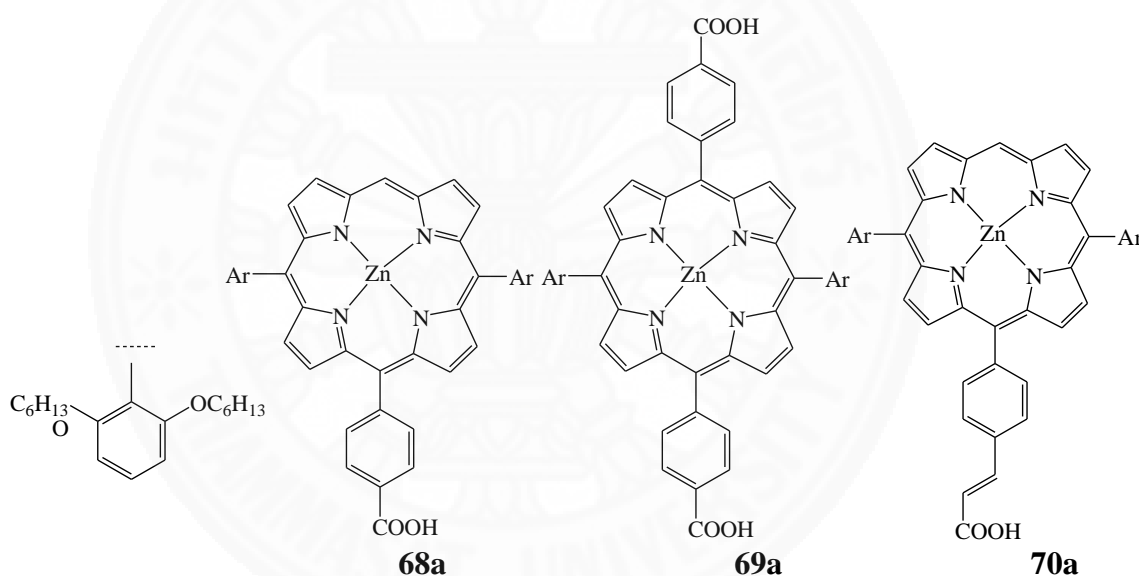


Figure 29. Molecular structure of the three *meso*- π -A-porphyrins.

In 2015, Huifang Z. *et al.* designed and synthesized three new donor- π -acceptor type unsymmetrical porphyrins (SF **71a**, BSF **72a** and NSF **73a**) for DSSCs. The photophysical, electrochemical and photovoltaic properties of these porphyrin dyes were considerably influenced by the donor units and π spacers. Compared with the absorption spectra of both **72a** and **73a** dyes in solution and broadened on TiO_2 films, it found that the amount of the two dyes absorbed on TiO_2 film significantly increased and **72a**-based DSSC exhibited the highest power conversion efficiency (PCE). [74]

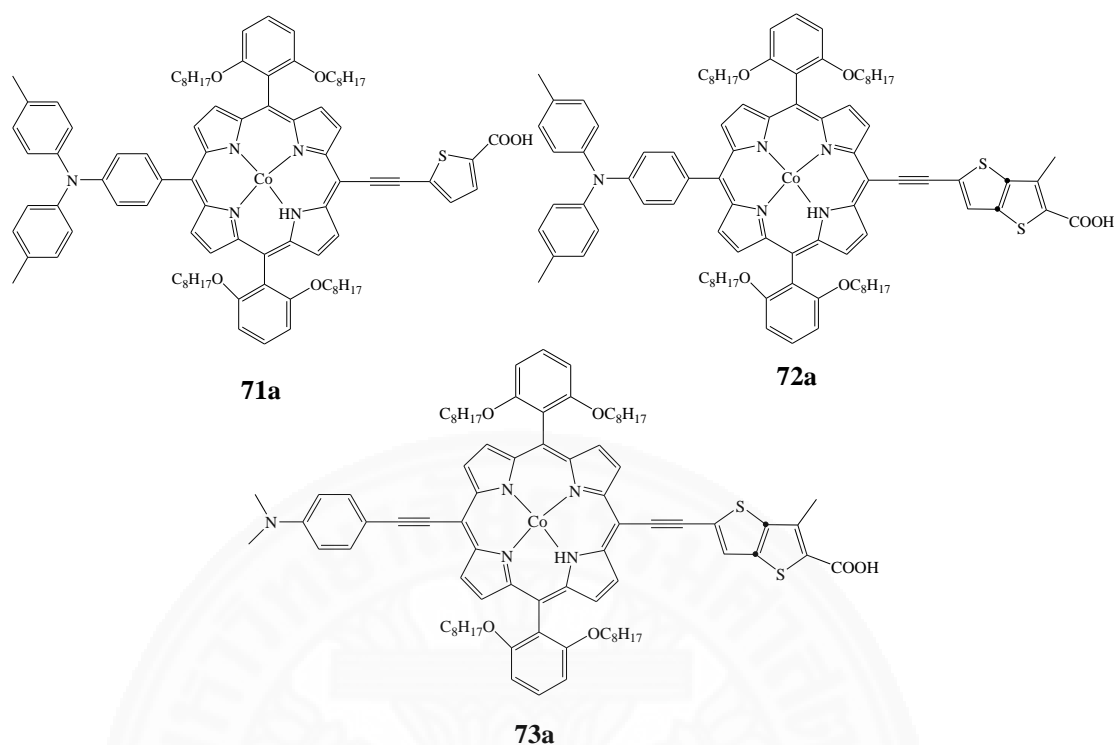


Figure 30. The structure of synthesized three new donor- π -acceptor porphyrins.

In 2016, Hao-Liang C. *et al.* synthesized the two novel zinc porphyrin dyes as **74a** and **75a**. Figure 31 shows the structure of **74a** and **75a** for dye-sensitized solar cells. The compounds have been characterized by ^1H -, ^{13}C -NMR and mass spectroscopy. The photochemical and electrochemical properties of both compounds were investigated. The results exhibited both dyes can efficiently convert the visible light into photocurrent. [75]

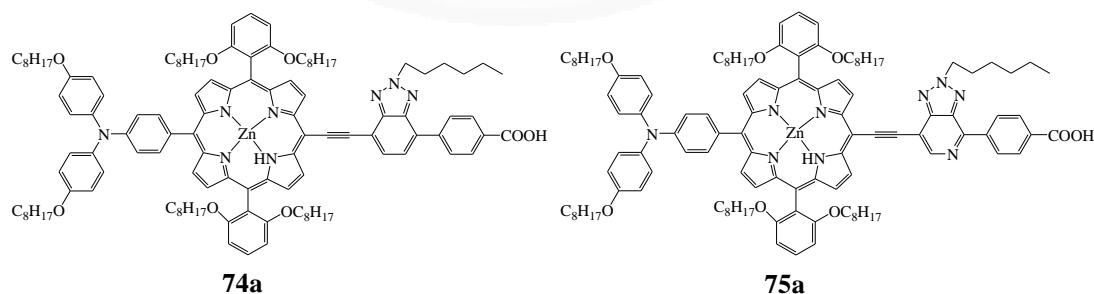


Figure 31. Structure of **74a** and **75a**.

In 2017, Heli S. *et al.* synthesized four alkoxy-wrapped push-pull porphyrin dyes bearing branched or linear alkoxy chains at the ortho-positions of the meso-phenyl moieties **76a-79a** for use as sensitizers in fabricating efficient dye-sensitized solar cells (DSSCs). The effect of alkoxy chains of porphyrin dyes was investigated. For the porphyrin dyes containing the ethynylbenzoic acid group as the acceptor found that the changes in the both branched and linear alkoxy chains make little difference in the photovoltaic performance, while for dyes containing the BTD unit as the acceptor, resulting shows branched chains provided obviously better photovoltaic behavior than the linear ones. [76]

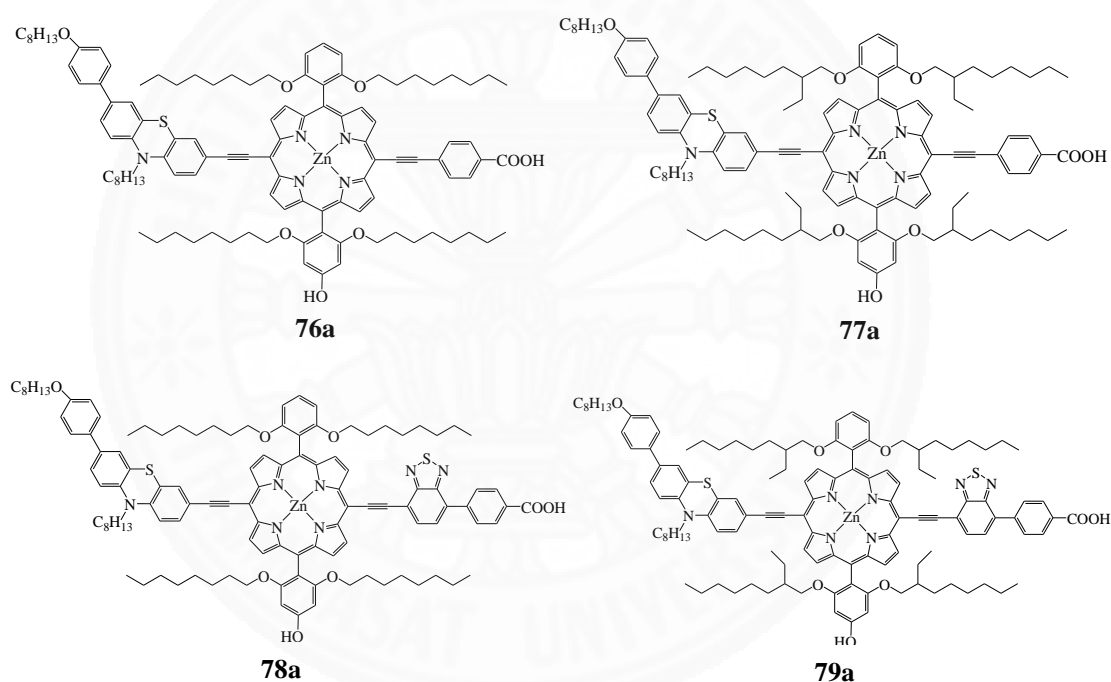


Figure 32. Molecular structure of **76a-79a**.

Also, the semiconducting material based porphyrins or metalloporphyrins have been investigated.

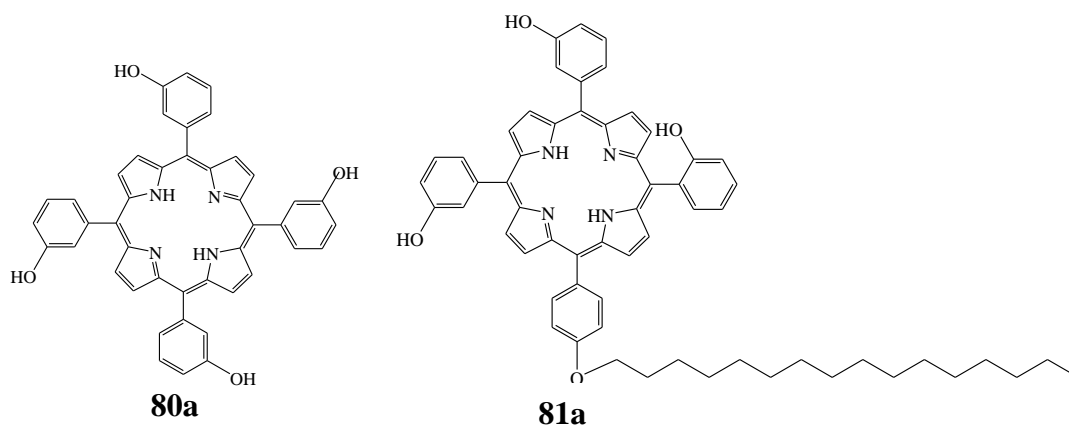
In 2016, Seung H.C. *et al.* designed and synthesized new solution processable semiconducting porphyrin derivatives, 5,10,15,20-tetrakis((4-hexylphenyl)ethynyl)porphyrin H₂TPEP and zinc complex via the Sonogashira coupling reaction of 4-iodohexylbenzene with corresponding tetraethynylporphyrins and their use in the fabrication of high-performing their film and single-crystal OFET

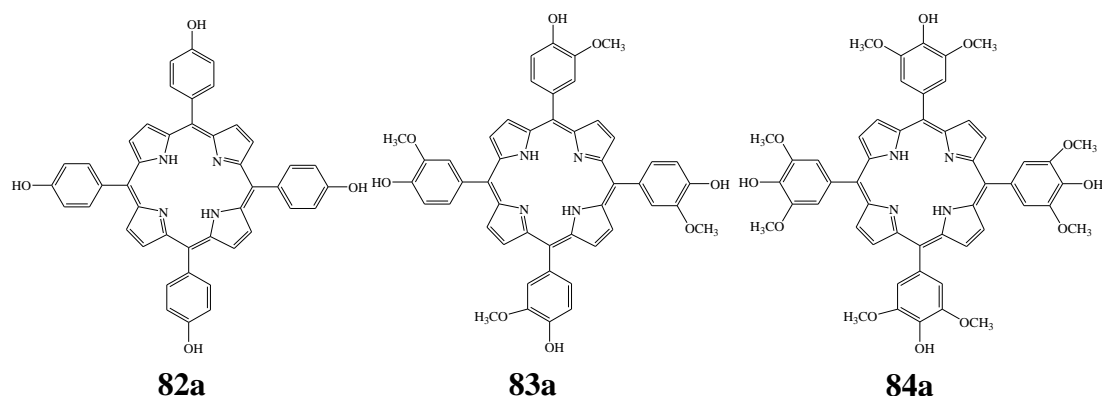
devices. Both porphyrins exhibited high crystallinity in film state and displayed excellent electrical characteristics with high carrier mobility due to strong π - π interactions. [77]

Moreover, porphyrins have gained much attention in the application of photodynamic therapy (PDT) for cancer and ophthalmic diseases. Porphyrins and metalloporphyrins were used as photosensitizers because photophysical properties contained long wavelength absorption and high singlet oxygen quantum yield.

In 2008, Xu X-J. *et al.* presented the antibacterial activity of manganese(II), tetraphenylporphyrin, ebselen-porphyrin conjugate, and its Mn(II) porphyrin derivatives. The stop-flow microcalorimetry was used to study the antibacterial effect of all compounds. *S. aureus* was used as the testing bacteria. The result shows all compounds have potential to antibacterial reagent and especially the tetraphenylporphyrin has IC₅₀ value less than other compounds. [78]

In 2013, Marcin R. *et al.* synthesized the tetrakis-(hydroxyphenyl) porphyrins with long alkyl chain at the different position for potential photosensitizers in anti-cancer photodynamic therapy. The summaries of all synthesized structure porphyrins are shown in Figure 33. Compounds **80a** – **84a**, **93a** and **96a** have been synthesized by condensation reaction of the appropriate aldehyde with pyrrole in propionic acid. Other porphyrins were gained from further modified synthetic route. Mass spectrometry, UV-Vis and fluorescence spectroscopy have been confirmed characterization of all compounds. Lipophilicity and photostability were investigated. These data confirm that compounds can usefulness as potential photosensitizers in anti-cancer photodynamic therapy. [79]





Compound	R ₁	R ₂	R ₃	R ₄	R ₅	R ₆
85a	OC ₁₆ H ₃₃	H	H	OH	H	H
86a	H	OC ₁₆ H ₃₃	H	H	OH	H
87a	OCOC ₁₅ H ₃₁	H	H	OH	H	H
88a	H	OCOC ₁₅ H ₃₁	H	H	OH	H
89a	OC ₁₆ H ₃₃	OCH ₃	H	OH	OCH ₃	H
90a	OCOC ₁₅ H ₃₁	OCH ₃	H	OH	OCH ₃	H
91a	OC ₁₆ H ₃₃	OCH ₃	OCH ₃	OH	OCH ₃	OCH ₃
92a	OCOC ₁₅ H ₃₁	OCH ₃	OCH ₃	OH	OCH ₃	OCH ₃
93a	NHCOCH ₃	H	H	OCH ₃	H	H
94a	NH ₂	H	H	OCH ₃	H	H
95a	NHCOC ₁₅ H ₃₁	H	H	OCH ₃	H	H
96a	NHCOC ₁₅ H ₃₁	H	H	OH	H	H

Figure 33. Structure of investigated compounds.

In 2014, Artak T. *et al.* synthesized a novel amphiphilic meso-substituted porphyrin, **97a** and its Ag(II) complex **98a** (Figure 34) through incorporation of long hydrophobic chain into the meso-position of porphyrin ring. The activity of **97a** and **98a** as potential photosensitizing and chemotherapeutic agent have been investigated compares with these of tetracationic porphyrins. Ag(II) porphyrin exhibited less toxicity to normal cells and greater toxicity to their cancerous counterparts as a promising new class of anticancer. [80]

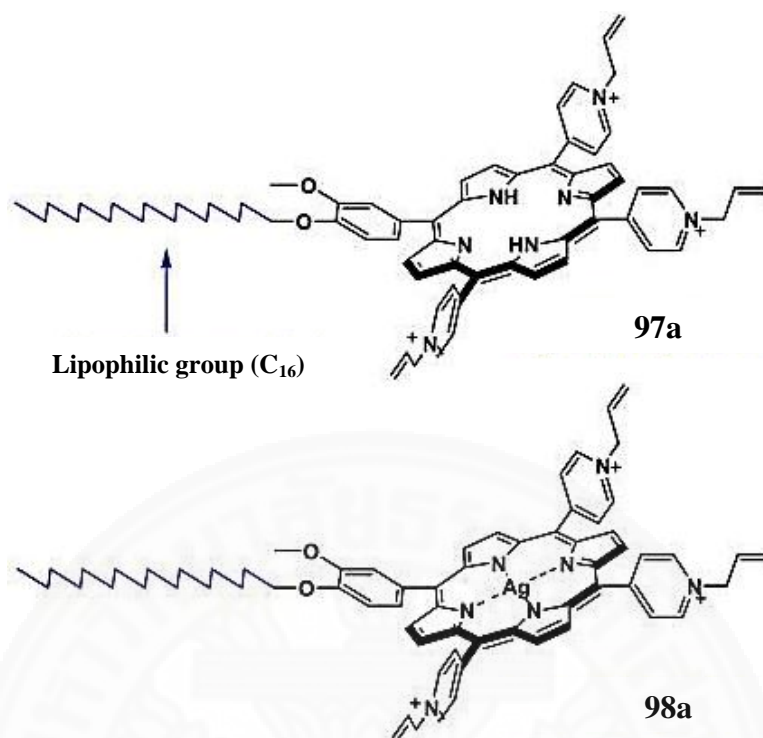


Figure 34. Chemical structures of porphyrins **97a** and Ag(II) complex **98a**.

In 2016, Mamone L. *et al.* reported the new synthetic porphyrin 5,10,15,20-tetrakis[4-(3-N,N-dimethylammonio)propoxy]phenyl]porphyrin (TAPP) bearing four basic groups in periphery of the tetrapyrrolic macrocycle for the treatment of planktonic and biofilm culture of *S.aureus* and *Pseudomonas aeruginosa*. The result exhibits the TAPP is an efficient photosensitizer of promoting the photodynamic killing of both bacteria. [81]

In 2016, Nela M. *et al.* studied the photodynamic activity of a new amphiphi porphyrin **99a** and hydrophilic porphyrin **100a**. $^1\text{H-NMR}$, UV-Vis and fluorescence spectroscopy and MALDI-TOF/TOF spectrometry were characterized the compounds. These two porphyrins exhibited drug dose-responses as well as a light dose-response relationship, but the compound **99a** showed significantly lower IC_{50} values than compound **100a**. [82]

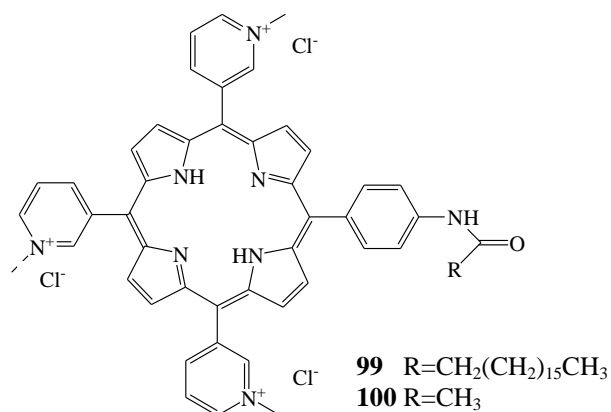


Figure 35. The structure of amphiphi porphyrin **99a** and hydrophilic porphyrin **100a**.

Furthermore, the porphyrins and their derivative porphyrins can also be used in other applications such as a catalyst in the various reaction, fluorescent markers in fuel and material device.

Siriorn P. *et al.* (2009) and Ana C. B.F. *et al.* (2011) have interested porphyrins modified to become fluorescent markers in the fuel. The resulting, *meso*-tetrakis(2-methoxy-4-pentadecylphenyl)porphyrin shows high solubility in diesel fuel and its strong fluorescence was monitored. The porphyrin marker was stable in diesel for at least 3 months. The physical properties of the porphyrin marker in diesel were unaffected at a concentration of 2 ppm. [83] While, *meso*-tetrakis(pentafluorophenyl)porphyrin (TPPF₂₀) using ethanol and hexadecan-1-ol have been studied on a spectrofluorometric detection method for the markers and the stability of the marked biodiesel fuel were investigated. Furthermore, the marked and unmarked biodiesel fuel physical properties of the synthesized porphyrins as biodiesel markers were tested. The fluorescent markers were stable in in storage conditions for at least 3 months and were unaffected at a concentration of 4 ppm. [84]

In 2013, Bianca S. *et al.* reported the preparation of a nanostructured films with an amphiphilic *meso*-porphyrin with side chains, which are derived from cardanol as a by-product of the cashew industry. The structure is shown in Figure 36. The applicability of the nanostructured ultrathin films as electrochemical sensor for promethazine was tested. The porphyrin with the linear chains provide a value greater than those obtained by other nanostructured systems. [85]

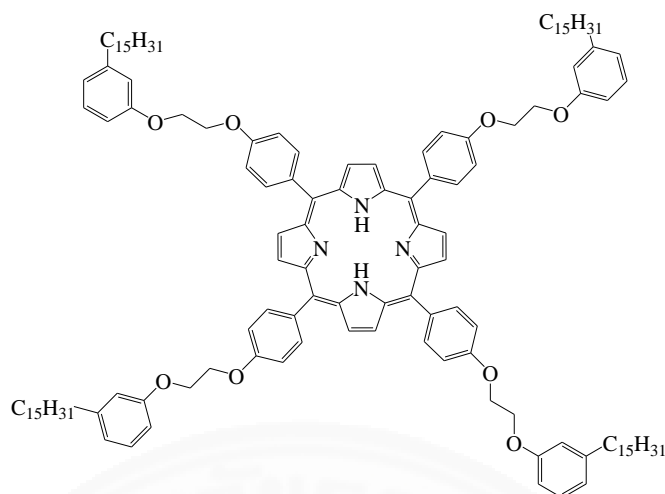


Figure 36. The structure of 5,10,15,20-tetrakis-{4-[2-(3-pentadecyl) phenoxy]-ethoxy} phenylporphyrin.

In 2016, Xu J. *et al.* reported a new type of lower symmetric prophyrinatozinc-based ionic liquids modified by quaternary ammonium halogenides at various positions. Their complexes were characterized by NMR, MS and elemental analysis. They were applied as bifunctional homo-sensor catalyst to the formation of cyclic carbonates from epoxides and CO₂. The result shows **105a** catalyst can convert to the corresponding cyclic carbonate with moderate to excellent yield and selectivity in the presence of the best catalyst. Moreover, phenoxypropylene carbonate can be obtained under atmosphere pressure of CO₂ and in large-scale. [86]

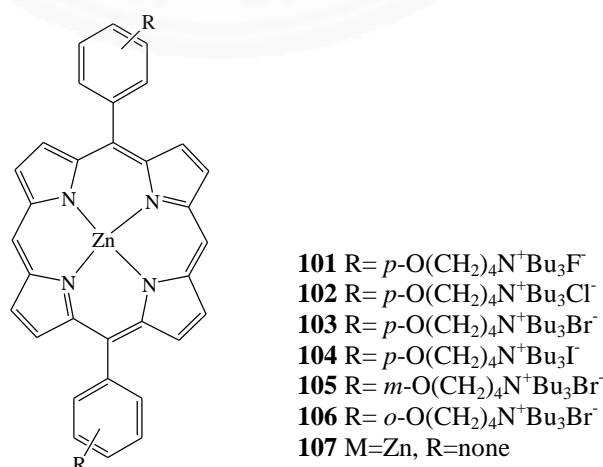


Figure 37. Structures of porphyrin catalysts **101-107a**.

2.4 Porphyrins in sensing applications

In the later years, porphyrins and metalloporphyrins have gained increasing interest in the vapor sensing field because of the richness of their properties. The electrical and optical properties of porphyrins and metalloporphyrins are strongly influenced by electron donor and acceptor with the gas molecule. Therefore, porphyrins and metalloporphyrins materials are favorable choices for gas sensors.

In 2004, Spadavecchia J. *et al.* reported the photochemical sensing properties for the detection of methanol, ethanol and isopropanol vapors by using Cu(II)tetrakis(p-tert-butylphenyl)porphyrin (CuP) – dropped Zn(II)tetra-4-(2,4-di-tert-amylphenoxy)-phthalocyanine (ZnPc) film. Figure 38 show macromolecule structures of the ZnPc and CuP used as sensing layers. All the sensing layers were prepared by spin-coating on cleaned quartz substrates. In particular, a mixed layer (ZnPc-CuP) thin film was obtained by spinning at 200 rpm for 30 s 2 mL of a chloroform solution including 12 mg of ZnPc and 1 mg of CuP. In the experiment, they use a specific optical technique from UV-Vis spectral range obtained by the exposure of the single ZnPc and CuP sensing layers to the considered vapors compared with mixing the two metal complexes sensing layer for analysis. The performance at ZnPc/CuP sensor evaluated in term of response and selectivity is different from single ZnPc and CuP films. [87]

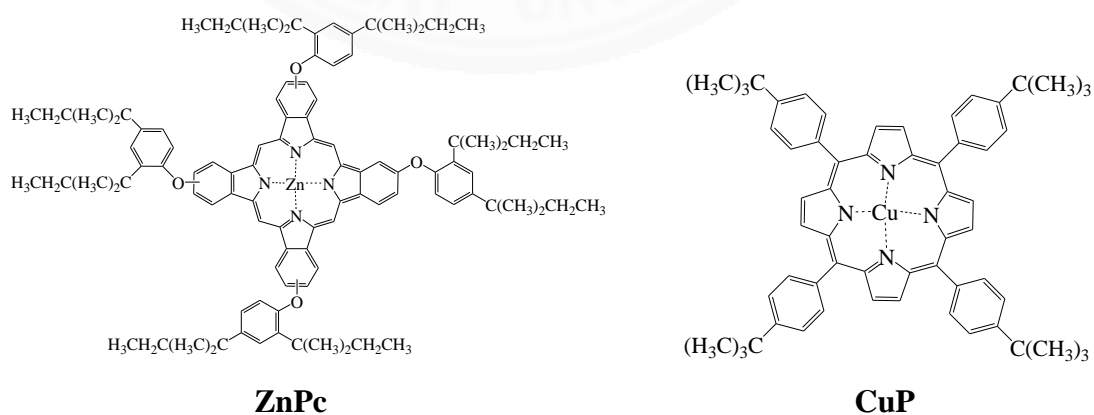


Figure 38. Macromolecule structures of the ZnPc and CuP used as sensing layers.

In 2006, Larisa L. *et al.* studied to develop an analytical instrument for detection of alcohols in beverages, which may permit rapid, online control of ethanol content in beverages of various sources in a wide range of concentrations. The evaluation of potentiometric response of PVC-based solid membranes contact sensors dropped with several porphyrins (5, 10, 15, 20-tetrakis-phenyl porphyrin, H₂TPP), Co- and Pt- porphyrin complexes) towards various alcohols (methanol, ethanol, and isobutanol) and their application in Electronic tongue system for the classification and evaluation of alcoholic degree of beverages has been performed. Discrimination and classification of qualitative sample applied by principal component analysis (PCA) and soft independent model classification analysis (SIMCA) methods. It found that the sensitivity of membranes in single-component alcohol solutions decreased in the following order: ethanol > methanol > isobutanol. The alcoholic strength of many commercial sorts of wine, beers, grappa, and whiskey were successfully evaluated. [88]

In next years, Tonezzer M. *et al.* (2007) studied thin solid films of three tetraphenyl porphyrins (H₂TPP, Fe(TTP)Cl and CoTPP) have been deposited by means of vacuum evaporation technique. These samples were characterized by means of Fourier Transform (FT-IR) and UV-Vis absorption spectra. The behavior of porphyrin films exposed to methyl, ethyl and isopropyl alcohol vapors have been investigated and compared to the behavior of the porphyrin films deposited through spin coating technique. It found that the vacuum evaporated samples show more pronounced and faster responses and higher sensitivity than spin-coated films for gas sensing application. [89]

Sureeporn U. *et al.* (2007) reported the fabrication of organic thin film sensor for detecting specific alcoholic volatile organic compounds (VOCs) by using zinc(II)-2,9,16,23-tetra-tert-butyl-29H,31H-phthalocyanine (ZnTTBPc) and zinc(II)-5,10,15,20-tetraphenyl-prorophyrin (ZnTPP). The ZnTTBPc and ZnTPP thin films were prepared by spin coating technique onto glass substrates. Responses of the thin films to various alcohols and Thai whisky were observed by optical absorption spectroscopy and were analyzed by principal component analysis (PCA) for classification of alcohol volatile organic compounds (VOCs). The result found that

both thin film sensors were able to distinguish ethanol, methanol and Thai whisky. Furthermore, the interaction of ZnTTBPc and ZnTPP with alcohol molecules (methanol, ethanol and isopropanol) have been investigated by Density Function Theory (DFT) calculations, which indicates a charge transfer mechanism between the oxygen atom in alcohol and the central Zn atom of both ZnTTBPc and ZnTPP in the sensing molecules. [90]

In 2008, Sumana K. *et al.* studied optical gas sensors based on magnesium 5,10,15,20-tetraphenyl porphyrin (MgTPP) thin films for detecting various kinds of gases. MgTPP thin films were prepared by spin coating technique using chloroform as solvent to dissolve samples, and then it was spin-coated onto clean glass substrates. The thin film was placed in furnace under the argon atmosphere to a thermal annealing at 280 °C. These MgTPP optical gas sensors have higher sensitivity with methanol than ethanol based on dynamic flow of alcohol vapors at 25 °C. The model the structure and electronic properties of MgTPP and its interactions with alcohols were calculated by Density Functional Theory (DFT). It showed that the interaction energy between MgTPP with methanol is higher than ethanol at the optimized Mg-O distance. Principal component analysis (PCA) was used to discriminate three types of alcohol, which are MeOH (100%), EtOH (100%) and a mixture of MeOH (50%) and EtOH (50%). The result found that MgTPP thin film can be distinguished all alcohol samples which an efficient optical sensing material. [91]

Furthermore, Sumana K. *et al.* (2012) studied detection of alcohol vapors, i.e. methanol, ethanol and isopropanol based on the optical sensing of MgTPP thin film by using electronic nose for detection. Figure 39 shows MgTPP thin film, as the selected material, was provided to be very effective in the discrimination of these alcohols. In addition, Density Functional theory (DFT) calculations were performed to model the underlying mechanism of this selectivity. [92]

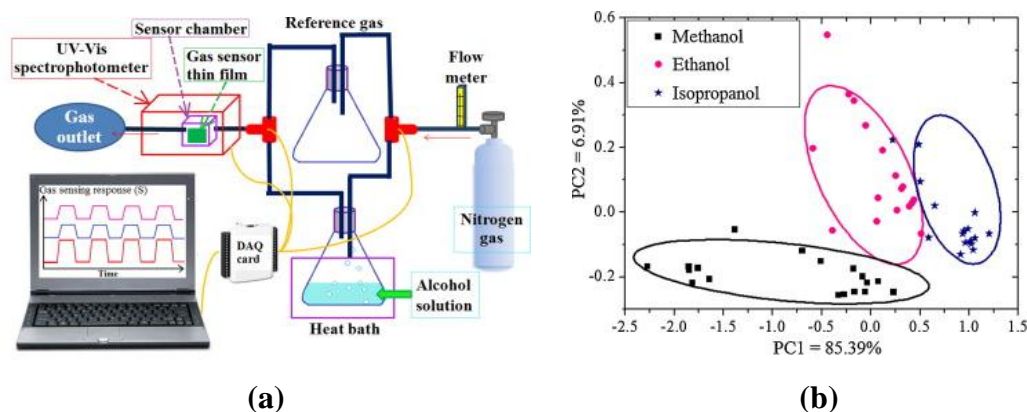


Figure 39. (a) Diagram of the optical electronic nose system in experiment
(b) Principal component analysis plot of the MgTPP thin film to alcohol vapors.

In 2011, Javier R. *et al.* reported the optimization of Langmuir-Blodgett films by using the mixture of 5,10,15,20-tetrakis[3,4-bis(2ethylhexyloxy)phenyl]-21H,23H-porphine (EHO) and p-tert-butylcalix[8]arene (C8A) as shown in Figure 40. This mixed monolayer had been prepared on pure water with a molar ratio of 3:2 (C8A:EHO). The properties of the surface of the mixed films were analyzed through AFM analysis. The result found that, the mixed film's architecture leads to a fast response NO_2 sensor, better than only EHO. [93]

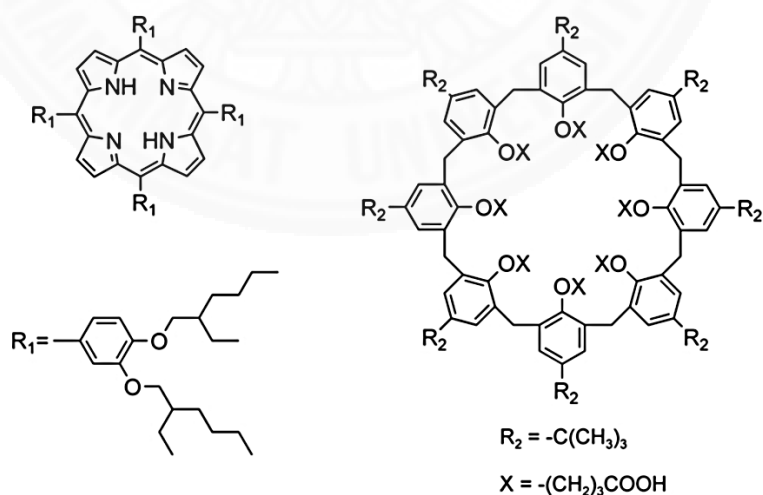


Figure 40. The structure of 5,10,15,20-tetrakis[3,4-bis(2ethylhexyloxy)phenyl]-21H,23H-porphine (EHO, left) and p-tert-butylcalix[8]arene (C8A, right).

In 2012, Mahendra D.S. *et al.* studied fabrication of single-walled carbon nanotubes (SWNTs) – porphyrins hybrid based chemiresistive nanosensor array for monitoring volatile organic carbons (VOCs) in the air. Surface modification of SWNTs used various porphyrins such as octaethylporphyrin (OEP), ruthenium OEP (RuOEP), iron OEP (FeOEP), manganese OEP (MnOEP), tetraphenylporphyrin (TPP), ruthenium TPP (RuTPP) and iron TPP (FeTPP). These SWNTs – porphyrins give good sensitivity to various VOCs under test. Furthermore, PCA was used for analysis of the test data which generated by the hybrid nanosensor array. It found that this discriminating power of the hybrid devices can be developed a highly dense nanosensor array for E-nose application. [94]

In the same years, Yu-Hui L. *et al.* (2012) reported a simple way to prepare a meso-tetra (4-pyridyl) porphyrin (MTPyP) film for ammonia (NH_3) and hydrochloric (HCl) gas sensor. The MTPyP film was prepared on the glass substrate by dip-dry coating method. The ratio of absorption peaks values at 418 nm and 450 nm was used to identify the vapor types and to determine the concentrations. The result shows MTPyP film provides a good potential to identify the HCl and NH_3 gas at room temperature. [95]

Carolyn P. *et al.* (2012) studied a novel optical gas sensor base on 5,10,15,20-terraphenylporphyrin-zinc as gas-reactive dye. The working principle for detection of gases is based on the gasochromic behavior. The ZnTPP was embedded into a polymeric matrix (PVC). The color change of the porphyrin dye can be detected with photodiodes as a variation of the out-coupled light intensity. Figure 41 show mechanism of ZnTPP to NO_2 by two steps. In the first step, NO_2 oxidizes the complex. Another NO_2 molecule can be reacted with oxidized complex, which is covalently bound to one phenyl ring. Next reaction step leads to the visible color change. The sensor exhibits no unwished sensitivities to CO_2 and CO and only low to NH_3 . NO_2 gas was detectable with a resolution of 1 ppm. [96]

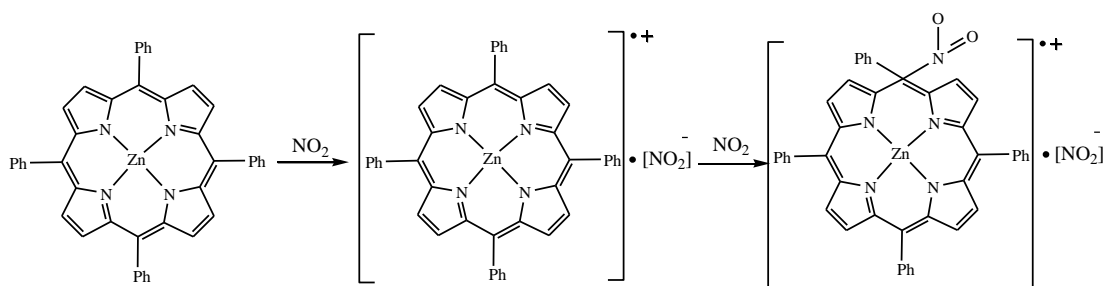


Figure 41. Two-step reaction mechanism of ZnTPP to NO_2 .

In 2013, Paladea A. *et al.* reported the silver colloids of different sizes by reduction of silver nitrate with sodium citrate in bare form and stabilized with polyethyleneglycol was intended in the purpose of developing new hybrid porphyrin-based materials with extended optoelectronic properties. The plasmon was comparatively analyzed by UV-vis and AFM investigations. A new complex based on 5-(4-carboxy-phenyl)-10,15,20-triphenyl-porphyrin and freshly synthesized with silver colloids were obtained and can be further used as a new optical sensor for Ag^0 detection in very small concentrations (2.5×10^{-9} M to 0.82×10^{-7} M), broadening the known detectable concentration range for rare metals and improving their recovery. The investigation of the behaviour of Ag^+ ions towards the same bare porphyrin led to obtaining of Ag(II) 5-(4-carboxy-phenyl)-10,15,20-triphenyl-porphyrin as a result of disproportionation of Ag(I) ion. [97]

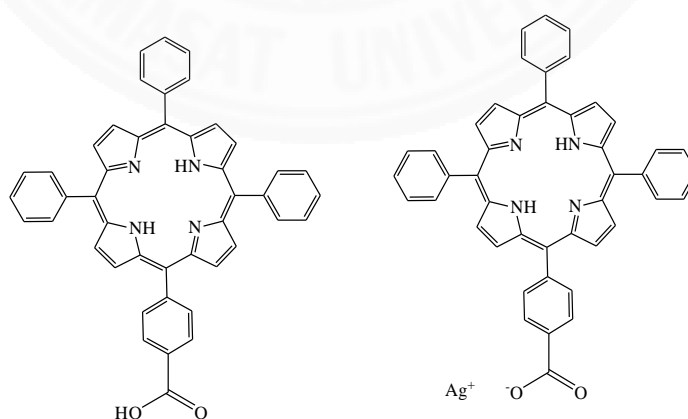


Figure 42. The 5-(4-carboxy-phenyl)-10,15,20-triphenyl-porphyrin (Left) and the silver(I) ion with 5-(4-carboxy-phenyl)-10,15,20-triphenyl-porphyrin at carboxylic group (Right).

In next years, Carlos H.A.E. *et al.* (2014) reported a new kind of composite gas sensors in which the conducting polymer doped with porphyrins including 3,4,5,6-pentafluorophenylporphyrin (H_2TPFP), *meso*-Tetra(phenyl) porphyrin (H_2TPP), and their Zinc, Nickel, Cobalt complexes instead of organic Lewis acid. The sensor was prepared by spin-coating the solution of Poly(2-phenyl-1,4-xylylene) (PPPX) and each porphyrin onto metallic (chrome) interdigitated electrodes. Ethyl acetate, ethanol, propanone, and toluene were used to the test sample. The Figure 43 shows a schematic representation of the e-nose system for used to test these polymers doped with porphyrin sensors. Both of sensors were successfully tested in the identification of four volatile solvents. [98]

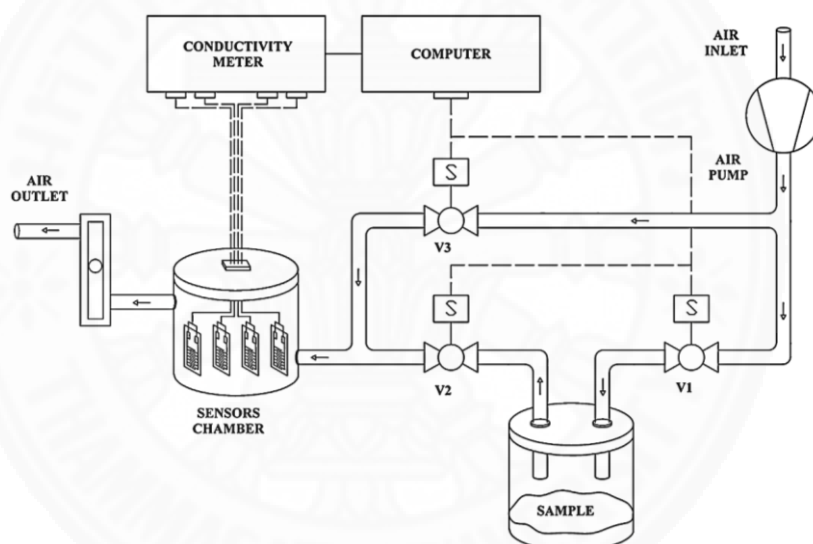


Figure 43. Schematic view of the e-nose measuring system

Swasti S. *et al.* (2014) prepared nano-composites by non-covalent functionalization of multiwall carbon nanotubes (MWNTs) with metal-tetraphenyl porphyrins (M-TPP) where nano-sized clusters of M-TPP molecular aggregates anchor the MWNTs surface. This nano-composite sensor made from cobalt-, and copper-tetraphenyl porphyrins functionalized MWNTs. The prepared nano-composites can be fabricated very fast, portable, low cost, reversible, stable and sensitive sensors for detection of benzene, toluene, and xylene in vapor form at normal temperature. [99]

Alfredo F.G. *et al.* (2014) reported a new sensor incorporating a porphyrin coated phototransistor for detection of volatile organic compounds (VOCs). The 5, 10, 15, 20-tetrakis[3,4-bis(2-ethylhexyloxy)phenyl]-21H, 23H-porphyrinato magnesium(II) used in the experiment for coating on phototransistor. The Mg-porphyrin sensor materials can be interacted with alcohol vapors such as methanol, ethanol, propanol, octanol, and methylbutanol, which it has stable, provide a good repeatability and can work at room temperature. [100]

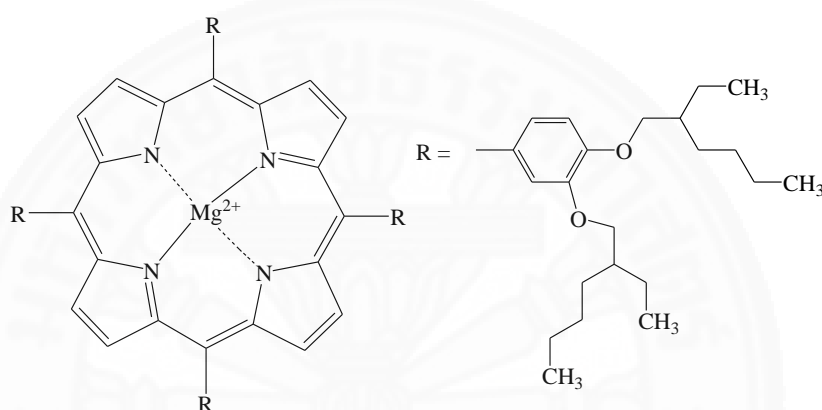


Figure 44. The chemical structure of 5, 10, 15, 20-tetrakis[3,4-bis(2-ethyl hexyloxy)phenyl]-21H, 23H-porphyrinato magnesium(II) (MgEHO).

In 2016, Feifei S. *et al.* reported the NO₂ gas sensor by using the porphyrin nanotubes. The nanoporous anodized aluminum oxide (AAO) membrane was to the template to fabricated the highly ordered nanotube of 5, 10, 15, 20-tetrakis(4-aminophenyl)porphyrin zinc (ZnTAP). The porphyrin nanotubes were characterized by electrical absorption spectra, fluorescence spectra TEM, SEM, and XRD techniques. This nanotube exhibited a good conductivity and can apply as NO₂ gas sensor. The proposed sensor shows fast response and recovery behavior, high sensitivity, and good reproducibility. Moreover, this sensor can achieve a detection limit as low as 1 ppm. [101]

The gradual increase in research of porphyrin sensing in the gas/vapor sensor application is shown in Figure 45. The data was collected from sciencedirect.com in 1990-2016, resulting to 179 papers. In 2006, there was only 2 paper use for alcohol sensing. However, current year shows many application of porphyrin in this field. The list of potential porphyrin sensor includes TPP, M-TPP (M = Co, Pt, Zn, and Mg) and its derivatives. The current study focuses on in preparing Ag-TPP and its derivatives to use as alcohol sensor.

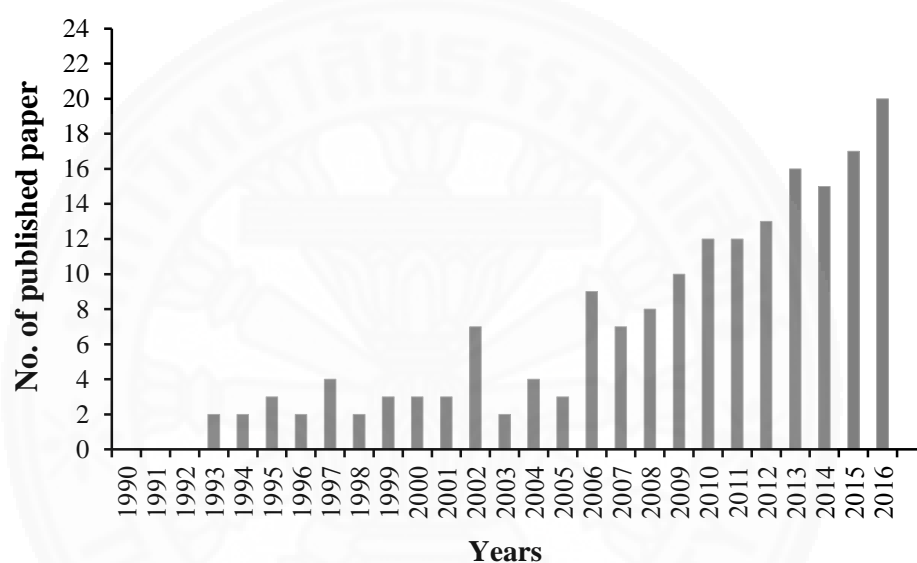


Figure 45. Trends of published paper for porphyrin-based sensor application in year 1990 to 2016. [102]

CHAPTER 3

RESEARCH METHODOLOGY

3.1 Materials

3.1.1 Reagents

- *l*-Bromobutane (C_4H_9Br , Assay 99%, Sigma-aldrich, USA)
- *l*-Bromooctane ($C_8H_{17}Br$, Assay 99%, Sigma-aldrich, USA)
- *l*-Bromodecane ($C_{10}H_{21}Br$, Assay 98%, Sigma-aldrich, USA)
- *l*-Bromo-4-nitrobenzene ($BrC_6H_4NO_2$, Assay 99%, Sigma-aldrich, USA)
- 4-Hydroxybenzaldehyde ($C_7H_6O_2$, Assay 99%, Sigma-aldrich, USA)
- Potassium carbonate anhydrous (K_2CO_3 , Assay 99%, Unilab, Australia)
- *N,N*-Dimethylformamide (C_3H_7NO , Analytical grade, MAY&BAKER, England)
- Pyrrole (C_4H_5N , A.R. grade, Sigma-aldrich, USA)
- *p*-Anisaldehyde ($C_8H_8O_2$, Assay 99%, Sigma-aldrich, USA)
- Propionic acid ($C_3H_6O_2$, Assay 95%, Poison, Australia)
- Silver nitrate ($AgNO_3$, RCI Labscan, Thailand)
- Methyl methacrylate ($C_5H_8O_2$, Assay 99% stabilized, Acros organics)
- Benzoyl peroxide (BPO) ($C_{14}H_{10}O_4$, Assay 70%, Sigma-aldrich, USA)
- Ethanol (C_2H_5OH , Assay 98%, RCI Labscan, Thailand)
- Methanol (CH_3OH , Assay 98%, RCI Labscan, Thailand)
- Methanol (CH_3OH , HPLC grade, Merck, Germany)
- Dichloromethane (CH_2Cl_2 , Assay 98%, RCI Labscan, Thailand)
- Dichloromethane (CH_2Cl_2 , HPLC grade, Merck, Germany)

- Acetone ($\text{C}_3\text{H}_6\text{O}$, Assay 98%, RCI Labscan, Thailand)
- Acetic anhydride ($(\text{CH}_3\text{CO})_2\text{O}$, Assay 98%, AnalaR, USA)
- Ethyl acetate ($\text{C}_4\text{H}_8\text{O}_2$, Assay 98%, RCI Labscan, Thailand)
- Toluene (C_7H_8 , Assay 98%, RCI Labscan, Thailand)
- Hexane (C_6H_{14} , Assay 98%, RCI Labscan, Thailand)
- Chloroform (CHCl_3 , Assay 98%, RCI Labscan, Thailand)
- Chloroform-*d* (CDCl_3 -*d*, A.R. grade, Cambridge Isotope, USA)
- DMSO ($(\text{CH}_3)_2\text{SO}$)
- Magnesium sulphate anhydrous (MgSO_4 , QP Panreac Quimica Sa, Barcelona)
- Thin layer chromatography (Macherey-nagel, Germany)

3.1.2 Apparatus

Elemental analysis (C, H, and N) was performed by a Vario EL-III CHNOS instrument. The FT-IR spectra were registered in KBr pellet using Perkin Elmer infrared spectrophotometer (Spectrum GX) in the range $4000\text{--}400\text{ cm}^{-1}$. ^1H -NMR (400 MHz) and ^{13}C -NMR (100 MHz) spectra were recorded using a Bruker (FT-NMR advance 400 MHz) spectrometer and chemical shifts were expressed in ppm. Mass spectra were recorded on Thermo Finnigan mass spectrometer (LCQ Advantage). All absorption and fluorescence measurements are performed with Shimadzu UV-spectrometer (UV-1700) and a Jasco spectrofluorometer (FP-6200), respectively.

3.1.2.1 NMR spectroscopy

The samples for NMR analysis were prepared in 0.0020 g NMR tubes and were dissolved in 1.0 mL of chloroform-*d*. The sample depth was at least 4.5 cm in the tube.

3.1.2.2 FT-IR spectroscopy

The samples for infrared spectroscopy analysis were mixed with solid KBr (transparent in the $4000\text{--}400\text{ cm}^{-1}$ region).

3.1.2.3 Mass spectrometry

The solutions of samples for measurement were prepared by dissolving 0.0100 g in 5.0 mL dichloromethane (HPLC grade).

3.1.2.4 The elemental analysis

The sample for analysis is weighed in a tin capsule. The required amount is 0.0015-0.0025 g of samples. After folding the capsule (looking rather like wrapped tin foil) the sample is loaded into the instrument.

3.1.2.5 Absorption and fluorescence emission spectroscopy

For the preparation of 0.002 mM solution, 0.010 g of samples were dissolved and made up to 10.0 mL volumetric flask by dichloromethane. Properties of porphyrin and metalloporphyrins were characterized by UV-Vis spectroscopy in the wavelength range of 300 to 700 nm.

3.2 Methods

The preparation, purification, and reaction of the long chain aldehyde, porphyrin, and their Ag-porphyrin were carried out under an ambient atmosphere. The reaction mixtures were magnetically stirred and the process of the reaction monitored by thin layer chromatography where appropriate. Column chromatography was performed by using Aldrich silica with an optimal solvent system. Each complex was purified using a mixture of two solvents eluent in chromatography. The impure solid was dissolved in the more polar solvent; such as CH_2Cl_2 prior applied in hexane silica column and the polarity was gradually increased. All complexes are stable at ambient condition.

The alkyloxybenzaldehyde reactant was prepared by the modification of published method [50]. While, the synthetic method of porphyrins and their derivatives was the well-known Adler-Longo method [26].

The synthesis of aldehyde, porphyrins and their metal derivatives were separately explained in 3 parts.

Part 1: Synthesis of alkyloxybenzaldehydes

3.2.1 Synthesis of Butyloxybenzaldehyde 1, octyloxybenzaldehyde 2 and decyloxybenzaldehyde 3

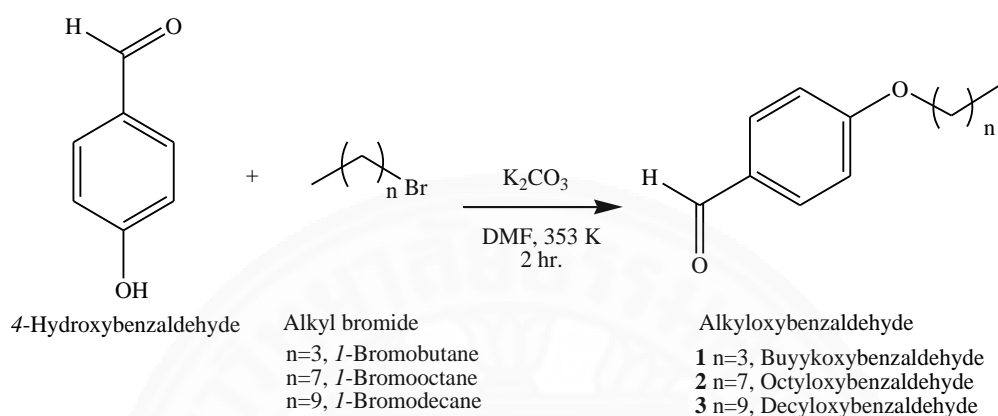


Figure 46. Synthesis of aldehydes.

The aldehyde synthetic method used in the study was modified by Ioannis D.K *et al.* [50]. To a stirred solution of 4-hydroxybenzaldehyde (2.00 g, 17.5 mmol) in DMF was added K_2CO_3 (2.7 g, 18 mmol) and followed by 1-Bromobutane (~18 mmol). After heating the mixture under reflux at 353 K for 2 hours, the DMF solution was evaporated to dryness in vacuum. The reaction mixture was quenched with distilled water and extracted with CH_2Cl_2 . The bright yellow in organic layer was further cleaned with water before dried with magnesium sulfate anhydrous (MgSO_4). The product was afforded Butyloxybenzaldehyde **1** as a yellow oil. The Octyloxybenzaldehyde **2** and decyloxybenzaldehyde **3** were prepared similarly by replacing 1-bromobutane with 1-bromooctane and 1-bromodecane, respectively. The observed structure of aldehyde **1**, **2** and **3** were shown in Figure 47. The products were used without further purification.

Butyloxybenzaldehyde **1** was obtained in 58 % yield (1.81 g). $^1\text{H-NMR}$ (400 MHz, CDCl_3): δ 9.87 (1H, CHO), 7.82 (2H, $J = 8.65$ Hz, Phenyl, *o*-H), 6.99 (2H, $J = 8.78$ Hz, Phenyl, *m*-H), 4.05 (2H, $-\text{OCH}_2$), 1.79 (2H, $J = 8.49$ Hz, $-\text{OCH}_2\text{CH}_2$), 1.51 (2H, $J = 6.71$ Hz, $-\text{CH}_2\text{CH}_3$), 0.99 (3H, $J = 7.39$ Hz, $-\text{CH}_3$). $^{13}\text{C-NMR}$ (100 MHz, CDCl_3): δ 190.55, 166.28, 131.86, 129.85, 114.97, 68.11, 31.06, 19.10, 13.64 ppm.

IR (NaCl): 3074, 2957, 2873, 2736, 1689, 1599, 1509, 1467, 1393, 1159, 1024, 883 cm^{-1} . Mass m/z (ESI) calcd for $\text{C}_{11}\text{H}_{14}\text{O}_2$: 178.23. Found 178.90 $[\text{M}+\text{H}]^+$.

Octyloxybenzaldehyde **2** was obtained as yellow oil (2.87 g, 70 % yield). ^1H -NMR (400 MHz, CDCl_3): δ 9.87 (1H, CHO), 7.82 (2H, $J = 8.81$ Hz, Phenyl, *o*-H), 6.98 (2H, $J = 8.43$ Hz, Phenyl, *m*-H), 4.03 (2H, $J = 6.59$ Hz, $-\text{OCH}_2$), 1.81 (2H, $-\text{OCH}_2\text{CH}_2$), 1.46 (2H, $J = 7.54$ Hz, $-\text{CH}_2\text{CH}_3$), 1.31 (8H, $-\text{CH}_2\text{CH}_2\text{CH}_2$), 0.89 (3H, $J = 6.54$ Hz, $-\text{CH}_3$). ^{13}C -NMR (100 MHz, CDCl_3): δ 190.34, 164.24, 131.77, 129.88, 114.75, 68.41, 31.69, 29.19, 29.08, 29.01, 25.88, 22.51, 13.84 ppm. IR (NaCl): 3073, 2928, 2856, 2734, 1691, 1599, 1509, 1468, 1393, 1159, 1019, 883 cm^{-1} . Mass m/z (ESI) calcd for $\text{C}_{15}\text{H}_{22}\text{O}_2$: 235.33. Found 235.30 $[\text{M}+\text{H}]^+$.

Decyloxybenzaldehyde **3** was obtained as yellow oil (3.35 g, 73 % yield). ^1H -NMR (400 MHz, CDCl_3): δ 9.87 (1H, CHO), 7.82 (2H, $J = 8.82$ Hz, Phenyl, *o*-H), 6.99 (2H, $J = 8.67$ Hz, Phenyl, *m*-H), 4.04 (2H, $J = 6.58$ Hz, $-\text{OCH}_2$), 1.81 (2H, $-\text{OCH}_2\text{CH}_2$), 1.44 (2H, $-\text{CH}_2\text{CH}_3$), 1.28 (12H, $-\text{CH}_2\text{CH}_2\text{CH}_2$), 0.88 (3H, $J = 6.68$ Hz, $-\text{CH}_3$). ^{13}C -NMR (100 MHz, CDCl_3): δ 190.15, 164.30, 131.69, 129.82, 114.76, 68.41, 32.81, 31.73, 29.44, 29.37, 29.18, 29.01, 25.85, 22.45, 13.76 ppm. IR (NaCl): 3073, 2924, 2854, 2732, 1693, 1602, 1509, 1467, 1391, 1159, 1015, 883 cm^{-1} . Mass m/z (ESI) calcd for $\text{C}_{17}\text{H}_{26}\text{O}_2$: 262.39. Found 261.20 $[\text{M}+\text{H}]^+$.

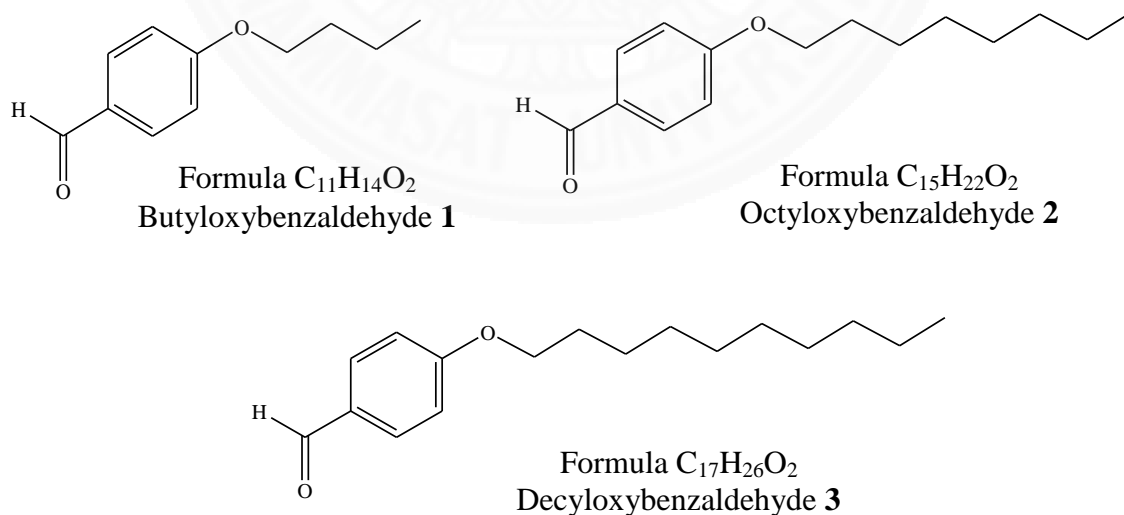


Figure 47. The structure of various alkyloxybenzaldehyde (**1-3**).

Part 2: Synthesis of porphyrin and its derivatives

3.2.2 Synthesis of Tetrakis(4-phenyl)porphyrin (TPP 4), Tetrakis(4-methoxyphenyl)porphyrin (TOMPP 5), Tetrakis (4-butyloxyphenyl)porphyrin (TOBPP 6), tetrakis(4-octyloxyphenyl) porphyrin (TOOPP 7) and tetrakis(4-decyloxyphenyl)porphyrin (TODPP 8)

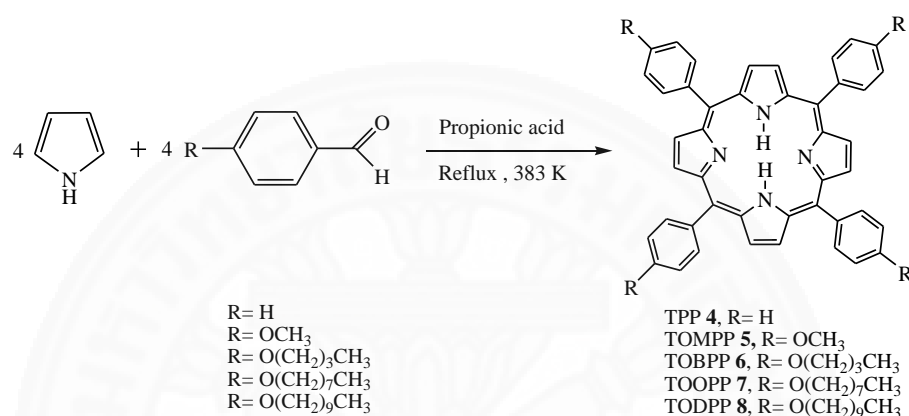


Figure 48. Synthesis of free base porphyrins.

The synthetic method was the known as Adler-Longo method [26]. Pyrrole 0.028 mole (2 mL) and benzaldehyde 0.03 mole (3.18 g) were refluxed in 40 mL propionic acid at 383 K for 2 hours. After the completed reaction, the mixture was cooled to room temperature and then added 40 mL of ethanol, before kept in the refrigerator overnight. The purple crystals were formed and vacuum- filtered, then washed with cold ethanol to remove traces of propionic acid. The crude product was purified on a silica-gel column chromatography, eluted with the mixture of dichloromethane and hexane to afford TPP 4.

Tetrakis (4-methoxyphenyl) porphyrin (TOMPP 5), The tetrakis(4-butyloxyphenyl) porphyrin (TOBPP 6), tetrakis(4-octyloxyphenyl)porphyrin (TOOPP 7) and tetrakis(4-decyloxyphenyl)porphyrin (TODPP 8) were prepared similarly to TPP 4, *p*-anisaldehyde (1.5 mL, 12.4 mmol), which various alkyloxybenzaldehyde 1-3 (~14 mmol) were used instead and benzaldehyde to obtain the product 5-8, respectively.

Tetrakis(4-phenyl)porphyrin (TPP **4**), a purple crystals (0.53 g, 24 %). ¹H-NMR (400 MHz, CDCl₃): δ 8.8 (8H, Pyrrole, β-H), 8.2 (8H, Phenyl, *o*-H), 7.7 (8H, Phenyl, *m*-H). ¹³C-NMR (100 MHz, CDCl₃): δ 127.70, 134.56, 131.12, 122.22, 120.15, 116.67 ppm. IR (KBr): 3310, 1597, 1469, 1212, 966, 794 cm⁻¹. Elemental analysis; calcd (%) for C₄₄H₃₀N₄ (614.70): C 85.97, H 4.92, N 9.11; found: C 86.0, H 4.9, N 9.1. Mass *m/z* (ESI): found 615 [M+H]⁺. UV-Vis (CH₂Cl₂): (λ_{abs}(nm), ε (10³M⁻¹cm⁻¹)): S-band; (417, 327.5), Q-band; (514, 14.1), (548, 6.1), (590, 4.6), (649, 3.9)

Tetrakis (4-methoxyphenyl) porphyrin (TOMPP **5**), a purple crystals (0.80 g, 26 %). ¹H-NMR (400 MHz, CDCl₃): δ 8.86 (8H, Pyrrole, β-H), 8.12 (8H, *J* = 8.06 Hz, Phenyl, *o*-H), 7.29 (8H, *J* = 8.10 Hz, Phenyl, *m*-H), 4.10 (12H, -OCH₃). ¹³C-NMR (100 MHz, CDCl₃): δ 158.75, 134.68, 133.99, 129.97, 127.89, 118.83, 111.44, 54.65 ppm. IR (KBr): 3317, 2928, 2832, 1606, 1509, 1247, 1175, 965, 802 cm⁻¹. Elemental analysis; calcd (%) for C₄₈H₃₈N₄O₄ (734.84): C 78.45, H 5.21, N 7.62; found: C 76.42, H 5.75, N 7.42. Mass *m/z* (ESI): found 735.4 [M+H]⁺. UV-Vis (CH₂Cl₂): (λ_{abs}(nm), ε (10³M⁻¹cm⁻¹)): S-band; (421, 115.4), Q-band; (517, 24.0), (556, 16.6), (594, 7.6), (651, 10.2)

Tetrakis (4-butyloxyphenyl)porphyrin (TOBPP **6**) was obtained as a purple crystals (0.11 g, 5% yield). ¹H-NMR (400 MHz, CDCl₃): δ 8.86 (8H, Pyrrole, β-H), 8.10 (8H, Phenyl, *o*-H), 7.29 (8H, Phenyl, *m*-H), 4.24 (-OCH₂), 1.98 (-OCH₂CH₂), 1.29 (-CH₂CH₃), 0.92 (-CH₃). ¹³C-NMR (100 MHz, CDCl₃): δ 159.12, 135.50, 134.64, 130.89, 128.75, 119.77, 112.87, 68.17, 31.60, 23.98, 13.78 ppm. IR (KBr): 3318, 2929, 2868, 1605, 1507, 1244, 1173, 965, 800 cm⁻¹. Elemental analysis; calcd (%) for C₆₀H₆₂N₄O₄ (903.16): C 79.79, H 6.92, N 6.20; found C 79.44, H 6.55, N 5.83. Mass *m/z* (ESI): found 903.6 [M+H]⁺. UV-Vis (CH₂Cl₂): (λ_{abs}(nm), ε (10³M⁻¹cm⁻¹)): S-band; (422, 115.4), Q-band; (517, 24.0), (556, 16.6), (594, 7.6), (651, 10.2).

Tetrakis(4-octyloxyphenyl)porphyrin (TOOPP **7**) was obtained as a purple crystals (0.50 g, 13 % yield). ¹H-NMR (400 MHz, CDCl₃): δ 8.86 (8H, Pyrrole, β-H), 8.10 (8H, Phenyl, *o*-H), 7.26 (8H, Phenyl, *m*-H), 4.24 (-OCH₂), 1.99 (-OCH₂CH₂), 1.36 (-CH₂CH₃), 1.26 (-CH₂CH₂), 0.91 (-CH₃). ¹³C-NMR (100 MHz, CDCl₃): δ 159.16, 135.48, 134.69, 130.80, 128.74, 119.76, 112.93, 68.56, 31.79, 29.57, 29.39,

29.19, 26.19, 22.55, 13.84 ppm. FT-IR (KBr): 3316, 2926, 2850, 1606, 1508, 1242, 1174, 965, 803 cm^{-1} . Elemental analysis; calcd (%) for $\text{C}_{76}\text{H}_{94}\text{N}_4\text{O}_4$ (1127.58): C 80.95, H 8.40, N 4.97; found C 81.10, H 8.25, N 4.93. Mass m/z (ESI): found 1127.9 $[\text{M}+\text{H}]^+$. UV-Vis (CH_2Cl_2): ($\lambda_{\text{abs}}(\text{nm})$, ϵ ($10^3\text{M}^{-1}\text{cm}^{-1}$)): S-band; (422, 120.4), Q-band; (519, 20.0), (556, 14.9), (595, 6.7), (651, 10.1).

Tetrakis(4-decyloxyphenyl)porphyrin (TODPP **8**) was obtained as a purple crystals (0.44 g, 11 % yield). ^1H -NMR (400 MHz, CDCl_3): δ 8.86 (8H, Pyrrole, β -H), 8.10 (8H, Phenyl, *o*-H), 7.26 (8H, Phenyl, *m*-H), 4.24 ($-\text{OCH}_2$), 1.98 ($-\text{OCH}_2\text{CH}_2$), 1.33 ($-\text{CH}_2\text{CH}_3$), 1.26 ($-\text{CH}_2\text{CH}_2$), 0.88 ($-\text{CH}_3$). ^{13}C -NMR (100 MHz, CDCl_3): δ 159.10, 135.51, 134.51, 130.68, 128.76, 119.77, 112.86, 68.48, 31.88, 29.60, 29.55, 29.53, 29.46, 29.28, 26.20, 22.60, 13.93 ppm. IR (KBr): 3310, 2923, 2852, 1606, 1509, 1243, 1175, 967, 804 cm^{-1} . Elemental analysis; calcd (%) for $\text{C}_{84}\text{H}_{110}\text{N}_4\text{O}_4$ (1239.78): C 81.37, H 8.94, N 4.52; found C 81.24, H 8.99, N 4.58. Mass m/z (ESI): found 1240.0 $[\text{M}+\text{H}]^+$. UV-Vis (CH_2Cl_2): ($\lambda_{\text{abs}}(\text{nm})$, ϵ ($10^3\text{M}^{-1}\text{cm}^{-1}$)): S-band; (422, 122.5), Q-band; (519, 16.7), (556, 12.5), (595, 5.5), (652, 9.2).

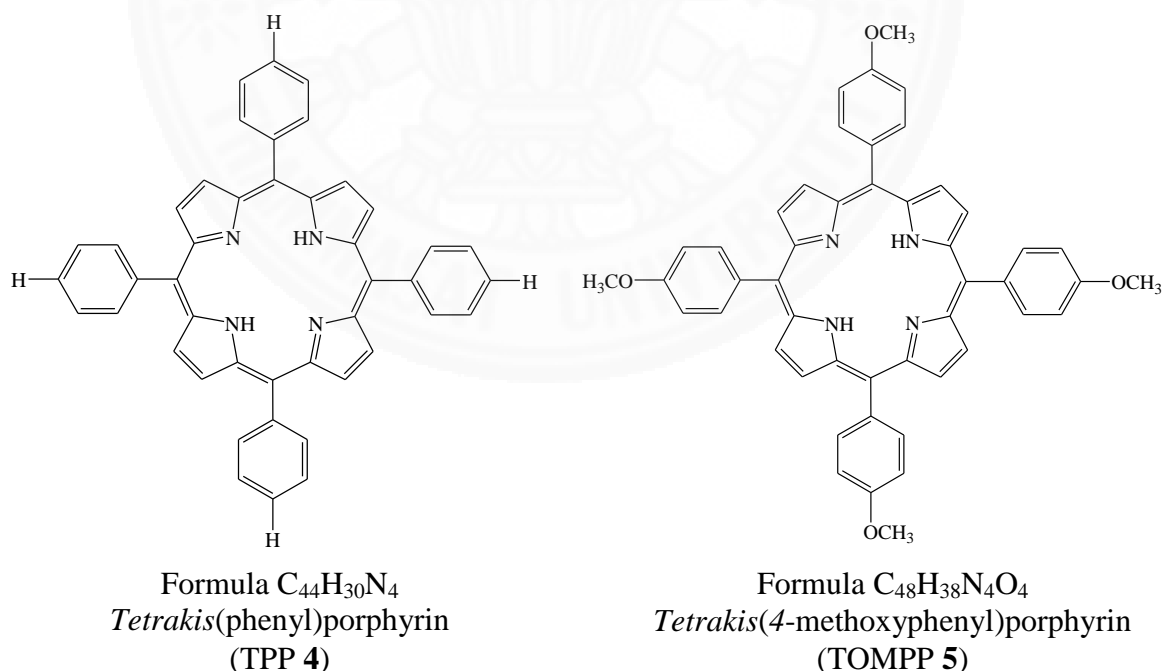


Figure 49. The expected structure of TPP **4**, TOMPP **5**.

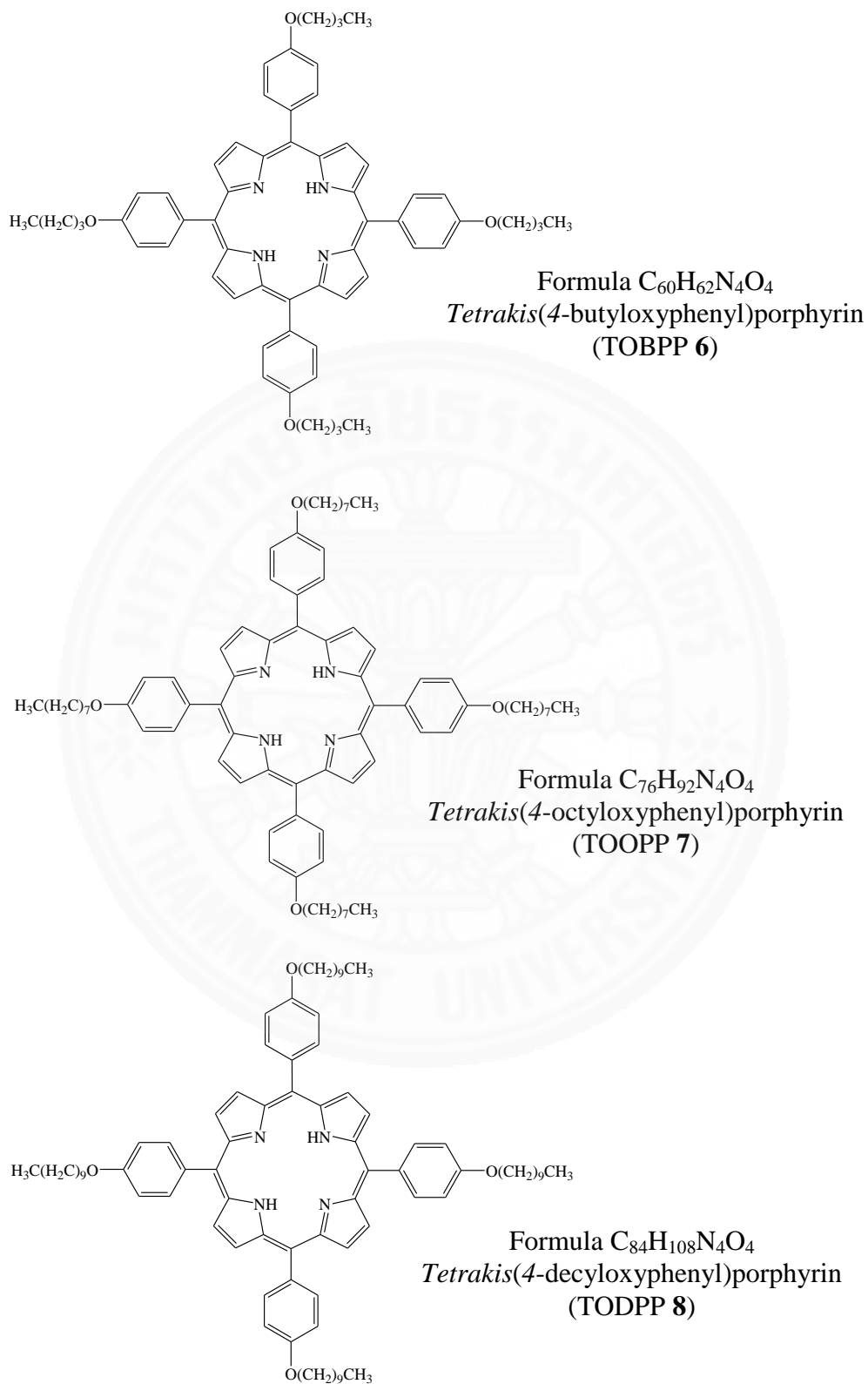


Figure 50. The expected structure of TOBPP **6**, TOOPP **7** and TODPP **8**.

Part 3: Synthesis of metalloporphyrins

3.2.3 Synthesis of silver-phenyl porphyrin (Ag-TPP), silver-methoxyphenyl porphyrin (Ag-TOMPP 9), silver-butyloxyphenyl porphyrin (Ag-TOBPP 10), silver-octyloxyphenyl porphyrin (Ag-TOOPP 11) and silver-decyloxyphenyl porphyrin (Ag-TODPP 12)

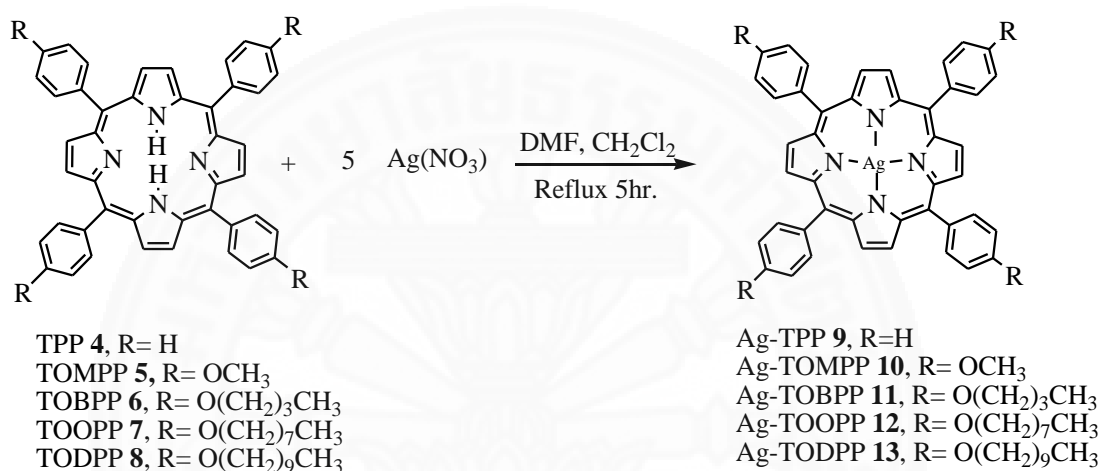


Figure 51. Synthesis of silver(II) porphyrins.

The synthesis of silver(II) porphyrins were followed the published procedure [62]. TPP 4 (0.5 mole, 0.3074 g) with an excess silver nitrate (AgNO₃) in the mixed solvent between DMF (15 mL) and dichloromethane (15 mL) at 383 K for 5 hours. After that reaction was completed, the reaction mixture was cooled to room temperature and kept in the refrigerator overnight after adding distilled water. The obtained purple crystal was vacuum-filtrated and washed with cold water. Further purification of the reaction product was carried out over a silica gel column with the mixture of dichloromethane and hexane as eluent to afford Ag-TPP 9. Similarly, the reaction of silver nitrate with TOMPP 5, TOBPP 6, TOOPP 7 and TODPP 8 gave purple macrocrystalline crystals of Ag-TOMPP 10, Ag-TOBPP 11, Ag-TOOPP 12 and Ag-TODPP 13. The ¹H- and ¹³C- NMR analysis of complexes 9-13 are unsuccessful due to the paramagnetic character. The ESR spectroscopy may require for further analysis.

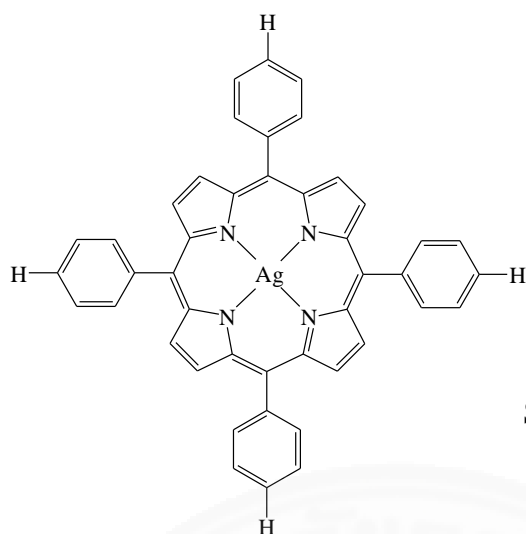
Silver-phenyl porphyrin (Ag-TPP **9**) was obtained yield 0.27 g, 74.94 % yield). IR (KBr): 1598, 1442, 1243, 794 cm^{-1} . Elemental analysis; calcd (%) for $\text{AgC}_{44}\text{H}_{28}\text{N}_4$ (720.59): C 73.34, H 3.92, N 7.77; found C 72.98, H 4.11, N 7.56. Mass m/z (ESI): found 721.3 $[\text{M}+\text{H}]^+$. UV-Vis (CH_2Cl_2): ($\lambda_{\text{abs}}(\text{nm})$, ϵ ($10^3\text{M}^{-1}\text{cm}^{-1}$)): S-band; (425, 542.78), Q-band; (542, 25.77).

Silver-methoxyphenyl porphyrin (Ag-TOMPP **10**) was obtained yield 0.24 g, 57.14 % yield). IR (KBr): 2934, 2833, 1606, 1548, 1250, 1175, 809 cm^{-1} . Elemental analysis; calcd (%) for $\text{AgC}_{48}\text{H}_{36}\text{N}_4\text{O}_4$ (840.69): C 62.47, H 4.53, N 6.13; found C 62.63, H 4.10, N 5.92. Mass m/z (ESI): found 841.6 $[\text{M}+\text{H}]^+$. UV-Vis (CH_2Cl_2): ($\lambda_{\text{abs}}(\text{nm})$, ϵ ($10^3\text{M}^{-1}\text{cm}^{-1}$)): S-band; (427, 442.21), Q-band; (542, 22.95).

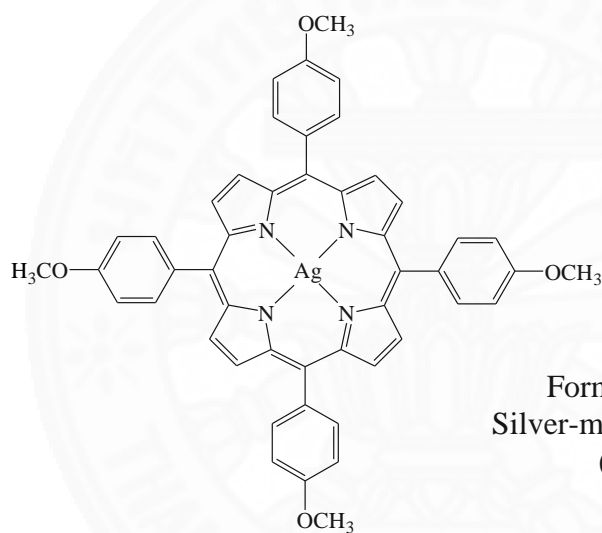
Silver-butyloxyphenyl porphyrin (Ag-TOBPP **11**) was obtained yield 0.09 g, 18 % yield). IR (KBr): 2932, 2834, 1609, 1506, 1248, 1176, 805 cm^{-1} . Elemental analysis; calcd (%) for $\text{AgC}_{60}\text{H}_{60}\text{N}_4\text{O}_4$ (1009.01): C 71.42, H 5.99, N 5.55; found C 74.51, H 6.25, N 5.76. Mass m/z (ESI): found 1010.1 $[\text{M}+\text{H}]^+$. UV-Vis (CH_2Cl_2): ($\lambda_{\text{abs}}(\text{nm})$, ϵ ($10^3\text{M}^{-1}\text{cm}^{-1}$)): S-band; (427, 356.56), Q-band; (543, 25.00).

Silver-octyloxyphenyl porphyrin (Ag-TOOPP **12**) was obtained yield 0.38 g, 63.33 % yield). IR (KBr): 2934, 2843, 1609, 1506, 1247, 1177, 805 cm^{-1} . Elemental analysis; calcd (%) for $\text{AgC}_{76}\text{H}_{92}\text{N}_4\text{O}_4$ (1233.44): C 73.42, H 7.47, N 4.50; found C 73.19, H 7.71, N 4.21. Mass m/z (ESI): found 1233.9 $[\text{M}+\text{H}]^+$. UV-Vis (CH_2Cl_2): ($\lambda_{\text{abs}}(\text{nm})$, ϵ ($10^3\text{M}^{-1}\text{cm}^{-1}$)): S-band; (430, 444.97), Q-band; (544, 22.97).

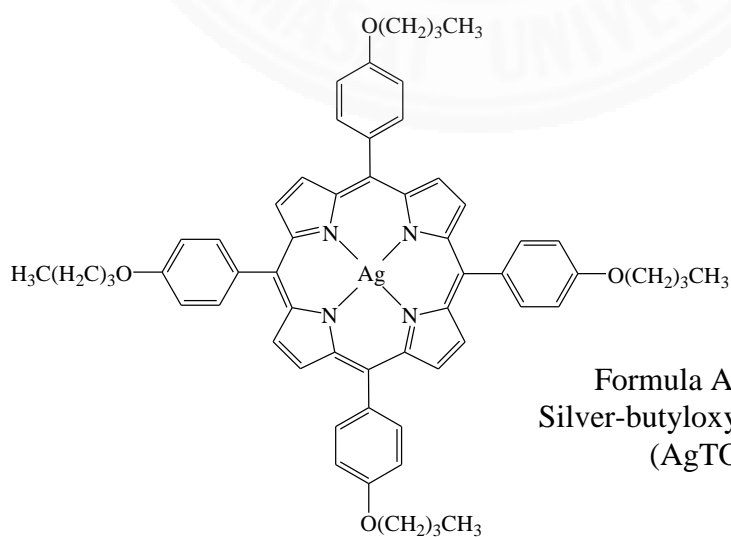
Silver-decyloxyphenyl porphyrin (Ag-TODPP **13**) was obtained yield 0.35 g, 52.24 % yield). IR (KBr): 2928, 2845, 1609, 1507, 1249, 1177, 805 cm^{-1} . Elemental analysis; calcd (%) for $\text{AgC}_{84}\text{H}_{108}\text{N}_4\text{O}_4$ (1345.65): C 69.71, H 7.59, N 3.80; found C 69.66, H 7.70, N 3.88. Mass m/z (ESI): found 1346.0 $[\text{M}+\text{H}]^+$. UV-Vis (CH_2Cl_2): ($\lambda_{\text{abs}}(\text{nm})$, ϵ ($10^3\text{M}^{-1}\text{cm}^{-1}$)): S-band; (430, 590.27), Q-band; (544, 25.96).



Formula $\text{AgC}_{44}\text{H}_{28}\text{N}_4$
Silver-phenyl porphyrin
(AgTPP 9)



Formula $\text{AgC}_{48}\text{H}_{36}\text{N}_4\text{O}_4$
Silver-methoxyphenyl porphyrin
(AgTOMPP 10)



Formula $\text{AgC}_{60}\text{H}_{60}\text{N}_4\text{O}_4$
Silver-butyloxyphenyl porphyrin
(AgTOBPP 11)

Figure 52. The expected structure of AgTPP 9, AgTOMPP 10 and AgTOBPP 11.

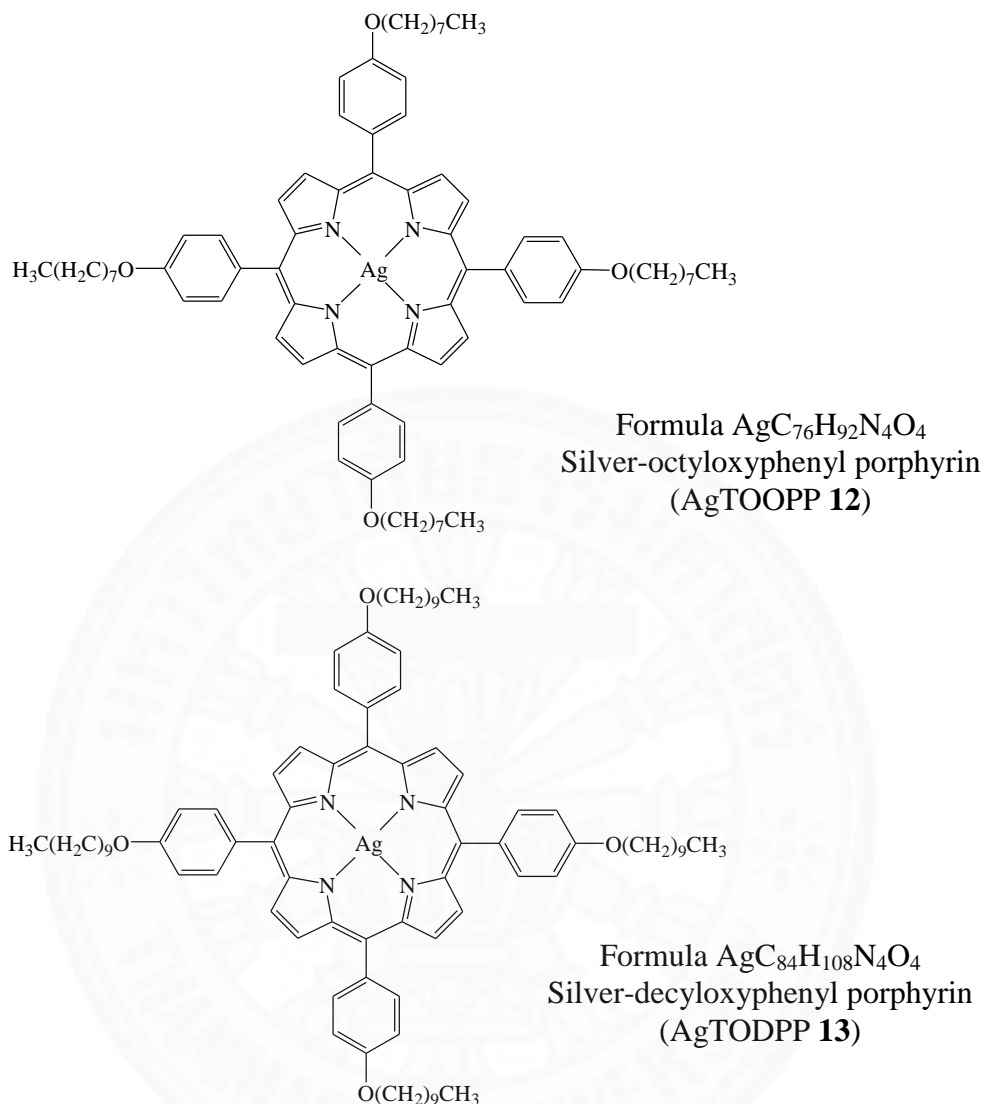


Figure 53. The expected structure of AgTOOPP 12 and AgTODPP 13.

3.3 Biological activity

Staphylococcus aureus (ATCC 25923) and *Escherichia coli* (ATCC 25922) were used to test the antibacterial activity of silver(II) porphyrins **9-13**. The antibacterial assay was evaluated by Agar-disk diffusion method [103]. The test compounds were dissolved in dimethyl sulfoxide (DMSO) to obtain a final concentration of 1 mg mL^{-1} . Sterilized Whatman no.1 filter paper (6 mm) was impregnated with $30 \mu\text{L}$ of compounds to get a concentration of 1000 ppm per disc. DMSO was taken as a control solvent and penicillin (1 mg mL^{-1}) was selected for

positive control, were load 30 μL in sterilized paper disc. The bacterial test pathogens were spread on fresh Agar plates and the filter paper discs impregnated with the test compound were placed on the surface of plates seeded with test bacteria. The compounds were incubated at 37 ± 2 $^{\circ}\text{C}$ for 24 hours. The inhibition zones around each disc were measured in millimeter (mm) units. Furthermore, the minimum inhibitory concentration (MIC) and the minimum bactericidal concentration (MBC) have been investigated. MIC values were determined by microbroth dilution method [104]. Stock solutions of all compounds were prepared by dissolving in DMSO solvent to make a concentration of 1280 ppm. Two-fold dilution of the test solution was made in the concentration range of 640-40 ppm in 96-well microplate. The wells of microplate were inoculated with 50 μL of standardized test organism of the bacterial cell. Negative controls were equally set up by using DMSO solvent and test solution. The microplate was incubated at 37 ± 2 $^{\circ}\text{C}$ for 18 hours. Then, 10 μL of 0.18% resazurin was added in all well and incubated at 37 ± 2 $^{\circ}\text{C}$ for 2 hours. The MIC value was identified visually and considered as the lowest concentration (highest dilution) of test solution without inhibiting bacterial growth (the color in well change to purple). From the well showing no apparent growth in MIC, 0.1 mL of each dilution was inoculated onto sterile nutrient agar using the streak plate method, with incubated 37 ± 2 $^{\circ}\text{C}$ for 18 hours. The MBC was determined as the lowest concentration that presented no bacterial growth.

3.4 Gases sensing application

3.4.1 Preparation of silver(II) porphyrin molecular films

The silver(II) porphyrin films were prepared by using chloroform as a solvent at a concentration of 5 mg mL^{-1} and dropped onto clean glass slide (microscope glass slide with a dimension of 21.2 mm x 25.3 mm x 1.3 mm)

3.4.2 E-nose measurement

For gas sensing application, the Ag-porphyrin films and their absorption were investigated. Figure 54 shows electronic nose (E-nose) instrument used in this work, which was modified a UV-Vis spectrophotometer and a schematic

representation of the electronic nose system of dynamic sampling. These instruments were supported by Faculty of Medical Technology, Mahidol University. Under gas sensing measurement, the silver porphyrins film was placed inside the chamber between light source and detector to allow them have an interact with of alcohol vapors. Methanol (MeOH, 100%), Ethanol (EtOH, 100%) and *iso*-propanol (i-PrOH, 100%) vapors were selected as alcohol samples in this experiment. The group of obtained data can be analyzed in real-time by in-house software based on Principal Component Analysis (PCA).

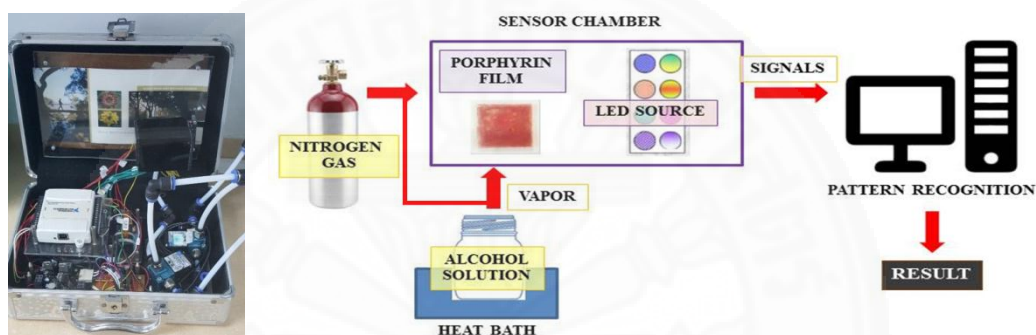


Figure 54. Electronic nose (E-nose) instrument in this experiment and the diagram of the electronic nose system set up.

CHAPTER 4

RESULTS AND DISCUSSION

4.1 Synthesis and characterization of various aldehydes

4.1.1 Aldehyde synthesis

The synthesis of long chain alkane aldehyde, including butyloxybenzaldehyde **1**, octyloxybenzaldehyde **2** and decyloxybenzaldehyde **3** are outlined in Figure 55. The compounds were prepared by refluxing 4-hydroxybenzaldehyde with an equivalent of various alkyl bromide in the presence of K_2CO_3 in DMF at 353 K for 2 hours, leading to yield of aldehyde products in the range of 55-75% as a yellow oil. The characterization data of all aldehydes were shown in Table 3.

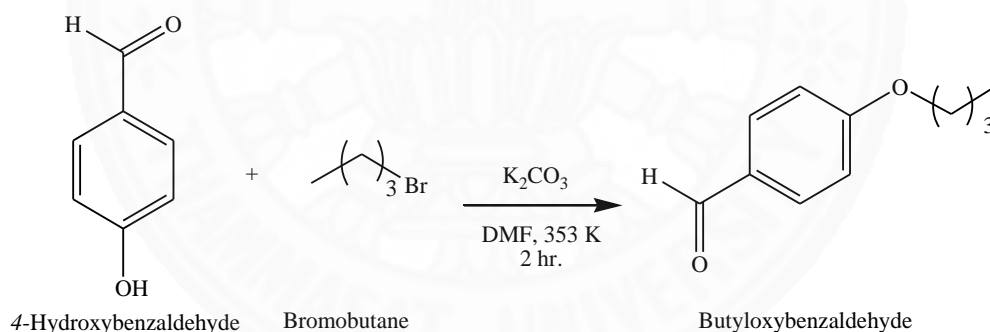


Figure 55. Synthesis of butyloxybenzaldehyde **1**

Table 3 Characteristic data of aldehydes **1-3**.

Compounds	Empirical formula	Yield (%)	Formula weight	MS (m/z) [M+H] ⁺
Butyloxybenzaldehyde 1	C ₁₁ H ₁₄ O ₂	58	178.2	178.9
Octyloxybenzaldehyde 2	C ₁₅ H ₂₂ O ₂	70	234.3	235.3
Decyloxybenzaldehyde 3	C ₁₇ H ₂₆ O ₂	73	262.4	261.2

4.1.2 Aldehyde characteristic

4.1.2.1 Mass spectrometry

The mass spectrometry data of these synthesized benzaldehydes were displayed in Table 3 and the butyloxybenzaldehyde **1** (representative example mass spectrum was shown in Figure 56). The result exhibits the strong molecular ion peak $[M+H]^+$ at m/z 178.9. It was found that the fragment peak at m/z 122.9 represents the loss of alkyl chain group, which was the mass spectrum of reactant compound (4-hydroxybenzaldehyde). Furthermore, the results of octyloxybenzaldehyde **2** and decyloxybenzaldehyde **3** spectra were obtained similarly of butyloxybenzaldehyde **1** due to the methyl and methylene group from the substituted alkyl long chain was the loss. The fragmentation pattern of all benzaldehydes was similar to the previous report by Domingues, M.R.M. [105]. Octyloxybenzaldehyde **2** and decyloxybenzaldehyde **3** showed the molecular ion peak $[M+H]^+$ at m/z 235.3 and 261.2, respectively. The analysis of mass data for these aldehydes gives a good signal peak which is in agreement with the theoretical value.

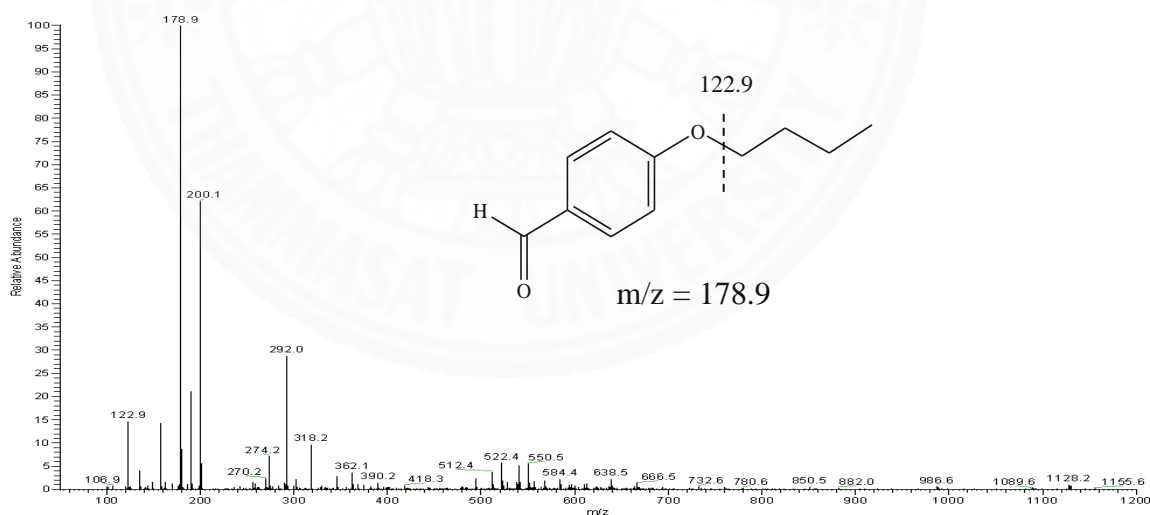


Figure 56. The mass spectrum of butyloxybenzaldehyde **1** in CH_2Cl_2

4.1.2.2 NMR spectroscopy

The ^1H and ^{13}C -NMR signals for aldehydes with alkyl long chain, including compounds **1-3**, were obtained in CDCl_3 at room temperature. The ^1H - and ^{13}C -NMR of butyloxybenzaldehyde **1**, as a representative example, shown in Figure 57 and 58, respectively.

For ^1H -NMR of butyloxybenzaldehyde **1**, the chemical shift was observed arising sharp single peak of CHO at 9.8 ppm due to the magnetic anisotropy the carbonyl group. The *ortho*- and *meta*- protons of phenyl ring were found as two doublets ($J=8.8$ Hz) peaks at 7.8 and 6.9 ppm, respectively. The signals of alkyl long chained protons were shifted significantly to 4.0, 1.7, 1.5 and 0.9 ppm. The triplet peak signal at 4.0 ppm exhibits $-\text{OCH}_2\text{-R}$ of the alkoxy group. The quintet and sextet signal peak at 1.7 ppm and 1.5 ppm, corresponded to protons of methylene groups ($-\text{OCH}_2\text{CH}_2-$). The proton of the methyl group at the end of alkyl long chain ($-\text{CH}_3$) was observed as triplet peaks at 0.9 ppm. The ^1H -NMR spectrum of octyloxybenzaldehyde **2** and decyloxybenzaldehyde **3** showed the signal similar to the butyloxybenzaldehyde **1**, which observed the signal of methylene proton around 1.3-1.1 ppm. However, the alkyl protons in the chain of butyloxybenzaldehyde **1** were found to be greater de-shielded than others due to the inductive effect and the electronegativity of the ether group (electron-donating) in the side chain.

The ^{13}C -NMR spectrum of the butyloxybenzaldehyde **1** was shown as a representative example in Figure 58. The signal peak showed the downfield peak at 190.55 ppm, corresponding to carbonyl carbon (CHO). The disubstituted phenyl ring causes four peaks at 114-77-166.28 ppm, the similar result was reported by Aline T. *et al* [106]. The methyl carbon at the end of the chain (d position) was shown a signal at 13.64 ppm, and the methylene carbon (b and c position) were founded the signal at 31.25 and 19.20 ppm respectively. Finally, the signal at 68.14 ppm showed the signal peak of methylene carbon that near the oxygen atom (a position). Octyloxybenzaldehyde **2** and decyloxybenzaldehyde **3** were founded similarly in butyloxybenzaldehyde **1**, and the result data were shown in Table 4. The results were in agreement with the previous reported by Ioannis D.K. *et al.* [50]. Both ^1H - and ^{13}C -NMR have been successfully confirmed as an expected corresponding aldehydes **1-3**.

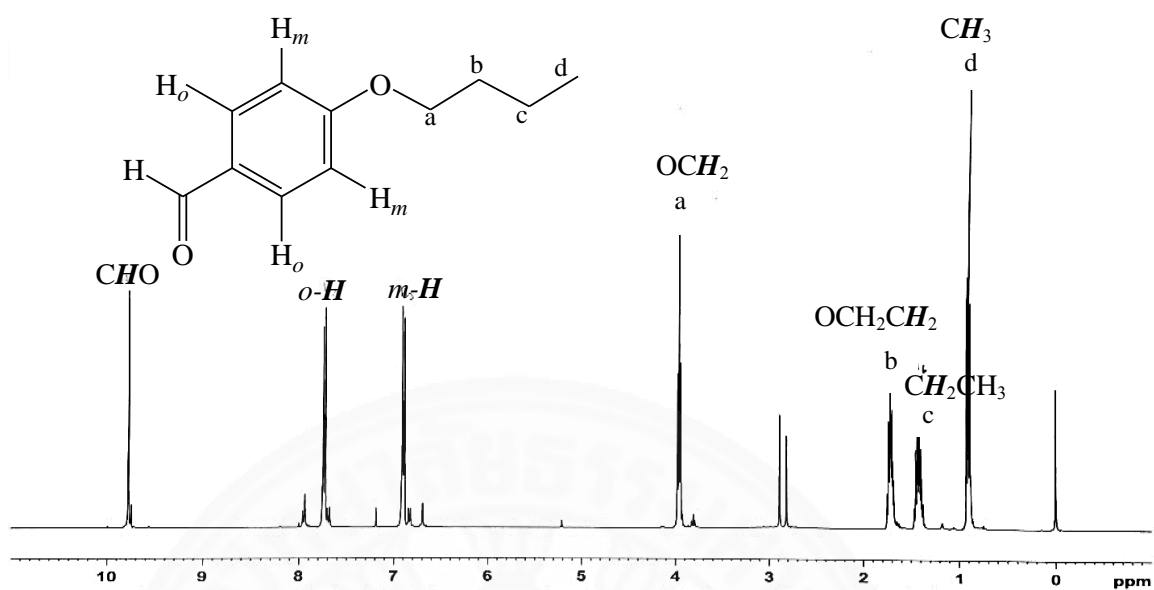


Figure 57. The ^1H NMR spectrum of butyloxybenzaldehyde **1** in chloroform- d .

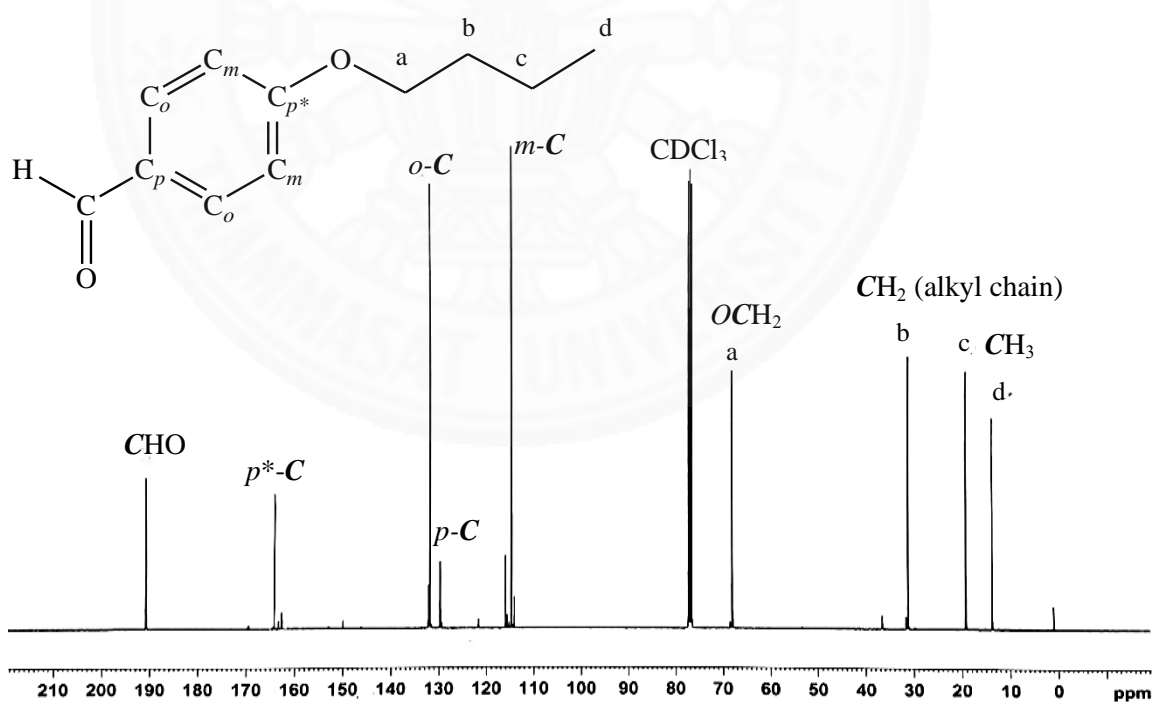


Figure 58. The ^{13}C NMR spectrum of butyloxybenzaldehyde **1** in chloroform- d .

Table 4 ^1H and ^{13}C NMR spectroscopic data for aldehydes **1-3**.

Aldehyde	^1H NMR (ppm), proton							
	<i>CHO</i>	Phenyl, <i>o-H</i>	Phenyl, <i>m-H</i>	<i>OCH</i> ₂	<i>OCH</i> ₂ <i>CH</i> ₂	<i>CH</i> ₂ <i>CH</i> ₃	<i>CH</i> ₂ <i>CH</i> ₂ <i>CH</i> ₂	<i>CH</i> ₃
Butyloxybenzaldehyde 1	9.8 (1H)	7.8 (2H)	6.9 (2H)	4.0 (2H)	1.7 (2H)	1.5 (2H)	-	0.9 (3H)
Octyloxybenzaldehyde 2	9.8 (1H)	7.8 (2H)	6.9 (2H)	4.0 (2H)	1.8 (2H)	1.4 (2H)	1.3 (8H)	0.8 (3H)
Decyloxybenzaldehyde 3	9.8 (1H)	7.8 (2H)	6.9 (2H)	4.0 (2H)	1.8 (2H)	1.4 (2H)	1.2 (12H)	0.8 (3H)

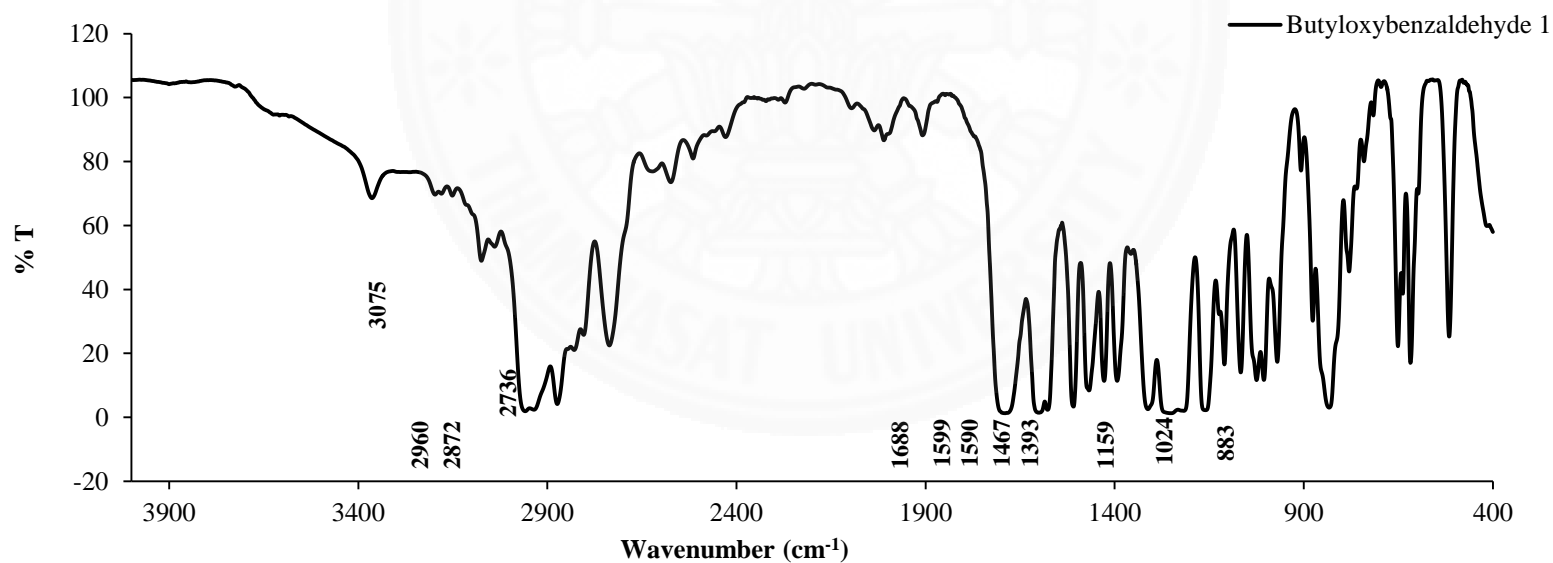
Aldehyde	^{13}C NMR (ppm), carbon								
	<i>CHO</i>	Phenyl, <i>p-C</i>	Phenyl, <i>o-C</i>	Phenyl, <i>m-C</i>	<i>OCH</i> ₂	<i>OCH</i> ₂ <i>CH</i> ₂	<i>CH</i> ₂ <i>CH</i> ₂ <i>CH</i> ₂	<i>CH</i> ₂ <i>CH</i> ₃	<i>CH</i> ₃
Butyloxybenzaldehyde 1	190 (1C)	166 (1C)	131 (1C)	115 (1C)	68 (1C)	31 (1C)	-	19 (1C)	13 (1C)
Octyloxybenzaldehyde 2	190 (1C)	164 (1C)	131 (1C)	114 (1C)	68 (1C)	31 (1C)	29 (4C)	22 (1C)	13 (1C)
Decyloxybenzaldehyde 3	190 (1C)	164 (2C)	131 (1C)	114 (1C)	68 (1C)	32 (1C)	29 (6C)	22 (1C)	13 (1C)

4.1.2.3 Infrared spectroscopy

The IR spectra recorded by nujol in NaCl disc for the synthesized alkyloxybenzaldehydes. The data were collected in the 4000-400 cm^{-1} region. The infrared data of all aldehydes were summarized in Table 5. The result found that all compounds show the similar wavenumber with a little peak shift, because of the effect of alkyl long chain group was substituted in porphyrin ring. The IR spectrum of butyloxybenzaldehyde **1** was shown as a representative example in Figure 59. The presence of C-H stretching at 2872 and 2736 cm^{-1} and C=O stretching at 1088 cm^{-1} were showed the characteristic peak of aldehyde functional group. The typical vibrational modes of phenyl and alkyl substituents were observed. The IR spectral signal at 3075 cm^{-1} was assigned to the C-H sp^2 stretching of the phenyl group and two peak at 1599 and 1509 cm^{-1} were corresponded the stretching of C=C in the phenyl ring. Another band at 2960 cm^{-1} in the infrared spectra of the butyloxybenzaldehyde **1** was assigned to the C-H sp^3 stretching band of alkyl long chain. The decreasing of wavenumber was founded in octyloxybenzaldehyde **2** and decyloxybenzaldehyde **3**, which they showed the signal peak at 2928 and 2924 cm^{-1} , respectively. The signal peaks at 1467 and 1393 cm^{-1} were assigned to CH_3 bend in alkyl long chain group. The position of alkyl long chain substitution at 883 cm^{-1} was agreed with the out of the plane in para disubstitution. Finally, the signal peak at 1159 and 1024 cm^{-1} were showed the signal of the ether group. The result of this study was generally in agreement with the previous report [107].

Table 5 The IR data of aldehydes **1 – 3**.

Aldehyde	C-H sp ² str. in phenyl	C-H sp ³ str. in long chain	C-H str. in aldehyde	C=O str. in aldehyde	C=C str. in phenyl	CH ₃ bend	C-O-C ether	Oop, para disubt.
Butyloxybenzaldehyde 1	3075	2960	2872, 2736	1688	1599, 1509	1467, 1393	1159, 1024	883
Octyloxybenzaldehyde 2	3073	2928	2856, 2732	1691	1599, 1509	1468, 1393	1159, 1019	883
Decyloxybenzaldehyde 3	3073	2924	2854, 2732	1693	1602, 1509	1467, 1391	1159, 1015	883

**Figure 59.** The IR spectrum of butyloxybenzaldehyde **1** in NaCl.

4.2 Synthesis and characterization of porphyrins and silver(II) porphyrins

4.2.1 Synthesis of porphyrins and silver(II) porphyrins

The modification of Adler-Longo method was used for synthesis of free based porphyrins, including Tetrakis(4-phenyl)porphyrin (TPP **4**), Tetrakis(4-methoxyphenyl)porphyrin (TOMPP **5**), Tetrakis (4-butyloxyphenyl)porphyrin (TOBPP **6**), tetrakis(4-octyloxyphenyl) porphyrin (TOOPP **7**) and tetrakis(4-decyloxyphenyl)porphyrin (TODPP **8**). Start with refluxing of aldehyde in a mixture of propionic acid and distilled pyrrole, for 2 hours. After completed reaction, the mixture was added ethanol and kept in the refrigerator overnight. Then, the precipitate was filtered and washed with ethanol. The crude product was purified on a silica gel column to give pure target compound as purple microcrystals. The free base porphyrins were obtained amount of yield range from 5 to 25 %. TOMPP **5** gave the highest yield as 26%, while the long chain derivative porphyrins such as TOBPP **6**, TOOPP **7** and TODPP **8** gave the lower yield than TOMPP **5**, due to the steric hindrance effect and the substitution of the donating group on para- position of alkyl long chain derivative.

The metalloporphyrins, silver(II) cation has been interested into the central hole of free base porphyrin. All silver(II) porphyrins, including Ag-TPP **9**, Ag-TOMPP **10**, Ag-TOBPP **11**, Ag-TOOPP **12** and Ag-TODPP **13** were synthesized by refluxing porphyrin and silver nitrate (AgNO_3) in a mixed solvent 1:1 ratio of *N,N*-dimethylformamide (DMF) and dichloromethane (CH_2Cl_2), for 5 hours. Then, the solvent was removed by a rotary evaporator and the crude product was purified by column chromatography to obtain purple products. The silver(II) porphyrins had a higher yield than free base porphyrin due to the size of silver ion that perfectly fitted into the central hole of the porphyrin ring. The long time reaction and the excess silver nitrate lead to drive forward reaction and give achievement product. However, the Ag-TOBPP **11** was obtained in the lowest yield (48%), while other porphyrins were received more than 50% yield, suggesting the influence of steric hindrance of *para* substituent of alkyl chain, the similar behavior found in Cu-TPP derivatives

[108]. The characterization data of free base porphyrins and silver(II) complexes were collected in Table 6.

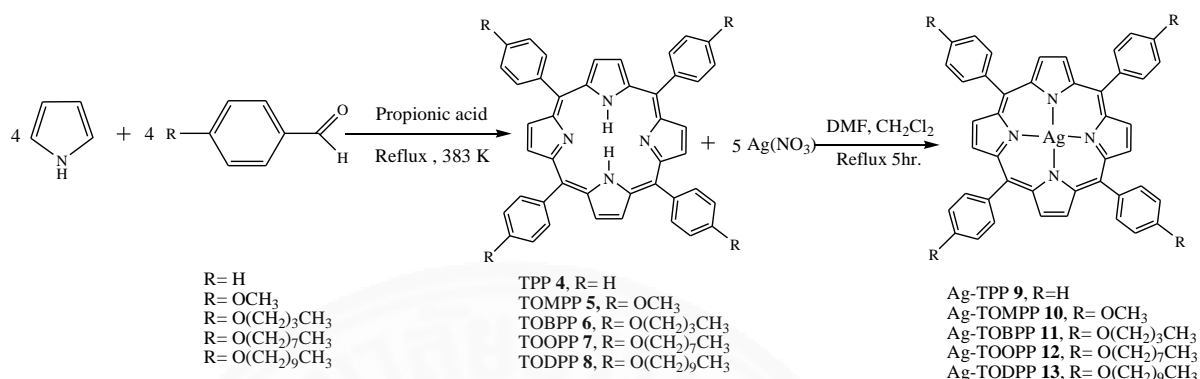


Figure 60. The route synthesis of silver(II) porphyrins.

4.2.2 Porphyrins and silver(II) porphyrins characterization

4.2.2.1 CHN elemental analysis

The characterization by using CHN elemental analysis of porphyrins and their silver(II) complexes were displayed in Table 6. The elemental analysis data for all complexes have been strongly confirmed the expected their structure and the result data was agreed with the theoretical value. However, some synthesized porphyrins, especially for silver(II) porphyrins, were afforded difference theoretical composition due to the trace of solvent (CH₂Cl₂) in their molecule.

Table 6 The characteristic data for free base porphyrins, and silver(II) porphyrins.

Compounds	Empirical formula	Yield (%)	Formula weight ^a	MS (m/z)	Elemental analysis (^b) %		
					C	H	N
TPP 4	C ₄₄ H ₃₀ N ₄	24	614.7	615.0	86.0(85.97)	4.9(4.92)	9.1(9.11)
TOMPP 5	C ₄₈ H ₃₈ N ₄ O ₄	26	734.8	735.4	76.42(78.45)	5.75(5.21)	7.42(7.62)
TOBPP 6	C ₆₀ H ₆₂ N ₄ O ₄	5	903.2	903.6	79.44(79.79)	6.55(6.92)	5.83(6.20)
TOOPP 7	C ₇₆ H ₉₄ N ₄ O ₄	14	1127.6	1127.9	81.10(80.95)	8.25(8.40)	4.93(4.97)
TODPP 8	C ₈₄ H ₁₁₀ N ₄ O ₄	11	1239.8	1240.0	81.24(81.37)	8.99(8.94)	4.58(4.52)
AgTPP 9	AgC ₄₄ H ₂₈ N ₄	74	720.6	719.2	72.98(73.34)	4.11(3.92)	7.57(7.78)
AgTOMPP 10	AgC ₄₈ H ₃₆ N ₄ O ₄ ·1.25CH ₂ Cl ₂	57	840.7	841.6	62.63(62.47)	4.53(4.10)	6.13(5.92)
AgTOBPP 11	AgC ₆₀ H ₆₀ N ₄ O ₄	48	1009.0	1010.1	74.51(71.42)	6.25(5.99)	5.76(5.55)
AgTOOPP 12	AgC ₇₆ H ₉₂ N ₄ O ₄ ·0.15 CH ₂ Cl ₂	63	1233.4	1233.9	73.19(73.39)	7.71(7.47)	4.21(4.50)
AgTODPP 13	AgC ₈₄ H ₁₀₈ N ₄ O ₄ ·1.5 CH ₂ Cl ₂	52	1345.7	1346.0	69.66(69.71)	7.70(7.59)	3.88(3.80)

^a Calculated without solvent^b Theoretical values are given in parentheses.

4.2.2.2 Mass spectrometry

The expected structure of all free base porphyrins had been confirmed by using mass spectrometry and the data shown in Table 6. The representative mass spectrum example of TOBPP **6** was shown in Figure 61, exhibited the molecular ion peak $[M+H]^+$ at m/z 903.6, as a major peak. In addition, the spectra of the other free base porphyrins showed the similar result with TOBPP **6**. However, the mass spectra of some free base porphyrins found to be a protonated hydrogen, yielding a strong $M+1$ peak such as TPP **4**, TOMPP **5** and TODPP **8** (shown in Appendix A). The mass spectra of all free base porphyrins displayed very intense molecular ion peak due to the fragmentation of porphyrins required a great deal of energy from the delocalization in macromolecules. Therefore, such fragmentation was not observed to any significant extent. The molecular ion peak $[M+H]^+$ at 615.0, 735.4, 1127.9 and 1240.0 were founded in the structure of TPP **4**, TOMPP **5**, TOOPP **7** and TODPP **8**, respectively.

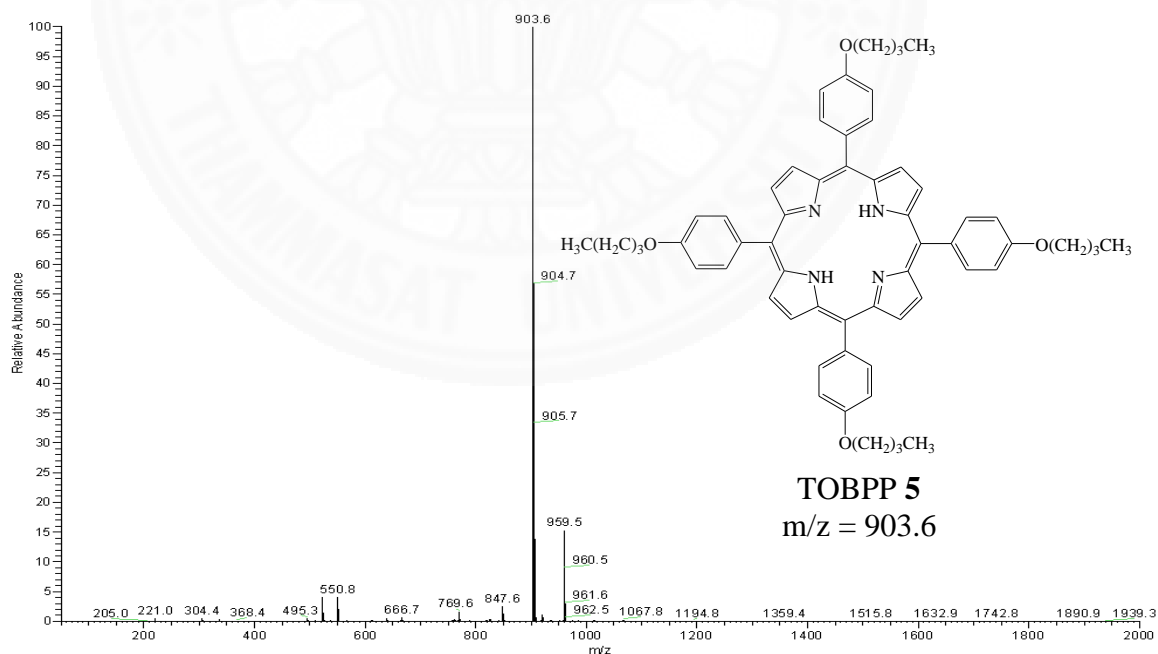


Figure 61. The mass spectrum of TOBPP **6** in CH_2Cl_2 .

The silver(II) porphyrins and the result data was shown in Table 6. The Ag-TOBPP **11** was used as a representative example of the mass spectrum of silver(II) porphyrins and was displayed in Figure 62. The strong molecular ion peak $[M+H]^+$ at m/z 1010.1 was assigned as a protonated molecule of $[Ag-TOBPP+H]^+$. However, the mass spectrum of Ag-TOBPP **11** was showed the fragmentation peak at m/z 904.3 that was related to the elimination of silver(II) ion from metal porphyrin structure. The fragment showed the peak at m/z = 705.0, that represent the butyloxyphenyl group substituents at 2 positions of the Ag(II)-porphyrin ring. The mass spectra of all silver(II) porphyrins showed very intense molecular ion peaks due to they had high energy from the delocalized electrons in the molecule, which the result similar in free base porphyrins. Ag-TPP **9**, Ag-TOMPP **10**, Ag-TOOPP **12** and Ag-TODPP **13** mass spectrum were founded the molecular ion peaks $[M+H]^+$ at 719.2, 841.6, 1233.9 and 1346.0, respectively. The mass spectra have been successfully received to confirm expect corresponding structure of the porphyrins and silver(II) porphyrins.

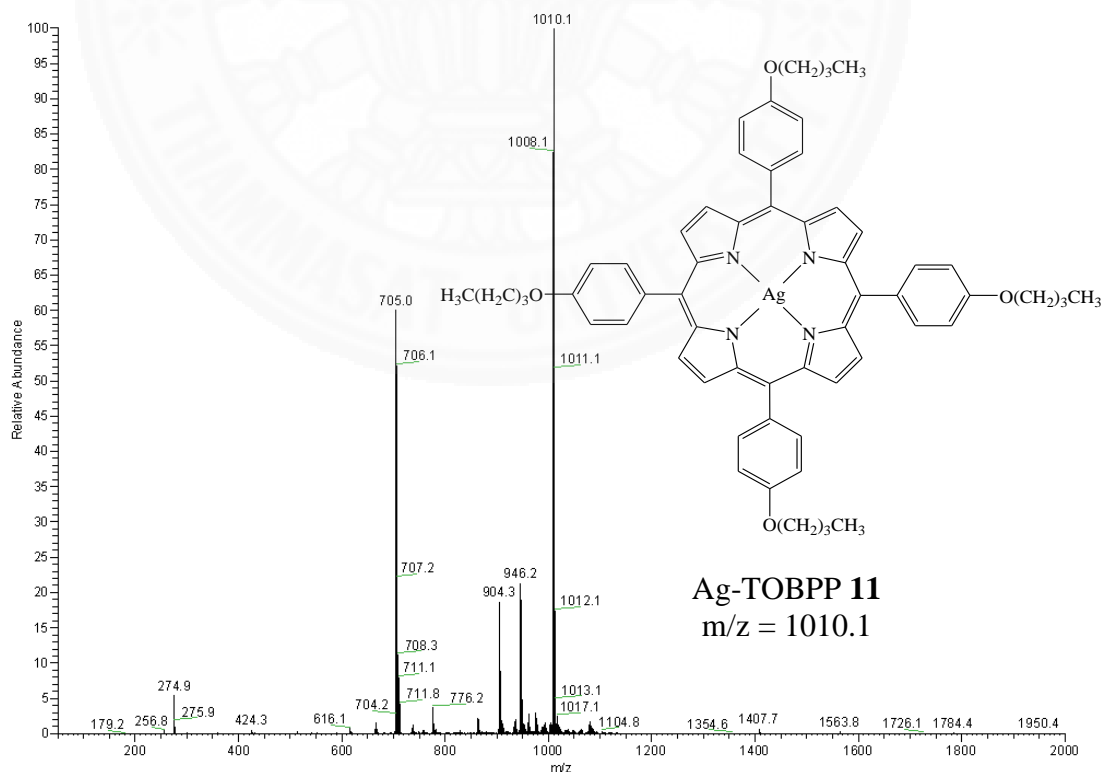


Figure 62. The mass spectrum of Ag-TOBPP **11** in CH_2Cl_2 .

4.2.2.3 NMR spectroscopy

The NMR spectra of free base porphyrins were highly characteristic and provide structural information of these compounds in CDCl_3 solvent. The assignment of spectral peaks of compounds was carried out by comparison with previous report data [103]. The important chemical shift data for analyzed were given in Table 7.

For the ^1H -NMR spectra of free base porphyrins, the signal of β -pyrrole protons was showed the chemical shift at 8.86 ppm, which was slightly downfield shift from TPP due to the deshielding effect. As the result, the deshielding effect of different substituted group in the peripheral position on phenyl ring in porphyrin may relate with the donating electrons of alkyl long chain.

The protons of *ortho*- and *para*- position in the phenyl group of all free based porphyrin had chemical shift in range from 8.20-8.10 and 7.77 to 7.26 ppm, respectively. This result data was similar in previous reported [109], when compared with TPP, the *para*- alkoxy substituted on the phenyl ring of other free base porphyrin show the up field shifts of chemical shift value. The alkoxy group, $-\text{OCH}_3$, $-\text{O}(\text{CH}_2)_3\text{CH}_3$, $-\text{O}(\text{CH}_2)_7\text{CH}_3$ and $-\text{O}(\text{CH}_2)_9\text{CH}_3$, were the electron-donating group that cause the phenyl protons displayed more shielding (up field chemical shifts). From the Table 7, the extent of shielding effect. The methoxy group is the lowest, shielding effect, when compared with other long chain alkoxy group due to the increasing number of carbon. The similar results on electron donating were reported by Dehghani, H. *et al.* [110]. The proton at *para*- substituent position in TOMPP **4** ($-\text{OCH}_3$) was assigned at 4.10 ppm. The alkyl proton in the short chain (TOBPP **5**) was found to be de-shielded than the TOOPP **6** and TODPP **7** due to the inductive effect and the electron-donating of the ether group in the side chain.

The limitation of equipment, the $-\text{NH}$ proton was unsuccessful to identify. The previous report by Zabardasti A [111] explained that the proton signal of $-\text{NH}$ group in porphyrin ring was up field shifted to -2.90 ppm due to the more shielding effect of the porphyrin ring. The spectrum of TOBPP **5** was as a representative example and shows in Figure 63.

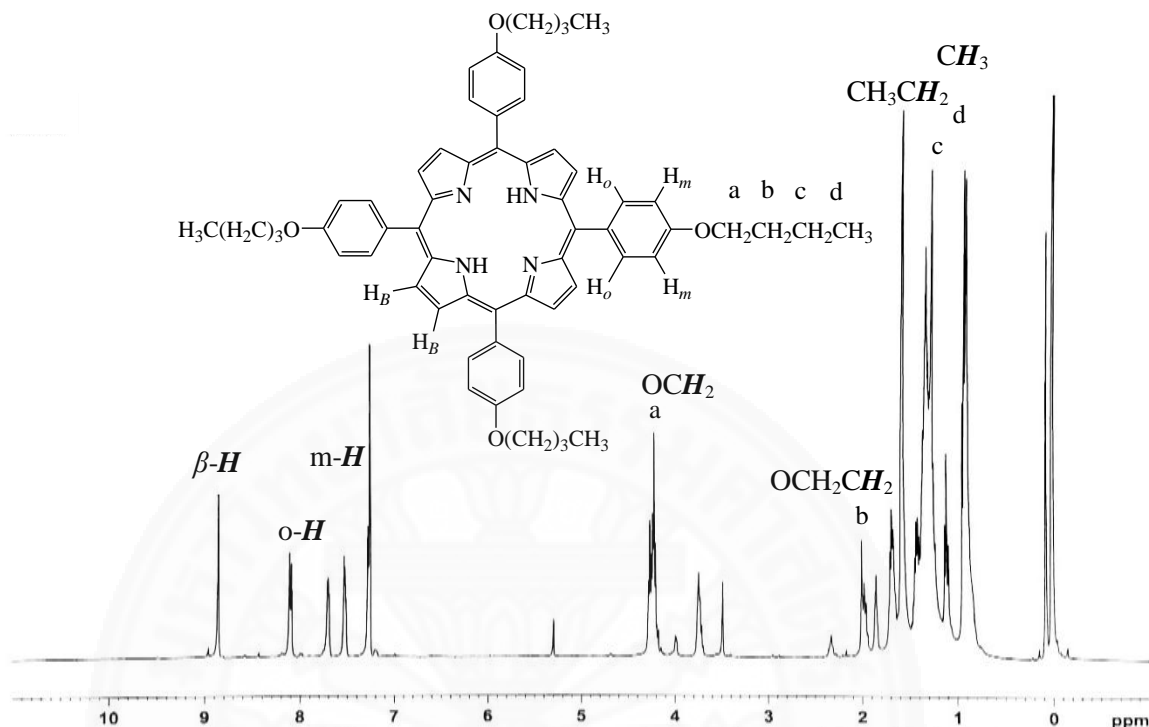


Figure 63. ^1H NMR spectrum of TOBPP **6** in chloroform-d (CDCl_3).

The ^{13}C -NMR of TOBPP **5** was shown as a representative example in Figure 64. ^{13}C -NMR spectrum of TOBPP **5** was assigned the signal at 135.50 (α -C, pyrrole), 130.89 (β -C, pyrrole) and 119.77 (meso-C, methane bridge) ppm. The carbons in the position of phenyl ring were shown only 4 signals at 159.12 (p^* -C), 134.64 (o-C), 128.75 (p-C) and 112.87 (m-C) ppm because of the symmetry of phenyl group in ortho and *para* position. Moreover, the signal of alkyl long chain group was shown in the same range of aldehyde. The other free base porphyrin was observed similar with TOBPP **5** and was related with the same reported by I-Chin L. and Jyh-Horung C. [112], especially for TOMPP **4**.

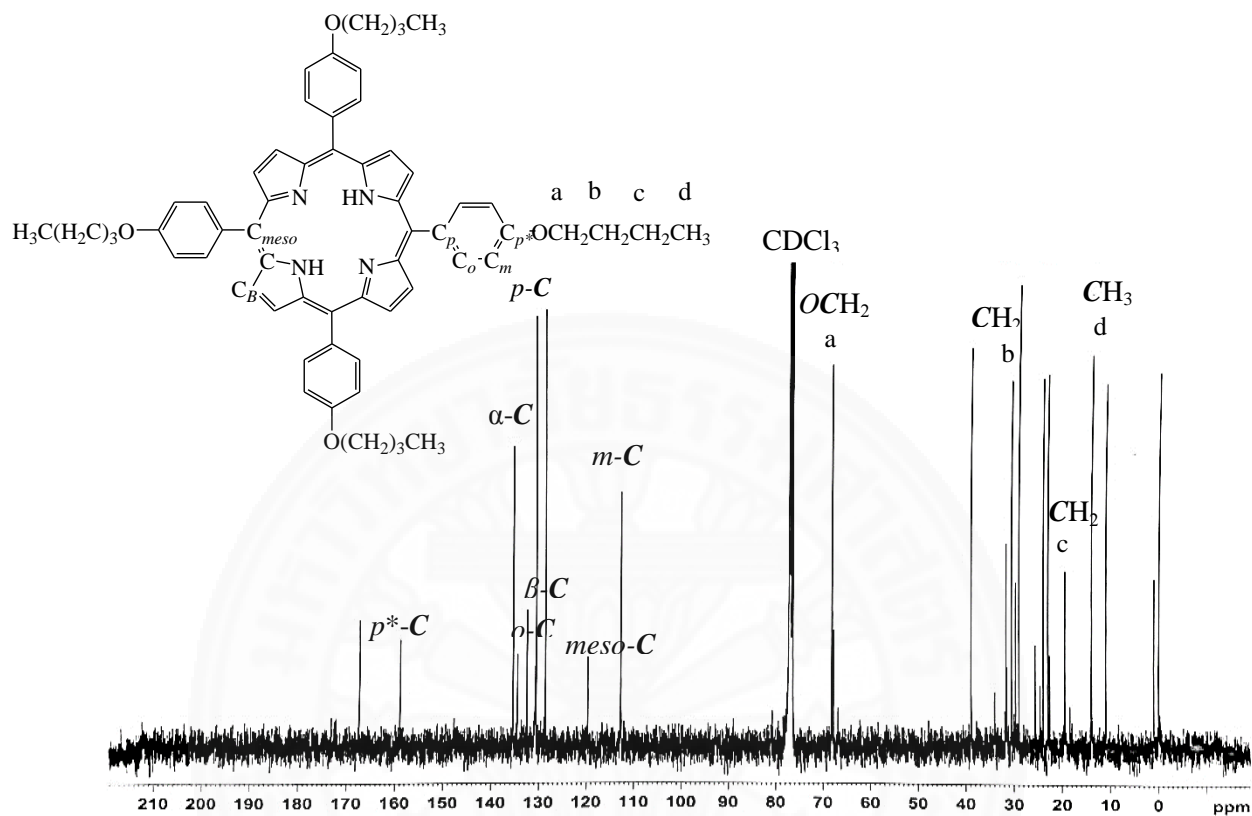


Figure 64. ^{13}C NMR spectrum of TOBPP 6 in chloroform-d (CDCl_3).

For the expected porphyrin with silver(II) ion were unsuccessful identified by using ^1H and ^{13}C NMR due to the paramagnetic silver(II) porphyrin, so the chemical shifts of silver porphyrin and their derivatives were observed as the broad peaks related with free base porphyrin information only. Further analysis, including ESR spectroscopy and Mossbauer spectroscopy, may required studying the information of inside into the complexes for confirm the structure.

Table 7 ^1H and ^{13}C NMR spectroscopic data for free base porphyrins.

Porphyrins	¹ H NMR (ppm), proton												
	Pyrrole, β- H	Phenyl, <i>o</i> - H	Phenyl, <i>m</i> - H	Phenyl, <i>p</i> - H	O CH ₃	O CH ₂	OCH ₂ CH ₂	CH ₂ CH ₃	CH ₂ CH ₂ CH ₂	CH ₃			
TPP 4	8.85	8.20	7.77	7.52	-	-	-	-	-	-			
TOMPP 5	8.86	8.12	7.29	-	4.10	-	-	-	-	-			
TOBPP 6	8.86	8.10	7.29	-	-	4.24	1.98	1.29	-	0.92			
TOOPP 7	8.86	8.10	7.26	-	-	4.22	1.99	1.36	1.26	0.91			
TODPP 8	8.86	8.10	7.26	-	-	4.22	1.98	1.33	1.26	0.88			
Porphyrins	¹³ C NMR (ppm), carbon												
	Phenyl, <i>p</i> *- C	α- C	Phenyl, <i>o</i> - C	β- C	Phenyl, <i>p</i> - C	<i>Meso</i> - C	Phenyl, <i>m</i> - C	OCH ₃	OCH ₂	OCH ₂ CH ₂	CH ₂ CH ₂ CH ₂	CH ₂ CH ₃	CH ₃
TPP 4	127.70	-	134.56	131.12	122.22	120.15	116.67	-	-	-	-	-	-
TOMPP 5	158.75	134.68	133.99	129.97	127.89	118.83	111.44	54.65	-	-	-	-	-
TOBPP 6	159.12	135.50	134.64	130.89	128.75	119.7	112.84	-	68.14	31.60	-	23.98	13.78
TOOPP 7	159.16	135.48	134.69	130.80	128.74	119.79	112.93	-	68.56	31.79	29.57, 29.39, 29.19, 26.19, 22.55	-	13.84
TODPP 8	159.10	135.51	134.51	130.68	128.76	119.77	112.86	-	68.48	31.88	29.60, 29.55, 29.53, 29.46, 29.28, 26.20, 22.60	-	13.93
Ag(II) porphyrin 9–13								- ^a					

^a Unable to identify due to paramagnetic character in ^1H and ^{13}C NMR data

4.2.2.4 Infrared spectroscopy

The IR spectra were recorded in KBr disc for the synthesized free base porphyrins and silver(II) porphyrin derivatives. The data were collected in the 4000-400 cm^{-1} region. The infrared data was concluded in Table 8. The important signal peaks of free base porphyrin were observed in the spectral range 3310-3320 cm^{-1} and 965-967 cm^{-1} , which were assigned to N-H stretching and N-H bending vibrations respectively [103]. Whereas, the IR spectra of silver(II) porphyrins were disappeared both of this signal. That can confirm, the silver(II) ion was inserted into the central hole of the porphyrin ring and replace of hydrogen in pyrrole ring. The comparison IR spectrum TOBPP **6** and Ag-TOBPP **11** were shown in Figure 65. As mention above, the free base porphyrin TOBPP **6** shows the characteristic signal peak of N-H stretching and N-H bending at 3318 and 965 cm^{-1} , respectively. Whereas, those of two peaks were disappeared in the spectrum of Ag-TOBPP **11**. The similar results were found in the previous report by Sandeep M. *et al.* [114]. In addition, the IR spectra of silver(II) porphyrins were corresponded the signal peak of Ag-N at $\sim 460 \text{ cm}^{-1}$, which similar result was reported by Tyulyaeva, E.Y. and Lomova, T.N. [115].

Furthermore, both free base porphyrin and its silver(II) complexes displayed the signal peak of C-H stretching (long chain) and C-N stretching in porphyrin ring. When increasing the number of carbon atom in the long chain, the frequency of both signals found to be slightly decreased because of the electronic effect of long chain substituent. The substituent saturated alkyl chain group exhibited electron delocalize from the *para* position of the phenyl ring to the electronegativity of the porphyrin. The frequencies were observed downshifts of carbon in alkyl chain substituted group, which related to the interactions intrinsically decrease the bond strength of the molecule [116-118]. However, the three signal peak including C=C stretching, C-O stretching and C-H bending for all synthesized porphyrins showed with a little peak shift in IR spectra.

Table 8 The IR spectroscopic data of free base porphyrins.

Compounds	N-H str. in porphyrin	C-H str. in phenyl and long chain	C=C str. in phenyl	C-N str. in porphyrin	C-O str. in long chain	N-H bend in porphyrin	C-H bend in porphyrin
TPP 4	3310	-	1597, 1469	1212	-	966	794
TOMPP 5	3317	2928, 2832	1606, 1509	1247	1175	965	802
TOBPP 6	3318	2929, 2868	1605, 1507	1244	1173	965	800
TOOPP 7	3316	2926, 2850	1606, 1508	1242	1174	965	803
TODPP 8	3310	2923, 2852	1606, 1509	1243	1175	967	804
AgTPP 9	-	-	1598, 1442	1243	-	-	794
AgTOMPP 10	-	2934, 2833	1606, 1522	1250	1176	-	807
AgTOBPP 11	-	2932, 2834	1609, 1516	1248	1176	-	805
AgTOOPP 12	-	2931, 2943	1609, 1516	1247	1177	-	805
AgTODPP 13	-	2928, 2845	1609, 1517	1249	1175	-	805

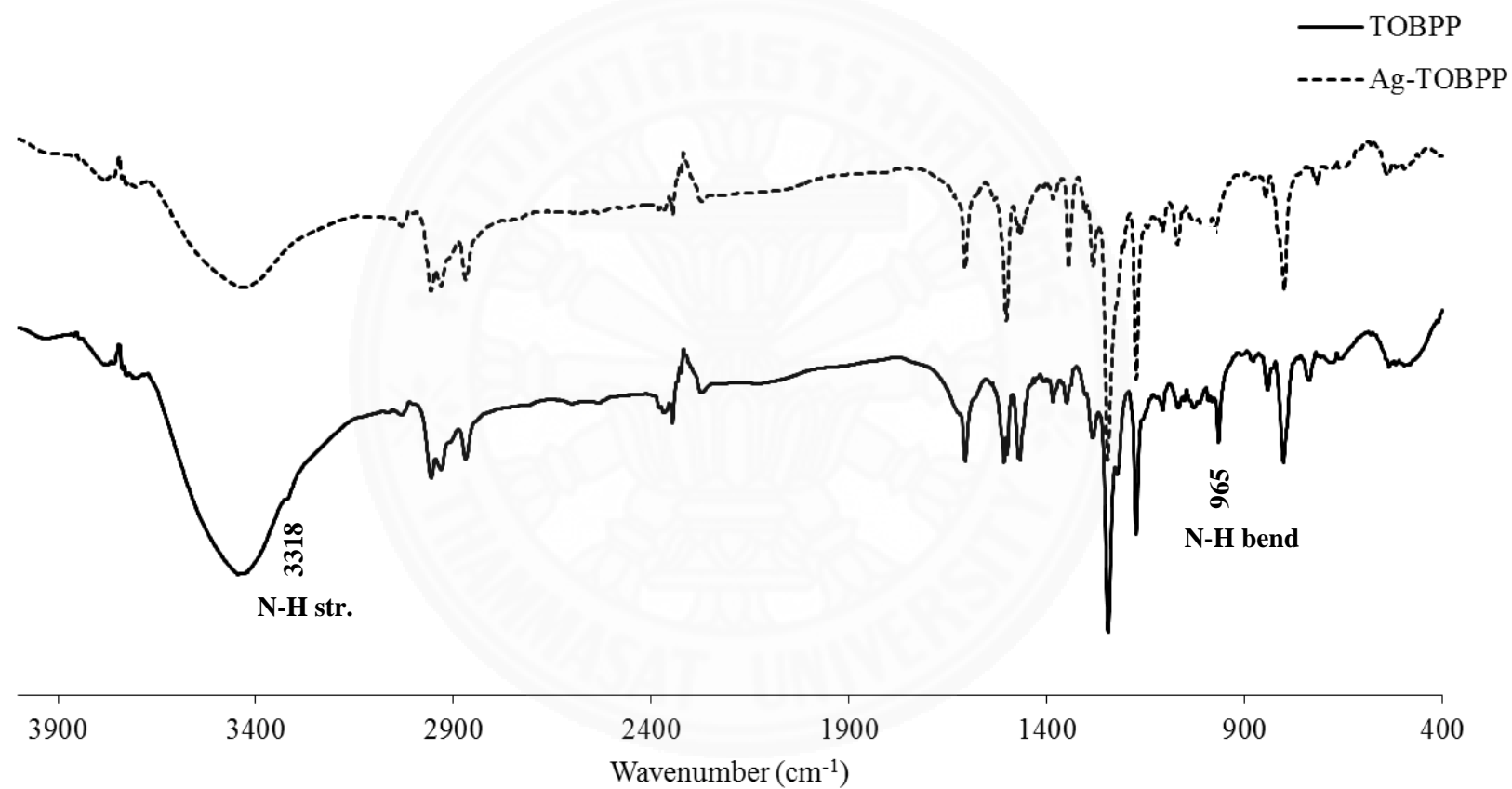


Figure 65. IR spectrum of TOBPP **6** and Ag-TOBPP **11** in KBr.

4.2.2.5 UV-Vis spectroscopy

The UV-Vis absorption spectra of porphyrins and metalloporphyrins are contained one intense band as the Soret band, which absorbed energy in the near-ultraviolet region around 350-430 nm, assigned to a higher singlet excited state $S_0 \rightarrow S_2$ transition [119]. While, the four low-intensity absorption from 500-655 nm in the visible region represent the Q bands, typically labeled Q_1 , Q_2 , Q_3 and Q_4 , which can be assigned to the $S_0 \rightarrow S_1$ transitions. Figure 66 depicts the UV-Vis spectra for all the free base porphyrins in dichloromethane solvent with molar absorptivity in the range ca $2\text{-}5 \times 10^5 \text{ molL}^{-1}$. According to UV-Vis spectroscopic data, the Soret band and Q band of the *para*-substituted porphyrin lead to a small red shift when compare with TPP 4. The absorption data and molar extinction coefficient (ϵ) of all free base porphyrins were showed in Table 9.

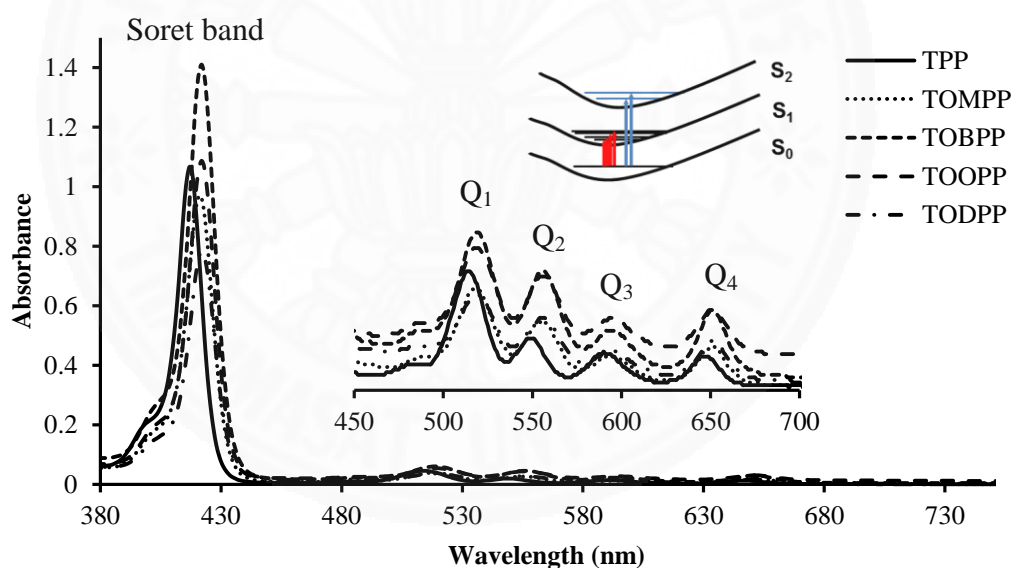


Figure 66. UV-Vis spectra of free base porphyrins in dichloromethane.

In silver(II) porphyrin derivatives show an intense absorption band around 425-430 nm (Soret band) and displayed only one Q band around 542-544 nm, which was similar result found in the report by Wootthiphan J [120]. The absorption band of *para*-substituted Ag-porphyrins shows red-shift when compared with Ag-TPP 9, which was the similar result in the free base porphyrins, suggesting the electron effects from long chain alkyl group.

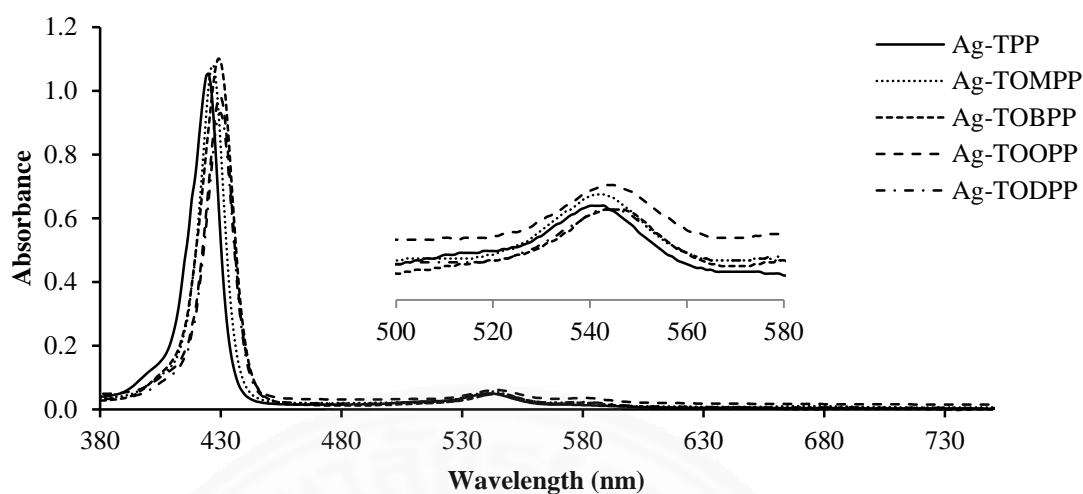


Figure 67. UV-Vis spectra of silver(II) porphyrins in dichloromethane.

A comparison of the spectra of free base porphyrin and its silver(II) porphyrin, which showed the representative UV-Vis spectrum example of TOBPP **6** and Ag-TOBPP **11**, as shown in Figure 68. The TOBPP exhibits a strong Soret band at 422 nm and four Q band at 517, 556, 595 and 651 nm. Then, the proton on NH group of porphyrin ring was deprotonated and the nitrogen atom binds with silver ion to yield the Ag-TOBPP. The absorption band at 543 nm represent the Q band of Ag-TOBPP, which shifted to red due to the signature of an effective intramolecular charge transfer [121]. This result has been observed in all silver(II) porphyrins.

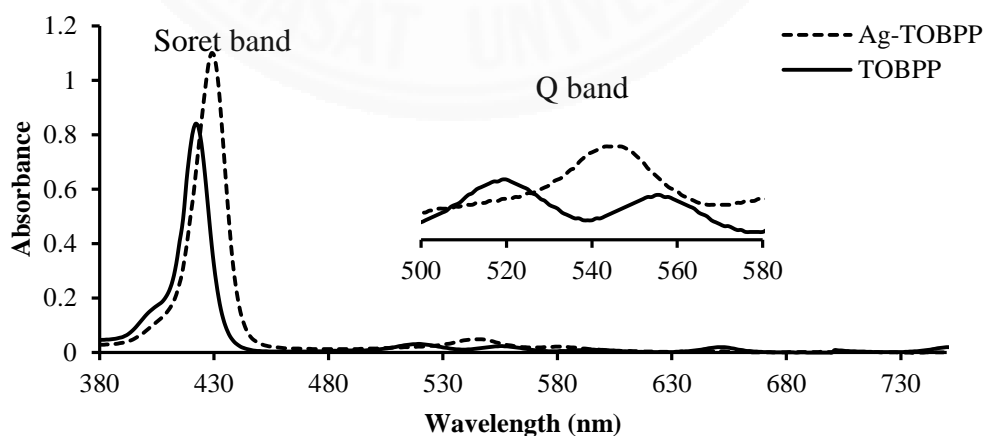


Figure 68. UV-Vis spectra of TOBPP **6** and Ag-TOBPP **11** in dichloromethane.

Table 9 The absorption data of all compounds.

Porphyrin	Dichloromethane ^a				
	S band (nm)	Q band (nm), ϵ (M ⁻¹ cm ⁻¹)			
		Q ₁	Q ₂	Q ₃	Q ₄
TPP 4	417	514, 14162	548, 6140	590, 4605	649, 3991
TOMPP 5	421	517, 24045	556, 16662	594, 7625	651, 10265
TOBPP 6	422	517, 24017	556, 16684	595, 7646	651, 10257
TOOPP 7	422	519, 20953	556, 14952	595, 6781	651, 10166
TODPP 8	422	519, 16782	556, 12539	595, 5589	652, 9258
AgTPP 9	425	-	542, 257779	-	-
AgTOMPP 10	427	-	542, 229512	-	-
AgTOBPP 11	427	-	543, 250043	-	-
AgTOOPP 12	430	-	544, 229723	-	-
AgTODPP 13	430	-	544,259617	-	-

^a All solution were prepared in the concentration of $2\text{-}5 \times 10^{-5}$ mol/L, in CH₂Cl₂(n =3, %RSD \leq 1.6) and measured in the wavelength range of 200-800 nm.

4.2.2.6 Fluorescence spectroscopy

Fluorescence spectroscopy can be used to identify the presence of the free base porphyrin and silver(II) porphyrin. The fluorescence emission spectra were recorded in dichloromethane at room temperature with a concentration about $2\text{-}5 \times 10^{-5} \text{ mol L}^{-1}$ and fluorescence spectral data of all porphyrins are presented in Table 10, when the selected excitation wavelength is the maximum absorption of the first Q-band. Figure 69 illustrates the fluorescence spectra of all free base porphyrins at emission wavelength from 654 nm (excitation at 534 nm) excepted for the TPP 4. The TPP showed a strong wavelength from 649 nm (excitation 529 nm). The present work selects the wavelength of maximum absorption the first Q band as the excitation wavelength. The spectra also exhibited the strong fluorescence intensity similar to the previous report [122].

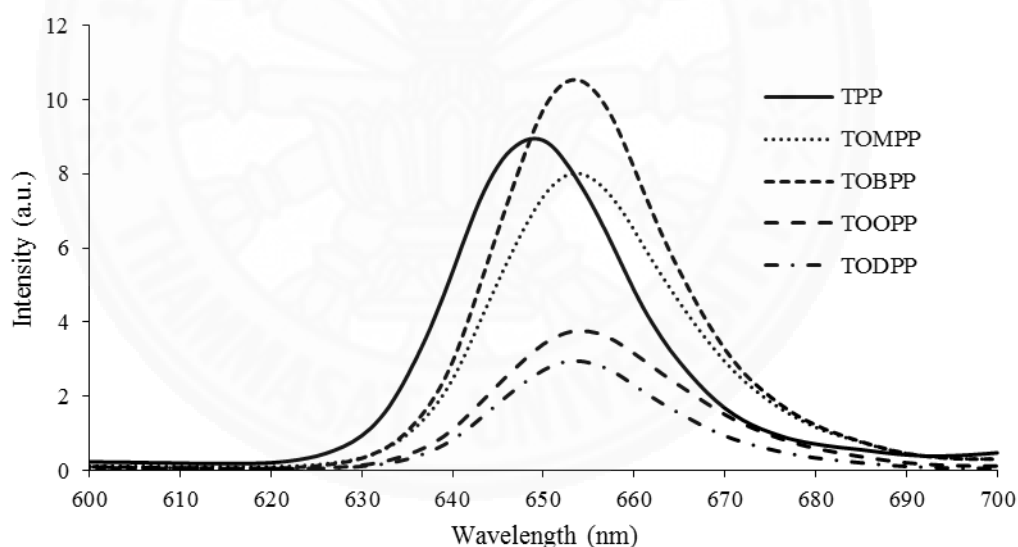


Figure 69. The emission spectra of the free base porphyrins in dichloromethane.

The fluorescence emission spectra of silver(II) porphyrins have been observed. The major emission bands showed at 605 nm for Ag-TPP, Ag-TOOPP, while Ag-TOMPP, Ag-TOBPP, and Ag-TODPP were observed at 607, 604 and 609 nm, respectively (excitation at 557 nm for all complexes). However, the emission spectra show a slight difference due to electron donating ability of alkoxy in the chain

[123]. The silver(II) porphyrins exhibited the blue shift when compared with free base porphyrin due to the interaction between the metal ion in the porphyrinic substituents and the solvent molecules. [124]

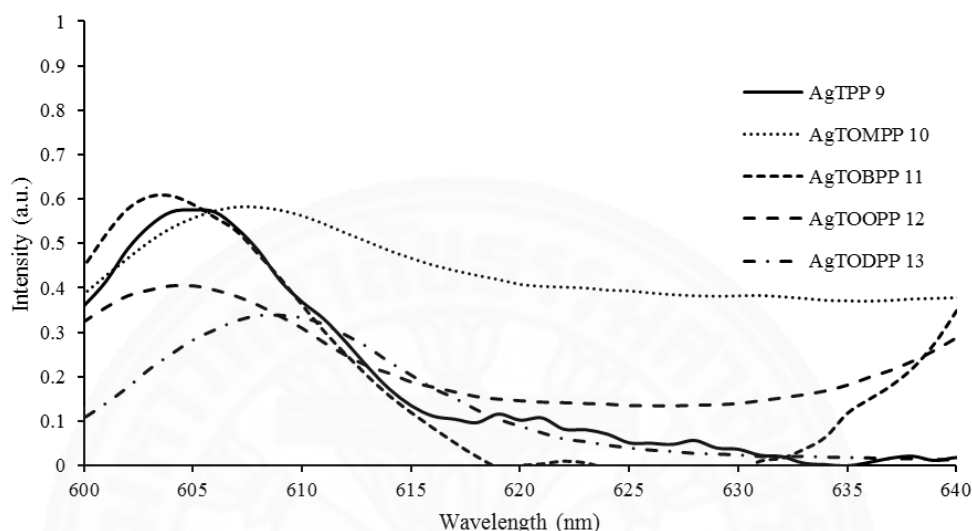


Figure 70. The emission spectra of the silver(II) porphyrins in dichloromethane.

The term of energy gap (E_{gap}) refers to the energy difference between the top of the valence band (highest occupied molecular orbital, HOMO) to the bottom of the conduction band (lowest unoccupied molecular orbital, LUMO), electrons are able to jump from one band to another. In order for an electron to jump from a valence band to a conduction band, it requires a specific minimum of energy for the transition, the band gap energy. The estimated energy gap determined from an intersection of UV-Vis absorption (Q_4 band) and fluorescence emission spectrum was following the equation [125].

$$\text{Energy gap } (E_{\text{gap}}) = hc/\lambda$$

$$\text{When } h = \text{Planks constant } (6.626 \times 10^{-34} \text{ J}\cdot\text{s})$$

$$c = \text{speed of light } (3.0 \times 10^8 \text{ ms}^{-1})$$

$$1 \text{ eV} = 1.602 \times 10^{-19} \text{ J}$$

In contrast, the silver(II) porphyrins did not exhibit the absorption spectra at Q_4 band. Therefore, the estimated energy gap of silver(II) porphyrin cannot be calculated. The calculated energy gap of all porphyrins was summarized in Table 10.

The energy gap of the long chain substituted free base porphyrins showed the lower energy gap at 1.90 eV that related to the donating electron of long chain substituent group at *para*- position.

Table 10. The absorption-emission wavelength and the estimated energy gap of free base porphyrins in dichloromethane.

porphyrins	Dichloromethane		
	Absorption wavelength (nm)	Emission wavelength (nm)	E _{gap} (ev)
TPP 4	529	649	1.92 [76]
TOMPP 5	534	654	1.90
TOBPP 6	534	654	1.90
TOOPP 7	534	654	1.90
TODPP 8	534	654	1.90
AgTPP 9	557	605	2.14 ^a
AgTOMPP 10	557	607	2.13 ^a
AgTOBPP 11	557	604	2.14 ^a
AgTOOPP 12	557	605	2.14 ^a
AgTODPP 13	557	609	2.13 ^a

^a Calculate by using average of wavelength between Q-band and emission band.

4.3 Biological activity of porphyrins and silver(II) porphyrins

In the present work, the free base porphyrin and silver(II) porphyrin were also tested for their antibacterial activities. The activities of free base porphyrins were compared with these silver(II) porphyrins. Their antibacterial activity against gram positive bacteria *Staphylococcus aureus* (ATCC 25923) and gram negative bacteria *Escherichia coli* (ATCC 25922) by disc diffusion method, minimum inhibitory concentration (MIC) and minimum bactericidal concentration (MBC) were determined.

4.3.1 Disc diffusion method

The antibacterial screening data by agar disc diffusion method at concentration 1 mg mL^{-1} show in Table 11. Zones of inhibition of both bacteria were measured as the diameter of the inhibitory area in millimeter (mm). The standard disc of drug penicillin was served as positive control and DMSO solvent was used for control experiments, which DMSO had no discernible biological effect. All free base porphyrins and silver(II) porphyrin complexes were found to be potentially effective against both gram-positive and gram-negative bacteria. However, the silver(II) porphyrins are more potent antibacterial against than free base porphyrins due to faster diffusion of metal complexes as a whole through the cell membrane which combined effect of metal atom and the ligand [126].

In the case of free base porphyrins, TOMPP **5** shows the greatest value of inhibition zone of $7.8 \pm 0.3 \text{ mm}$ for against *S.aureus*. The larger zone of inhibition around an antibiotic-containing disc of all free base porphyrins indicates in the order as follow: $\text{TOMPP} \geq \text{TPP}$, $\text{TOOPP} \geq \text{TODPP} \geq \text{TOBPP}$. Whereas, the result of silver(II) porphyrins were displayed effectively of inhibiting the growth of the *S.aureus* and *E.coli* strain. The Ag-TODPP has more effective inhibitory activity than other complexes, suggesting that the activity was dependent on the chain length [127]. Tovmasyan A. *et al.* [128] reported that structural modification of the Ag porphyrin molecule from water-soluble (Ag porphyrin with allyl functional group at the periphery) to amphiphilic porphyrin (Ag porphyrin with long hydrophilic chain into

the *meso* position of porphyrin ring) resulted in a certain decrease in cell line specificity and increase in the cytotoxicity. The standard drug penicillin showed 23 mm inhibition against *S.aureus*, while it cannot against *E.coli* due to *E.coli* was penicillin resistant.

Table 11 Antibacterial screening data for the synthesized porphyrins **9 – 13**.

Complexes	Inhibition zone (mm) ^a	
	<i>Staphylococcus aureus</i>	<i>Escherichia coli</i>
TPP 4	7.5 ± 0.0	6.5 ± 0.0
TOMPP 5	7.8 ± 0.3	6.5 ± 0.0
TOBPP 6	6.8 ± 0.3	6.5 ± 0.0
TOOPP 7	7.5 ± 0.0	6.5 ± 0.0
TODPP 8	7.3 ± 0.0	6.5 ± 0.0
Ag-TPP 9	7.5 ± 0.0	7.5 ± 0.5
Ag-TOMPP 10	7.5 ± 0.0	7.5 ± 0.5
Ag-TOBPP 11	11.5 ± 0.5	10.0 ± 0.0
Ag-TOOPP 12	11.5 ± 0.6	11.4 ± 0.6
Ag-TODPP 13	12.5 ± 0.5	11.5 ± 0.5
DMSO	6 ± 0.0	6 ± 0.0
Penicilin	23 ± 0.0	-

^a Inhibition zone value observed was not minus the negative control value.

4.3.2 MIC/MBC method

The minimum inhibitory concentration (MIC) and the minimum bactericidal concentration (MBC) of the silver(II) porphyrins were showed in Table 12. The MIC determination of complexes of silver(II) porphyrins against all the test bacteria were done in concentrations of 640, 320, 160, 80 and 40 ug/mL for test bacteria which indicated all Ag complexes were active against *S. aureus* and *E. coli* bacteria. These silver(II) porphyrins displayed activity of MIC value against *S. aureus* and *E. coli* at concentration 320 ppm and 160 ppm respectively, excepting Ag-TODPP shows MIC value of *E. coli* at concentration 80 ppm.

Then, the concentration did not show growth was considered to be the MBC for the test in microbial death. The MBC value of all silver(II) porphyrins were founded in the same concentration at 640 ppm for *S. aureus*, excepting Ag-TPP and Ag-TODPP exhibit in concentration at 320 ppm. Whereas, the MBC value was shown at 160 ppm for *E. coli* against, except Ag-TODPP found in concentration at 80 ppm. From the result, Ag-TODPP were considerably more achieve (MIC = 320 and MBC 80 ppm) than other porphyrins, suggesting that the alkyl long chain may easily penetrate cell lipid barriers of the bacteria cell. [129]

Table 12. The MIC and MBC value of silver(II) porphyrin complexes **9 – 13**.

Silver(II) porphyrin complexes	minimum inhibitory concentration (MIC/ppm)		minimum bactericidal concentration (MBC/ppm)	
	<i>S. aureus</i>	<i>E. coli</i>	<i>S. aureus</i>	<i>E. coli</i>
AgTPP 9	320	160	320	160
AgTOMPP 10	320	160	640	160
AgTOBPP 11	320	160	640	160
AgTOOPP 12	320	160	640	160
AgTODPP 13	320	80	320	80

4.4 Alcohol vapor sensing application of silver(II) porphyrins film

The application of alcohol vapor sensing for all silver(II) porphyrins has been investigated. The Ag-TPP and its derivatives were prepared by using dichloromethane solvent at a concentration of 5 mgmL^{-1} porphyrin solution and then dropped onto a clean glass slide. The coated glass was shown in Figure 71. Then, the porphyrin films were tested by dynamic measurement so called “electronic nose” under the flow of alcohol vapors such as methanol, ethanol, and iso-propanol at 25°C and used principal component analysis (PCA) program to analyze the obtained data from an electronic nose.

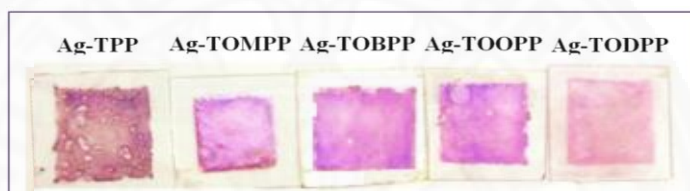


Figure 71. The texture thin film of Ag-TPP and its derivatives.

4.4.1 Optical sensing characteristic

For sensing test, the chemically-optical change of porphyrin film on various alcohols was analyzed by using eight LED light. Each LED light source with emitting wavelength shows in Table 13.

Table 13. The LED light sources used in this test.

No.	Color	Wavelength (nm)
Sensor 1	Infrared	>700
Sensor 2	Red	638
Sensor 3	Yellow	587
Sensor 4	Green	537
Sensor 5	Violet	399
Sensor 6	Pink	472
Sensor 7	Blue	457
Sensor 8	White	450-700

The synthesized Ag-TPP and their derivatives, including Ag-TOMPP, Ag-TOBPP, Ag-TOOPP and Ag-TODPP were fabricated as a film by dropped coated on the glass slide before study the sensor application. However, the film may not totally homogeneous but all film samples gave sensitive signals on various alcohol vapors (methanol, ethanol, and iso-propanol).

The Ag-TOBPP film gives the strongest gas sensing response signals, specific to methanol and ethanol in all ranges LED. While only sensor 2 was not responded with iso-propanol. Tonezzer M. *et al.* explained the porphyrin films possess an energy gap between the highest occupied molecular orbital (HOMO) and the lowest unoccupied molecular orbital (LUMO), before interacting with the alcohol molecules causes a rearrangement of the electrical dipoles and changing the energy gap between HOMO and LUMO orbitals, resulting different the absorption properties of the film. [89]

The result confirms by the absorption spectra band of Ag-TOBPP in the various alcohol solvent. It found that the absorption band in the range 360-600 nm exhibits the electronic $\pi - \pi^*$ transition of the absorption change, due to the alcohol vapor molecule interacting with the macrocycle, as report by Sumana K. *et al.* [92].

Figure 72-74 show the absorption signals of each LED light on the Ag-TOBPP film, representative example of each type of alcohol, methanol, ethanol, and iso-propanol, respectively. Alcohol vapor was purged at 25 °C in a chamber, switching between the alcohol vapor for 2 minutes and the reference gas (nitrogen, N₂) for 2 minutes. Thus the absorption signal showed as a clear/pulse. However, sensor 1 and 2 (related to infrared and red LED source) illustrated a uniform signal especially for iso-propanol vapor, which may relate to weak absorption of both complex and alcohol in these regions. Other LED sources were found to be a uniform signal (Figure 72-74).

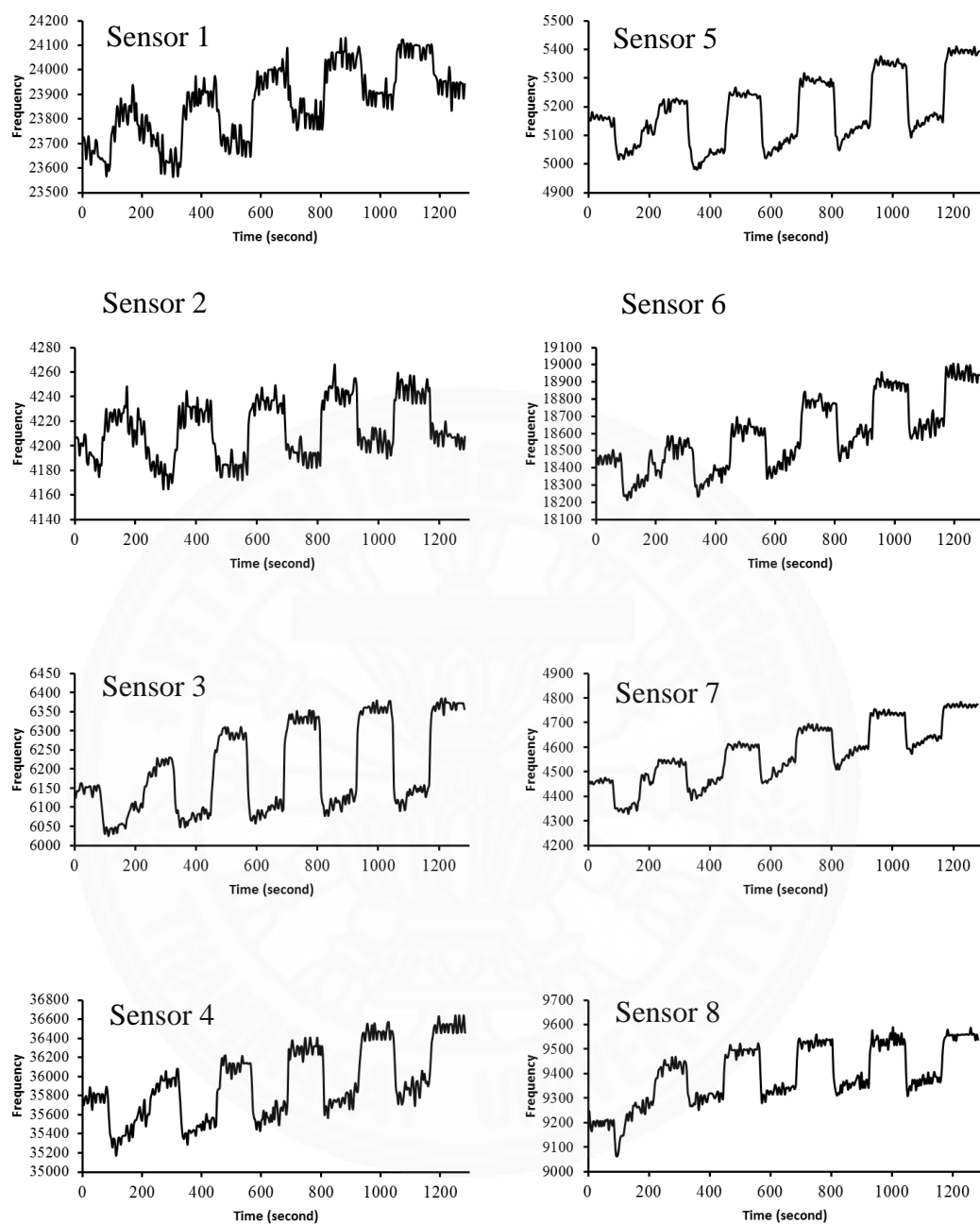


Figure 72. The dynamic response of Ag-TOBPP film in the presence of methanol vapor.

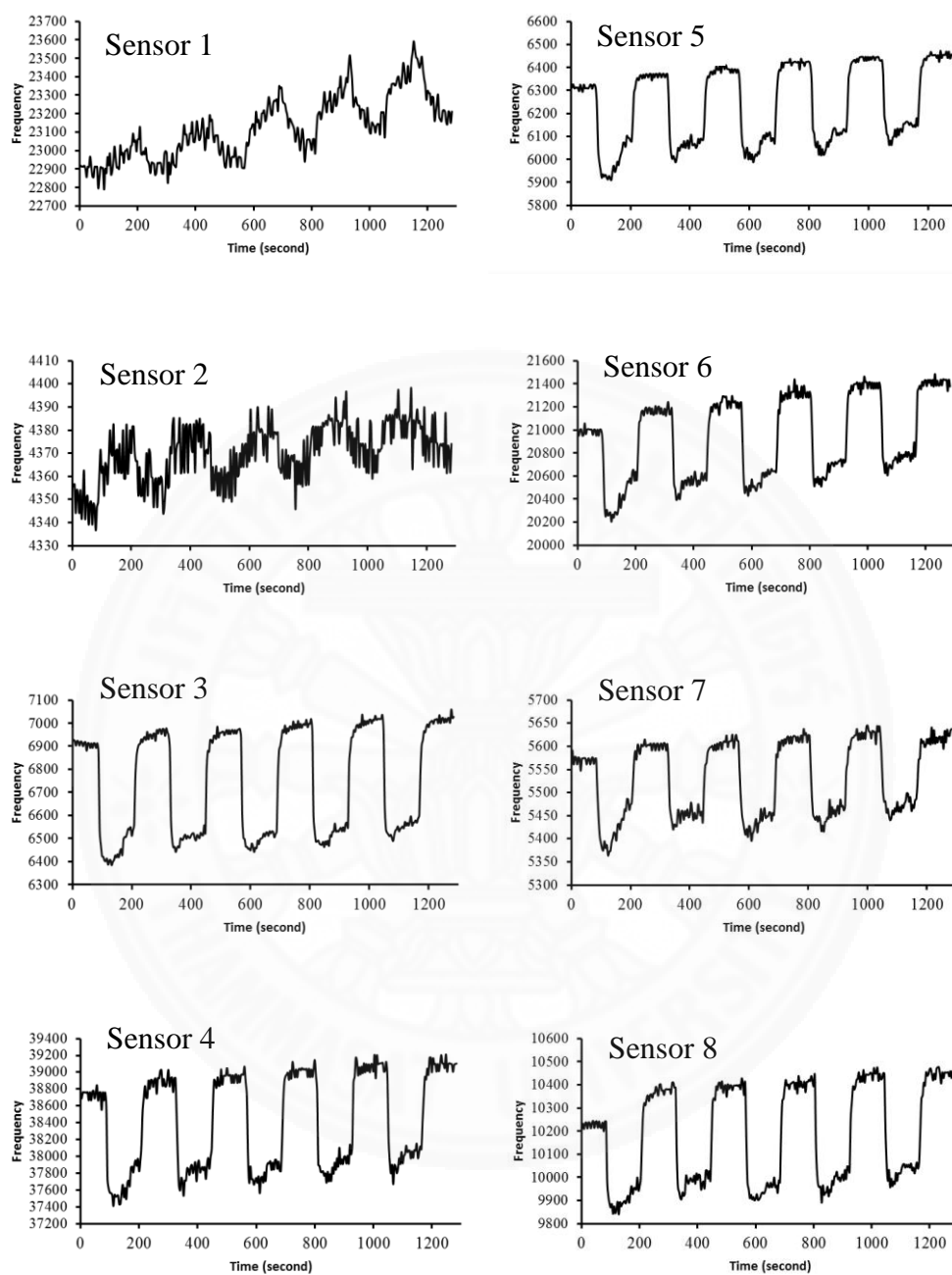


Figure 73. The dynamic response of Ag-TOBPP film in the presence of ethanol vapor.

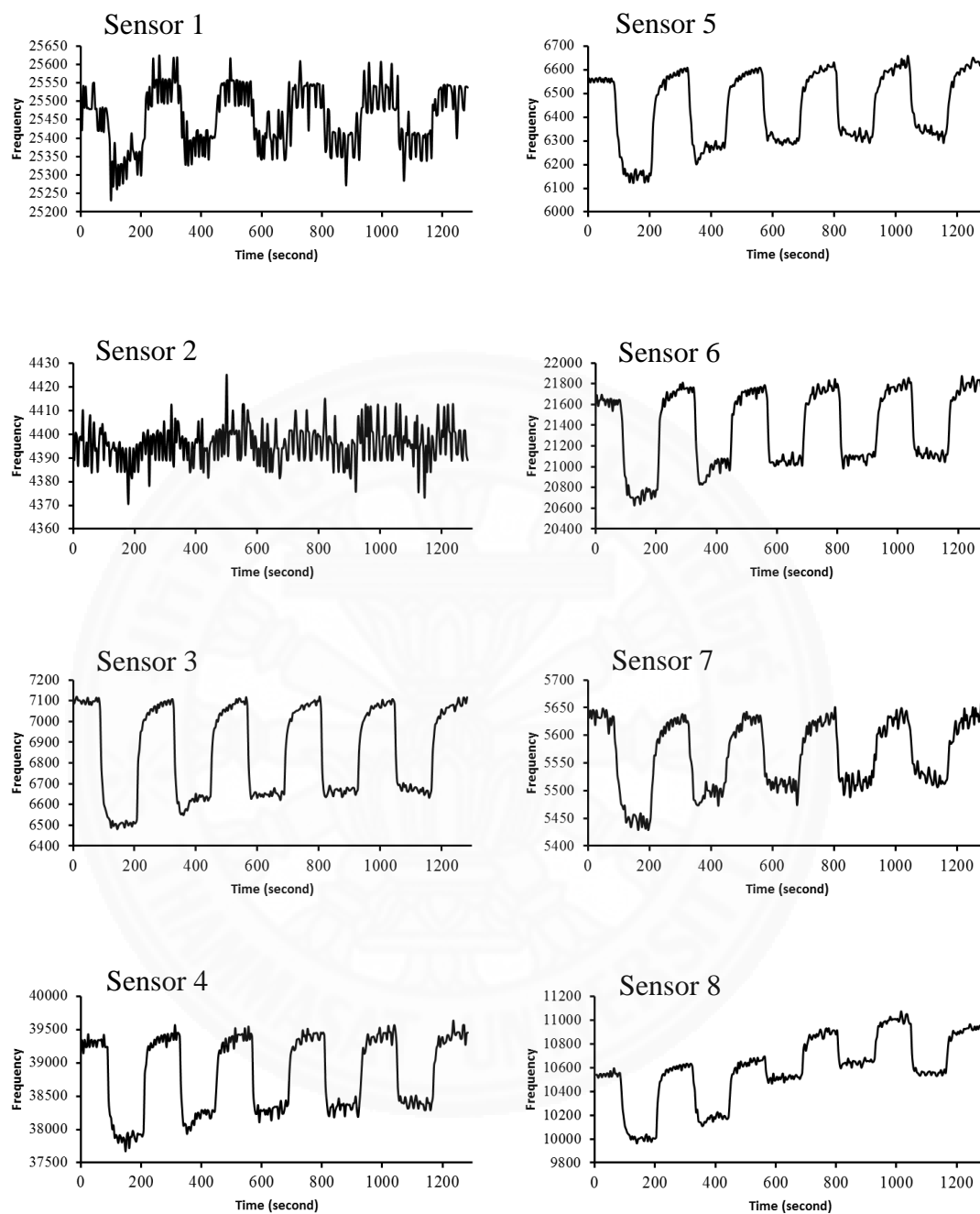


Figure 74. The dynamic response of Ag-TOBPP film in the presence of iso-propanol vapor.

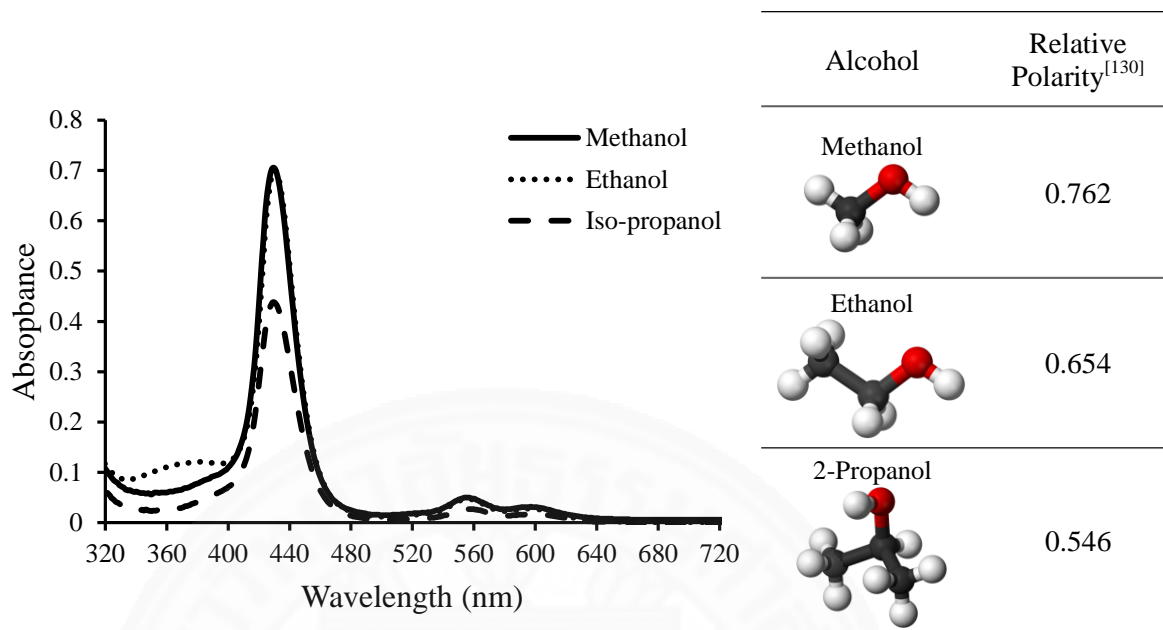


Figure 75. The UV-Vis spectra of Ag-TOBPP in various alcohol solvent.

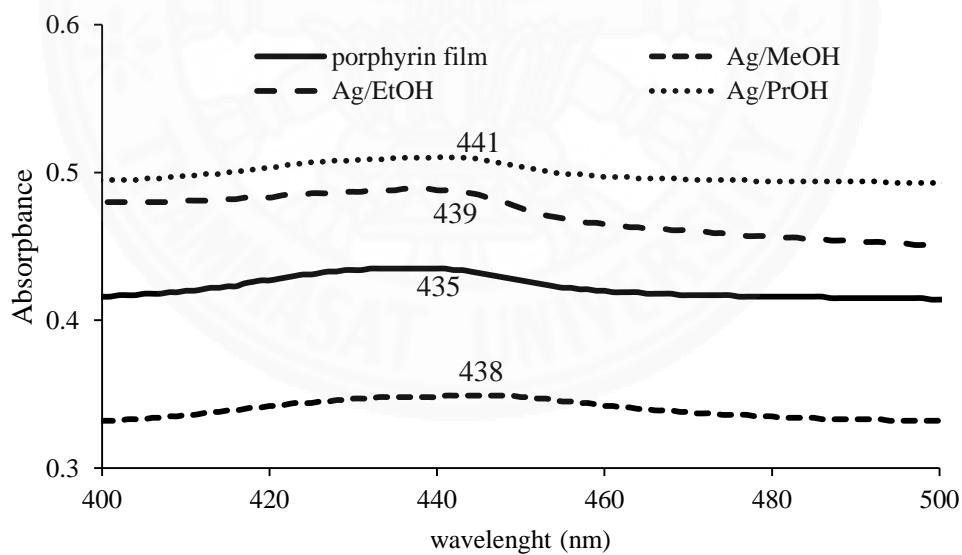


Figure 76. The UV-Vis spectra of Ag-TOBPP film.

To prove the weak absorption of red light and infrared radiation, the Ag-TOBPP was dissolved in various alcohols and the UV-vis absorption was shown in Figure 75. The methanol and ethanol gave better absorption spectra than iso-propanol and for all sample observed very weak absorption range for 638 nm (red) and >700 nm (infrared). The low absorption of iso-propanol related to the low polarity of the molecule and steric hindrance that slower the interaction between iso-propanol and Ag-TOBPP molecule.

4.4.2 Principal component analysis (PCA)

The absorption data from Figure 77-78 were detected and analyzed by using PCA program. PCA is a common tool for classification of the data by reducing abundant information into limited data space dimensions and a simple linear analysis method. In this experiment, PCA was used as a pattern recognition method to classify the data set produced from E-nose. The data sets for all Ag(II) porphyrins were analyzed independently by PCA. The principal components have been computed iteratively for separation of methanol, ethanol and iso-propanol vapors based on PC1 and PC2 axis. Figure 77-78 shows two-dimensional score plot PCA related to the optical response of the Ag(II) porphyrins film to alcohols. The long carbon chain number of PC1 and PC2 represented an effectiveness of data group, which can be implied that the sample is a good sensor.

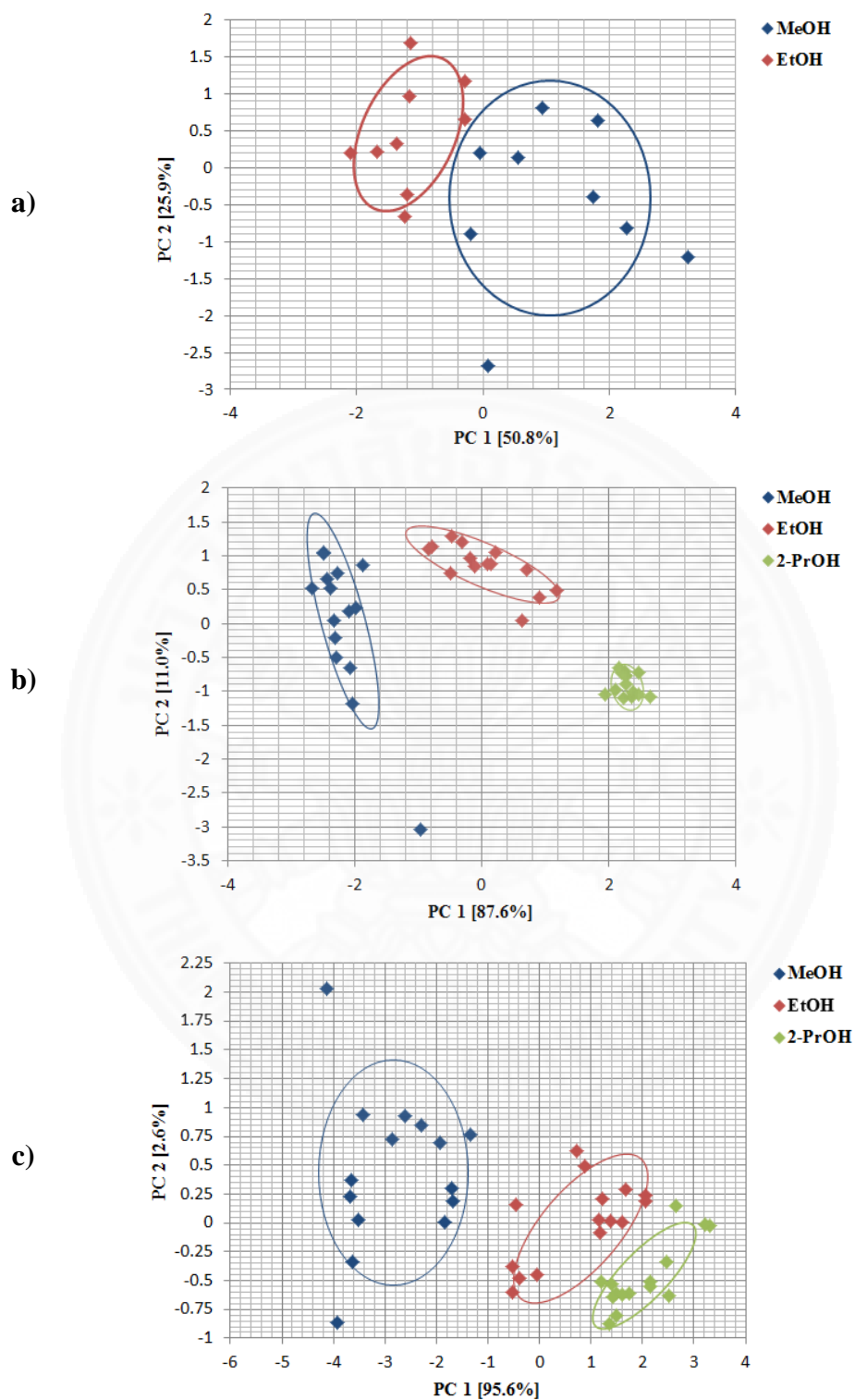


Figure 77. PCA plot of the optical response of the a) Ag-TTPP b) Ag-TOMPP c) Ag-TOBPP to alcohol vapors (methanol, ethanol and iso-propanol).

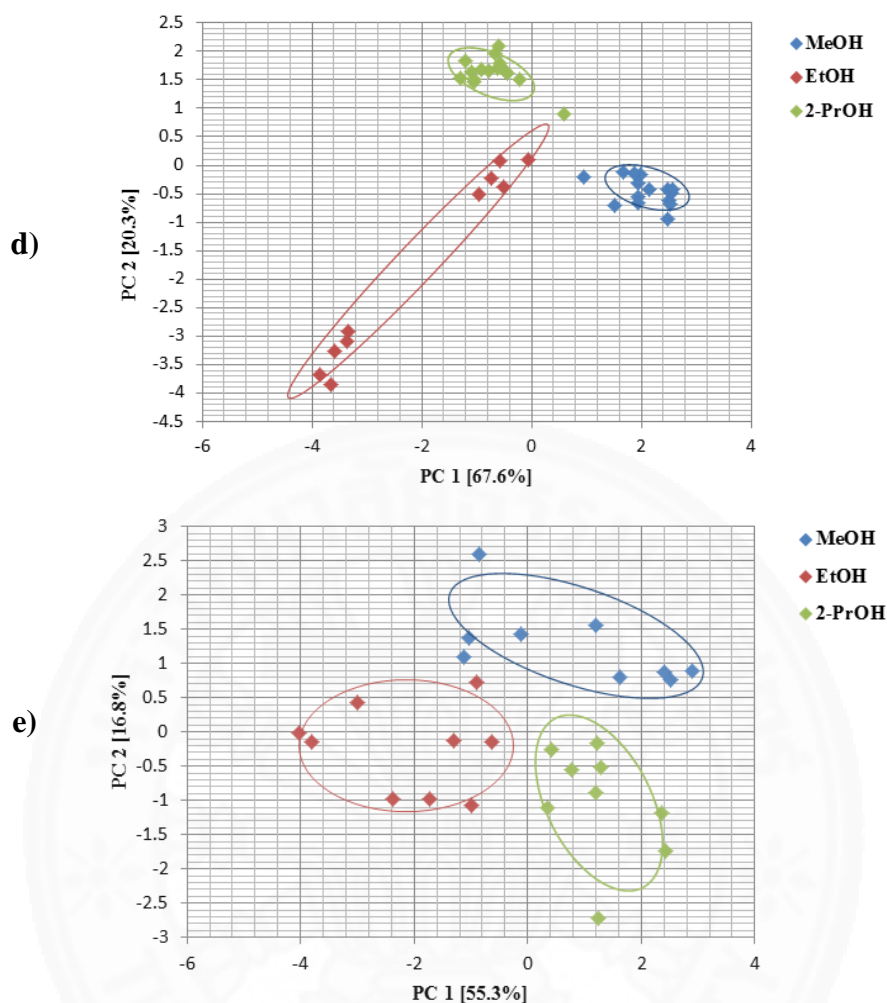


Figure 78. PCA plot of the optical response of the d) Ag-TOOPP and e) Ag-TODPP to alcohol vapors (methanol, ethanol and iso-propanol).

The results for all Ag(II) sensing evidently illustrated distinctive clustering of the data corresponding to methanol, ethanol, and iso-propanol with a good sensitivity, excepting the Ag-TPP sensing. The Ag-TPP film gives a sensitive signal only for only the methanol and ethanol, due to the electron transfer from alcohol molecules to Ag-TPP. The similar result was reported by Sureporn U. *et al.* [90]. Moreover, the iso-propanol molecule is larger than methanol and ethanol, thus the interaction between the oxygen atom in the alcohol molecule and the Ag atom in Ag-TPP complex is difficult. Also, the alkyl long chain in porphyrin ring causes decreasing sensitivity, due to the steric of the carbon-long chain, which it can block the interacted position of Ag atom.

The previous report, Sumana K. *et al.* presented the optical sensing respond of Mg-TPP thin film for the detection of alcohol vapors. They proposed the Mg-TPP film gives a very effective in the discrimination of methanol, ethanol and iso-propanol vapor with PC1 (85.39 %) and PC2 (6.91 %), already account for 92.3 % for the information. Moreover, the density functional theory (DFT) calculations were used to investigate the interaction energy between the oxygen of alcohol molecule with Mg atom in the central hole of porphyrin molecule. The result reveals the interaction energy between Mg-TPP with methanol is higher than ethanol due to the methanol exhibits the highest value of electron charge transfer from alcohol molecule to Mg-TPP [92].

Table 14. Summarized result of PCA data based on PC1 and PC2 axis.

Porphyrin film	PCA percentage (%)		
	PC1	PC2	PC1+PC2
Ag-TPP	50.8	25.9	76.7
Ag-TOMPP	87.6	11.0	98.6
Ag-TOBPP	95.6	2.6	98.2
Ag-TOOPP	67.6	20.3	87.6
Ag-TODPP	55.3	16.8	72.1

The data from Table 14 showed the relationship of long chained hydrocarbon on *para*- position of Ag-TPP derivatives vs. sensitive (PC1+PC2). The Ag-TPP has no substitution on *para*- position, while the other Ag-TPP derivatives have O-R (alkoxy group) at *para*- position, while –O- may form the hydrogen bond between alcohol and oxygen atom. However, the further study by DFT calculation may need.

The Ag-TOMPP sensing had the highest efficiency for discriminating alcohol vapor than another sensing with PC1 (87.6%) and PC2 (11.0%), already account for 98.6% for the information. The increasing of the alkyl long chain, the sensitivity is decreased as 98.2%, 87.6% and 72.1% of Ag-TOBPP, Ag-TOOPP and Ag-TODPP film, respectively. Therefore, it can be summarized that Ag-TOMPP, Ag-TOBPP has high potential for alcohol sensor.

CHAPTER 5

CONCLUSIONS AND RECOMMENDATIONS

Three benzaldehydes with long chain alkane, including butyloxybenzaldehyde **1**, octyloxybenzaldehyde **2** and dectyloxybenzaldehyde **3** have been successfully prepared from the modification of published method by Ioannis D.K. *et al.* The mass spectrometry (MS), ^1H , ^{13}C NMR and IR spectroscopy were confirmed their expected structure of alkyloxybenzaldehyde product without purification. The synthesized aldehyde (compound **1-3**) gave the high yield as over 60%.

The series substituent at the para- position of the alkoxy group of meso-tetraphenyl porphyrins were synthesized by a modification of Alder-Longo method. The suitable reaction condition by refluxing in propionic acid for 2 hours which used to synthesize free base porphyrins (TPP **4**, TOMPP **5**, TOBPP **6**, TOOPP **7** and TODPP **8**) and were obtained in range 5 to 25% yield, which the alkoxy long chain was substituted in porphyrin ring gave low yield while TOMPP **5** gave the highest yield as 26%.

Furthermore, the silver(II) porphyrin derivatives were synthesized by refluxing free base porphyrin product with silver(I) nitrate in the mixed solvent of dichloromethane and *N,N*-dimethylformamide. The reaction of ligands and silver nitrate provided Ag-TPP **9**, Ag-TOMPP **10**, Ag-TOBPP **11**, Ag-TOOPP **12** and Ag-TODPP **13** in 74% 57% 48% 63% and 52% yield, respectively. The yield of silver(II) porphyrins had higher than free base porphyrins due to the size of metal ion that perfectly fitted into the central hole of porphyrin ring. The structure of porphyrin and silver(II) porphyrin were confirmed by the elemental analysis (CHN), mass spectrometry (MS), ^1H and ^{13}C -NMR and IR spectroscopy.

The UV-Vis absorption spectra of free base porphyrins exhibited a strong intensity band (S-band) with four low intensity absorption (Q-band), while the silver(II) porphyrin complexes showed a single Soret band with only one Q band in dichloromethane solvent. The absorption spectra of all free base porphyrins and silver(II) porphyrins moved to small red shift when the carbon number of alkyl long chain was increased due to the signature of an effective intramolecular charge transfer

and may relate to the electron-donating effect. When excitation of the free base porphyrins at 534 nm, the products exhibited the emitted fluorescence spectra at 654 nm, when excited at 529 nm and showed the fluorescence spectrum at 649 nm. The calculated energy gap was observed at 1.92 for TPP **4** and 1.90 for other free base porphyrins.

For the antibacterial activity of all porphyrins indicated that the compounds have been sensitive against both of gram positive bacteria *Staphylococcus aureus* and gram negative bacteria *Escherichia coli*. In the case of disc diffusion method, TOMPP **5** shows the greater zone of inhibition while the metalloporphyrins as Ag-TODPP **13** has more effective inhibitory activity than others. The minimum inhibitory concentration (MIC) and the minimum bactericidal concentration (MBC) of silver(II) porphyrin derivatives have been investigated. The complexes founded the MIC value at concentration 320 ppm and 160 ppm for against *S. aureus* and *E. coli*, excepting Ag-TODPP **13** displayed MIC value of *E. coli* at 80 ppm. Whereas the MBC values of all porphyrins were found at 640 ppm and 160 ppm for *S. aureus* and *E. coli* respectively, excepting Ag-TPP **9** and Ag-TODPP **13** exhibited MBC value at 320 ppm for *S. aureus* and at 80 ppm for against *E. coli* of Ag-TODPP **13**.

Moreover, the synthesized silver(II) porphyrins were fabricated as a film by dropped coated on the glass slide for study the sensor application. The porphyrin films were tested by Electronic nose under the flow of alcohol vapors such as methanol, ethanol, and iso-propanol at 25 °C. The principal component analysis (PCA) program was used to analyze the obtained data from an electronic nose. The result found that all silver(II) complexes can be used as a gas sensor for alcohol vapors (methanol, ethanol, and iso-propanol) with a good sensitivity as 98.6%, 98.2%, 87.6% and 72.1% for Ag-TOMPP **10**, Ag-TOBPP **11**, Ag-TOOPP **12** and Ag-TODPP **13**, respectively.

The result shows that all silver porphyrins derivative has high potential to develop for gas sensor and good antibacterial activity.

REFERENCES

1. Harrison, H. R., Hodder, O. J. R. and Crawfoot, H.D.(1971) Crystal and molecular structure of 8,12-diethyl-2,3,7,13,17,18-hexamethylcorrole. *Journal of the Chemical Society B: Physical Organic* 0. 640-645.
2. Porphyrin-http://shodhganga.inflibnet.ac.in/bitstream/10603/323/3/06_chapter1.pdf. Retrieved October 07, 2015.
3. Merritt, J. and Loening, K. L. (1979) Nomenclature of Tetrapyrroles. *Pure And Applied Chemistry* 51, 2251–2304.
4. Abraham, R.J., Medforth, C.J., Mansfield, K.E., Simpson, D.J. and Smith, K.M. (1988). *Perkin Transactions 2. Journal of the Chemical Society*, 1365.
5. Milgrom L. R. (1997). *The colours of life: an introduction to the chemistry of porphyrins and related compounds*. Oxford University Press, Oxford.
6. Battersby, A. R., Fookes, C. J. R., Matcham, G. W. J. and McDonald, E. (1980) Biosynthesis of the pigments of life: formation of the macrocycle. *Nature* 285, 17-21.
7. Messerschmidt, A., Huber, R., Poulos, K. and Wieghardt K. (2001). *Handbook of metalloproteins*, vols 1 & 2. John Wiley & Sons, Ltd, Chichester.
8. Heme -<http://en.wikipedia.org>. Retrieved September 10, 2014.
9. Heme-www.chemistry.wustl.edu/~edudev/LabTutorials/Hemoglobin/MetalComplexinBlood.html. Retrieved October 22, 2015.
10. Heme -<http://www.bio.davidson.edu>. Retrieved September 10, 2014.
11. Brockmann, H. JR.(1978). In *Porphyrins*. Dolphin, D. Ed., Academic Press: New York.
12. Chlorophyll -<http://www.ch.ic.ac.uk>. Retrieved September 10, 2014.
13. Mauzerall, D.(1977) In *Photosynthesis I*. Trebst, P. D. A., Avron, P. D. M., Eds.; *Encyclopedia of Plant Physiology*, Springer Berlin Heidelberg, 117–124.
14. Scott, J. M. and Molloy, A. M. (2012) The Discovery of Vitamin B12. *Annals of Nutrition and Metabolism* 61(3), 239–245.
15. Thackray, S. J., Mowat, C. G. and Chapman, S. K. (2008) Exploring the mechanism of tryptophan 2,3-dioxygenase. *Biochemical Society Transactions* 36(Pt 6), 1120–1123.

16. Vitamin B12 -<http://en.wikipedia.org>. Retrieved September 10, 2014.
17. Smith, E.L., Hill, R.L., Lehman, I.R., Lefkowitz, R.J., Handler, P. and White, A. (1983) Principles of Bio-Chemistry-General Aspects (7th Edition), McGraw-Hill Inc., Singapore.
18. Hughes, M. N. (1988). The Inorganic Chemistry of Biological Processes, (2nd Edition), John Wiley and Sons, New York.
19. Lehuyet, A.L. (1978). Biochemistry, (2nd Edition), Kalyan publishers, New Delhi.
20. Enzyme-<http://en.wikipedia.org/wiki/Enzyme>. Retrieved October 22, 2015.
21. Marsh, E.N. (1999) Coenzyme B12 (cobalamin)-dependent enzymes. Essays Biochem 34, 54-139.
22. Bajju, G.D., Singh, N. and Deepmala. (2014) Synthesis and Characterization of New Meso-Substituted and β -Substituted Unsymmetrical Metalloporphyrins. Chemical Science Transactions 3(1), 314-322.
23. Dehghani, H. and Fathi, F. (2008) Molecular complexation of meso-tetraphenylporphyrins with SO₂. Dyes and Pigments 77, 323-326.
24. Rothmund, P. (1935) Formation of porphyrins from pyrrole and aldehydes. Journal of the American Chemical Society 57, 2010-2011.
25. Rothmund, P. (1936) A new porphyrin synthesis. The synthesis of porphin. Journal of the American Chemical Society 58(4), 625-627.
26. Adler, A.D., Longo, F.R. and Shergalis, W. (1964) Mechanistic investigations of porphyrin syntheses I. Preliminary studies on meso-tetraphenylporphin. Journal of the American Chemical Society 86, 3145-3149.
27. Shy, H., Mackin, P., Orvieto, A.S., Gharbharan, D., Peterson, G.R., Bampos, N. and Hamilton, T.D. (2014) Two-step Mechanochemical Synthesis of Porphyrins. Faraday Discuss 170, 59-69.
28. Lindsey, J.S., Hsu, H.C. and Schreiman, I.C. (1986) Synthesis of Tetraphenylporphyrins Under Very Mild Conditions. Tetrahedron Letters 27, 4969-4970.
29. Arsenault, G.P., Bullock, E. and MacDonald, S.F. (1960) Pyrromethanes and porphyrins therefrom¹. Journal of the American Chemical Society 82, 4384-4389.

30. Zhou, W., Cao, Z., Jiang, S., Huang, H., Deng, L., Liu, Y. *et al* (2012) Porphyrins modified with a low-band-gap chromophore for dye-sensitized solar cells. *Organic Electronics: physics, materials, applications* 13, 560–569.
31. Mathew, S., Yella, A., Gao, P., Humphry-Baker, R., CurchodBasile, F.E., Ashari-Astani, N. *et al* (2014) Dye-sensitized solar cells with 13% efficiency achieved through the molecular engineering of porphyrin sensitizers. *Nature Chemistry* 6(3), 242–247.
32. Arteaga, D., Cotta, R., Ortiz, A., Insuasty, B., Martin, N. and Echegoyen, L. (2015) Zn (II)-porphyrin dyes with several electron acceptor groups linked by vinyl-fluorene or vinyl-thiophene spacers for dye-sensitized solar cells. *Dyes Pigments* 112, 127–137.
33. Waltera, M.G., Rudineb, A.B. and Wamser, C.C. (2010) Porphyrins and phthalocyanines in solar photovoltaic cells. *Journal of Porphyrins and Phthalocyanines* 14, 759–792.
34. Groves, J.T. and Kruper, W.J. (1985) Metalloporphyrins in Oxidative Catalysis. Oxygen Transfer Reactions of Oxochromium Porphyrins. *Israel Journal of Chemistry* 25, 148-154.
35. Lammer, A.D., Cook, M.E. and Sessler, J.L. (2015) Synthesis and anti-cancer activities of a water soluble gold(III) porphyrin. *Journal of Porphyrins and Phthalocyanines* 19(01-03), 398–403.
36. Stojiljkovic, I., Evavold, B.D. and Kumar, V. (2001)Antimicrobial properties of porphyrins. *Expert Opinion on Investigational Drugs*10, 309–320.
37. Kondo, H., Nara, J. and Ohno, T. (2011) Possibility of Gas Sensor Using Electronic Transport Properties of Iron–Porphyrin Molecular Junction System. *The Journal of Physical Chemistry C* 115(14), 6886–6892.
38. Sternberg, E.D. and Dolphin, D. (1998) Porphyrin-based Photosensitizers for Use in Photodynamic Therapy. *Tetrahedron* 54, 4151-4202.
39. Yoon, I., Li, J.Z. and Shim, Y.K. (2013) Advance in Photosensitizers and Light Delivery for Photodynamic Therapy. *Clinical Endoscopy* 46(1), 7–23.
40. Dunbar, A. D. F., Brittle, S., Richardson, T.H., Hutchinson, J. and Hunter, C.A. (2010) Detection of Volatile Organic Compounds Using Porphyrin Derivatives. *Journal of Physical Chemistry B* 114(36), 11697–11702.

41. Li, L.L. and Diau, E.W. (2013) Porphyrin-sensitized solar cells. *Chemical Society Reviews* 42(1), 291-304.
42. Yuichi T., Brian O. P. and David H.D. (2002). Synthesis, crystal structures, and redox potentials of 2,3,12,13-tetrasubstituted 5,10,15,20-tetraphenylporphyrin zinc(II) complexes. *Inorganic Chemistry*, 41, 6703-6710.
43. Ana, P.J., Antonio C.T., Cláudio, R.N., Maria, E.F.G., Osvaldo, A.S. and Yassuko, I. (2004). Synthesis, spectroscopy and photosensitizing properties of hydroxyl nitrophenylporphyrins. *Journal of the Brazilian Chemical Society*, 15, 708-713.
44. Temelli, B. and Unaleroglu, C. (2009) Synthesis of meso-tetraphenyl porphyrins via condensation of dipyrromethanes with N-tosyl imines. *Tetrahedron* 65(10), 2043-2050.
45. Xue, Z., Lee, P.P.S., Wang, Y., Kwong, D.W.J., Li, J., Xin, J.H., Wong, W.-K. and Cheuk, K.K.L. (2011) Further insight into aryl nitration of tetraphenylporphyrin. *Tetrahedron* 67(33), 6030-6035.
46. Gal, E., Brem, B., Perețeanu, I., Găină, L., Lovasz, T., Perde-Schrepler, M., Silaghi-Dumitrescu, L., Cristea, C. and Silaghi-Dumitrescu, L. (2013) Novel meso-phenothiazinylporphyrin dyes: Synthesis, optical, electrochemical properties and PDT assay. *Dyes and Pigments* 99(1), 144-153.
47. Fagadar-Cosma, E., Sebarchievici, I., Lascu, A., Creanga, I., Palade, A., Birdeanu, M., Taranu, B. and Fagadar-Cosma, G. (2016) Optical and electrochemical behavior of new nano-sized complexes based on gold-colloid and Co-porphyrin derivative in the presence of H₂O₂. *Journal of Alloys and Compounds* 686, 896-904.
48. Wu, Y., Liu, J.-C., Guo, W.-B., Li, R.-Z. and Jin, N.-Z. (2016) Three horizontal anchor porphyrins for dye-sensitized solar cells: An optical, electrochemical and photovoltaic investigation. *Polyhedron* 117, 155-160.
49. Yadav, P. and Sankar, M. (2017) Facile synthesis, photophysical and electrochemical redox properties of octa- and tetracarboxamidophenylporphyrins and the first example of amido-imidol tautomerism in porphyrins. *Dyes and Pigments* 139, 651-657.

50. Kostas, I.D., Coutsolelos, A.G., Charalambidis, G. and Skondra, A. (2007) The first use of porphyrins as catalysts in cross-coupling reactions: a water-soluble palladium complex with a porphyrin ligand as an efficient catalyst precursor for the Suzuki–Miyaura reaction in aqueous media under aerobic conditions. *Tetrahedron Letters* 48(38), 6688-6691.
51. Fedulova, I.N., Bragina, N.A., Novikov, N.V., Ugol'nikova, O.A. and Mironov, A.F. (2007) Synthesis of lipophilic tetraphenylporphyrins to design lipid-porphyrin ensembles. *Russian Journal of Bioorganic Chemistry* 33(6), 589-593.
52. Fedulova, I.N., Bragina, N.A., Novikov, N.V., Mironov, A.F., Bykova, V.V., Usol'tseva, N.V. and Ananieva, G.A. (2008) Synthesis and mesomorphism of tetraphenylporphyrin derivatives. *Mendeleev Communications* 18(6), 324-326.
53. Cao, H., Zhao, H.-B., Zhou, F.-H., Liu, J.-P. and Liu, Y.-L. (2008) Crystal Structure of Meso-tetrakis[4-(pentyloxy)phenyl]porphyrin. *Journal of Chemical Crystallography* 39(1), 51-54.
54. Wang, C., Yang, G., Li, J., Mele, G., Slota, R., Broda, M., Duan, M., Vasapollo, G., Zhang, X. and Zhang, F. (2009) Novel meso-substituted porphyrins: Synthesis, characterization and photocatalytic activity of their TiO₂-based composites. *Dyes and Pigments* 80(3), 321-328.
55. Sun, E., Sun, Z., Yuan, M., Wang, D. and Shi, T. (2009) The synthesis and properties of meso-tetra(4-alkylamidophenyl)porphyrin liquid crystals and their Zn complexes. *Dyes and Pigments* 81(2), 124-130.
56. Novikov, N.V., Formirovsky, K.A., Bragina, N.A., Mironov, A.F., Anan'eva, G.A., Bykova, V.V. and Usol'tseva, N.V. (2010) Synthesis and mesomorphism of cationic derivatives of meso-aryl-substituted porphyrins and their metal complexes. *Mendeleev Communications* 20(4), 239-241.
57. Kirll A.F., Natal'ya A.B. Andrey F.M., Galina A.A., Venera V.B. and Nadezhda V.U. (2011). Novel alkoxyaryl substituted porphyrins with terminal carboxymethyl and carboxy groups: synthesis and mesomorphic properties. *Macroheterocycles*, 4(2), 127-129.
58. Formirovsky, K.A., Bragina, N.A., Mironov, A.F., Anan'eva, G.A., Bykova, V.V. and Usol'tseva, N.V. (2012) Synthesis and Liquid-crystal Properties of

- New Amphiphilic Long-chain Derivatives of Meso-arylporphyrins with Terminal Polar Groups. *Mendeleev Communications* 22(5), 278-280.
59. Moonsin, P., Sirithip, K., Jungsuttiwong, S., Keawin, T., Sudyoadsuk, T. and Promarak, V. (2011) meso-Multi(iodophenyl) porphyrins: synthesis, isolation, and identification. *Tetrahedron Letters* 52(37), 4795-4798.
 60. Zyablikova, E.S., Bragina, N.A. and Mironov, A.F. (2012) Covalent-bound Conjugates of Fullerene C₆₀ and Metal Complexes of Porphyrins with Long-chain Substituents. *Mendeleev Communications* 22(5), 257-259.
 61. Zhao, H.B., Chen, L., Wang, B.Y., Liao, J.X. and Xu, Y.J. (2013) meso-Tetrakis[4-(heptyloxy)phenyl]porphyrin. *Acta Crystallogr C* 69(Pt 6), 651-653.
 62. Liao, J.X., Zhao, H.B., Yang, D.L., Chen, L. and Wang, B.Y. (2011) {meso-Tetra-kis[p-(hept-yloxy)phen-yl]-porphyrinato}silver(II). *Acta Crystallogr Sect E Struct Rep Online* 67(Pt 9), m1316.
 63. Liu, W., Shi, Y., Shi, T., Liu, G., Liu, Y., Wang, C. and Zhang, W. (2003) Synthesis and characterization of liquid crystalline 5, 10, 15, 20-tetrakis(4-n-alkanoyloxyphenyl)porphyrins. *Liquid Crystals* 30(11), 1255-1257.
 64. Wu, Y.-h., Chen, L., Yu, J., Tong, S.-l. and Yan, Y. (2013) Synthesis and spectroscopic characterization of meso-tetra (Schiff-base substituted phenyl) porphyrins and their zinc complexes. *Dyes and Pigments* 97(3), 423-428.
 65. Zhang, Y.J., Shi, J., Liu, W. and Yu, M. (2013) 5, 10, 15, 20-Tetra (N-Long Chain-Alkyl Carbazole) Porphyrin and Their Lanthanide Complexes. *Synthesis and Reactivity in Inorganic, Metal-Organic, and Nano-Metal Chemistry* 43(5), 640-646.
 66. Gautam, R. and Chauhan, S.M. (2014) Surfactant assisted self-assembly of zinc 5,10-bis (4-pyridyl)-15,20-bis (4-octadecyloxyphenyl) porphyrin into supramolecular nanoarchitectures. *Mater Sci Eng C Mater Biol Appl* 43, 447-457.
 67. Jiblaoui, A., Leroy-Lhez, S., Ouk, T.S., Grenier, K. and Sol, V. (2015) Novel polycarboxylate porphyrins: synthesis, characterization, photophysical properties and preliminary antimicrobial study against Gram-positive bacteria. *Bioorg Med Chem Lett* 25(2), 355-362.

68. Misra, R. and Gautam, P. (2015) Meso-tetrakis(ferrocenylethynylphenyl) porphyrins: Synthesis and properties. *Journal of Organometallic Chemistry* 776, 83-88.
69. Korolev, V.V., Lomova, T.N., Maslennikova, A.N., Korolev, D.V., Shpakovsky, D.B., Zhang, J. and Milaeva, E.R. (2016) Magnetocaloric properties of manganese(III) porphyrins bearing 2,6-di-tert-butylphenol groups. *Journal of Magnetism and Magnetic Materials* 401, 86-90.
70. Lu, F., Wang, X., Zhao, Y., Yang, G., Zhang, J., Zhang, B. and Feng, Y. (2016) Studies on D-A- π -A structured porphyrin sensitizers with different additional electron-withdrawing unit. *Journal of Power Sources* 333, 1-9.
71. Deyab, M.A., Mele, G., Al-Sabagh, A.M., Bloise, E., Lomonaco, D., Mazzetto, S.E. and Clemente, C.D.S. (2017) Synthesis and characteristics of alkyd resin/M-Porphyrins nanocomposite for corrosion protection application. *Progress in Organic Coatings* 105, 286-290.
72. Angaridis, P.A., Lazarides, T. and Coutsolelos, A.C. (2014) Functionalized porphyrin derivatives for solar energy conversion. *Polyhedron* 82, 19-32.
73. Zhang, N., Zhang, B., Yan, J., Xue, X., Peng, X., Li, Y., Yang, Y., Ju, C., Fan, C. and Feng, Y. (2015) Synthesis of π -A-porphyrins and their photoelectric performance for dye-sensitized solar cells. *Renewable Energy* 77, 579-585.
74. Zhao, H., Long, J., Luo, X., Zhao, B. and Tan, S. (2015) 2-Ethynyl-6-methylthieno[3,2- b]thiophene as an efficient π spacer for porphyrin-based dyes. *Dyes and Pigments* 122, 168-176.
75. Cheng, H.-L., Huang, Z.-S., Wang, L., Meier, H. and Cao, D. (2017) Synthesis and photovoltaic performance of the porphyrin based sensitizers with 2 H - [1,2,3]triazolo[4,5- c]pyridine and benzotriazole as auxiliary acceptors. *Dyes and Pigments* 137, 143-151.
76. Song, H., Li, X., Ågren, H. and Xie, Y. (2017) Branched and linear alkoxy chains-wrapped push-pull porphyrins for developing efficient dye-sensitized solar cells. *Dyes and Pigments* 137, 421-429.
77. Chae, S.H., Kim, H., Kim, J.Y., Kim, S.-J., Kim, Y. and Lee, S.J. (2016) Preparation of new semiconducting tetraphenylethynyl porphyrin derivatives

- and their high-performing organic field-effect transistors. *Synthetic Metals* 220, 20-24.
78. Xu, X.-J., Xue, Z., Qi, Z.-D., Hou, A.-X., Li, C.-H. and Liu, Y. (2008) Antibacterial activities of manganese(II) ebselen–porphyrin conjugate and its free components on *Staphylococcus aureus* investigated by microcalorimetry. *Thermochimica Acta* 476(1-2), 33-38.
 79. Rojkiewicz, M., Kuś, P., Kozub, P. and Kempa, M. (2013) The synthesis of new potential photosensitizers [1]. Part 2. Tetrakis-(hydroxyphenyl)porphyrins with long alkyl chain in the molecule. *Dyes and Pigments* 99(3), 627-635.
 80. Tovmasyan, A., Babayan, N., Poghosyan, D., Margaryan, K., Harutyunyan, B., Grigoryan, R., Sarkisyan, N., Spasojevic, I., Mamyan, S., Sahakyan, L., Aroutiounian, R., Ghazaryan, R. and Gasparyan, G. (2014) Novel amphiphilic cationic porphyrin and its Ag(II) complex as potential anticancer agents. *J Inorg Biochem* 140, 94-103.
 81. Mamone, L., Ferreyra, D.D., Gándara, L., Di Venosa, G., Vallecorsa, P., Sáenz, and D., Calvo, G. *et al.* (2016) Photodynamic inactivation of planktonic and biofilm growing bacteria mediated by a meso-substituted porphyrin bearing four basic amino groups, *Journal of Photochemistry and Photobiology B: Biology* 161, 222-229.
 82. Malatesti, N., Harej, A., Kraljevic Pavelic, S., Loncaric, M., Zorc, H., Wittine, K., Andjelkovic, U. and Josic, D. (2016) Synthesis, characterisation and in vitro investigation of photodynamic activity of 5-(4-octadecanamidophenyl)-10,15,20-tris(N-methylpyridinium-3-yl)porphyrin trichloride on HeLa cells using low light fluence rate. *Photodiagnosis Photodyn Ther* 15, 115-126.
 83. Puangmalee, S., Petsom, A. and Thamyongkit, P. (2009) A porphyrin derivative from cardanol as a diesel fluorescent marker. *Dyes and Pigments* 82(1), 26-30.
 84. Figueira, A.C.B., de Oliveira, K.T. and Serra, O.A. (2011) New porphyrins tailored as biodiesel fluorescent markers. *Dyes and Pigments* 91(3), 383-388.
 85. Sandrino, B., Clemente, C.d.S., Oliveira, T.M.B.F., Ribeiro, F.W.P., Pavinatto, F.J., Mazzetto, S.E., de Lima-Neto, P., Correia, A.N., Pessoa, C.A. and Wohnrath, K. (2013) Amphiphilic porphyrin-cardanol derivatives in Langmuir

- and Langmuir–Blodgett films applied for sensing. *Colloids and Surfaces A: Physicochemical and Engineering Aspects* 425, 68-75.
86. Jiang, X., Gou, F., Fu, X. and Jing, H. (2016) Ionic liquids-functionalized porphyrins as bifunctional catalysts for cycloaddition of carbon dioxide to epoxides. *Journal of CO2 Utilization* 16, 264-271.
 87. Spadavecchia, J., Ciccarella, G., Siciliano, P., Capone, S. and Rella, R. (2004) Spin-coated thin films of metal porphyrin–phthalocyanine blend for an optochemical sensor of alcohol vapours. *Sensors and Actuators B: Chemical* 100(1-2), 88-93.
 88. Lvova, L., Paolesse, R., Di Natale, C. and D’Amico, A. (2006) Detection of alcohols in beverages: An application of porphyrin-based Electronic tongue. *Sensors and Actuators B: Chemical* 118(1-2), 439-447.
 89. Tonezzer, M., Quaranta, A., Maggioni, G., Carturan, S. and Mea, G.D. (2007) Optical sensing responses of tetraphenyl porphyrins toward alcohol vapours: A comparison between vacuum evaporated and spin-coated thin films. *Sensors and Actuators B: Chemical* 122(2), 620-626.
 90. Uttiya, S., Kerdcharoen, T., Na-Ayutthaya, P.D., Bhanthumnavin, W., Buntem, R. and Pratontep, S. (2007). Optical Gas Sensor Array Based on Metallo-Phthalocyanines and Metallo-Porphyrins, ECTI-CON 2007 The 2007 ECTI International Conference, 180-183.
 91. Kladsomboon, S., Pratontep, S., Uttiya, S. and Kerdcharoen, T. (2008) Alcohol gas sensors based on magnesium tetraphenyl porphyrins, Nanoelectronics Conference (INEC) 2008 2nd International, 585-588.
 92. Kladsomboon, S. and Kerdcharoen, T. (2012) A method for the detection of alcohol vapours based on optical sensing of magnesium 5,10,15,20-tetraphenyl porphyrin thin film by an optical spectrometer and principal component analysis. *Anal Chim Acta* 757, 75-82.
 93. Roales, J., Pedrosa, J.M., Castillero, P., Cano, M. and Richardson, T.H. (2011) Optimization of mixed Langmuir–Blodgett films of a water insoluble porphyrin in a calixarene matrix for optical gas sensing. *Thin Solid Films* 519(6), 2025-2030.

94. Shirsat, M.D., Sarkar, T., Kakoullis, J., Jr., Myung, N.V., Konnanath, B., Spanias, A. and Mulchandani, A. (2012) Porphyrins-Functionalized Single-Walled Carbon Nanotubes Chemiresistive Sensor Arrays for VOCs. *J Phys Chem C Nanomater Interfaces* 116(5), 3845-3850.
95. Lin, Y., Lin, H. and Lin C. (2012) Preparation of meso-tetra(4-pyridyl)porphyrin film for optical gas sensor, *Sensors Based on Optical Techniques, 14th International Meeting on Chemical Sensors - IMCS 2012*, 946 - 949
96. Peter, C., Schmitt, K., Apitz, M. and Woellenstein, J. (2012) Metallo-porphyrin zinc as gas sensitive material for colorimetric gas sensors on planar optical waveguides. *Microsystem Technologies* 18(7-8), 925-930.
97. Palade, A., Fagadar-Cosma, G., Lascu, A., Creanga, I., Birdeanu, M. and Fagadar-Cosma, E. (2013) New Porphyrin -Based Spectrophotometric Sensor For Ag⁰ Detection. *Digest Journal of Nanomaterials and Biostructures* 8. 1013–1022.
98. Esteves, C.H.A., Iglesias, B.A., Li, R.W.C., Ogawa, T., Araki, K. and Gruber, J. (2014) New composite porphyrin-conductive polymer gas sensors for application in electronic noses. *Sensors and Actuators B: Chemical* 193, 136-141.
99. Saxena, S. and Verma, A. L. (2014) Metal-tetraphenylporphyrin functionalized carbon nanotube composites as sensor for benzene, toluene and xylene vapors, *Advanced Materials Letters*. 5(8), 472-478
100. Gutiérrez, A.F., Brittle, S., Richardson, T.H. and Dunbar, A. (2014) A prototype sensor for volatile organic compounds based on magnesium porphyrin molecular films. *Sensors and Actuators B: Chemical* 202, 854-860.
101. Song, F., Ma, P., Chen, C., Jia, J., Wang, Y. and Zhu, P. (2016) Room temperature NO₂ sensor based on highly ordered porphyrin nanotubes. *J Colloid Interface Sci* 474, 51-57.
102. Porphyrin sensing-[http:// sciencedirect.com](http://sciencedirect.com). Retrieved May 1, 2017.
103. Kooriyaden, F.R., Sujatha, S. and Arunkumar, C. (2015) Synthesis, spectral, structural and antimicrobial studies of fluorinated porphyrins. *Polyhedron* 97, 66-74.

104. Vallekobia, A., Kostalova, D. and Sochorova, R. (2001): Isoquinolone alkaloid from *Ahonia aquifolium* stem bark is active against *Malassezia* species. *Folia Microbiology* 46: 107-111.
105. Domingues, M.R.M., S.-Marques, M.G.a.O., Vale, C.A.M., Neves, M.G.a., Cavaleiro, J.A.S. and Ferrer-Correia, A.J. (1998) Do Charge-Remote Fragmentations Occur under Matrix-Assisted Laser Desorption Ionization Post-Source Decompositions and Matrix-Assisted Laser Desorption Ionization Collisionally Activated Decompositions, *American Society for Mass Spectrometry* 10, 217 – 223.
106. Aline, T., Paulo, H.S. and Aloir A.M. (2009). 3,5-Disubstituted isoxazolines as potential molecular kits for liquid-crystalline materials. *European Journal of Organic Chemistry*, 889-897.
107. Mayank, J.M., Javed, G.M., Juvansinh, J.J., Rohit, B.M., and Manish K.S. (2015). An efficient suzuki reaction using a new benzothiazole/Pd(II) species as catalyst in aqueous media. *World Journal of Pharmaceutical Research* 4, 1046-1052.
108. Tossapon Phromsatit. synthesis and characterization of mesotetraphenyl porphyrin derivatives and their copper(II) complexes. Master's Thesis, Department of Chemistry, Faculty of Science and Technology, Thammasat University, 2015.
109. Meng, S., Xu, Z., Hong, G., Zhao, L., Zhao, Z., Guo, J., Ji, H. and Liu, T. (2015) Synthesis, characterization and in vitro photodynamic antimicrobial activity of basic amino acid-porphyrin conjugates. *Eur J Med Chem* 92, 35-48.
110. Dehghani, H. and Shaterian, M. (2009) New Cationic Sandwich-type Intermediate Sitting-atop Complexation between meso-Tetraarylporphyrins and Tantalum(V) Chloride: Synthesis, Spectroscopic Characterization and Photoluminescence Study. *Bulletin of the Korean Chemical Society* 30, 2792 -2794.
111. Zabardasti A. (2012). Molecular interactions of some free base porphyrins with ζ - and π -acceptor molecules, molecular interactions, Prof. Aurelia Meghea (Ed.), ISBN: 978-953-51-0079-9. In Tech, Available from:

<http://www.intechopen.com/books/molecular-interactions/molecular-interactions-of-some-free-basesporphyrins-with-sigma-and-pi-acceptor-molecules>.

112. I-Chin L. and Jyh-Horung C. (1996). Synthesis and characterization of antimony complexes of meso-tetraphenylporphyrin (TPP) and meso-tetra(4-methoxyphenyl)porphyrin (TMPP), and the X-ray crystal structure of [Sb(TMPP)Cl₂]⁺ OH⁻. *Polyhedron*, 15, 3947-3954.
113. Chen, W., El-Khouly, M.E., and Fukuzumi, S. (2011) Saddle Distortion of a Sterically Unhindered Porphyrin Ring in a Copper Porphyrin with Electron-Donating Substituents. *Inorganic. Chemistry* 50 (2). 671–678.
114. Mishira, S., Kaur, S., Tripathi, S.K., Mahajan, C.G. and Saini, G.S.S. (2006). Fourier-transform infrared spectroscopic studies of dithiatetraphenylporphine. *Journal of Chemical Sciences* 118(4), 361-369.
115. Tyulyaeva, E.Y. and Lomova, T.N. (2001) Interaction of Silver(II) and Gold(III) meso-Tetraphenylporphine Complexes with Concentrated Sulfuric Acid. *Russian Journal of Coordination Chemistry* 27, 433–438.
116. Horng Y.J., Wang C.L., Ya L.W. and Jing-Huei P. (2008). Substituent effects in porphyrin dimer complexes studied by IR spectroscopy. *Polyhedron*, 27, 3377-3382.
117. Kewei X., Graham R. and Timothy D.L. (1998). Infrared spectroscopy of geoporphyrins analysis of geochemically significant nickel(II) porphyrins. *Vibrational Spectroscopy*, 18, 157-174.
118. Alexander V.U., Anastasia V.B. and Johannes G.V. (2014). Highly ordered surface structure of large-scale porphyrin aggregates assembled from protonated TPP and water. *Journal of Molecular Structure*, 1065-1066, 170–178.
119. Xu, Z., Mei, Q., Hua, Q., Tian, R., Weng, J., Shi, Y. and Huang, W. (2015) Synthesis, characterization, energy transfer and photophysical properties of ethynyl bridge linked porphyrin–naphthalimide pentamer and its metal complexes. *Journal of Molecular Structure* 1094, 1-8.
120. Wootthiphan Jantayot. Synthesis and characterization of long-chained porphyrin derivatives and their cobalt complex. Master's Thesis, Department of Chemistry, Faculty of Science and Technology, Thammasat University, 2014.

121. Siri, O., Jaquinod, L. and Smith, K.M. (2000) Coplanar conjugated β -nitroporphyrins and some aspects of nitration of porphyrins with N_2O_4 Tetrahedron Letters 41, 3583 - 3587.
122. Maestrin, A.P.J., Tedesco, A.C., Neri, C.R., Gandini, M.E.F., Serra, O.A. and Iamamoto, Y. (2004) Synthesis, Spectroscopy and Photosensitizing Properties of Hydroxynitrophenylporphyrins. Journal of The Brazilian Chemical Society 15, 708 - 713.
123. Lu, F., Zhang, J., Zhou, Y., Zhao, Y., Zhang, B. and Feng, Y. (2016). Novel D- π -A porphyrin dyes with different alkoxy chains for use in dye-sensitized solar cells. Dyes and Pigments 125, 116–123.
124. Boscencu, R. (2012) Microwave Synthesis Under Solvent-Free Conditions and Spectral Studies of Some Mesoporphyrinic Complexes. Molecules 17(5), 5592-5603.
125. Barbara V., Lucia F.G.M., Fabio L. and David L.O. (2008). Extending the porphyrin core: synthesis and photophysical characterization of porphyrins with p-conjugated β -substituents. New Journal of Chemistry, 32, 166-178.
126. Bajju, G.D., Kundan, S., Bhagat, M., Gupta, D., Kapahi, A. and Devi, G. (2014). Synthesis and Spectroscopic and Biological Activities of Zn(II) Porphyrin with Oxygen Donors. Bioinorganic Chemistry and Applications 2014. 1-13.
127. Kumar, S.V., Scottwell, S., Waugh, E., McAdam, C.J., Hanton, L.R., Brooks, H.J.L. and Crowley, J.D. (2016) Antimicrobial Properties of Tris(homoleptic) Ruthenium(II) 2-Pyridyl-1,2,3-triazole “Click” Complexes against Pathogenic Bacteria, Including Methicillin-Resistant Staphylococcus aureus (MRSA). Inorganic. Chemistry 55 (19). 9767–9777.
128. Tovmasyan, A., Babayan, N., Poghosyan, D., Margaryan, K., Harutyunyan, B., and Grigoryan, R. *et al* (2014) Novel amphiphilic cationic porphyrin and its Ag(II) complex as potential anticancer agents. Journal of Inorganic Biochemistry 140. 94-103.
129. Burda, W.N., Fields, K.B., Gill, J.B., Burt, R., Shepherd, M., Zhang, X.P. and Shaw, L.N. (2012) Neutral Metallated and Meso-Substituted Porphyrins as

Antimicrobial Agents Against Gram-Positive Pathogens. *European Journal of Clinical Microbiology & Infectious Diseases* 31(3). 327-335.

130. Glazer, N. and Rosenheck, K.(1962) Solvent and Conformational Effects on the Ultraviolet Spectra of Polypeptides and Substituted Amides. *The journal of biological chemistry* 237(12). 3674-3678.



The seal of Thammasat University is a circular emblem. It features a central five-tiered umbrella (parasol) with a lotus flower at its base. Radiating from the center are eight stylized arms or rays. The outer ring of the seal contains the university's name in Thai script at the top and "THAMMASAT UNIVERSITY" in English at the bottom, separated by small floral motifs.

APPENDICES

APPENDIX A

MASS SPECTRA

Mass spectra of aldehyde

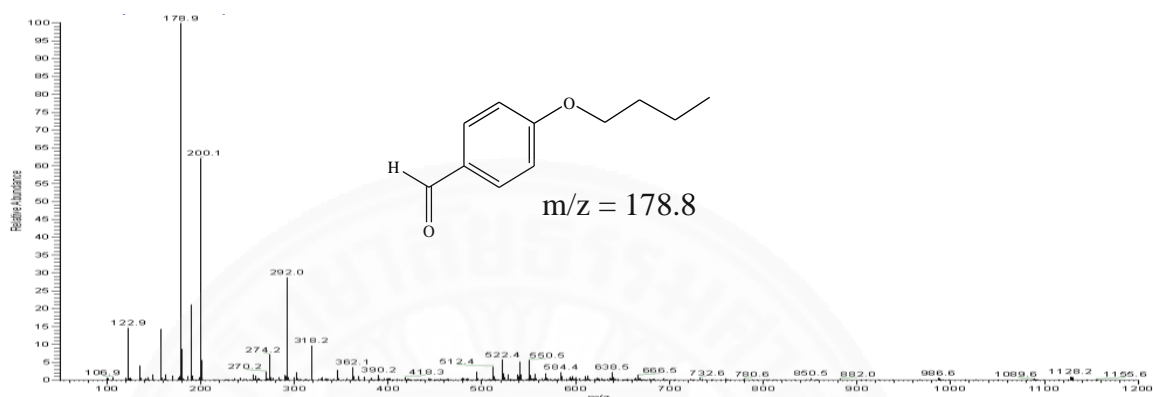


Figure A1. The mass spectrum of butyloxybenzaldehyde **1** in CH_2Cl_2 .

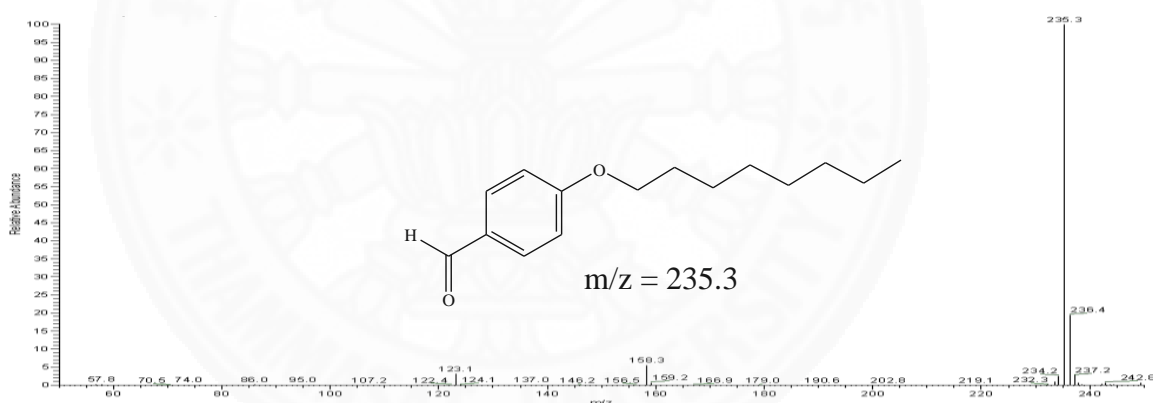


Figure A2. The mass spectrum of octyloxybenzaldehyde **2** in CH_2Cl_2 .

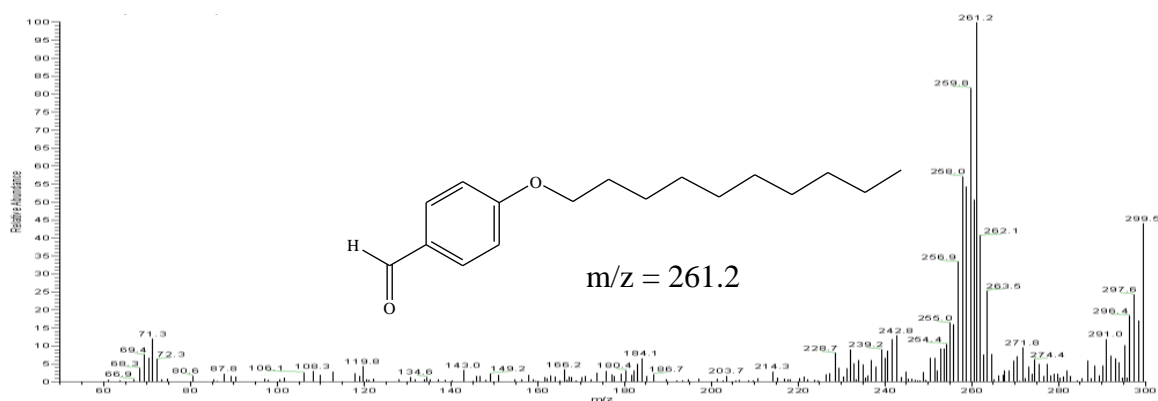


Figure A3. The mass spectrum of decyloxybenzaldehyde **3** in CH_2Cl_2 .

Mass spectra of free base porphyrins

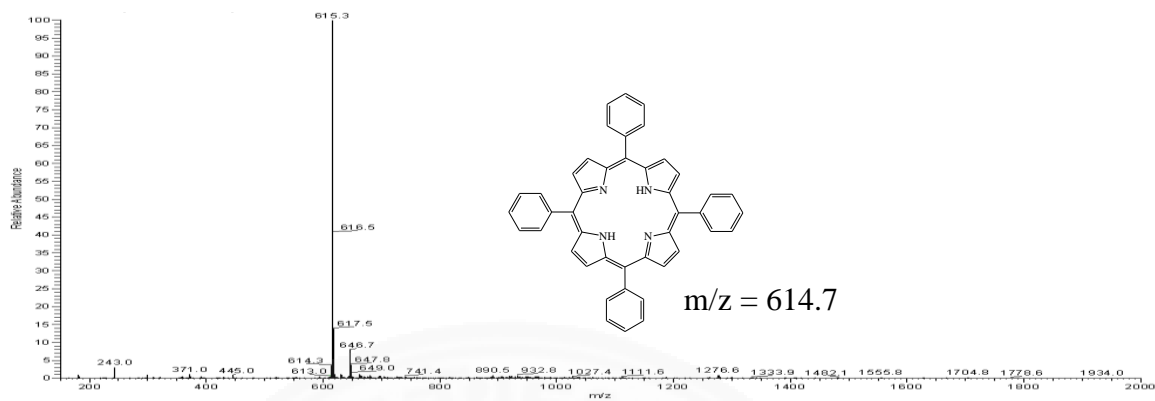


Figure A4. The mass spectrum of tetrakis(4-phenyl)porphyrin (TPP 4) in CH_2Cl_2 .

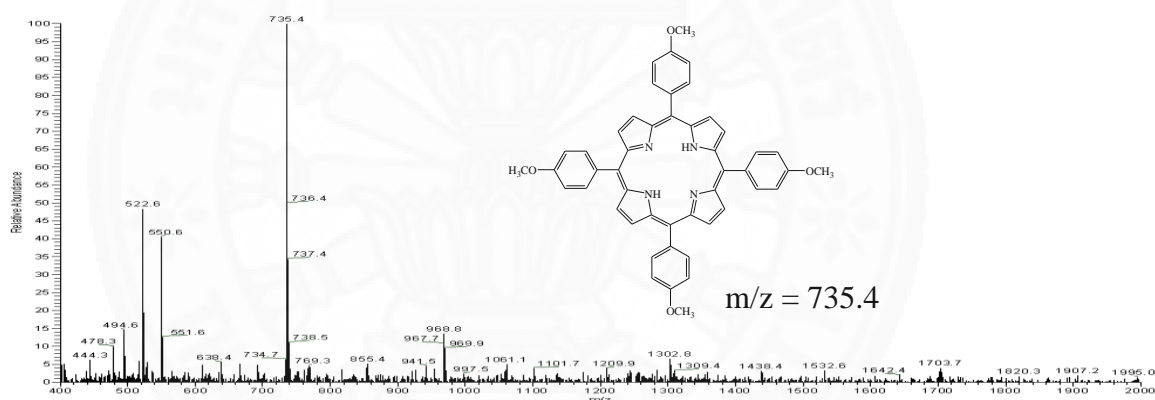


Figure A5. The mass spectrum of tetrakis(4-methoxyphenyl)porphyrin (TOMPP 5) in CH_2Cl_2 .

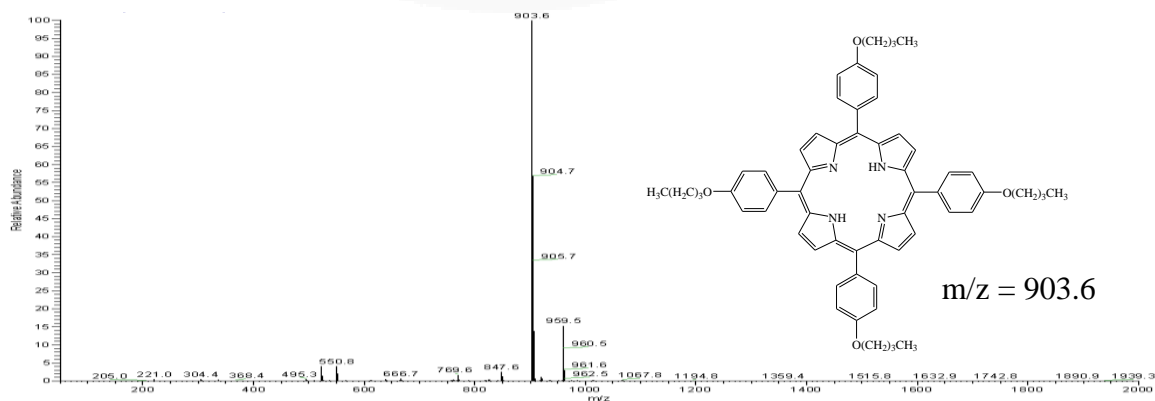


Figure A6. The mass spectrum of tetrakis(4-butyloxyphenyl)porphyrin (TOBPP 6) in CH_2Cl_2 .

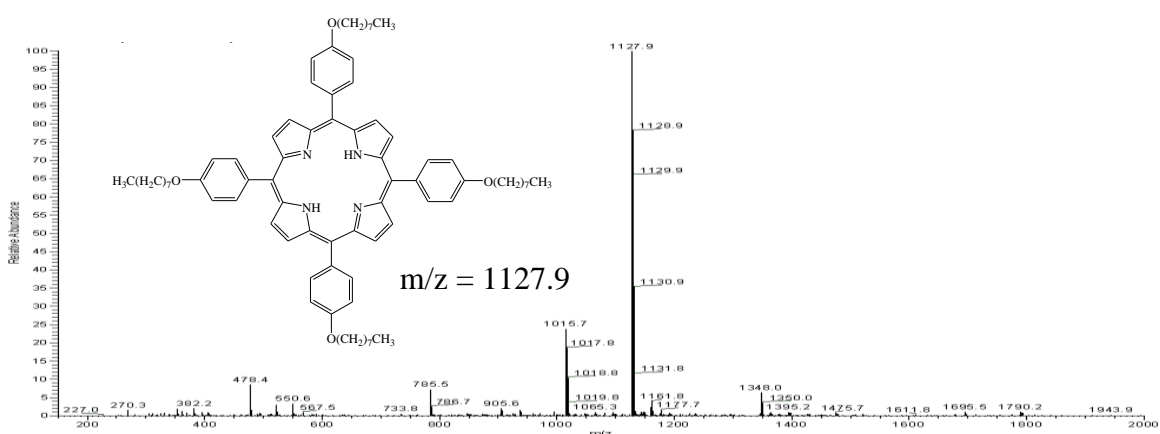


Figure A7. The mass spectrum of tetrakis(4-octyloxyphenyl) porphyrin (TOOPP 7) in CH_2Cl_2 .

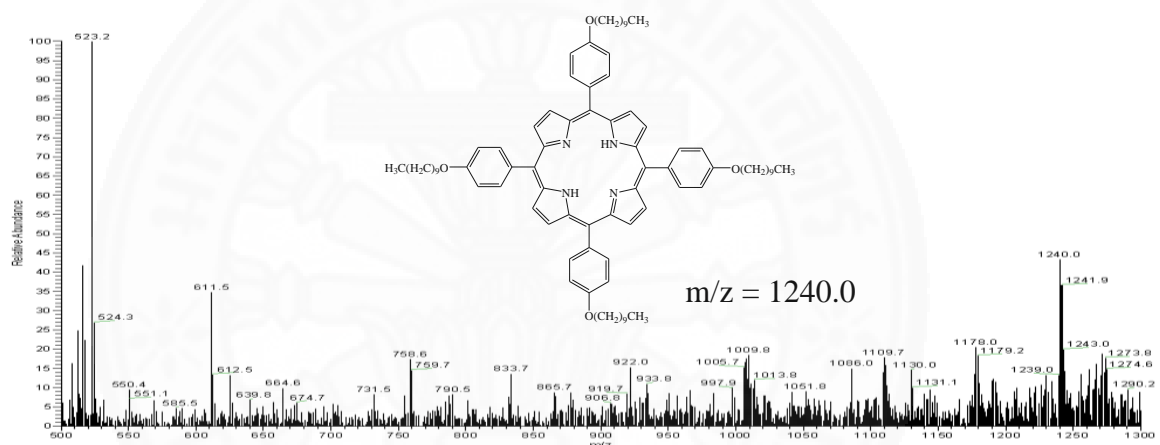


Figure A8. The mass spectrum of tetrakis(4-decyloxyphenyl)porphyrin (TODPP 8) in CH_2Cl_2 .

Mass spectra of silver(II) porphyrins

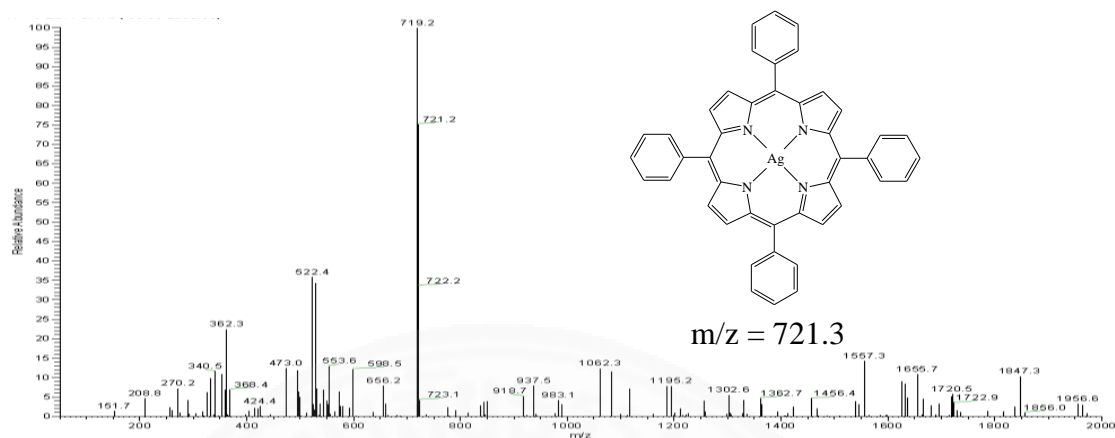


Figure A9. The mass spectrum of silver-phenyl porphyrin (Ag-TPP 9) in CH_2Cl_2 .

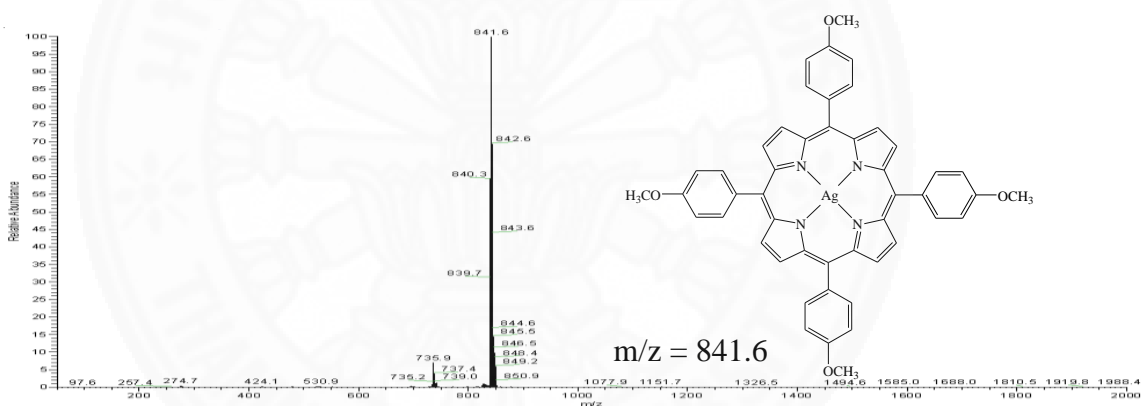


Figure A10. The mass spectrum of silver-methoxyphenyl porphyrin (Ag-TOMPP 10) in CH_2Cl_2 .

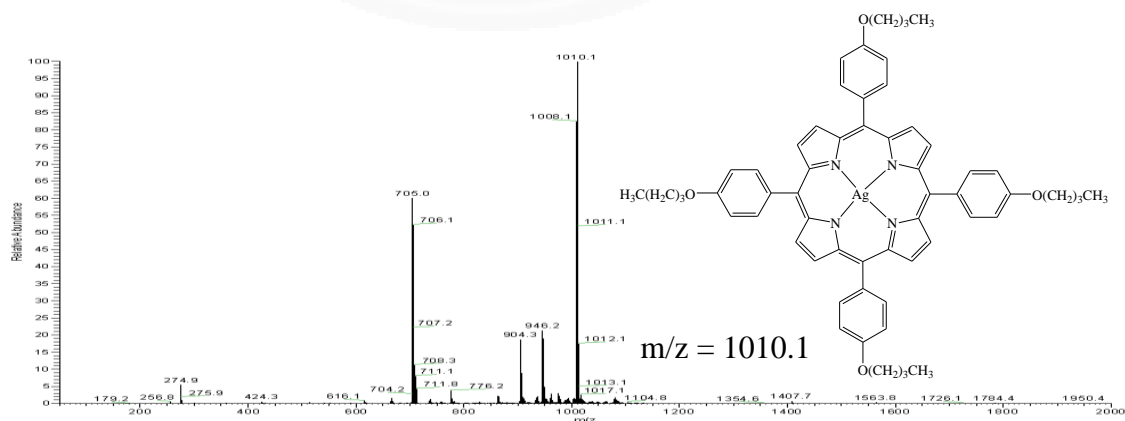


Figure A11. The mass spectrum of silver-butyloxyphenyl porphyrin (Ag-TOBPP 11) in CH_2Cl_2 .

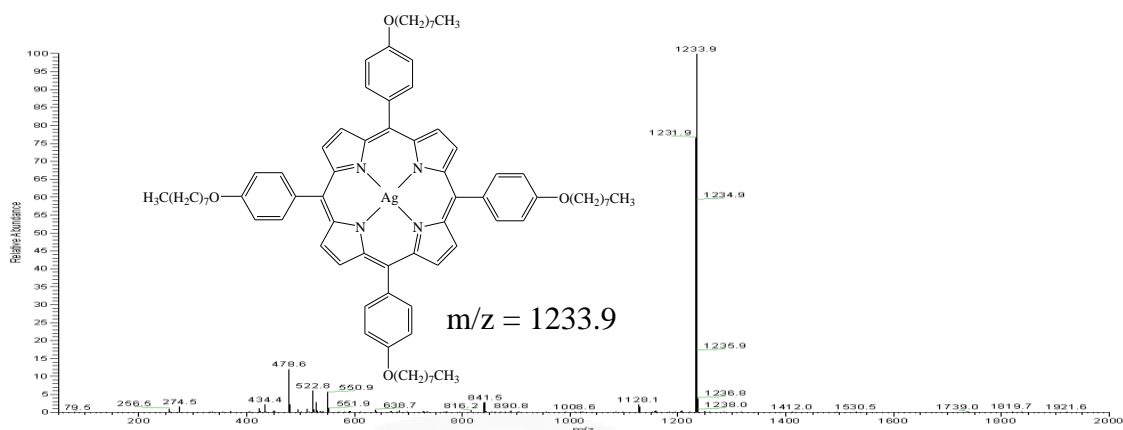


Figure A12. The mass spectrum of silver-octyloxyphenyl porphyrin (Ag-TOOPP 12) in CH_2Cl_2 .

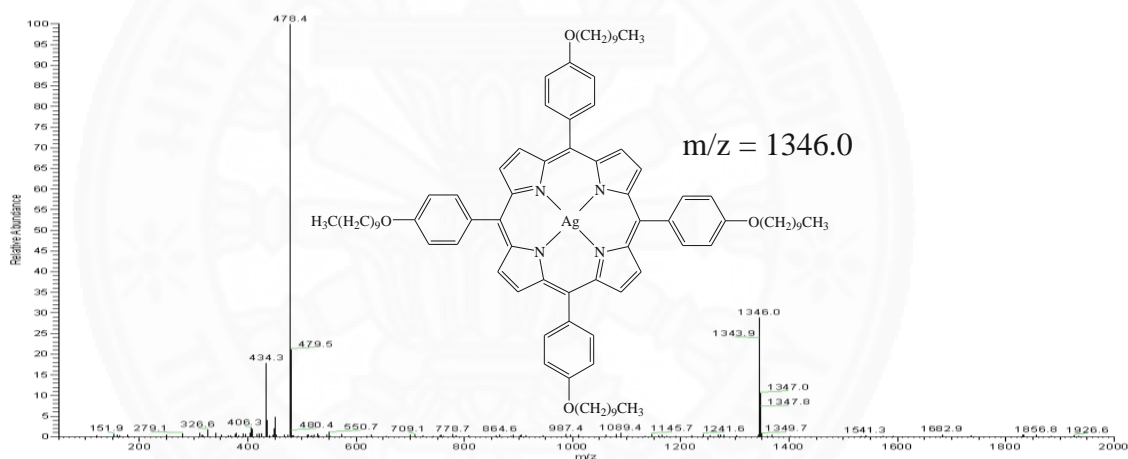


Figure A13. The mass spectrum of silver-decyloxyphenyl porphyrin (Ag-TODPP 13) in CH_2Cl_2 .

APPENDIX B

NMR SPECTRA

^1H NMR of aldehyde

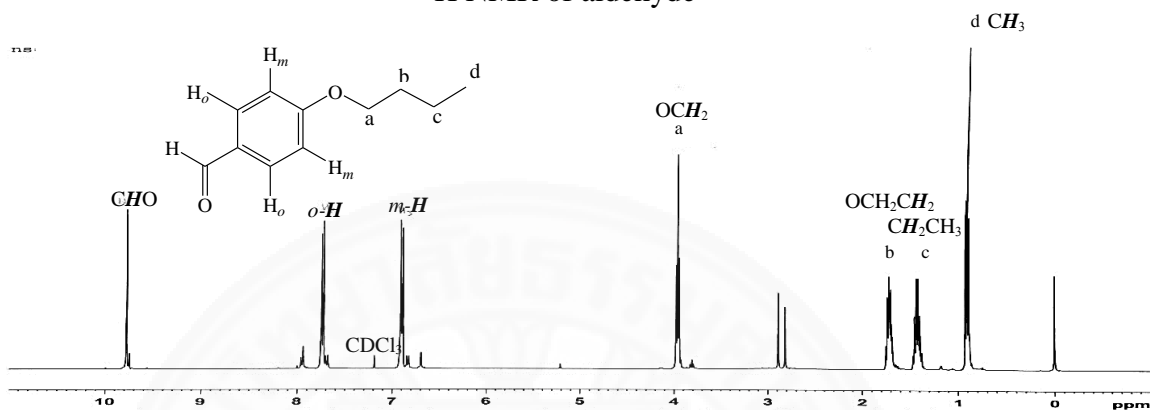


Figure B1. The ^1H NMR spectrum of butyloxybenzaldehyde **1** in chloroform-d.

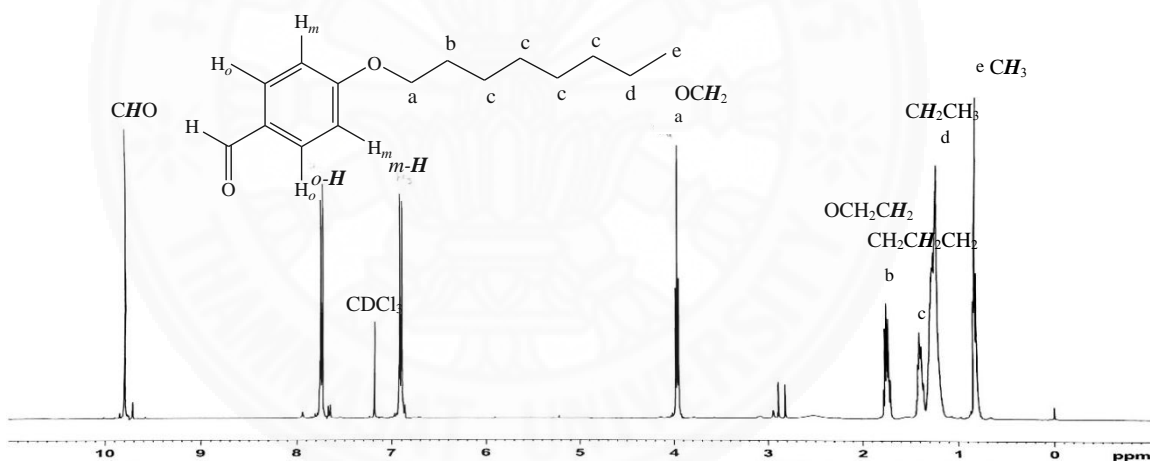


Figure B2. The ^1H NMR spectrum of octyloxybenzaldehyde **2** in chloroform-d.

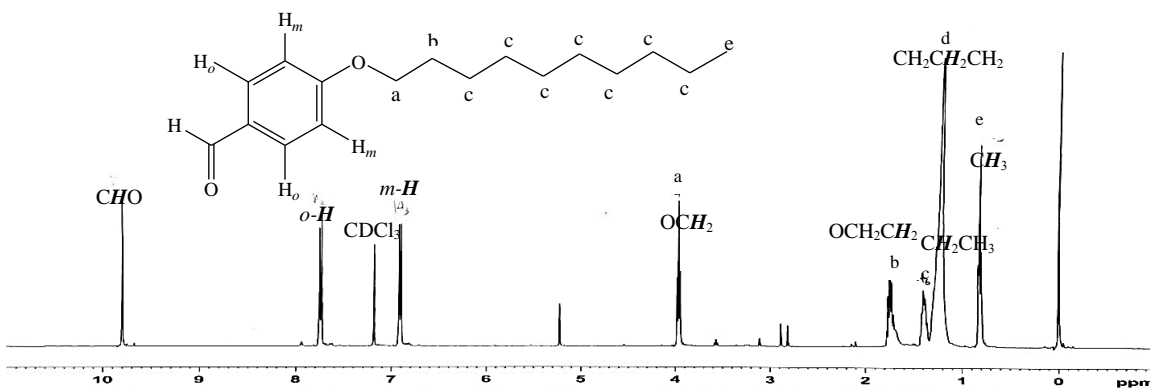


Figure B3. The ^1H NMR spectrum of decyloxybenzaldehyde **3** in chloroform-d.

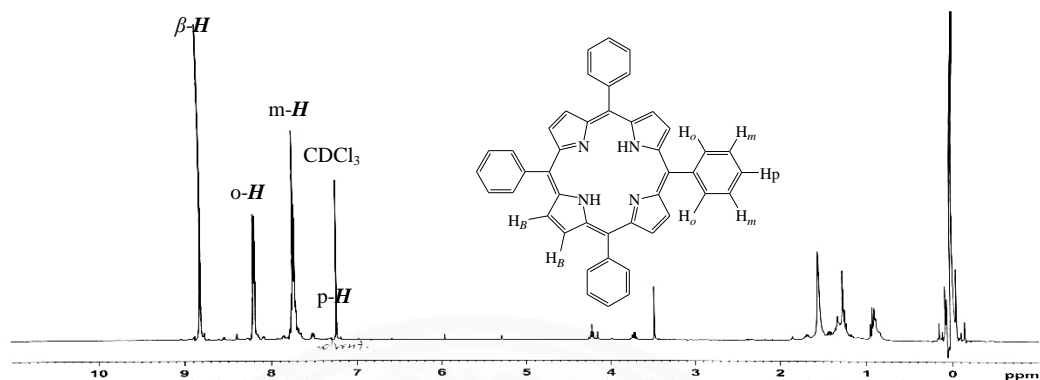
¹H NMR of free base porphyrins

Figure B4. The ¹H NMR spectrum of TPP 4 in chloroform-d (CDCl₃).

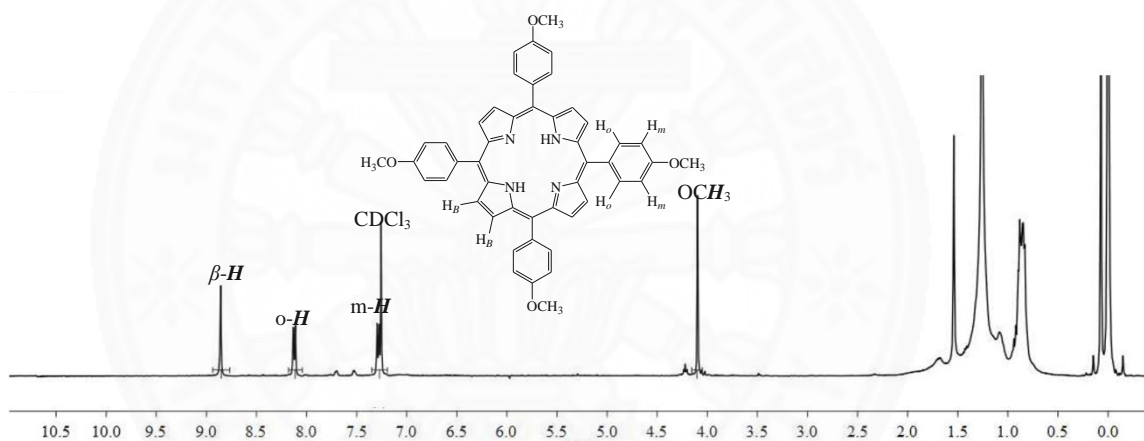


Figure B5. The ¹H NMR spectrum of TOMPP 5 in chloroform-d (CDCl₃).

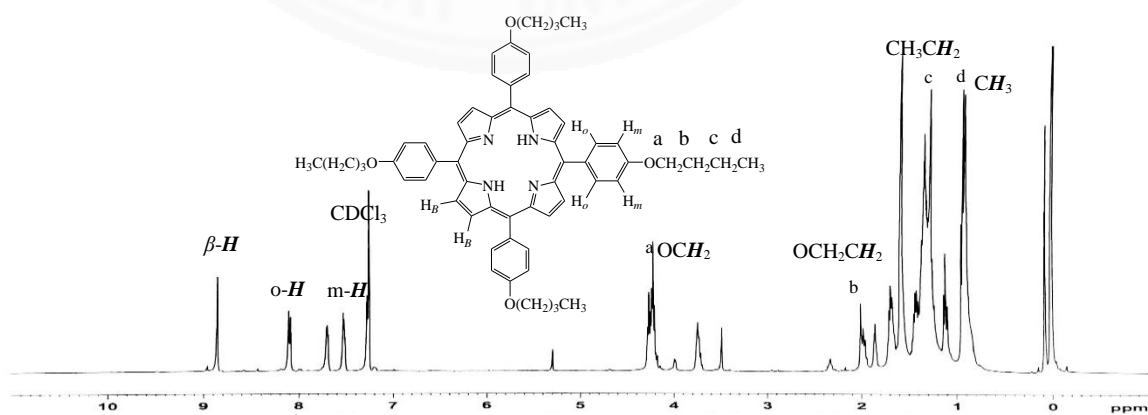
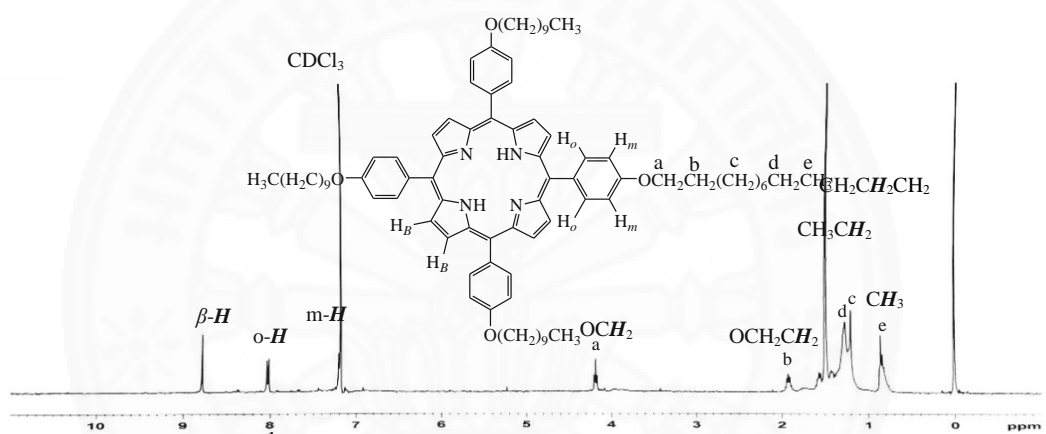
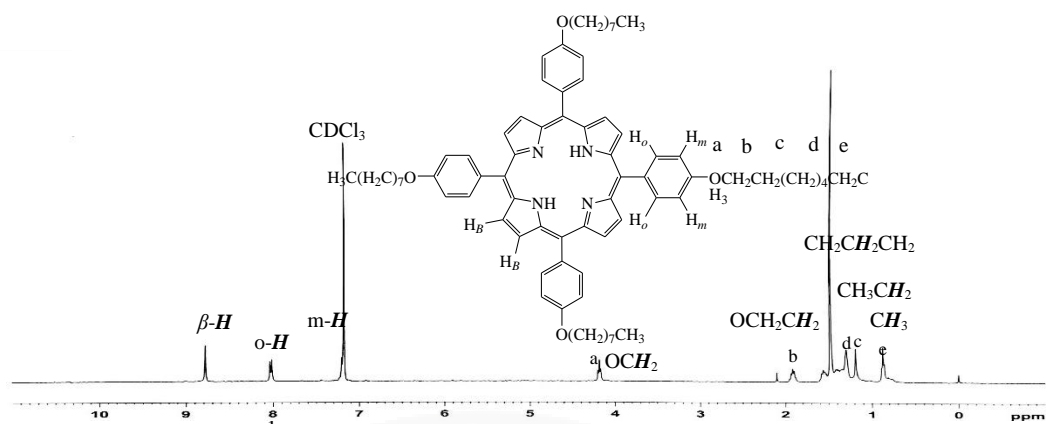


Figure B6. The ¹H NMR spectrum of TOBPP 6 in chloroform-d (CDCl₃).



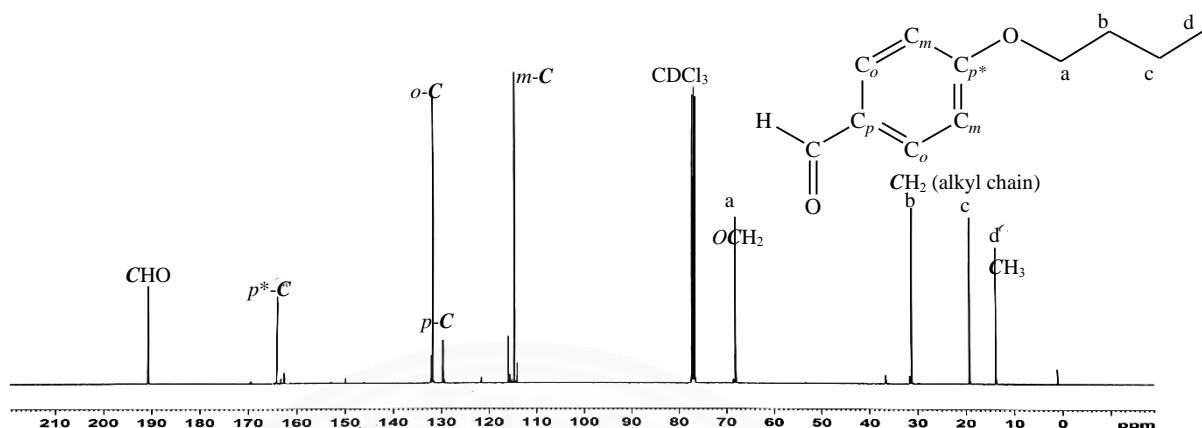
^{13}C NMR spectra of aldehyde

Figure B9. The ^{13}C NMR spectrum of butyloxybenzaldehyde **1** in chloroform- d .

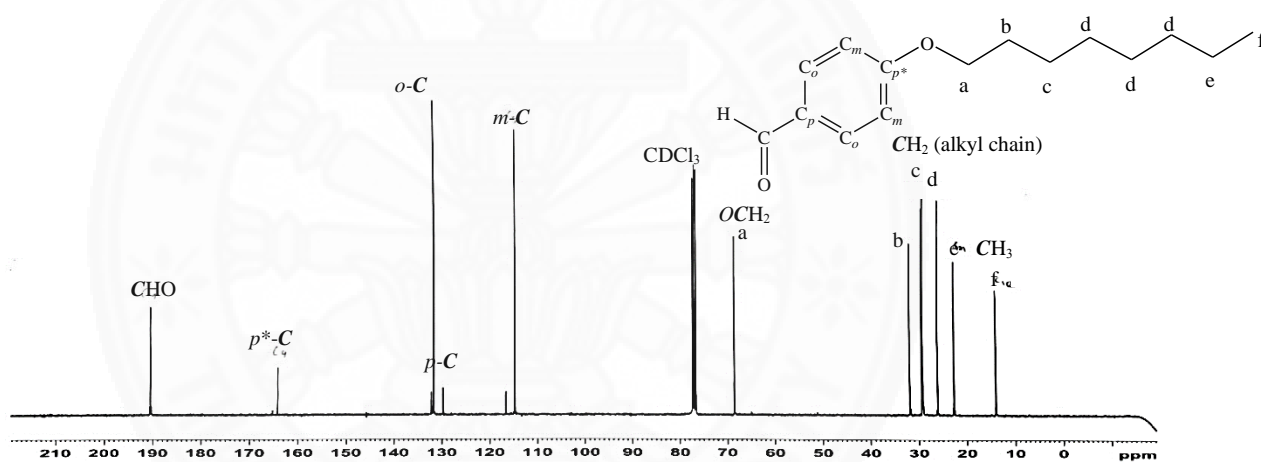


Figure B10. The ^{13}C NMR spectrum of octyloxybenzaldehyde **2** in chloroform- d .

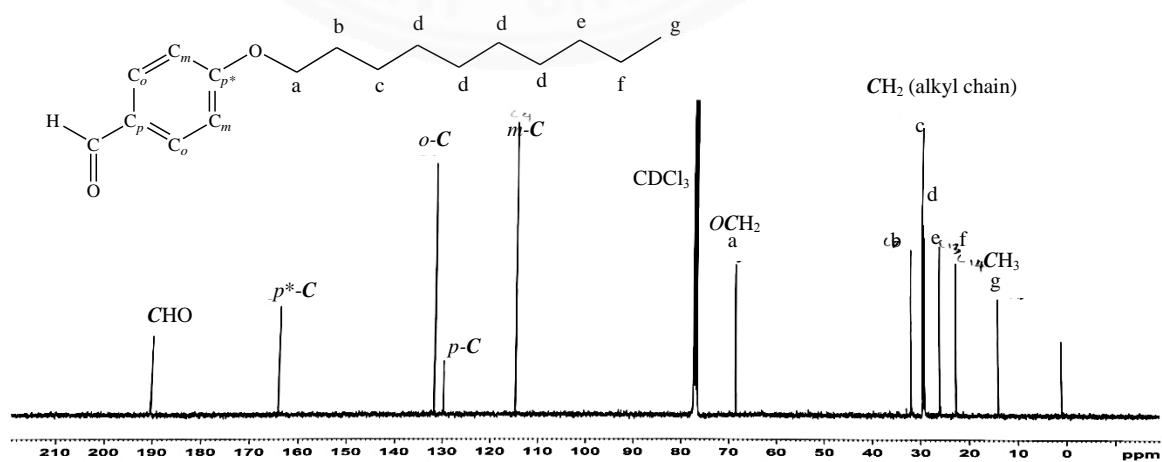


Figure B11. The ^{13}C NMR spectrum of decyloxybenzaldehyde **3** in chloroform- d .

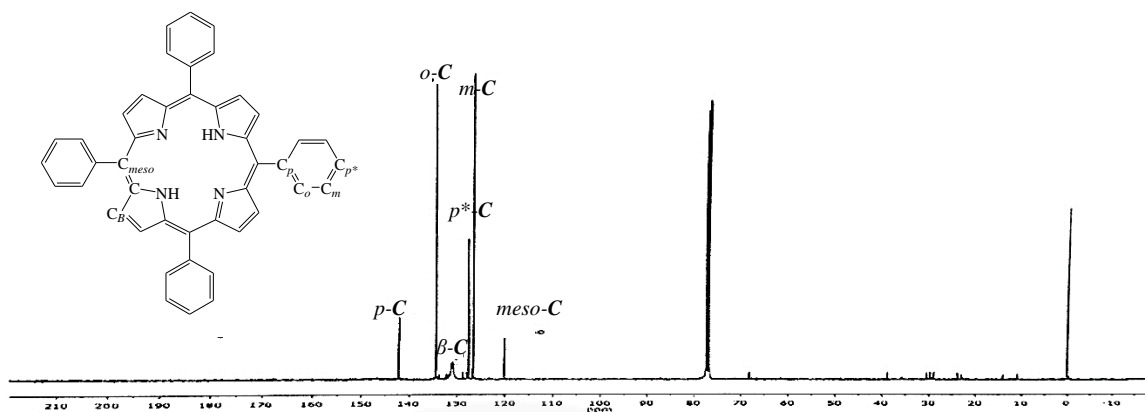


Figure B12. The ^{13}C NMR spectrum of TPP **4** in chloroform-d (CDCl_3).

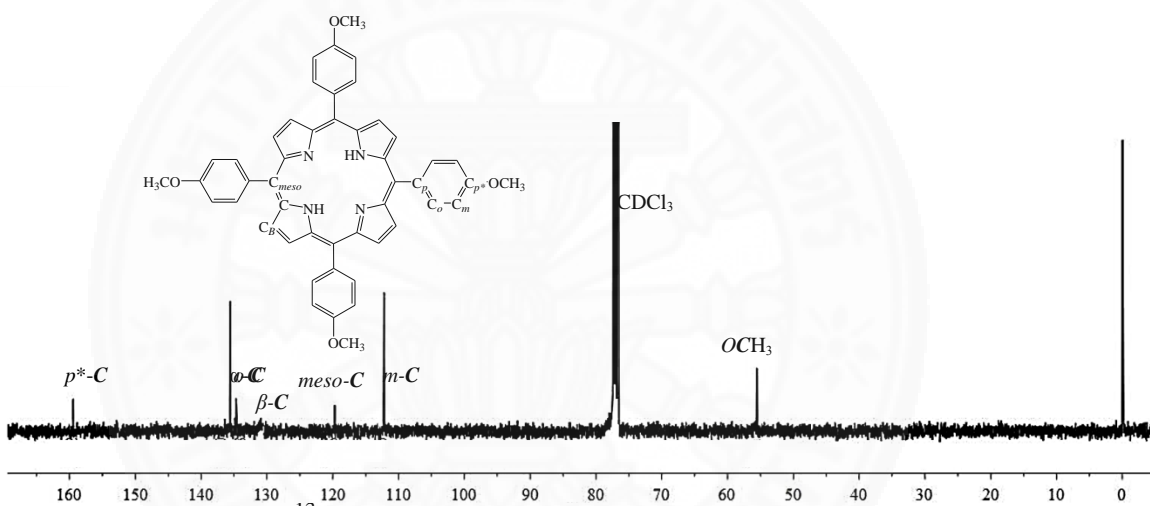


Figure B13. The ^{13}C NMR spectrum of TOMPP **5** in chloroform-d (CDCl_3).

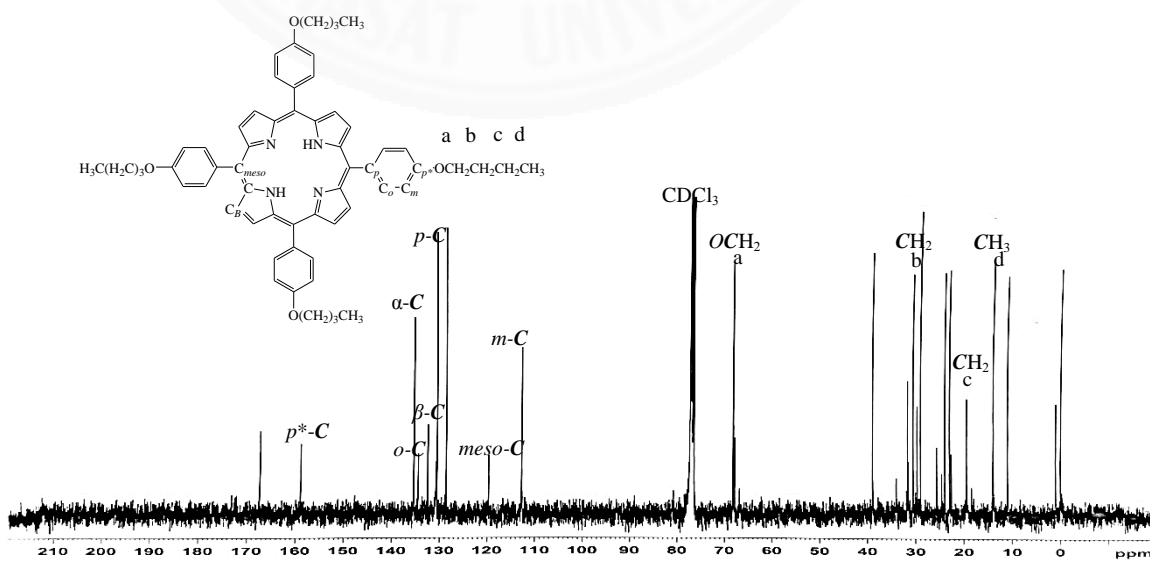


Figure B14. The ^{13}C NMR spectrum of TOBPP **6** in chloroform-d (CDCl_3).

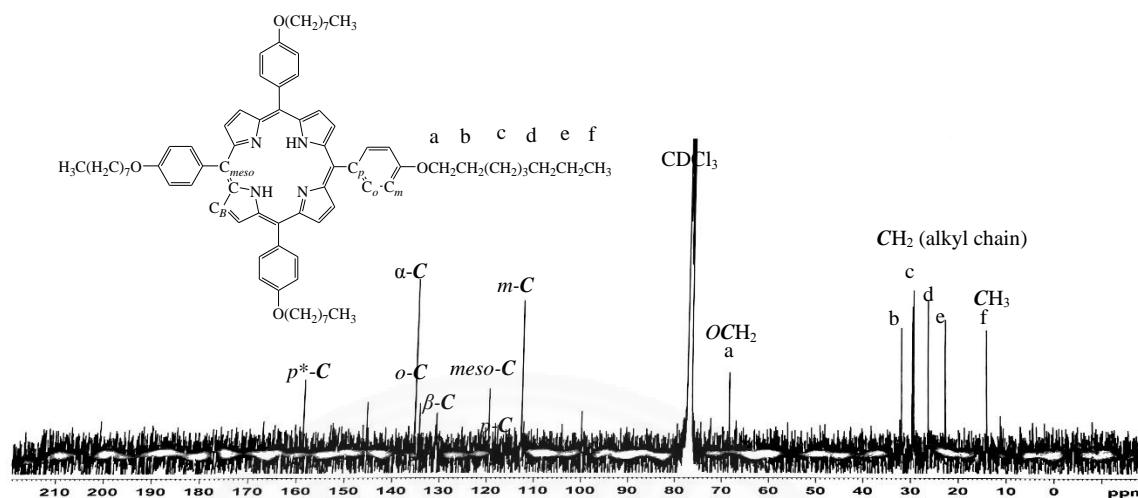


Figure B15. The ^{13}C NMR spectrum of TOOPP **7** in chloroform-d (CDCl_3).

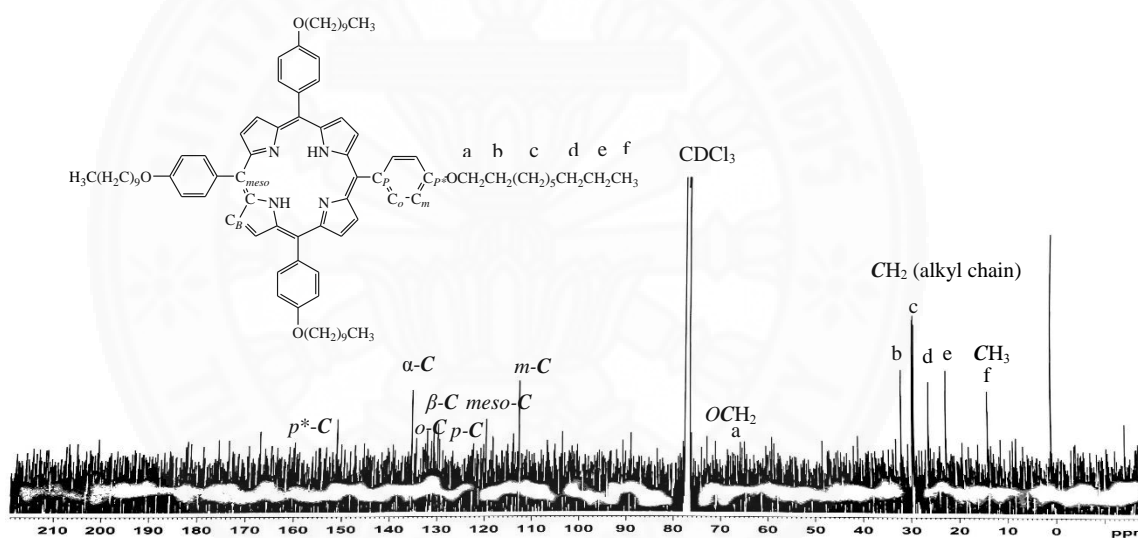


Figure B16. The ^{13}C NMR spectrum of TODPP **8** in chloroform-d (CDCl_3).

APPENDIX C

IR SPECTRA

IR spectra of aldehydes

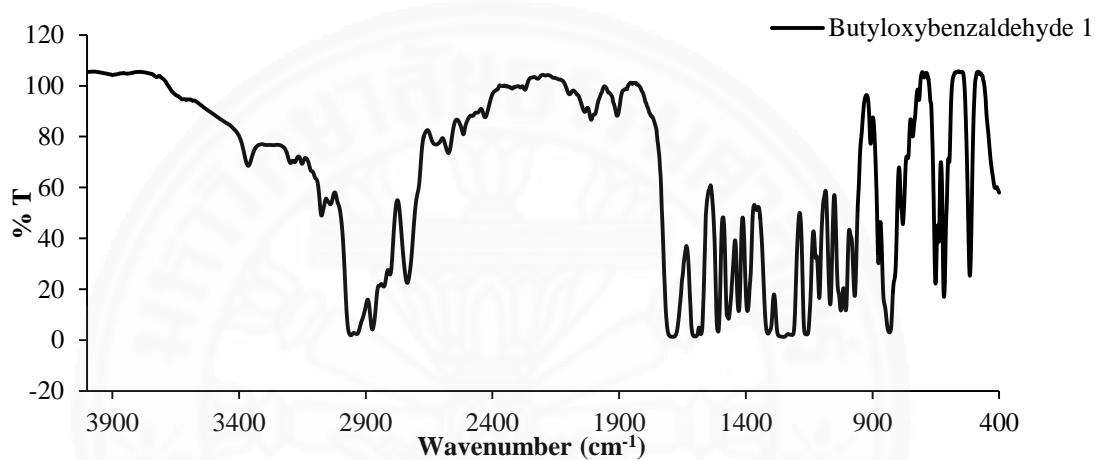


Figure C1. The IR spectrum of butyloxybenzaldehyde **1** in NaCl.

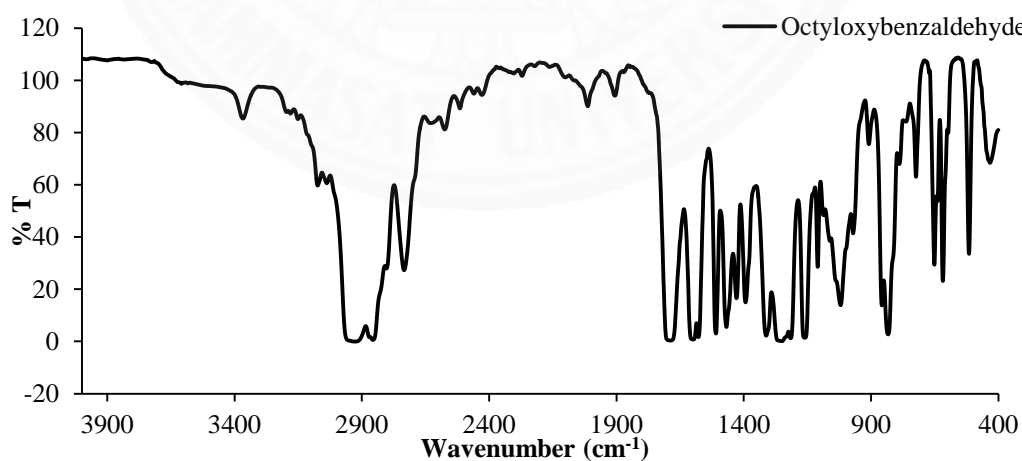


Figure C2. The IR spectrum of octyloxybenzaldehyde **2** in NaCl.

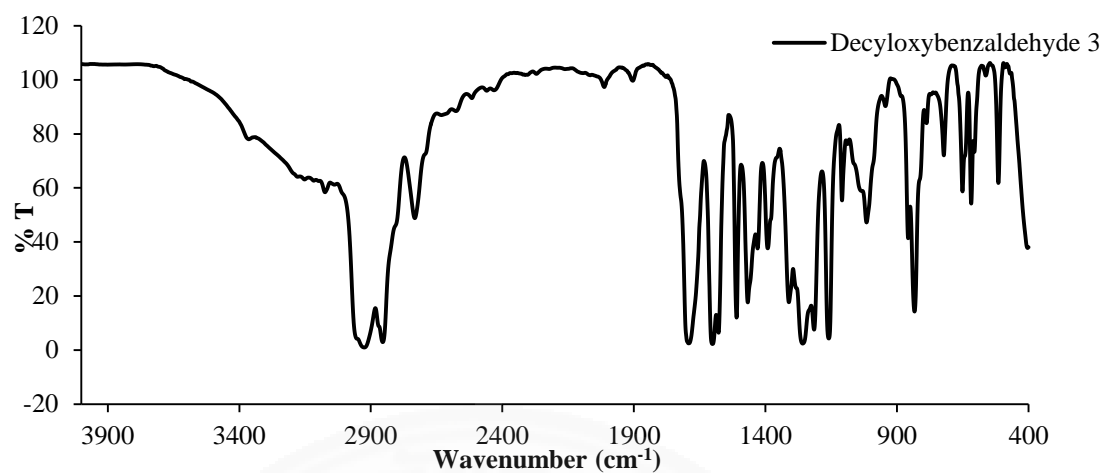
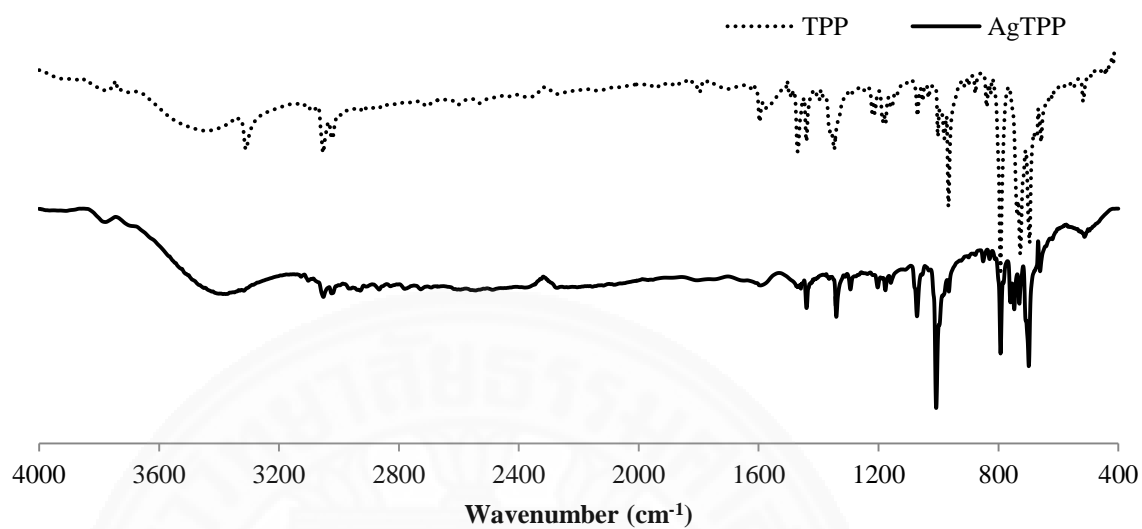
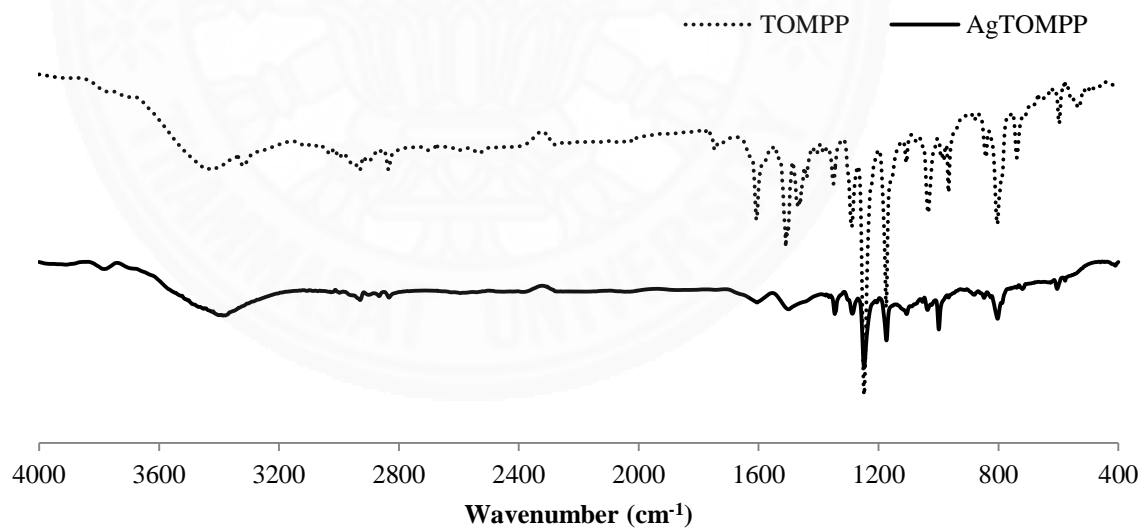


Figure C3. The IR spectrum of decyloxybenzaldehyde **3** in NaCl.

IR spectra of porphyrins and silver(II)porphyrins

**Figure C4.** The IR spectra of TPP 4 and AgTPP 9 in KBr.**Figure C5.** The IR spectra of TOMPP 5 and AgTOMPP 10 in KBr.

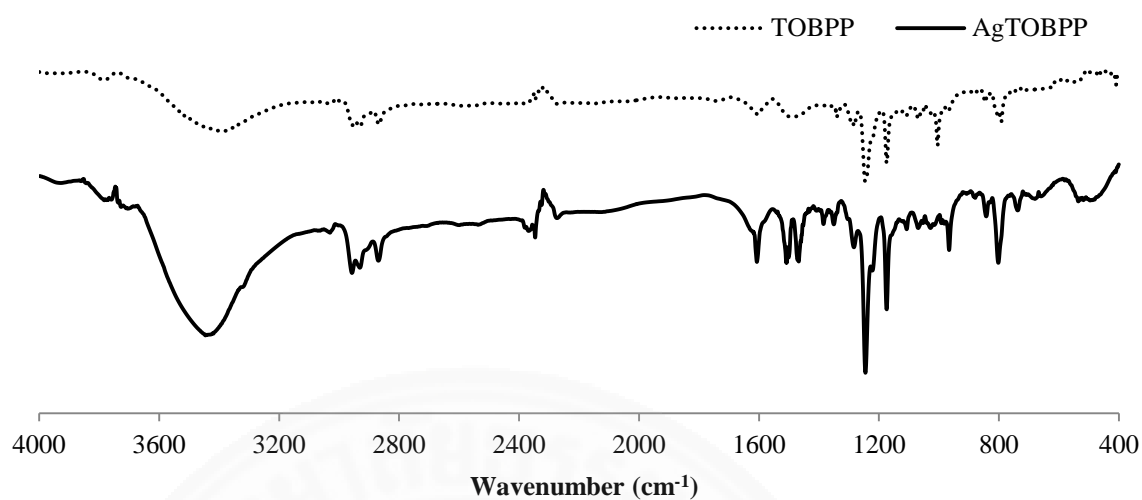


Figure C6. The IR spectra of TOBPP **6** and AgTOBPP **11** in KBr.

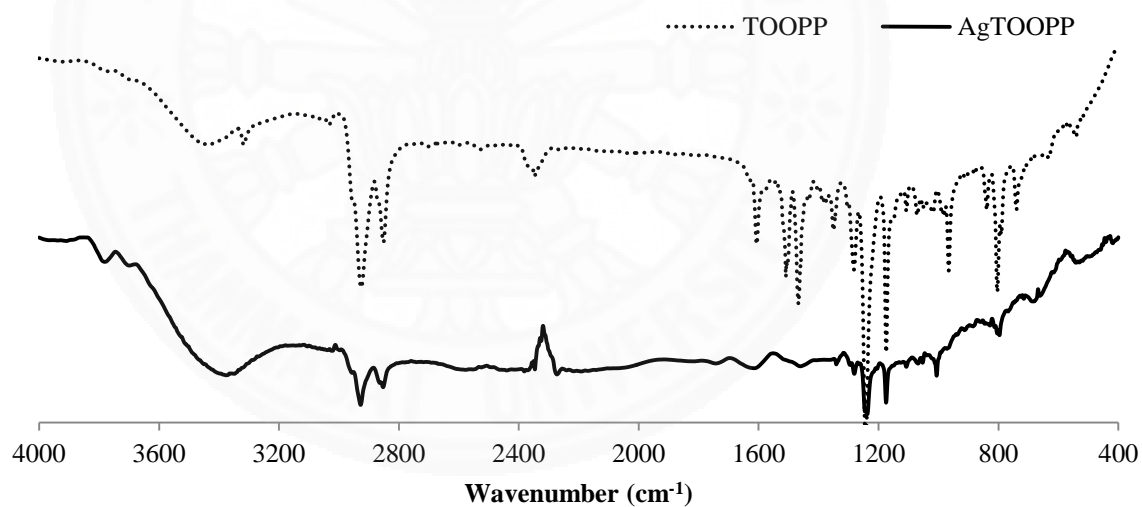


Figure C7. The IR spectra of TOOPP **7** and AgTOOPP **12** in KBr.

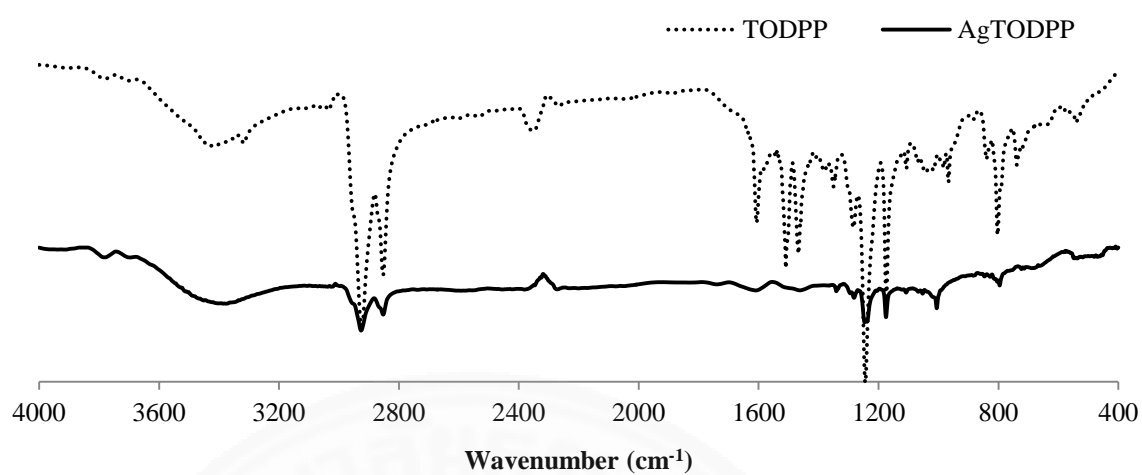


Figure C8. The IR spectra of TODPP **8** and AgTODPP **12** in KBr.

APPENDIX D

UV-VIS ABSORPTION SPECTRA

UV-Vis absorption spectra of free base porphyrins in dichloromethane

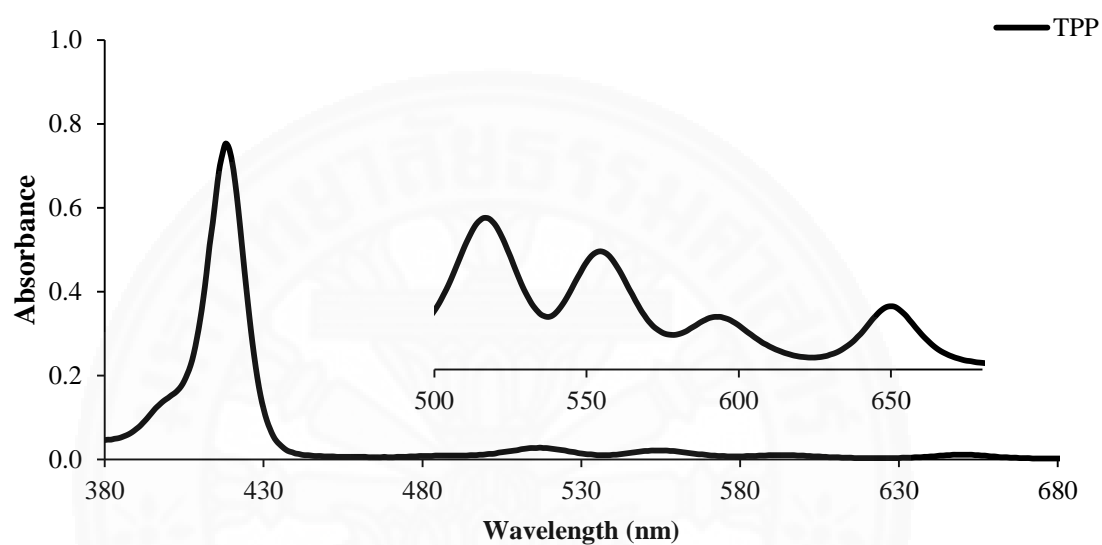


Figure D1. UV-Vis absorption spectra of TPP 4.

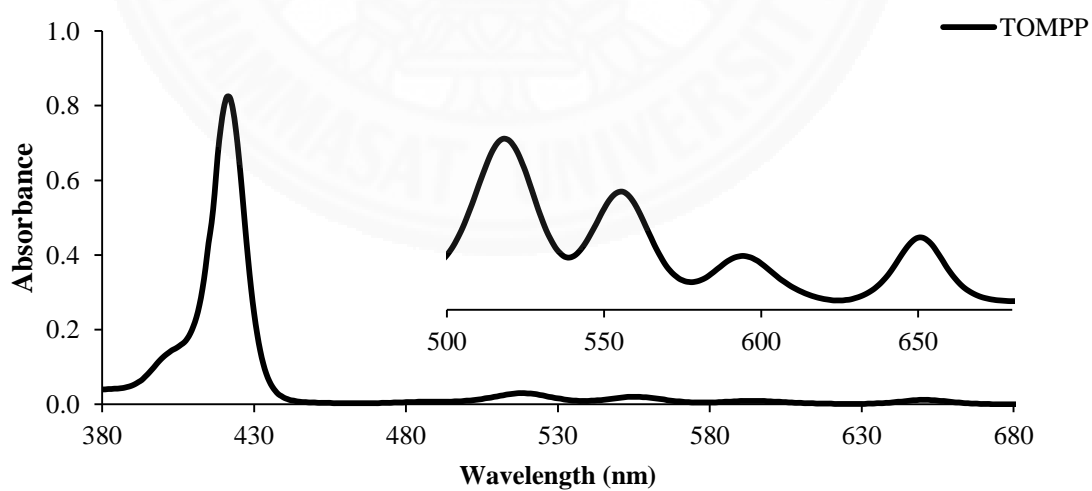


Figure D2. UV-Vis absorption spectra of TOMPP 5.

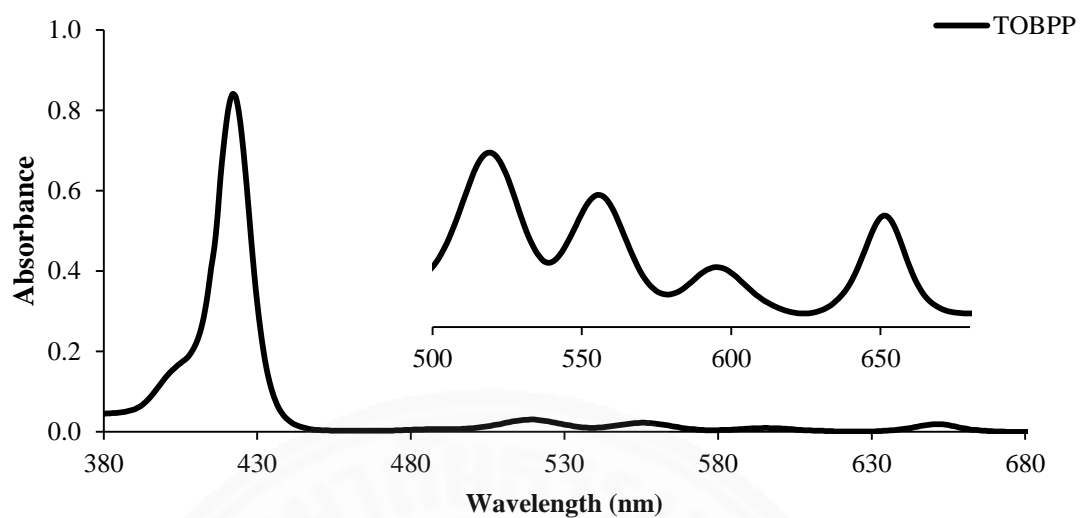


Figure D3. UV-Vis absorption spectra of TOBPP 6.

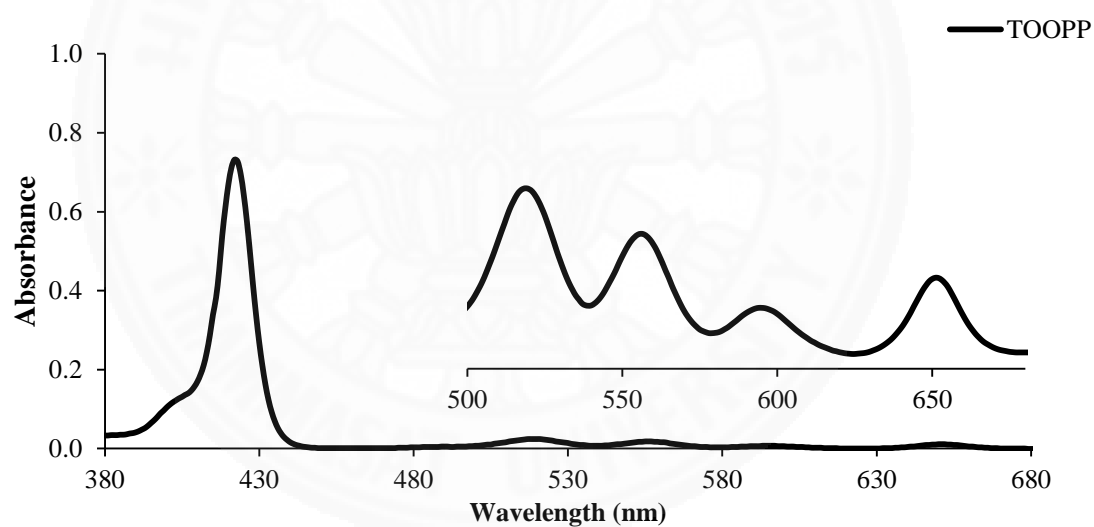


Figure D4. UV-Vis absorption spectra of TOOPP 7.

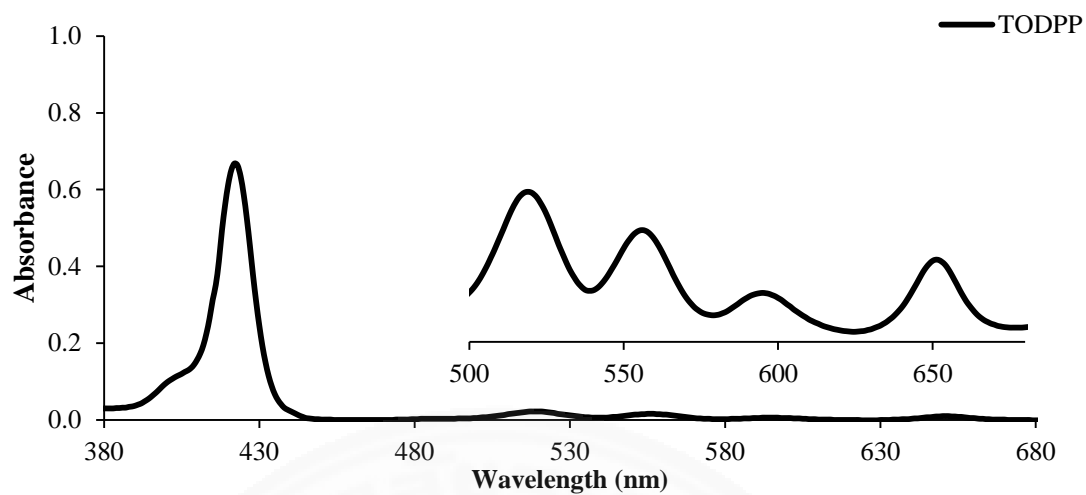


Figure D5. UV-Vis absorption spectra of TODPP 8.

UV-Vis absorption spectra of silver(II) porphyrins in dichloromethane

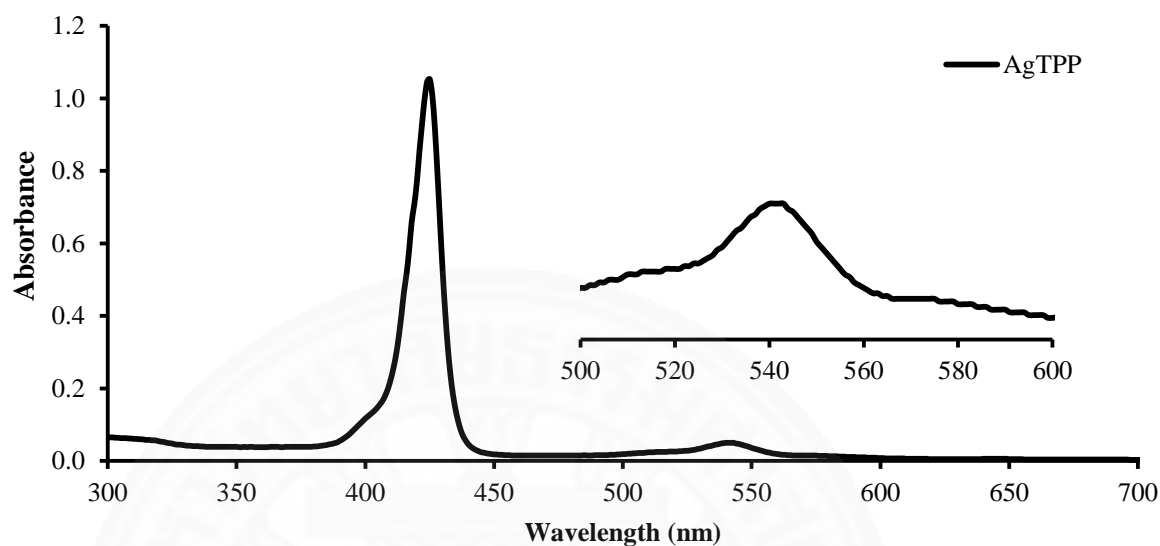


Figure D6. UV-Vis absorption spectra of AgTPP 9.

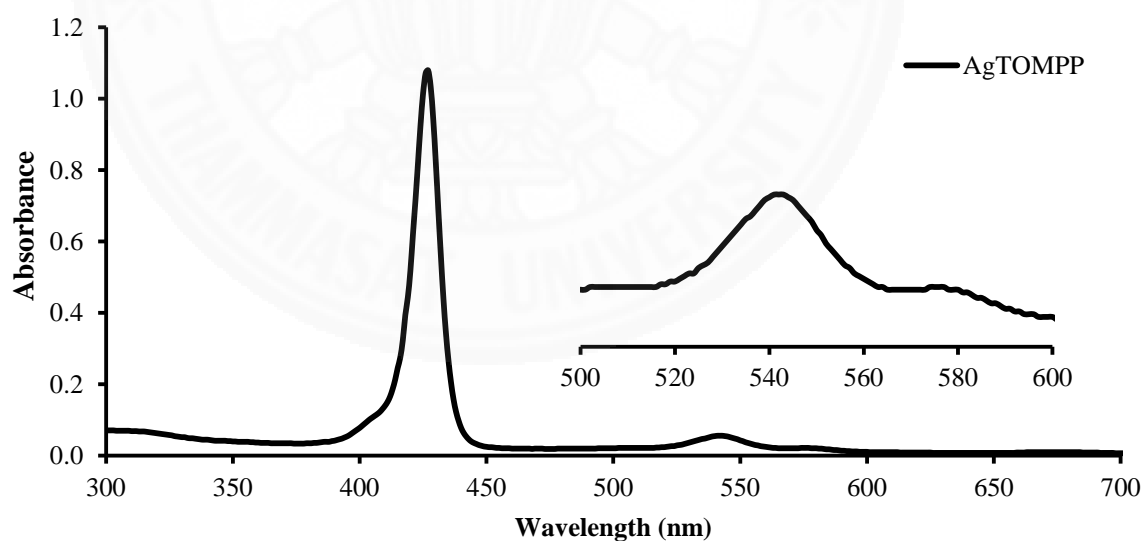


Figure D7. UV-Vis absorption spectra of AgTOMPP 10.

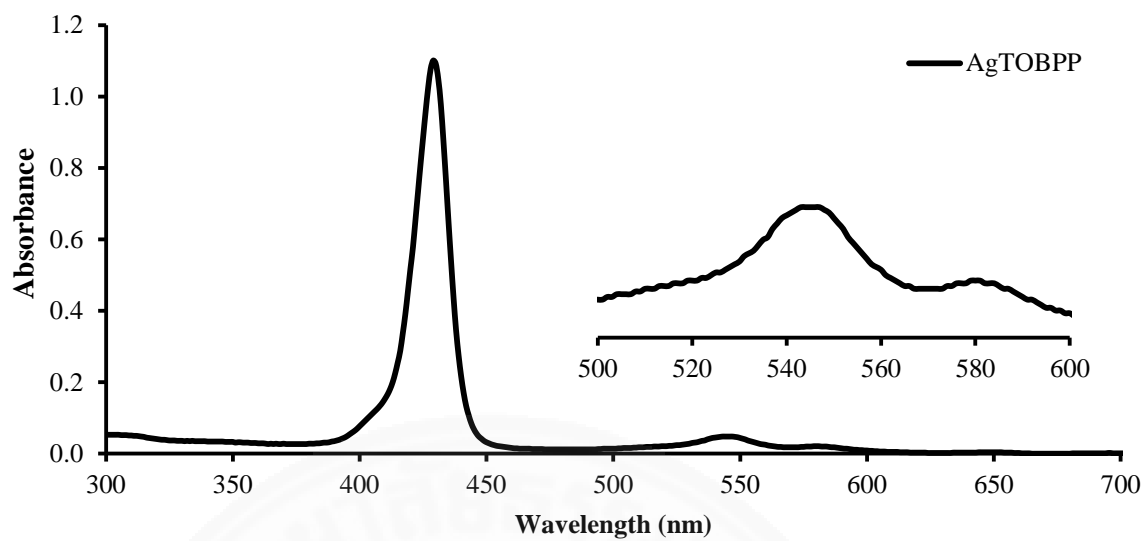


Figure D8. UV-Vis absorption spectra of AgTOBPP 11.

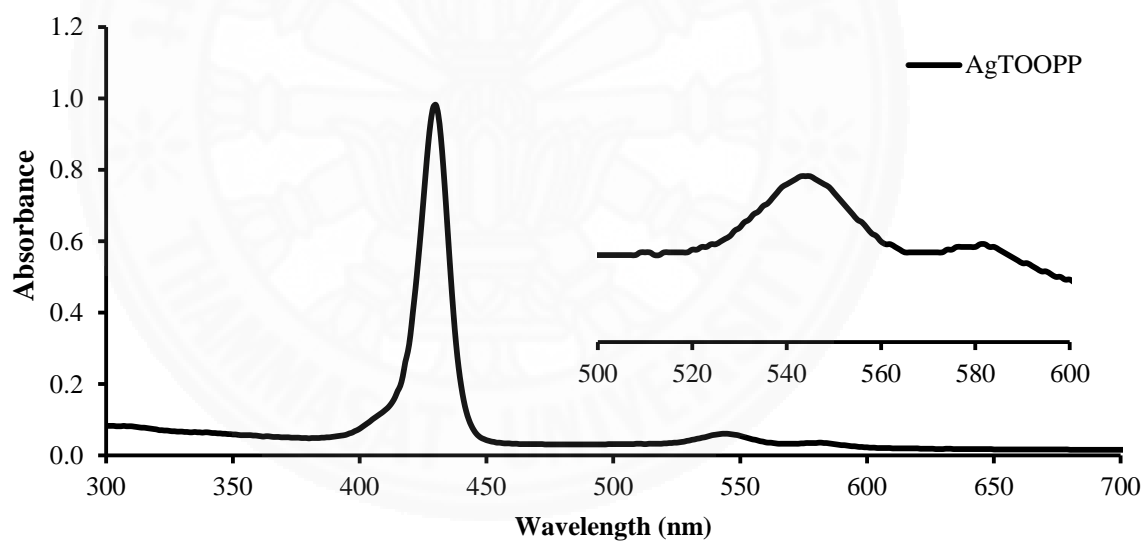


Figure D9. UV-Vis absorption spectra of AgTOOPP 12.

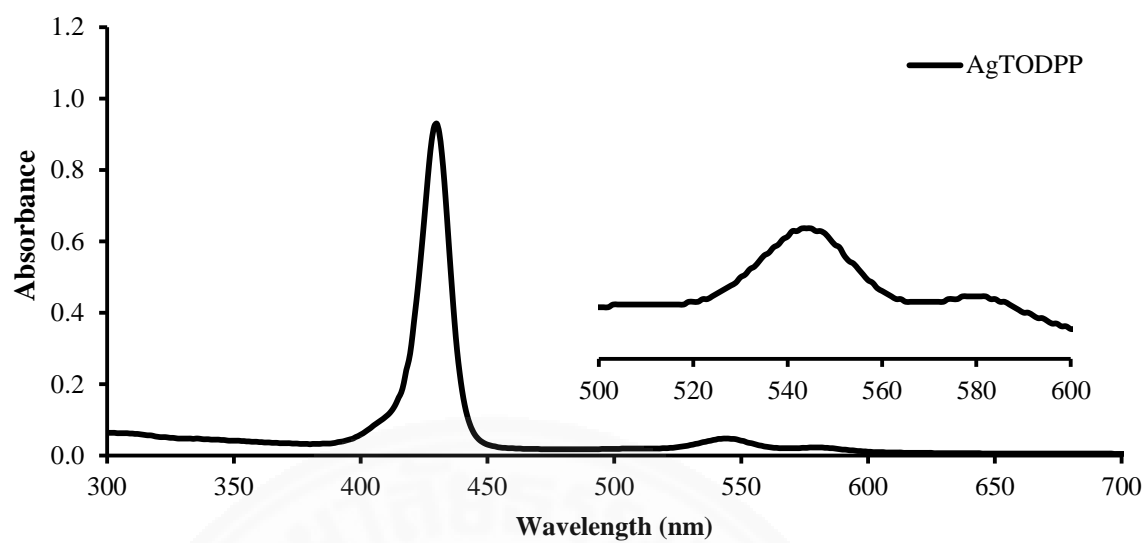


Figure D10. UV-Vis absorption spectra of AgTODPP 13.

APPENDIX E

FLUORESCENCE SPECTRA

Fluorescence spectra of free base porphyrins

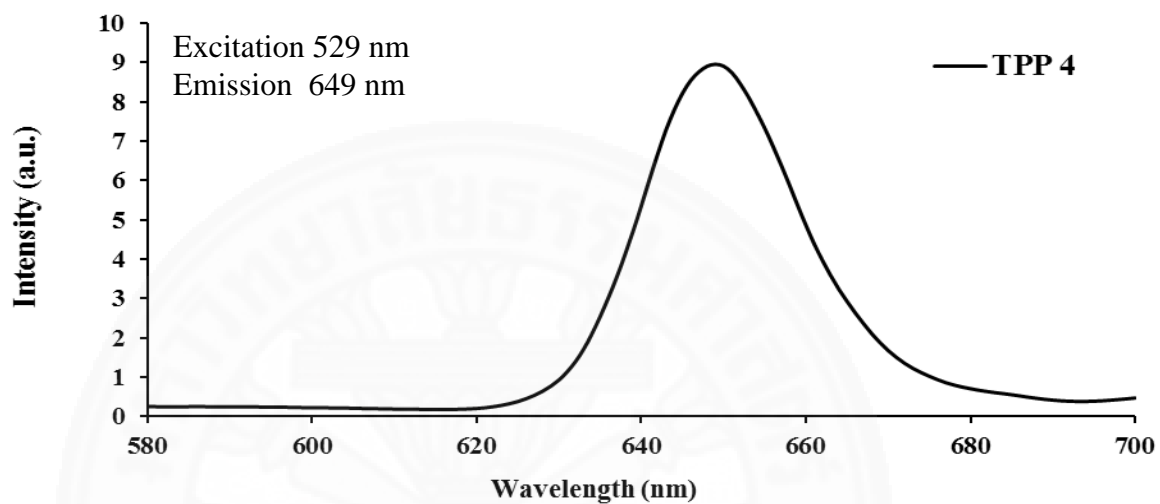


Figure E1. Fluorescence spectra of TPP 4.

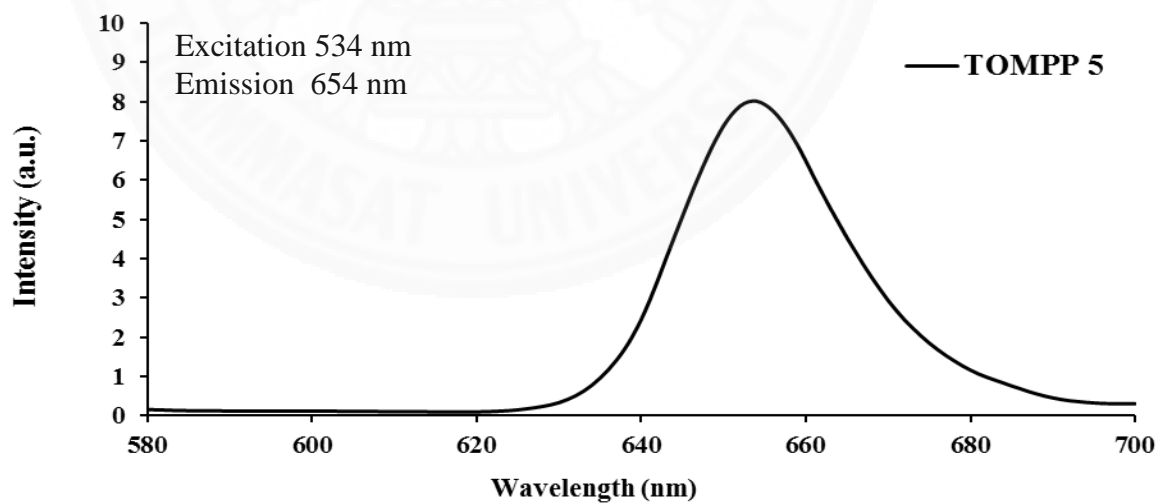


Figure E2. Fluorescence spectra of TOMPP 5.

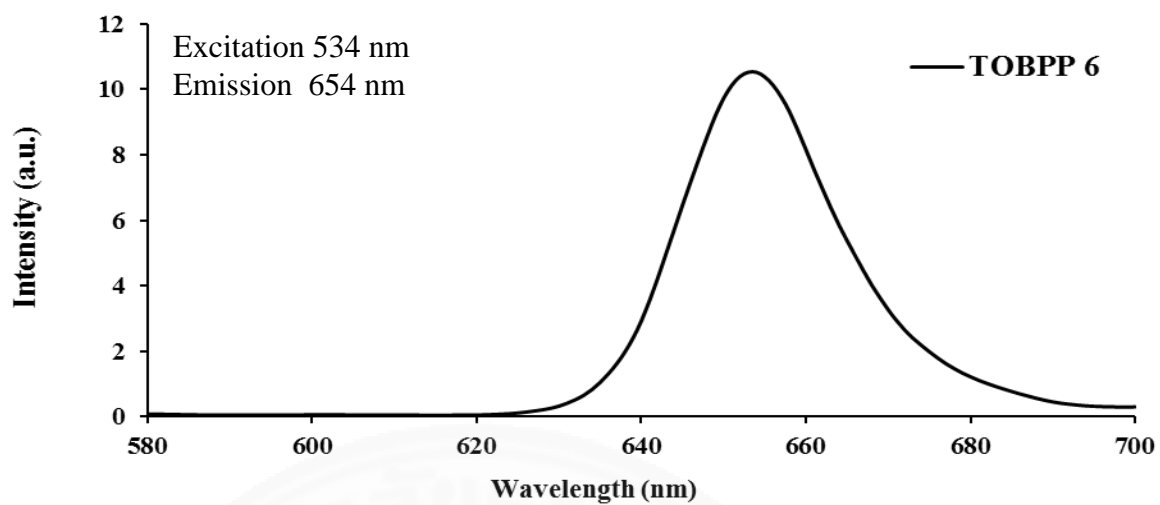


Figure E3. Fluorescence spectra of TOBPP 6.

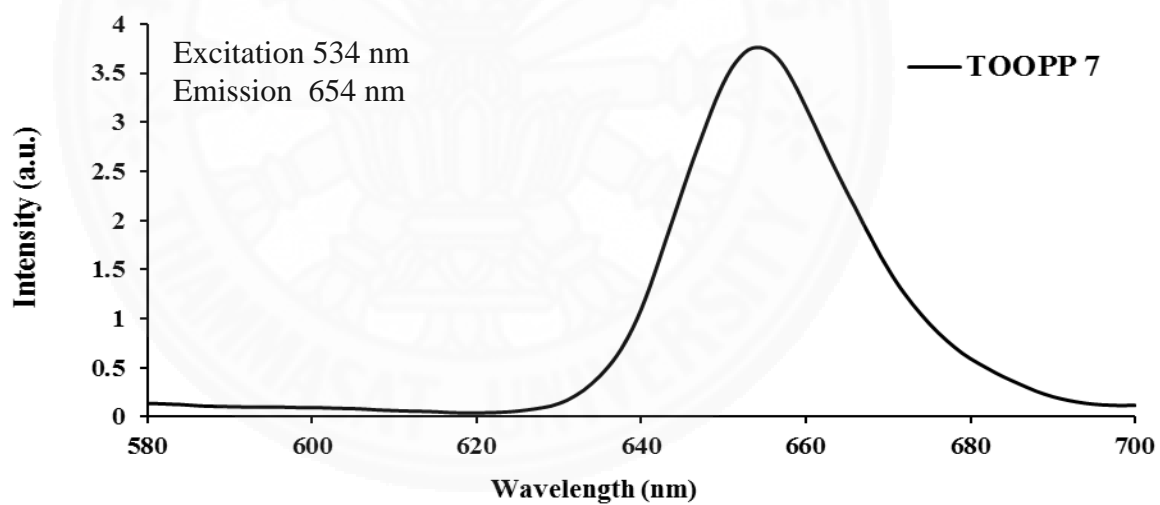


Figure E4. Fluorescence spectra of TOOPP 7.

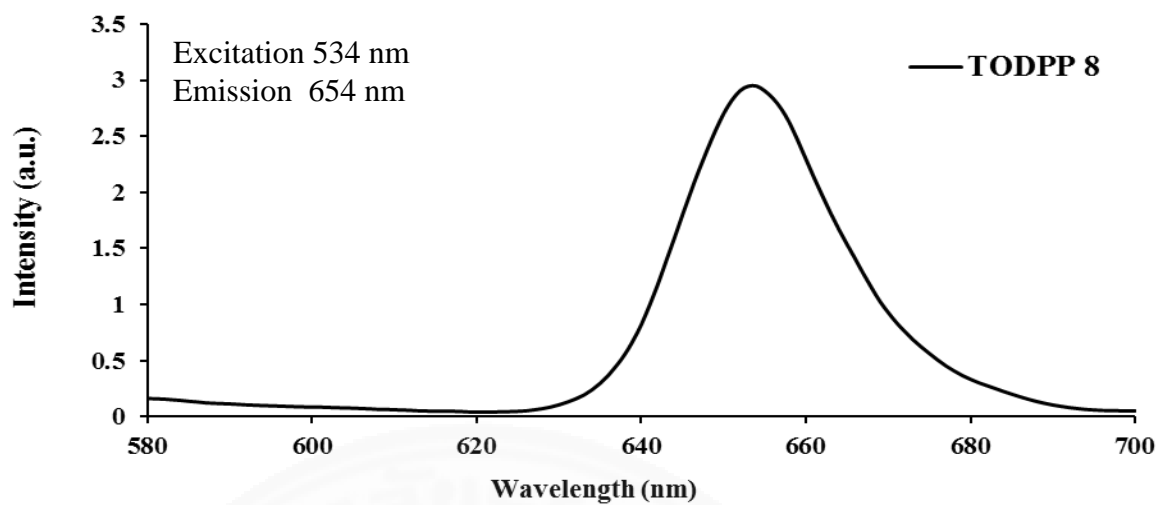


Figure E5. Fluorescence spectra of TODPP 8.

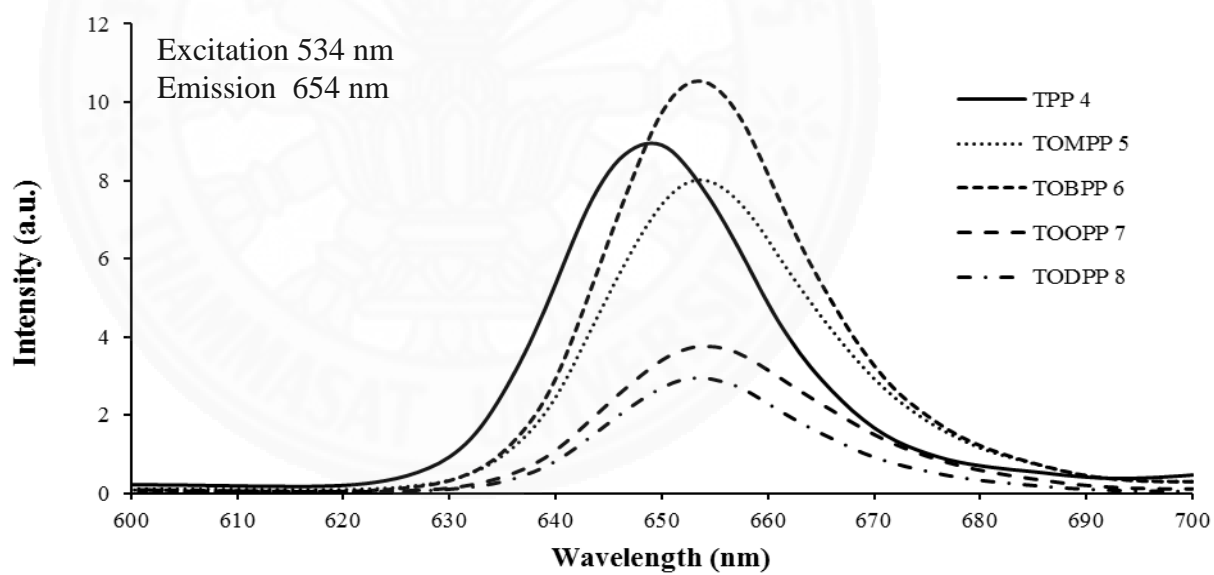
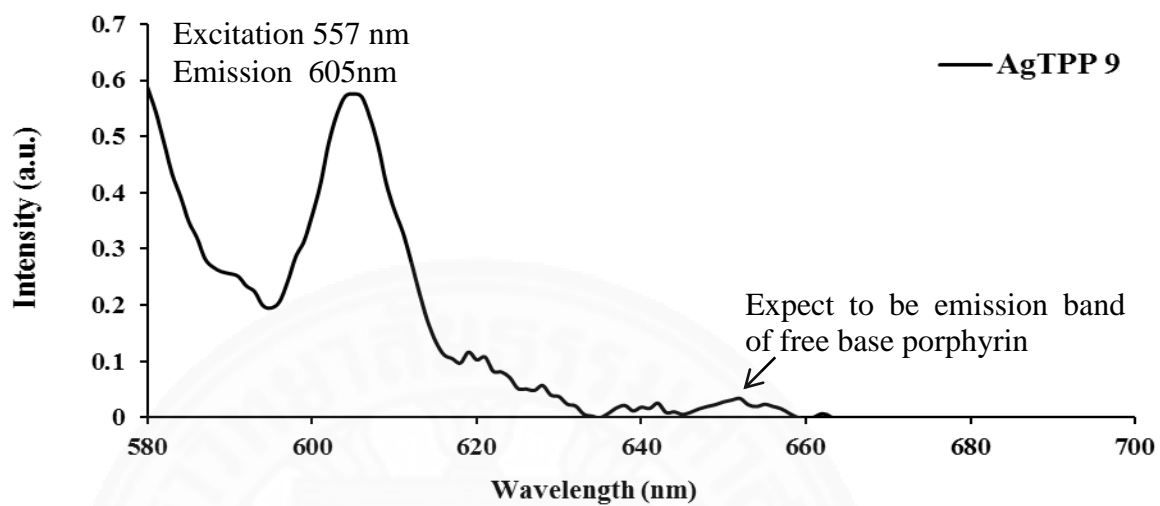
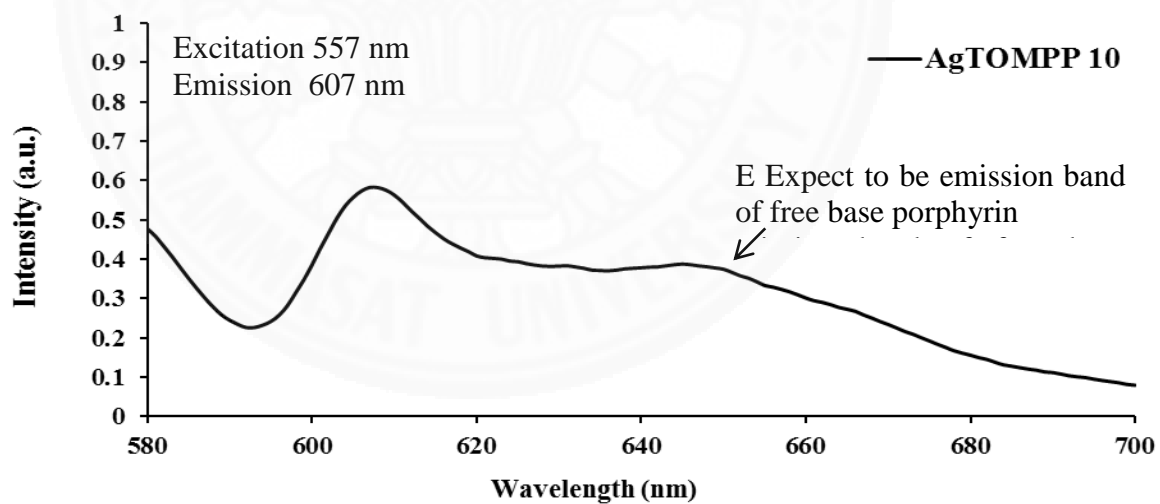


Figure E6. Fluorescence spectra of 4-8.

Fluorescence spectra of silver(II) porphyrins

**Figure E7.** Fluorescence spectra of Ag-TPP 9.**Figure E8.** Fluorescence spectra of Ag-TOMPP 10.

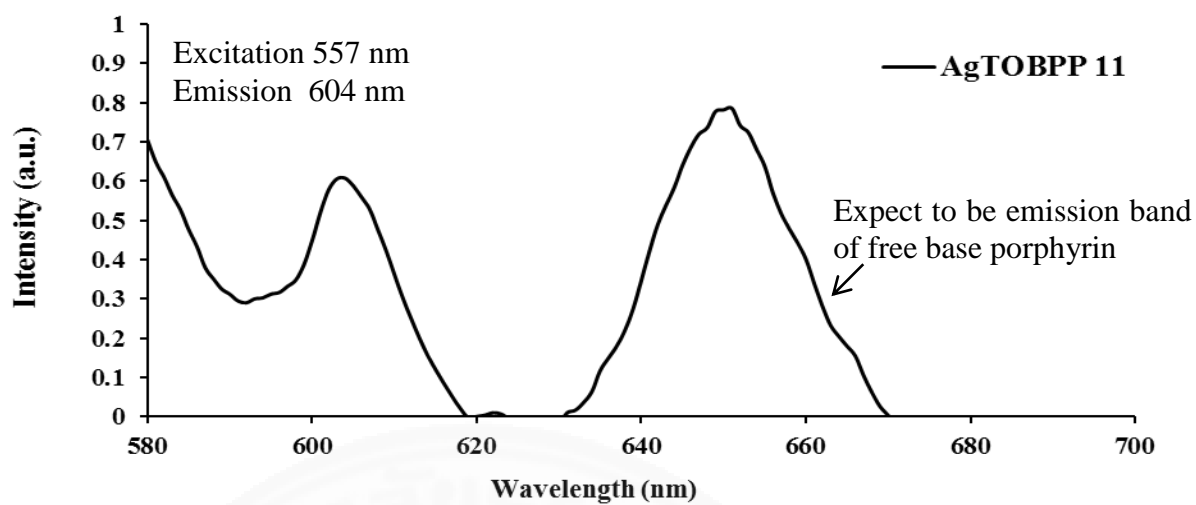


Figure E9. Fluorescence spectra of Ag-TOBPP 11.

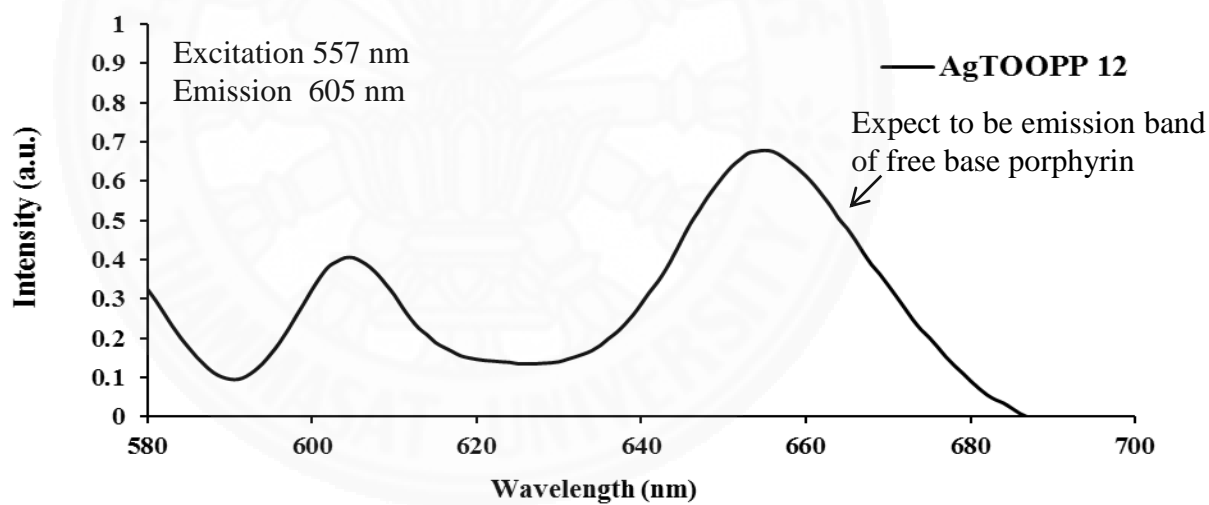


Figure E10. Fluorescence spectra of Ag-TOOPP 12.

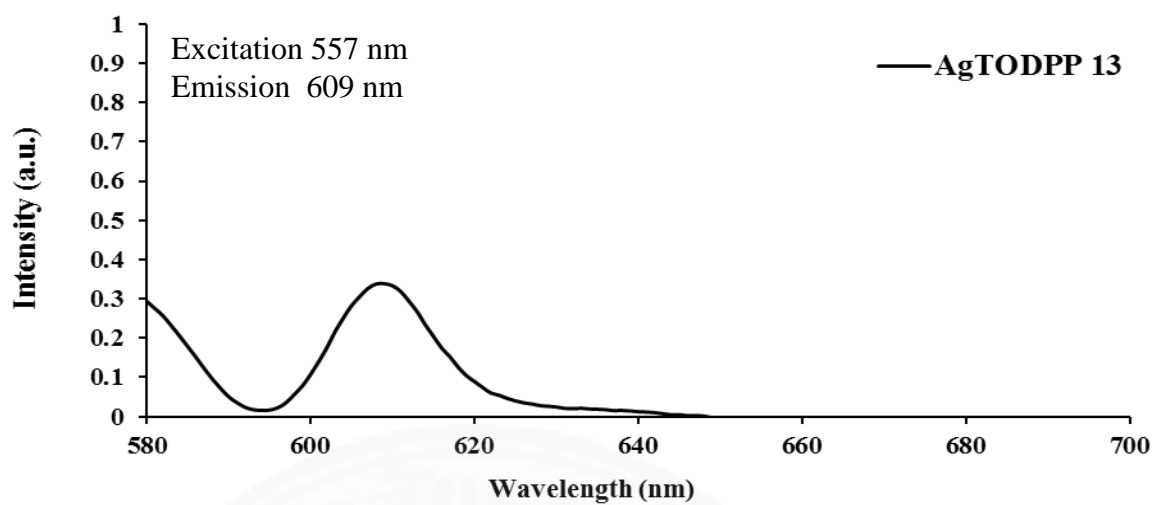


Figure E11. Fluorescence spectra of Ag-TODPP 13.

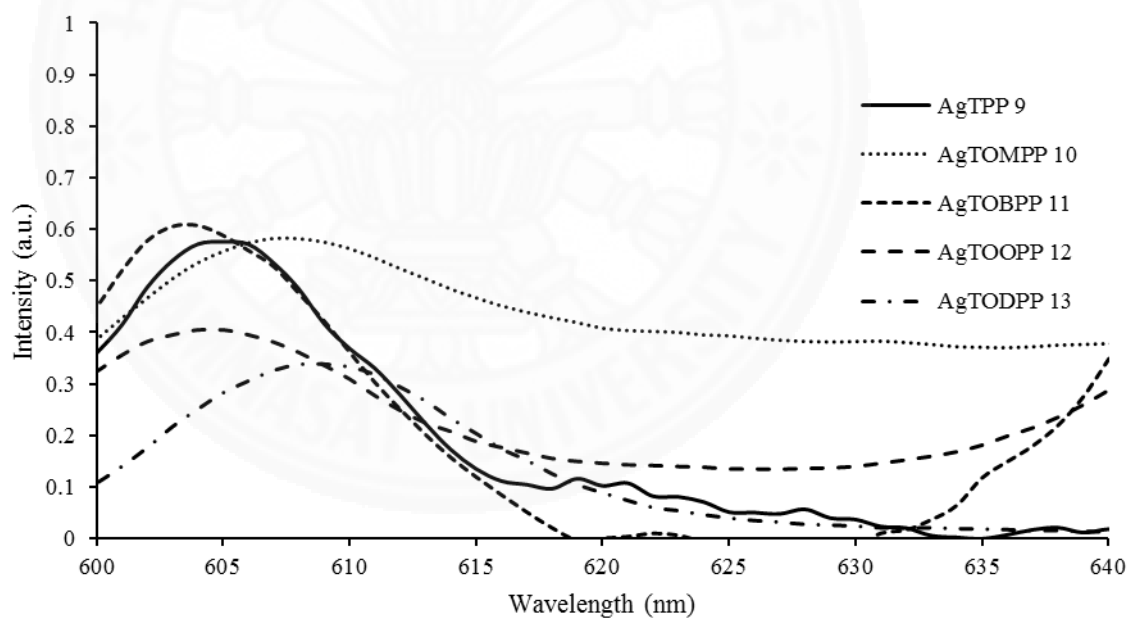


Figure E12. Fluorescence spectra of 9-13.

APPENDIX F

THE DYNAMIC RESPONSE

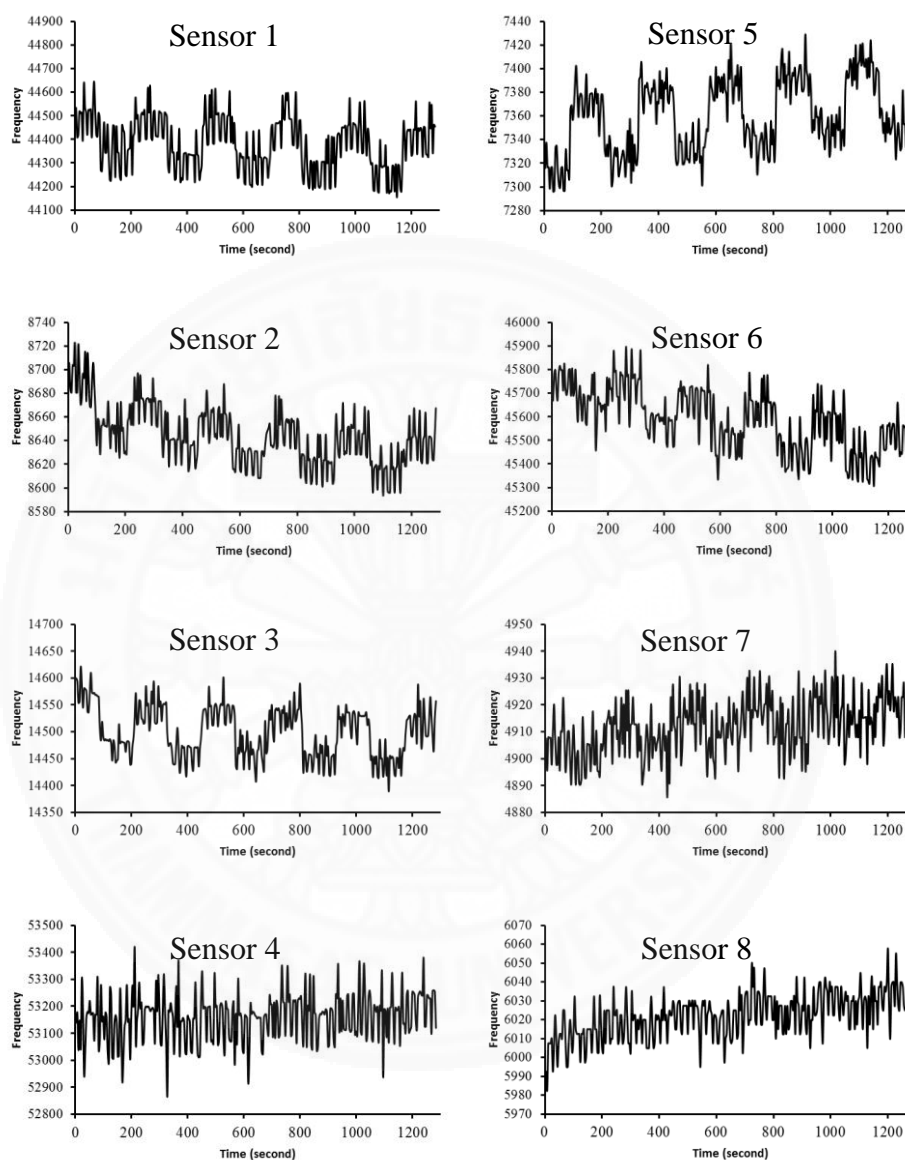


Figure F1. The dynamic response of Ag-TPP film in the presence of methanol vapor.

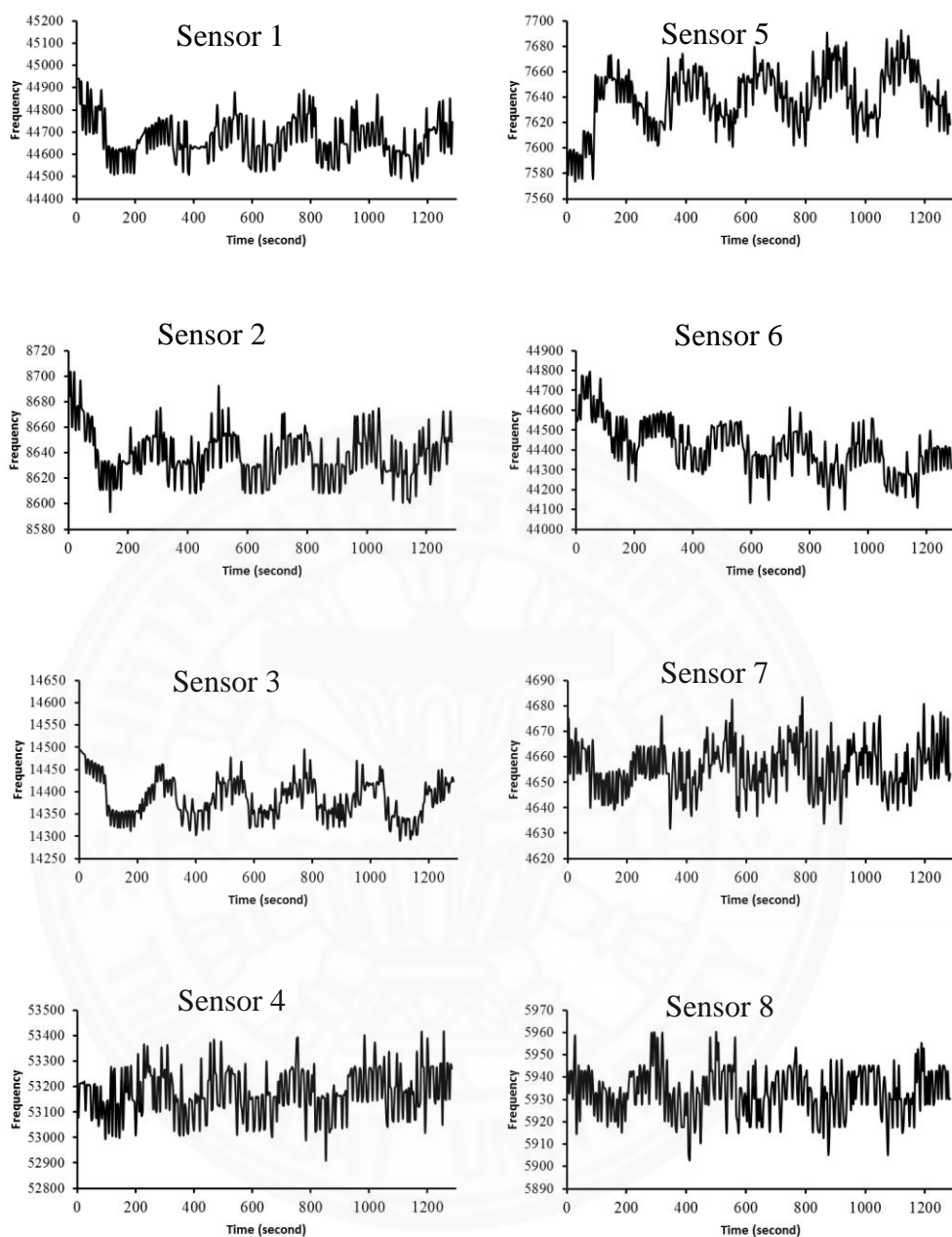


Figure F2. The dynamic response of Ag-TPP film in the presence of ethanol vapor.

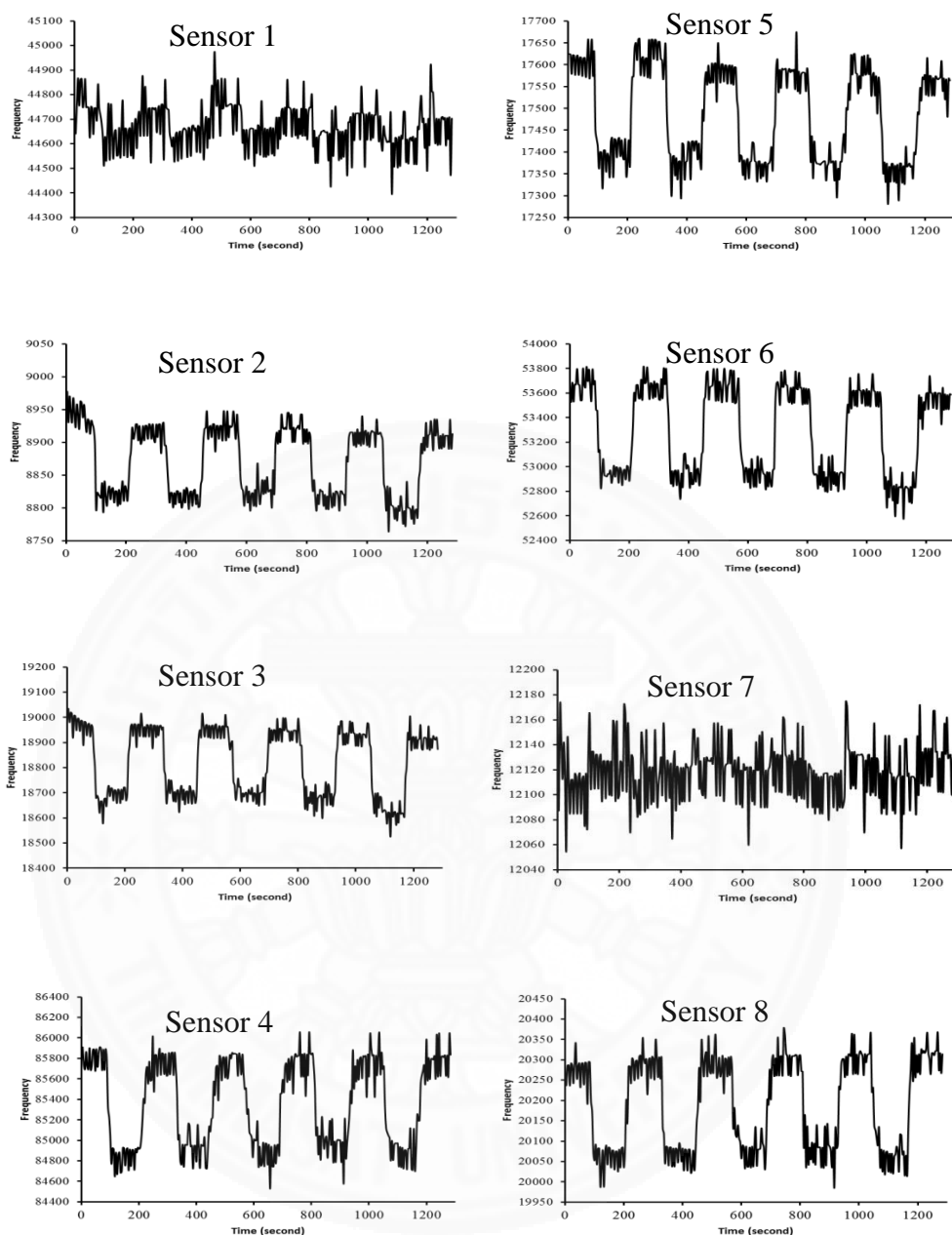


Figure F3. The dynamic response of Ag-TOMPP film
in the presence of methanol vapor.

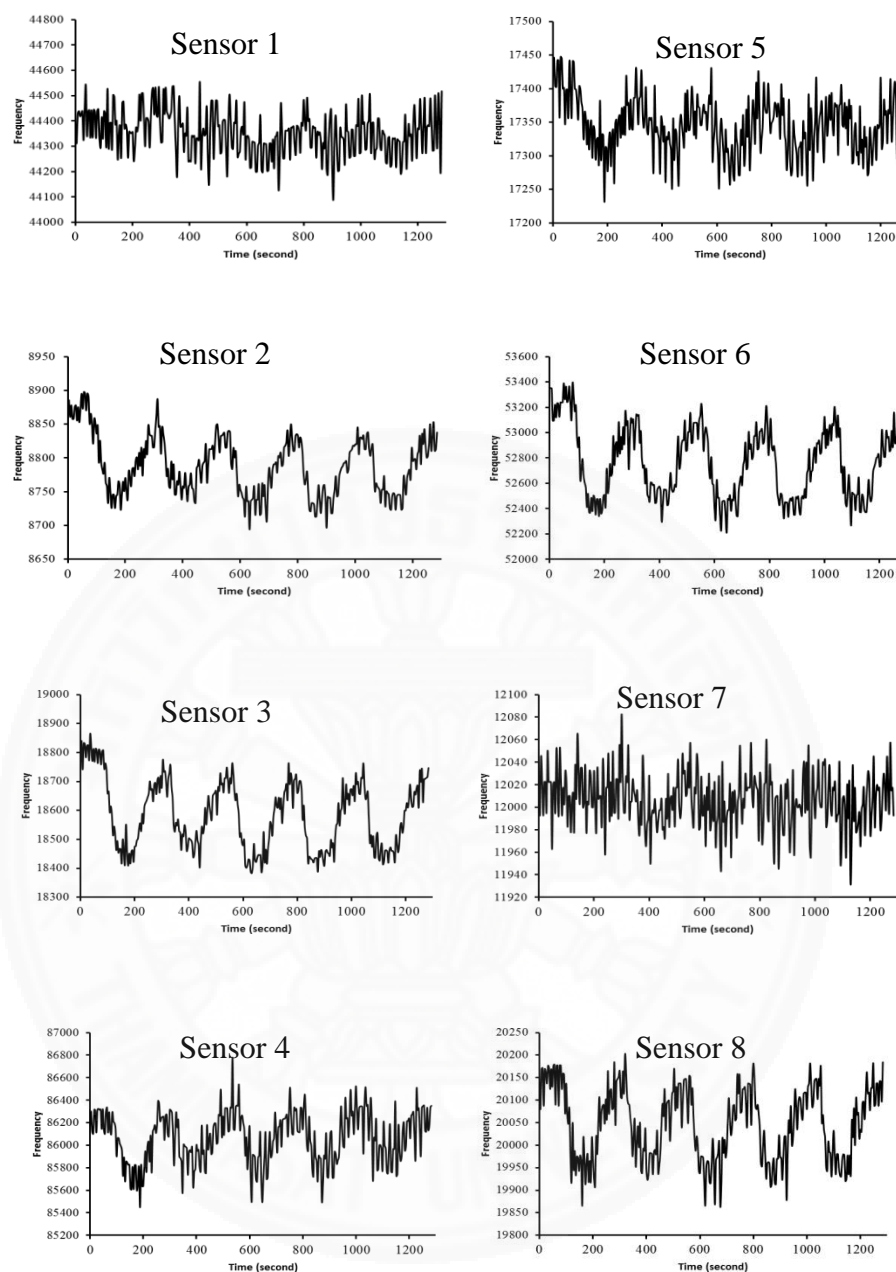


Figure F4. The dynamic response of Ag-TOMPP film in the presence of ethanol vapor.

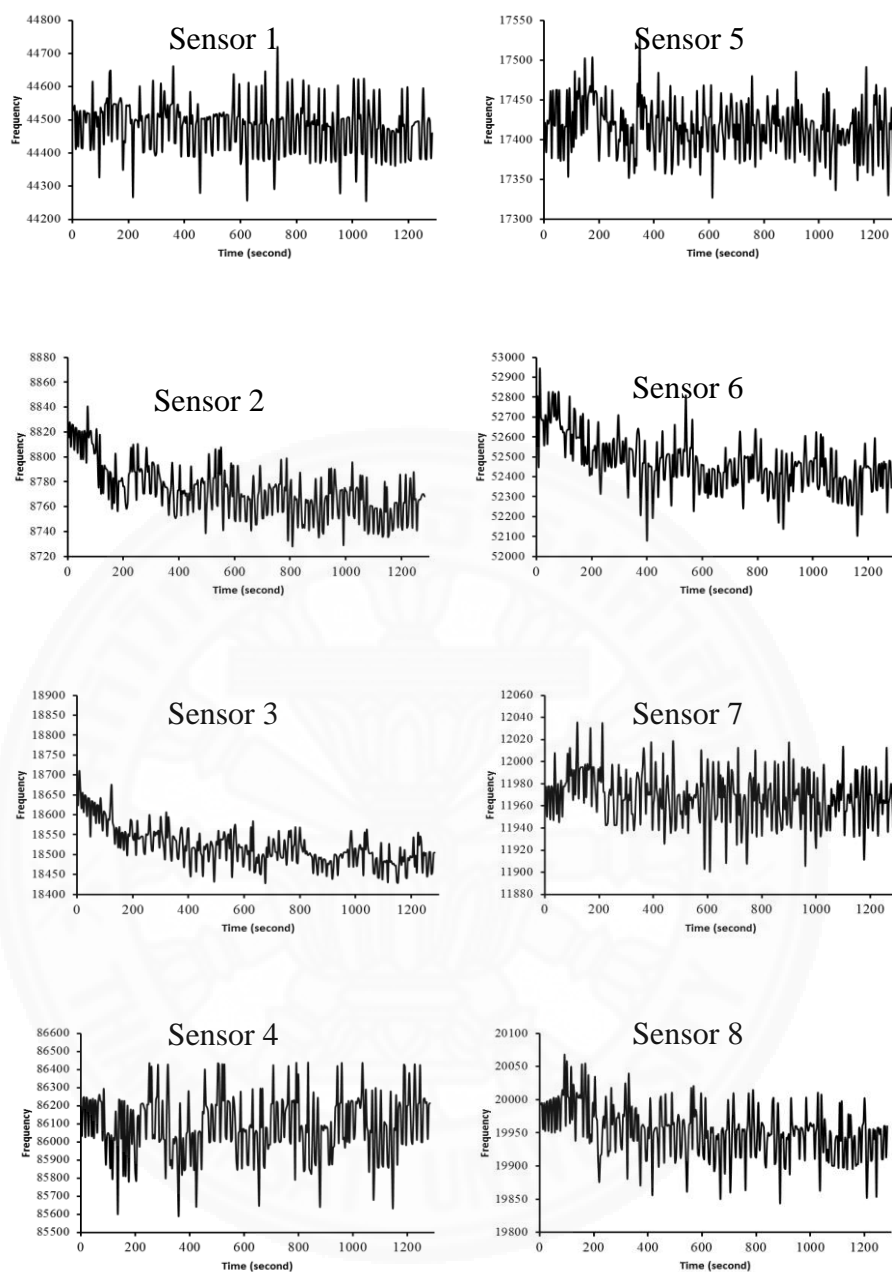


Figure F5. The dynamic response of Ag-TOMPP film in the presence of iso-propanol vapor.

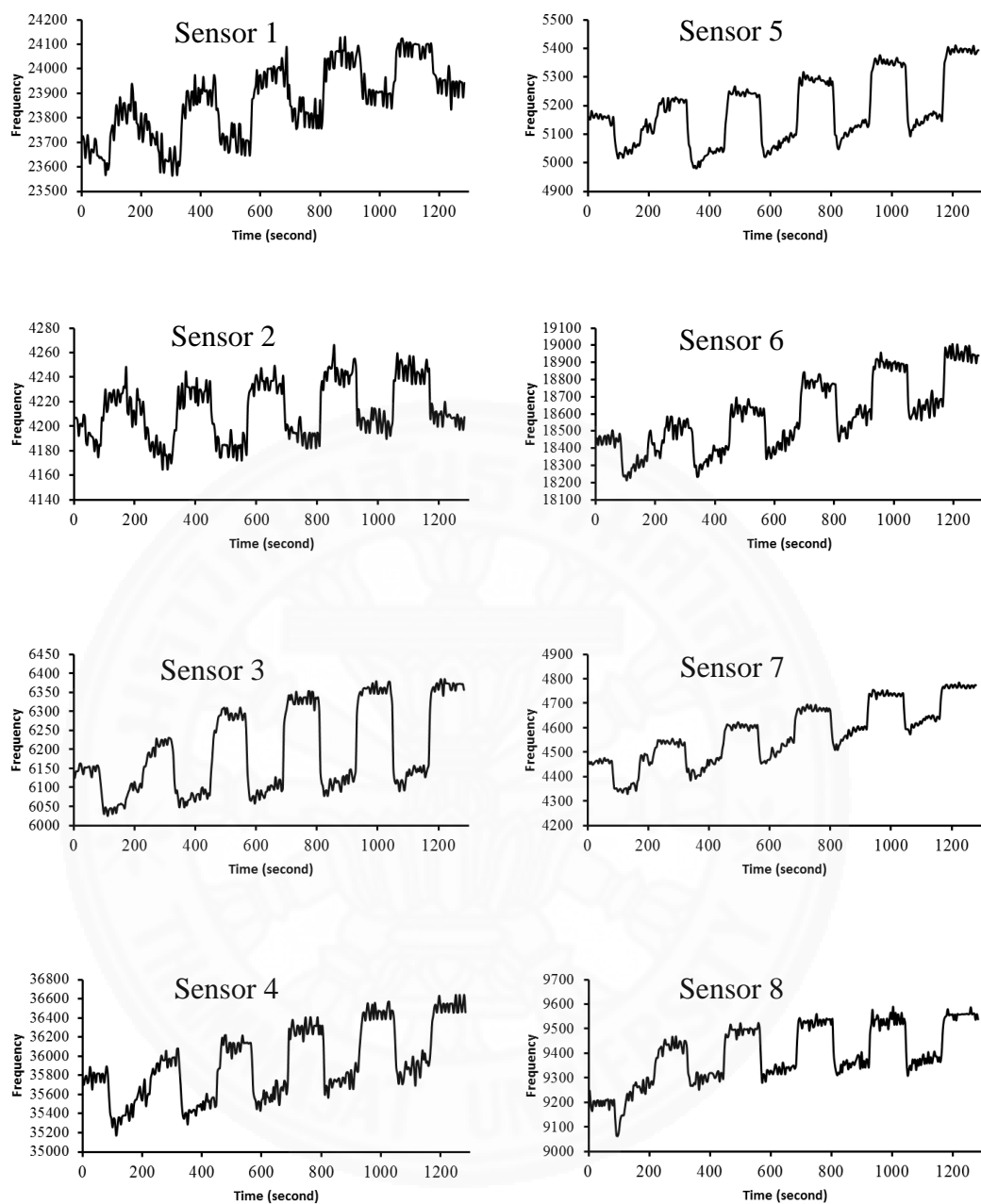


Figure F6. The dynamic response of Ag-TOBPP film in the presence of methanol vapor.

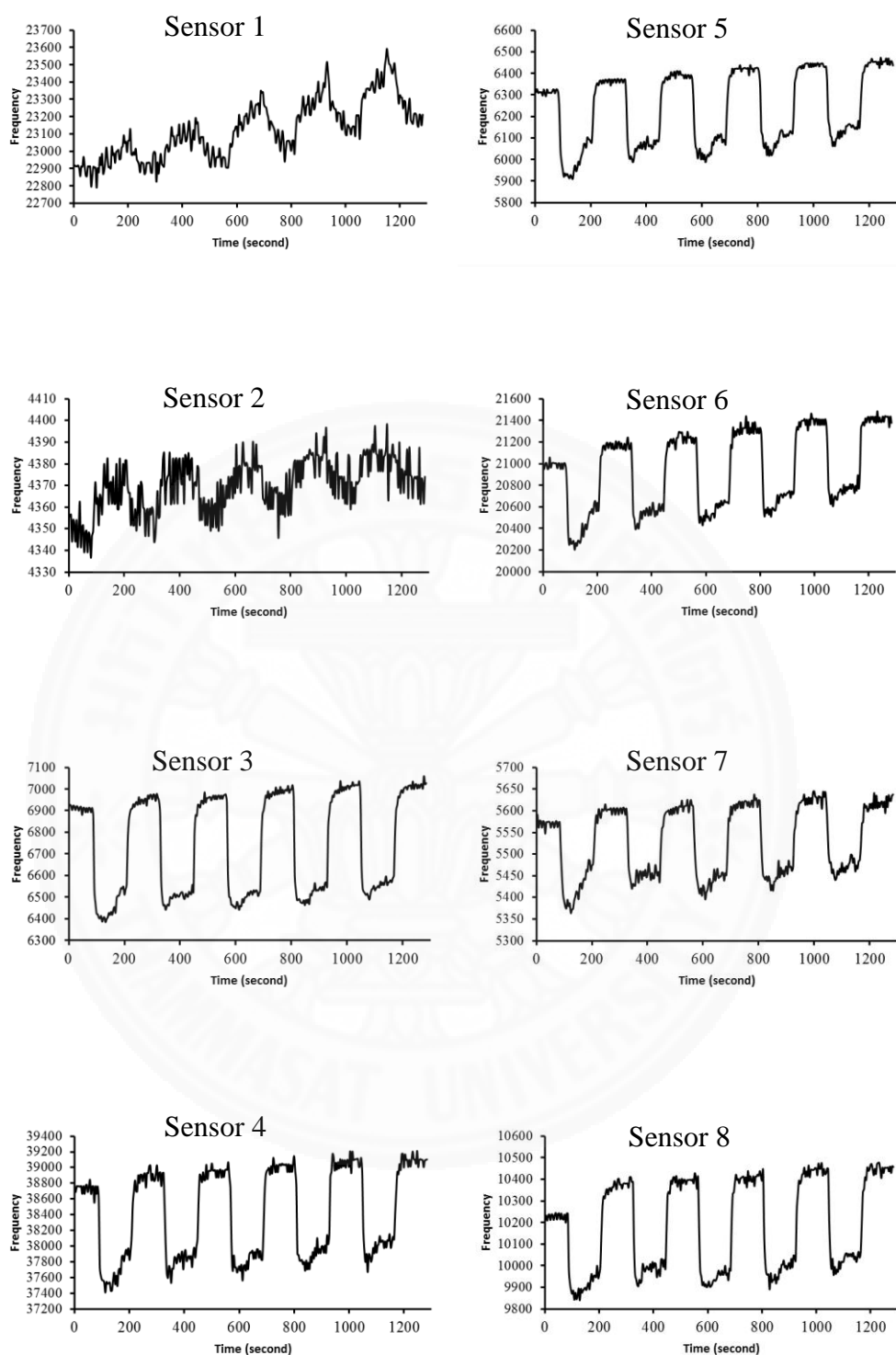


Figure F7. The dynamic response of Ag-TOBPP film in the presence of ethanol vapor.

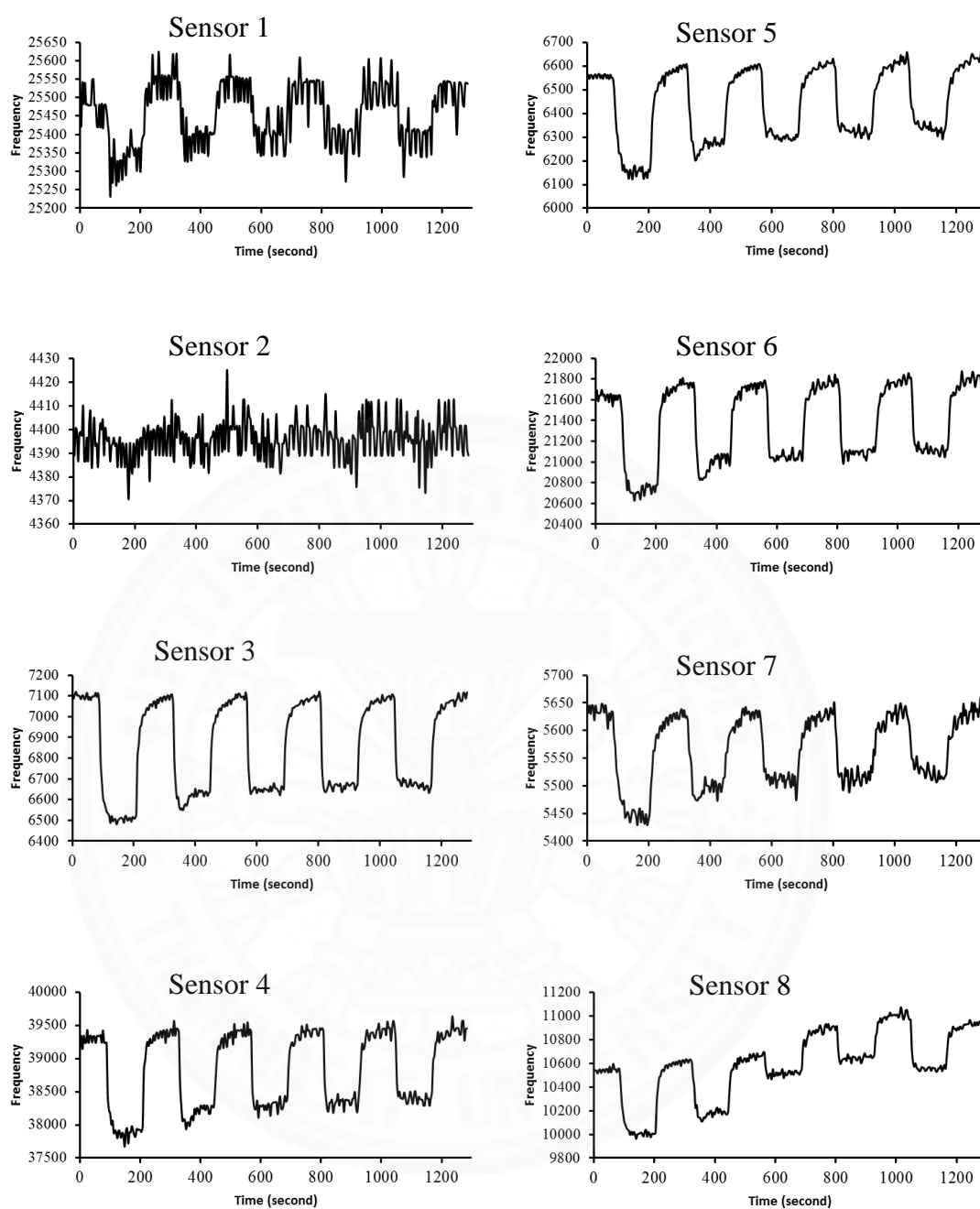


Figure F8. The dynamic response of Ag-TOBPP film in the presence of iso-propanol vapor.

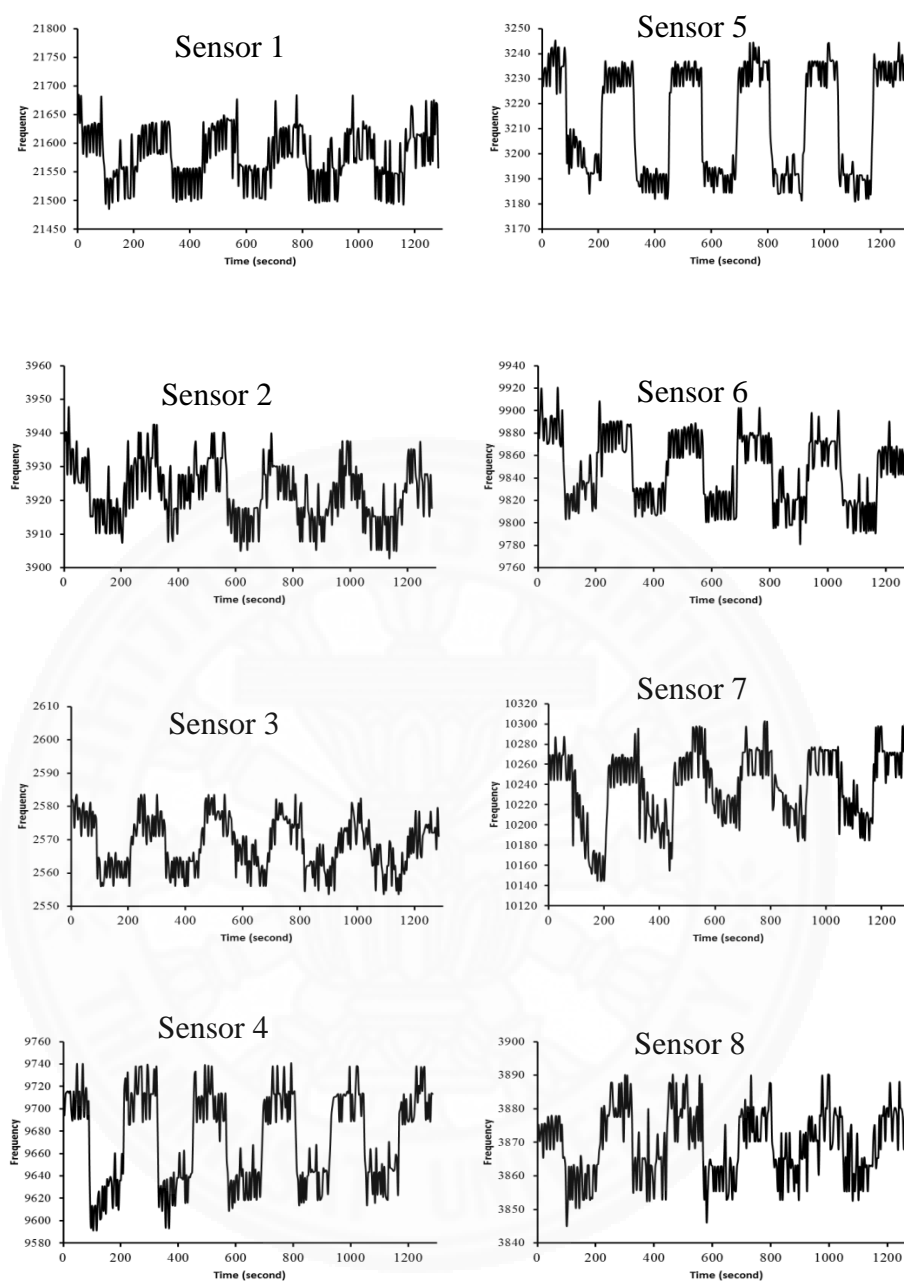


Figure F9. The dynamic response of Ag-TOOPP film in the presence of methanol vapor.

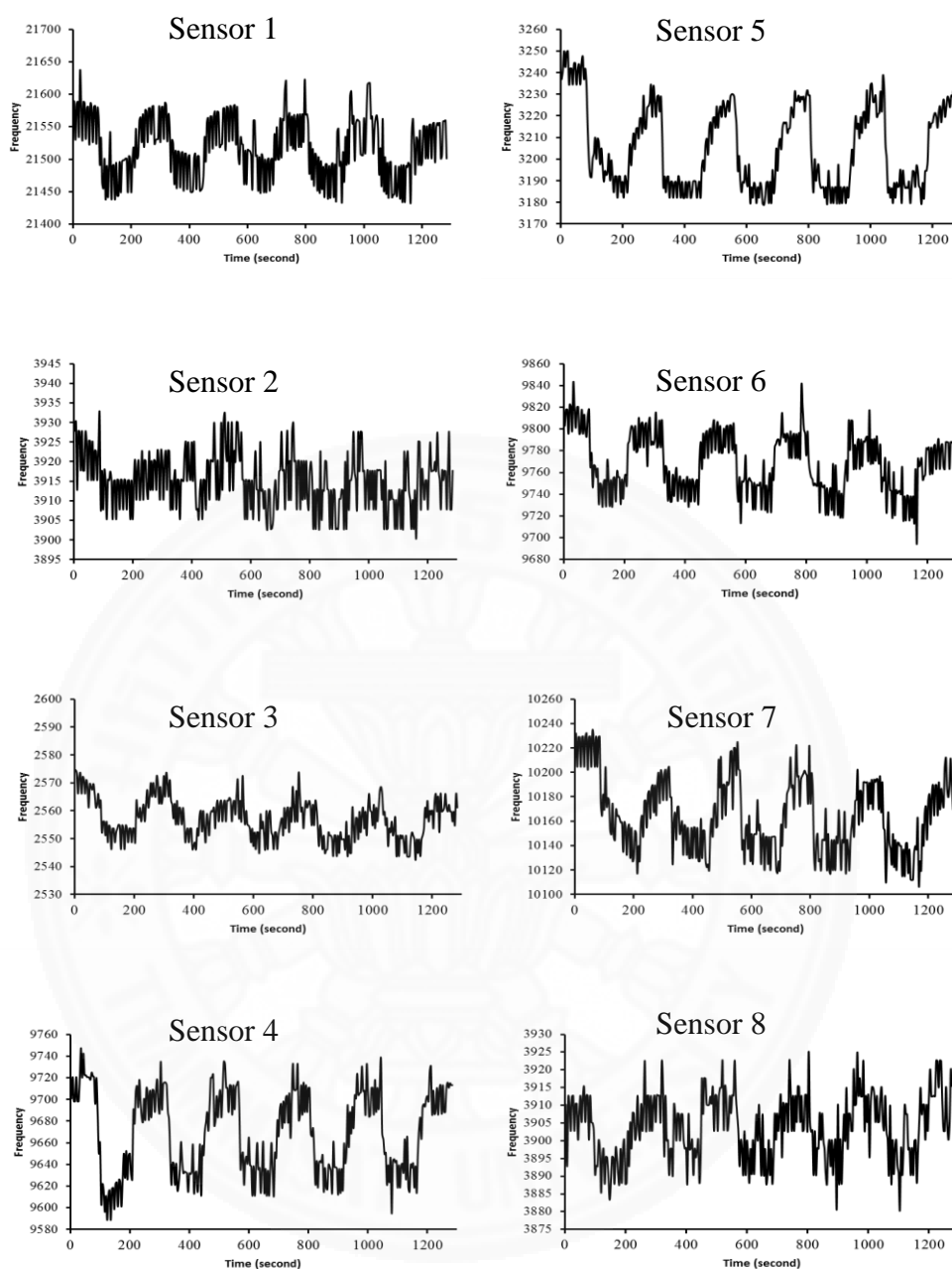


Figure F10. The dynamic response of Ag-TOOPP film in the presence of ethanol vapor.

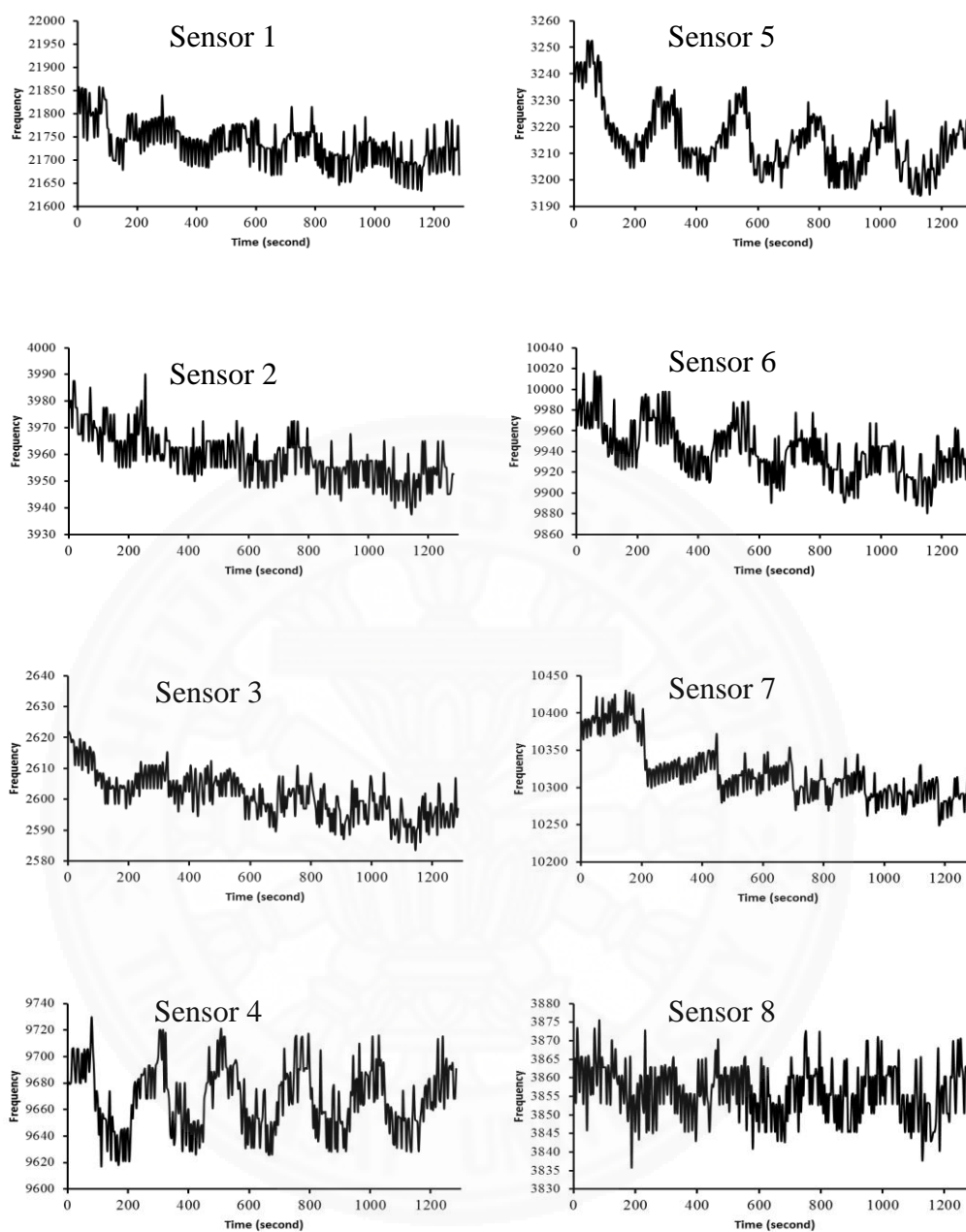


Figure F11. The dynamic response of Ag-TOOPP film in the presence of iso-propanol vapor.

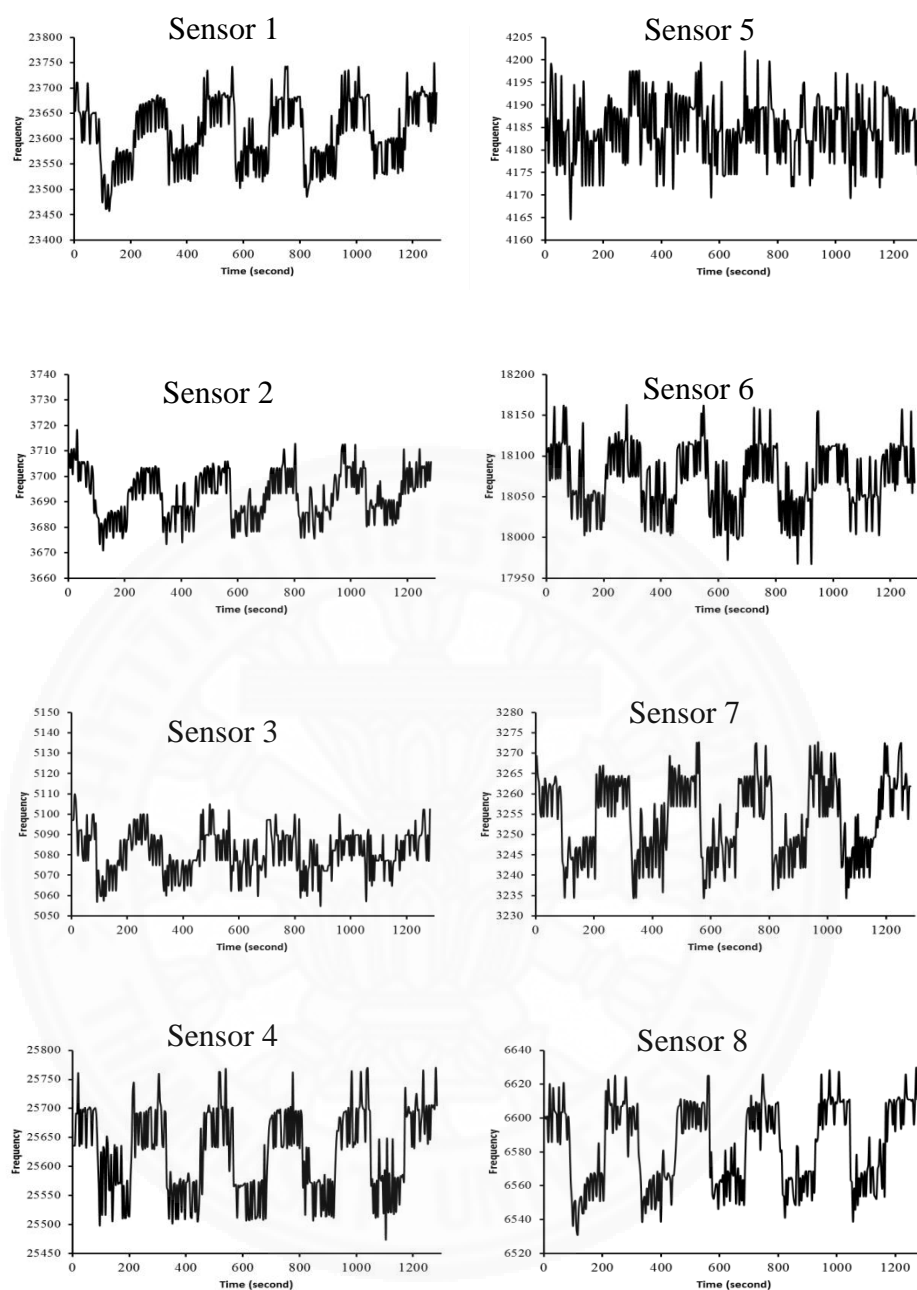


Figure F12. The dynamic response of Ag-TODPP film in the presence of methanol vapor.

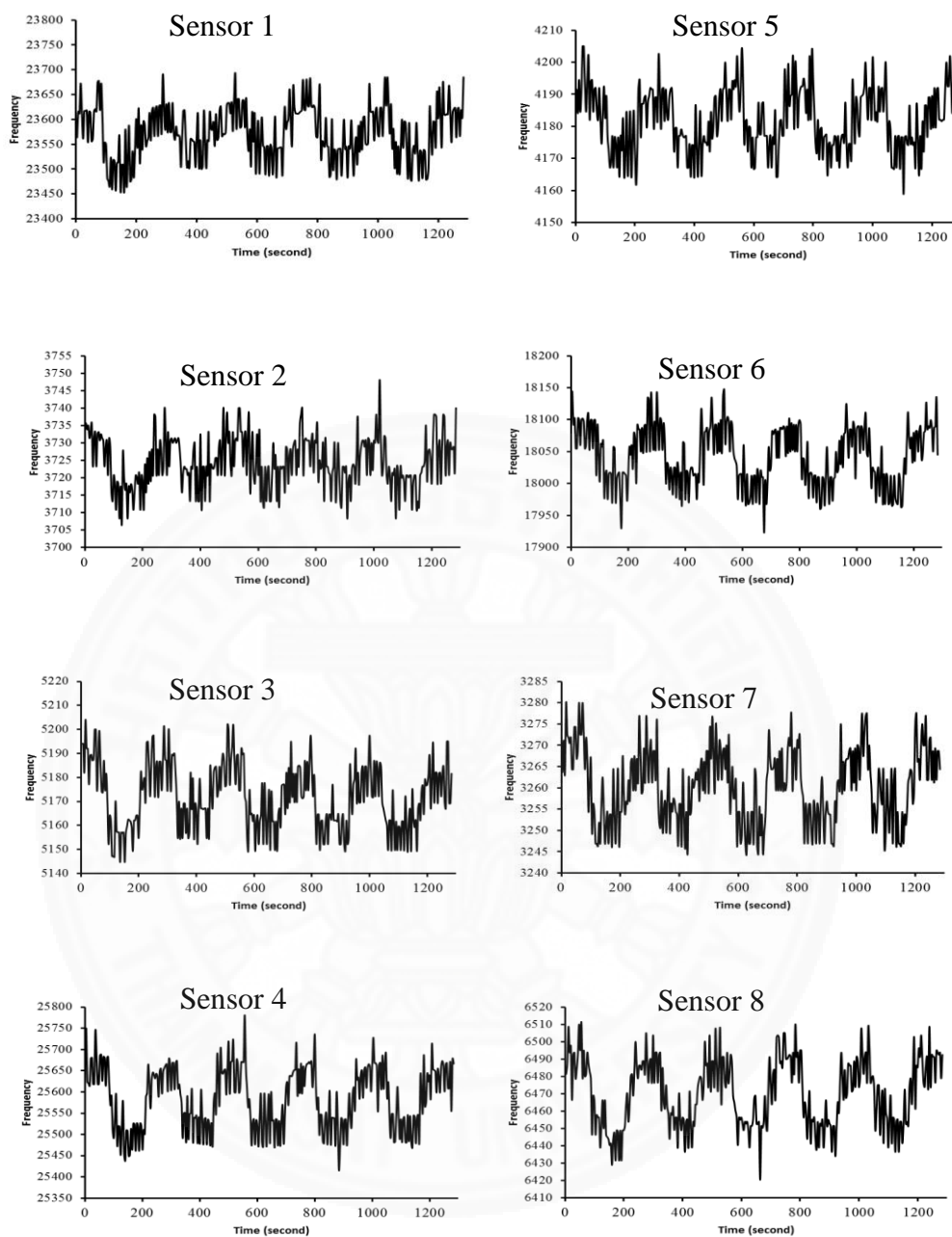


Figure F13. The dynamic response of Ag-TODPP film in the presence of ethanol vapor.

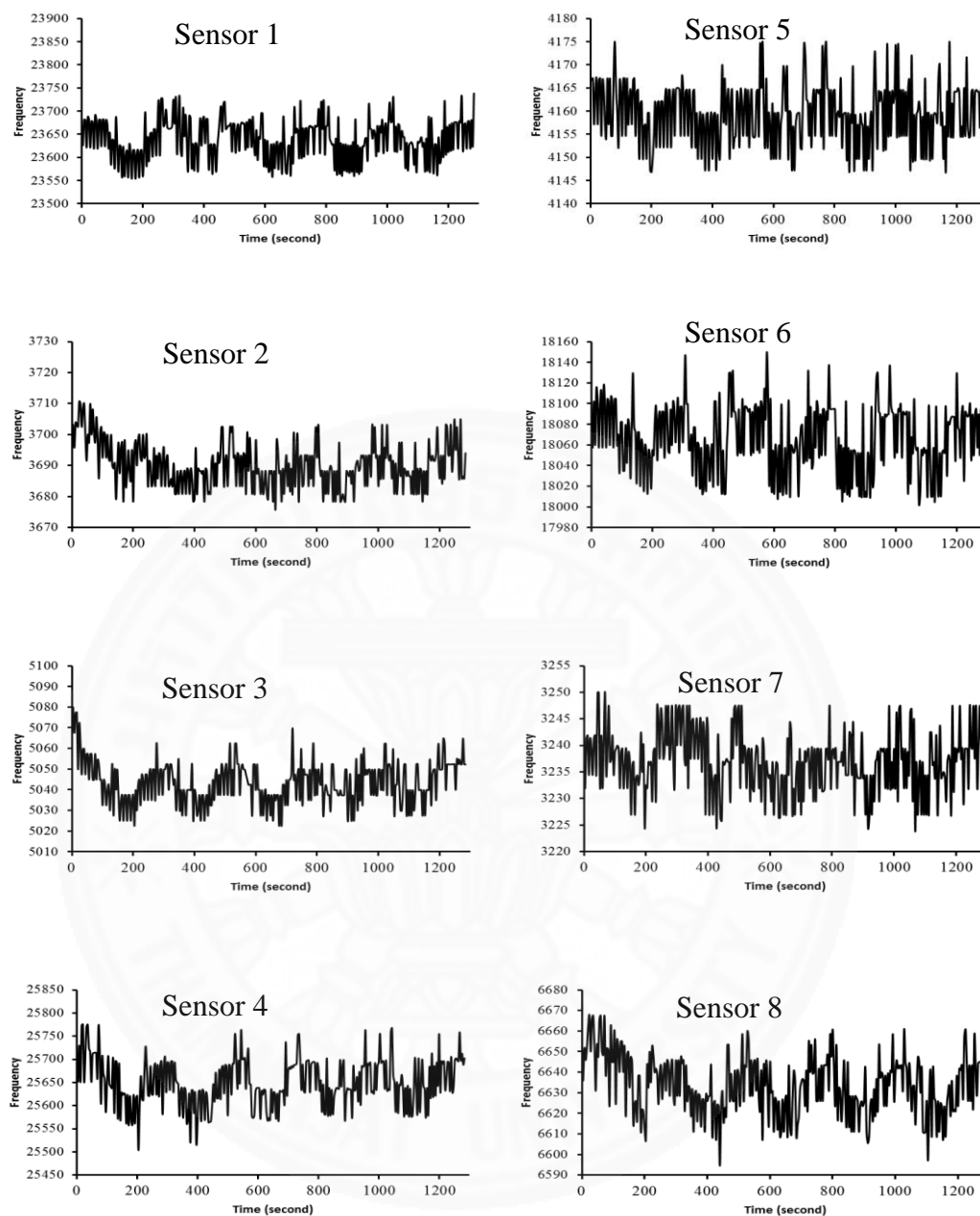


Figure F14. The dynamic response of Ag-TODPP film in the presence of iso-propanol vapor.

APPENDIX G

PUBLICATION

C3_177 PF: THE NOVEL 2-NITRO-TETRAKIS(4-ALKOXYPHENYL) PHENYLPORPHYRINATOCOPPER(II) COMPLEXES: SYNTHESIS, CHARACTERIZATION AND ITS BACTERIAL ACTIVITY

Marisa Matsathum,¹ Supakorn Boonyanon,¹ Teesaporn Pichmasit,¹ Anthevit Nuchthanon,¹ Pariya Na Nakorn,² Anujina Poomkiesag,²

¹ Department of Chemistry, Faculty of Science and Technology, Thammasat University, Pathumthani, 12121 Thailand

² Department of Biotechnology, Faculty of Science and Technology Thammasat University, Pathumthani 12120, Thailand

*email: chemistryna@gmail.com

Abstract: The complexes 2-nitro-tetrakis(4-alkoxyphenyl)phenylporphyrinatocopper(II): (CuTOMPP-NO₂ and CuTOBPP-NO₂) have been synthesized and fully characterized. Structures of synthesized compounds were confirmed by ¹H-NMR, ¹³C-NMR, UV-Vis, fluorescence spectroscopy, CHN elemental analysis and mass spectrometry. Infrared spectroscopy was used to confirm the functional groups especially for nitro (-NO₂) that attached to the β-position in this structure. The estimated energy gaps of Cu-TOMPP-NO₂ and CuTOBPP-NO₂ are 2.05 and 0.24 eV, respectively. Finally, CuTOMPP-NO₂ and CuTOBPP-NO₂ were tested for antibacterial activity using disc diffusion technique. The synthesized compounds were found to be effective for the inhibition of bacterial growth. The CuTOMPP-NO₂ complexes showed the inhibition capacity comparably to penicillin drug standard.

Keyword: porphyrin, β-nitro substituted porphyrin, bacterial activity.

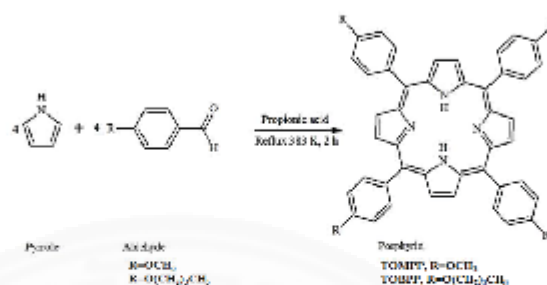
Introduction: Porphyrins are a large class of aromatic organic compounds of natural or synthetic origin, are heterocyclic macrocycles consisting of four pyrrole units connected by four methine bridges [1]. Porphyrins have been widely studied for their spectroscopy, electrochemical, luminescence properties and their biological activity [2]. Porphyrins and their metal complexes were used in many applications such as photodynamic therapy, dye sensitized solar cell (DSSC), catalysts and molecular sensor [3-5]. Porphyrins play very important roles in essential biological activity, and their synthesis arouses continuing interest in biological, material, and inorganic chemistry [6-7]. Photophysical properties of porphyrin derivatives have been the target of a huge amount of investigations during the past few decades, motivated by the possibilities of their use in a large variety of applications including light harvesting systems when the molecular orbital have been disturbed by substitution with electron-withdrawing or electron-donating group at meso- or β- position of the porphyrin rings [8]. Nitration is one substitution reaction of special interest, and porphyrin can be readily transformed into other derivative compounds [9].

The present work focused on the synthesized the 2-nitro-tetrakis(4-methoxyphenyl)phenylporphyrinatocopper(II) (CuTOMPP-NO₂) and the 2-nitro-tetrakis(4-methoxyphenyl)phenylporphyrinatocopper(II) (CuTOBPP-NO₂) via nitration reaction of copper porphyrin. Further antibacterial activity of ligands and their metal complexes have been primarily tested against various bacterial strains. The obtained results were compared with standard drug (penicillin) [10].

Methodology:

Apparatus: Nuclear magnetic resonance spectra were recorded at 400 MHz for ¹H NMR and at 100 MHz for ¹³C NMR using a Bruker (FT-NMR advance 400 MHz) spectrometer. The FT-IR (4000-400 cm⁻¹) spectra were recorded on Perkin Elmer infrared spectrophotometer (spectrum GX). Mass spectra were obtained on Thermo Finnigan mass spectrometer (LCQ Advantage). The elemental analysis was carried out on Perkin Elmer (2400) elemental analyzer. UV-Vis absorption and fluorescence spectroscopic measurements were carried out on a Shimadzu UV-spectrometer (UV-1700) and a Jascofluorimeter (FP-6300), respectively.

Synthesis of free base porphyrins



Free base porphyrins and their derivatives were synthesized by following a published procedure with slight modification [11]. Pyrrole 0.028 mole (2 mL) and *p*-anisaldehyde 0.03 mole (3.1600 g) were taken in a 100 mL round bottom flask containing 40 mL of propionic acid. The reaction mixture was stirred and refluxed at 383 K for 2 hours. After refluxing, the reaction mixture was cooled to room temperature and added 40 mL of ethanol. Then, the mixture was kept in a refrigerator overnight. The purple crystals were filtered, washed, and dried by vacuum filtration with cold ethanol to removed traces of propionic acid. The crude products were purified by silica gel column chromatography and eluted with the increasing polarity by the mixture of dichloromethane and hexane to afford the tetrakis(4-methoxyphenyl)porphyrin (TOMPP) as a purple crystal in 26% yield (0.5988 g). ¹H NMR (400 MHz, CDCl₃): 6.8.8 (8H, Pyrrole, β-H), 8.1 (8H, Phenyl, α-H), 7.2 (8H, Phenyl, m-H), 4.1 (12H, -OCH₃). ¹³C NMR (100 MHz, CDCl₃): 158.75, 134.68, 133.59, 129.97, 127.89, 118.83, 111.44, 54.65 ppm. IR (KBr): 3316, 2991, 2834, 1607, 1509, 1248, 1174, 966, 804 cm⁻¹. Elemental analysis; calcd (%) for C₂₈H₂₀N₄O₄: C 78.45, H 5.21, N 7.62; found: C 76.42, H 5.75, N 7.42. Mass m/z (ESI) calcd for C₂₈H₂₀N₄O₄: 734.84. Found 735.4 [M+H]⁺. UV-vis (CH₂Cl₂): (λ_{max}(nm), ε(10³M⁻¹cm⁻¹)): S-band; (421, 294.9), Q-band; (518, 11.9), (555, 8.2), (595, 3.9), (650, 5.2).

The TOBPP was prepared similarly to TOMPP, by changing *p*-anisaldehyde to *p*-tert-butoxybenzaldehyde. It was obtained 9 % yield. The tetrakis (4-*tert*-butoxyphenyl) porphyrin (TOBPP) was obtained as purple crystal in 9% yield. ¹H NMR (400 MHz, CDCl₃): 6.8.9 (8H, Pyrrole, β-H), 8.1 (8H, Phenyl, α-H), 7.4 (8H, Phenyl, m-H), 4.2 (-OCH₃), 1.9 (-OCH₂CH₃), 1.3 (-CH₂CH₃), 0.9 (-CH₃). ¹³C NMR (100 MHz, CDCl₃): 159.08, 155.32, 134.74, 130.70, 128.76, 119.7, 112.84, 68.14, 31.49, 23.98, 13.84 ppm. IR (KBr): 3320, 2931, 2868, 1607, 1509, 1245, 1174, 966, 802 cm⁻¹. Elemental analysis; cal. (%) for C₄₀H₄₀N₄O₄: C 79.79, H 6.92, N 6.20; found: C 79.44, H 6.55, N 5.83. Mass m/z (ESI) cal. for C₄₀H₄₀N₄O₄: 903.16. Found 903.6 [M+H]⁺. UV-vis (CH₂Cl₂): (λ_{max}(nm), ε(10³M⁻¹cm⁻¹)): S-band; (422, 590.6), Q-band; (519, 22.9), (556, 17.3), (595, 8.6), (651, 11.6).

Synthesis of β-nitro substituted porphyrins:

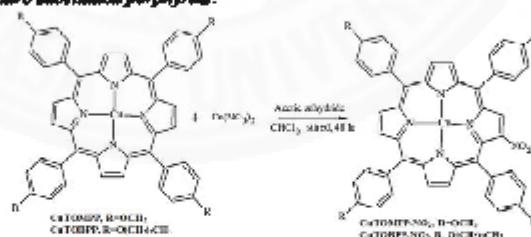


Figure 1. Synthesis of β-nitro-tetrakis(4-alkoxyphenyl)porphyrin/copper(II)

The β-nitro porphyrin derivatives have been synthesized via nitration reaction of copper porphyrin following a previous method [11]. The copper tetrakis(4-methoxyphenyl) (CuTOMPP) 0.3 mmole (0.2028g) was dissolved in 100 mL of chloroform solvent in 250 mL round bottom flask. The copper nitrate

[Cu(NO₃)₂·3H₂O] 0.5 mmole (0.1206g) and acetic anhydride 9 mL were added in the solution. The synthetic mixture was magnetically stirred for 48 hours at room temperature. After that the mixture was washed with water 4 × 50 mL. The organic solvent was removed. Then, the final products were purified by silica gel column chromatography and eluted with the increasing polarity by the mixture of dichloromethane and hexane to afford 2-nitro-tetakis(4-methoxyphenyl)porphyrinocopper(II) (CuTOMPP-NO₂) as a purple crystal in 13% yield. IR (KBr): 2928, 2830, 1607, 1502, 1248, 1174, 1515, 1340, 801 cm⁻¹. Elemental analysis, cal. (%) for CuC₂₈H₃₂N₂O₈: C 65.93, H 4.07, N 7.92; Found: C 66.94, H 4.17, N 7.68. Mass m/z (ESI) calcd for CuC₂₈H₃₂N₂O₈: 841.38. Found 841.8 [M+H]⁺. UV-vis (CH₂Cl₂): (λ_{max}(nm), ε(10³ M⁻¹cm⁻¹)): S-band; (428, 188.9), Q-band; (551, 15.0), (594, 11.5).

The 2-nitro-tetakis(4-hydroxyphenyl)porphyrinocopper(II) (CuTOHPP-NO₂) was prepared by nitration reaction of CuTOHPP. The product was obtained as purple crystal in 8% yield. IR (KBr): 2927, 2870, 1607, 1506, 1256, 1174, 1521, 1340, 800 cm⁻¹. Elemental analysis, calcd (%) for CuC₂₈H₂₀N₂O₈: C 71.43, H 5.85, N 6.94; Found: C 72.79, H 6.27, N 4.34. Mass m/z (ESI) calcd for CuC₂₈H₂₀N₂O₈: 1009.7. Found 1009.6 [M+H]⁺. UV-vis (CH₂Cl₂): (λ_{max}(nm), ε(10³ M⁻¹cm⁻¹)): S-band; (429, 238.1), Q-band; (552, 20.6), (596, 16.5).

Biological activity: The antibacterial activities were evaluated against *Staphylococcus aureus* (ATCC 25923) and *Escherichia coli* (ATCC 25922) by Disc diffusion method [12]. The compounds were dissolved in DMSO (solvent control) to obtain concentration of 1 mg/mL. Nutrient agar medium was prepared by using nutrient broth 4.00 g and agar 7.50 g in water. The disc of Whatmann No.1 filter paper having the diameter 5 mm, autoclave priors used. Both compound solution 30μL (1,000 ppm) was applied on disc then placed over the media. The DMSO was served as control solvent, while penicillin (1 mg/mL) was selected for standard drug. The samples were incubated for 24 hours at 37.00 ± 2.00 °C. The inhibition zone was carefully measured in mm.

Results and Discussion: The β-functionalized porphyrins were investigated. The nitro (-NO₂) functional group have been inserted into the β-position of copper porphyrin complexes followed the reported work by Hengshan H. [13]. The synthetic products (CuTOMPP-NO₂ and CuTOHPP-NO₂) have been obtained in the lowest yield (less than 15%), due to the steric of substituted group on para position, and the symmetry of porphyrin ring. The characteristic data were shown in Table 1.

Table 1: The characteristic data for β-nitro substituted porphyrin

Compounds	Empirical formula	Yield (%)	Formula weight ^a	Elemental analysis (%)			MS (m/z)
				C	H	N	
TOMPP	C ₂₈ H ₃₂ N ₂ O ₄	26	734.84	76.42 (78.45)	5.75 (5.21)	7.42 (7.62)	735.4
TOHPP	C ₂₈ H ₂₀ N ₂ O ₄	9	903.16	79.44 (79.79)	6.55 (6.92)	5.83 (6.28)	903.6
CuTOMPP-NO ₂	CuC ₂₈ H ₃₂ N ₂ O ₈ ·0.5 CH ₂ Cl ₂	13	841.38	66.04 (65.93)	4.17 (4.87)	7.68 (7.92)	841.8
CuTOHPP-NO ₂	CuC ₂₈ H ₂₀ N ₂ O ₈ ·0.5CH ₂ Cl ₂ ·3.5C ₆ H ₁₄	8	1009.7	72.79 (72.96)	8.27 (8.07)	4.38 (5.10)	1009.6

^aCalculated without solvent

^bTheoretical values are given in parentheses.

In complexes of porphyrins with the β-nitro substituted copper (II) porphyrin complexes the chemical shifts was observed the broad peaks related with ligands information only. The copper(II) porphyrins were unsuccessfully identified due to the paramagnetic copper porphyrin. Further analysis, including ESR spectroscopy, may be required for studying the information inside into the complexes.

The absorption spectrum of metalloporphyrin and 2-nitrometallaporphyrin are shown for comparison. The Cu-TOMPP displays the absorption at 541 nm (Q band). The signature of an effective intramolecular charge transfer [13]. However, when inserted the nitro (-NO₂) group in copper(II) porphyrin, the Soret-band of β-nitro substituted porphyrin was moved to red shift, compared with copper (II) porphyrin, the similar result was reported by Ravi K. and Muniappan S. [14]. Thus the energy gap (HOMO and LUMO) of β-nitro substituted porphyrin are less than other synthesized

complexes. The introduction of nitro (-NO₂) group at β -position does alter the absorbance spectra by lower the energy gap (Table 2).

Table 2: The absorption data of all compounds

Porphyrin	Dichloromethane ^a				
	S band (nm)	Q band (nm), ϵ (M ⁻¹ cm ⁻¹)			
		Q ₁	Q ₂	Q ₃	Q ₄
CuTOMPF	419	-	541, 18914	-	-
CuTOBPP	419	-	541, 24599	-	-
CuTOMPF-NO ₂	428	-	551, 15074	594, 11568	-
CuTOBPP-NO ₂	429	-	552, 20652	596, 16522	-

^a All solution were prepared in the concentration of 1×10^{-5} mol/L, in CH₂Cl₂ (n = 3, %RSD \leq 1.6) and measured in the wavelength range of 200–800 nm.

The fluorescence of CuTOMPF have been obtained at 654 nm and CuTOBPP at 605 nm when excited at 536 nm. While the β -nitro substituted porphyrin complexes were excited at 566 nm, the emission spectra were shown between 618 – 619 nm. The emission data of all compounds were summarized in Table 3.

Table 3: The absorption-emission wavelength and the estimated energy gap of free base porphyrins in dichloromethane

porphyrin	Dichloromethane		
	Absorption wavelength (nm)	Emission wavelength (nm)	E _{gap} (eV)
CuTOMPF	556	654	2.16 ^a
CuTOBPP	556	604	2.17 ^a
CuTOMPF-NO ₂	566	618	2.05 ^a
CuTOBPP-NO ₂	566	619	2.04 ^a

^a Calculated by using average of wavelength between Q-band and emission band

Biological activity: The antibacterial activity was evaluated against *Staphylococcus aureus* (*S. aureus*) and *Escherichia coli* (*E. coli*) by disc diffusion method. In the previous study, the antibacterial activity of TPF and metalloporphyrin derivative has been reported [15]. The antibacterial screening data (Table 3.) show that CuTOMPF and CuTOMPF-NO₂ were sensitive against *S. aureus*, where the inhibition zone was greater than control solvent (DMSO). The CuTOMPF exhibited clear zone for *S. aureus* and *E. coli*, 14.0 and 8.0 mm, respectively, while CuTOBPP exhibited clear zone for *S. aureus* and *E. coli*, 8.0 and 6.5 mm, respectively. When added nitro group, the trend of inhibition zone was founded to be similar to copper(II) porphyrin. Moreover, CuTOMPF showed greater inhibition activity than penicillin drug standard (*S. aureus* and *E. coli*, 12.5 and 8.0 mm, respectively). In complexes, the positively charge of metal ion is partially shared with the donor atom presented in ligands and may allow the π -electron delocalized over the whole complex, increasing the lipophilic character of the complex. The complex may permeate through the lipid layer of the bacterial membrane and cause the bacteria die.

Table 3: Antibacterial screening data for the synthesized porphyrins

Complex	<i>Staphylococcus aureus</i>	<i>Escherichia coli</i>
	Inhibition zone (mm)	Inhibition zone (mm)
CuTOMPP	14.0	8.0
CuTOBPP	8.0	6.5
CuTOMPP-NO ₂	11.5	8.0
CuTOBPP-NO ₂	9.0	6.5
DMSO	6.8	6.5
Penicillin	12.5	8.0

n=5

Conclusions: In this work, 2-nitro-1-triaza(4-alkoxyphenyl)phenylporphyrinocopper(II): (CuTOMPP-NO₂ and CuTOBPP-NO₂) have been successfully synthesized and characterized by IR spectroscopy, ¹H-NMR and ¹³C-NMR spectroscopy, CHN elemental analysis, and mass spectroscopy. Both β -nitro substituted porphyrin complexes were obtained in low reaction yields due to the steric of alkyl long chain and nitro group at β -position. The UV-Visible absorption showed that upon insertion of the nitro (-NO₂) group in copper(II) porphyrin, the Soret-band of β -nitro substituted porphyrin moved to the longer wavelength. The antibacterial activity indicated that CuTOMPP and CuTOMPP-NO₂ were sensitive against *S. aureus*. Moreover, the CuTOMPP-NO₂ complex showed the inhibition capacity comparably to penicillin drug standard.

References

1. Vicente MGH, Smith KM. *Curr Org Chem*. 2000; 4: 139–174.
2. Chitpakdee C, Namsangruk S, Saitisinsung K, Jongsattiwong S, Kanyin T, Sadyonchuk T, Rittitip K, Promrak V, Kungwan N. *Dyes Pigments* 2015;118: 64–75.
3. Kavin MS, Vicente MGH. *Curr Org Chem. Synthesis* 2014; 11:3–28.
4. Collman JP, Halbert TR, Smalick ES. *Metal Ions Biol*, 1980; 2:256–262.
5. Lu-Lin L, Eric D. (2013). *ChemSoc Rev*. 2013; 42: 297–304.
6. Dolmans DE, Dai F, Rakrak KI. *Nat Rev Cancer*. 2003; 3: 380–387
7. Bardi S, Caruso E, Buccellanti L, Battini V, Zaccaron S, Barbieri P, Orlandi V. *J Photochem Photobiol B*. 2006; 85: 28–38.
8. Adler A, Longo FR, Shergalis W. *J Am Chem Soc*. 1964; 86:3145–3149.
9. Lee Y-Y, Chen J-H, Hsieh H-Y. *Polyhedron* 2003; 22:1633–1639.
10. Fedulova IN, Bragina NA, Novikov NV, Ugol'nikova OA, Mironov AP. *Russ J Bioorganic Chem*. 2007; 33: 589–593.
11. Rittitip K, Meechai S, Namsangruk S, Kanyin T, Jongsattiwong S, Sadyonchuk T, Promrak V. *Tetrahedron Lett*. 2013; 54: 2435–2439.
12. Hblouci A, Leroy-Lhez S, Ouik TS, Grenier K, Sol V. *Bioorg Med Chem Lett*. 2015; 25: 355–362.
13. He H, Duhay M, Zhong Y, Shroff M, Sykes AG. *Eur J Inorg Chem*, 2011; 25:3733–3738.
14. Kumar R, Sankar M. *Inorg Chem*. 2014;53: 12706–12719.
15. Hu J, Pavel I, Maigne D, Wenzler M, Kistler W, Chen Z, Ye Y, Wu Q, Huang Q, Chen S, Niu F. *GuY.SpectrochimActa A Mol Biomol Spectrosc*. 2013;59:1929–1935.

Acknowledgements: The financial and all experiments equipment were supported by Department of Chemistry, Faculty of Science and Technology, Thammasat University. Central Scientific Instrument Center (CSIC) of Faculty of Science and Technology, Thammasat University.

Synthesis, spectroscopic characterization, crystallographic studies and antibacterial activity of 4-(4-nitrophenoxy) benzaldehyde

Monta Malaithong¹, Supakorn Boonyeun¹, Kittipong Chainok², Natthakorn Phadungsak^{1,2}, Pariya Na Nakorn³ and Ausjima Poomkleang³

¹ Department of Chemistry, Faculty of Science and Technology, Thammasat University, Pathumthani, 12121 Thailand

² Materials Innovation and Technology, Department of Physics, Faculty of Science and Technology, Thammasat University, Pathum Thani 12120, Thailand

³ Department of Biotechnology, Faculty of Science and Technology Thammasat University, Pathumthani 12120, Thailand

E-mail: Malaithongmonta@gmail.com

A diaryl ether, 4-(4-nitrophenoxy) benzaldehyde, has been successfully synthesized by the reaction refluxed of 4-hydroxybenzaldehyde and 4-bromonitrobenzene in dimethylformamide (DMF) solvent. The crude product was purified on a silica-gel column. The synthesized structure was characterized by infrared spectroscopy, mass spectroscopy, ¹H-NMR and single-crystal X-ray diffraction analyses. The compound crystallizes in the monoclinic, space group *P2₁/n* with *a*= 11.2089(4) Å, *b*= 7.8839(3) Å, *c*= 13.4165(5) Å, α = 90°, β = 102.9980(10)°, γ = 90°, *v*= 1155.24(7) Å³ and *z*= 4. The C-O-C angle at the central O atom is 119.71(11)°. The intermolecular hydrogen bonding interactions, π - π stacking, C-H \cdots π and N-O \cdots π , connect the molecules to generate supramolecular layers. Furthermore, the title compound was assayed for antibacterial activity for against *Staphylococcus aureus* (*S. aureus*) and *Escherichia coli* (*E. coli*) by minimum inhibitory concentration (MIC) and minimum bactericidal concentration (MBC). The pure compound showed the highest activity for *S. aureus* as MIC= 80 ppm and MBC= 160 ppm.

References

- [1] Yang Y., Wang Z., Yang J., Yang T., Pi W., Ang W., Lin Y., Liu Y., Li Z., Luo Y and Wei Y., "Design, synthesis and evaluation of novel molecules with a diphenyl ether nucleus as potential antitubercular agents", *Bioorganic & Medicinal Chemistry Letters*, 22, (2012), pp 954-957.
- [2] Sawyer JS., "Recent Advances in Diaryl Ether Synthesis", *Tetrahedron*, 56, (2000), pp 5045-5065.



Gas sensor for alcoholic volatile organic compounds based on silver porphyrin molecular film

Monta Malaithong¹, Supakorn Boonyeun^{1,*}, Tossapon Prohmsatit¹ and Sumana Kladsomboon²

¹ Department of Chemistry, Faculty of Science and Technology, Thammasat University, Pathumthani, 12121 Thailand

² Center for Research and Innovation, Faculty of Medical Technology, Mahidol University, Nakhon Pathom 73170, Thailand

*e-mail: chemistrytu@gmail.com

Abstract: A new 5,10,15,20-tetrakis(4-butyloxy)phenyl porphyrinatosilver(II) [Ag-TOBPP] compound has been successfully synthesized and characterized. The structure of the synthesized compounds was confirmed by Proton nuclear magnetic spectroscopy (¹H-NMR), Infrared Spectroscopy (IR), Mass Spectroscopy (MS), Fluorescence and UV-Vis absorption spectra. The dissolved [Ag-TOBPP] complex in chloroform was coated onto clean glass slide by dropping method. The dry film glass slide was used as a detector in an Electronic nose (E-nose) for methanol, ethanol and iso-propanol at ambient conditions. Principal component analysis (PCA) was used as a pattern recognition method to analyze the data set produced from a UV-Vis spectrophotometer. The result showed that the [Ag-TOBPP] organic film can perform efficiently as a selective alcohol sensor with PCA value as 98%.

Keywords: Metallo-porphyrin; Alcohol detection; Electronic nose

1. Introduction

Porphyrins, a large class of aromatic organic compounds of natural or synthetic origin, are heterocyclic macrocycles consisting of four pyrrole connected by four methine bridges.¹ Porphyrins have received much attention due to the use of these compounds in catalysis, as materials with novel electrical and as biomimetic model systems of primary processes of photosynthesis.²⁻⁵ The modified porphyrins, nanotube nanowire and nanorods, have been successfully reported for sensing applications.⁶⁻⁷ Moreover the supramolecular network of the porphyrin offers the interesting pathways for more selective and sensitive than single molecular unit.⁸

The aims of this research mainly focus on two different topics: a) the synthesis and characterization of synthesized porphyrins and b) study the alcohol vapors sensing applications. The first objective of this work is to synthesize and characterize

5,10,15,20-tetrakis(4-butyloxy)phenylporphyrinatosilver(II) [Ag-TOBPP]. The second objective is to prepared [Ag-TOBPP] film on glass slide for methanol, ethanol and iso-propanol vapors sensor in electronic nose.

2. Materials and Methods

2.1 Apparatus

The FT-IR (4000-400 cm⁻¹) spectra were recorded on Perkin Elmer infrared spectrophotometer (spectrum GX). Mass spectra were obtained on Thermo Finnigan mass spectrometer (LCQ Advantage). UV-Vis absorption and fluorescence spectroscopic measurements were carried out on a Shimadzu UV-spectrometer (UV-1700) and a Jasco spectrofluorometer (FP-6200), respectively.

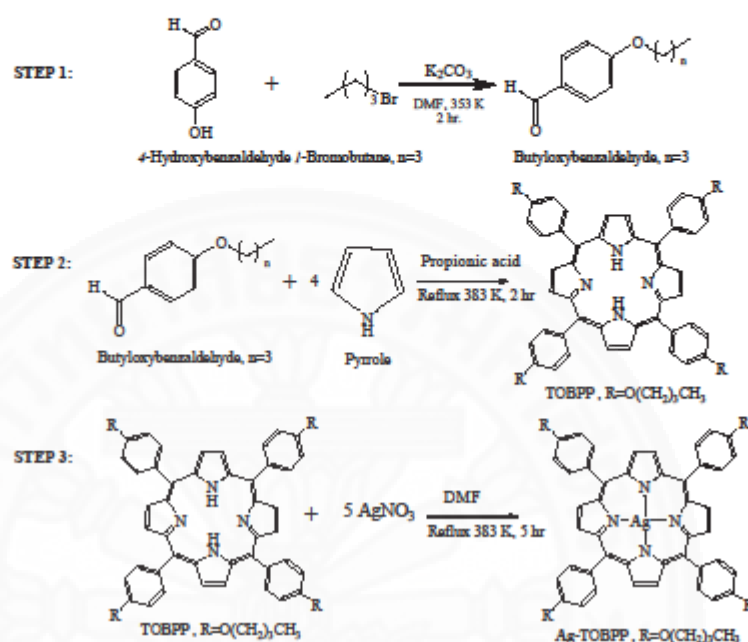


Figure 1. Steps of porphyrin synthesis: 1) synthesis of butyloxyaldehyde, 2) synthesis of free-based porphyrin and 3) synthesis of silver(II)porphyrin.

2.2 Synthesis of butyloxyaldehyde

A mixture of 4-hydroxy benzaldehyde (17.5 mmol) and K_2CO_3 (18 mmol) was stirred in DMF. Bromobutane (18 mmol) was added dropwise and the mixture was heated at 353 K for 2 hours. After cooling, the salts were filtered. DMF was evaporated to dryness, and the reaction mixture was re-dissolved in CH_2Cl_2 and washed with distilled water. Magnesium sulfate anhydrous was used for drying. Butyloxyaldehyde as yellow oil was afforded by filtration and evaporation.

2.3 Synthesis of tetrakis(4-butyloxy phenyl)porphyrin [TOBPP]

Free-based porphyrin was synthesized by following a published procedure with slight modification.⁹

Pyrrole 0.028 mole and butyloxyaldehyde 0.03 mole were taken in a 100 mL round-bottomed flask containing 40 mL of propionic acid. The reaction mixture was stirred and refluxed at 383 K for 2 hours. After refluxing, the reaction mixture was cooled down to room temperature, and added 40 mL of ethanol. Then, it was kept in the refrigerator overnight. The purple crystals were filtered, washed with cold ethanol to remove traces of propionic acid, and dried by vacuum. The crude products were purified by silica gel column chromatography with the mixture of dichloromethane and hexane as eluent to afford TOBPP as a purple crystal in 8.4% yield.

Tetrakis(4-butyloxyphenyl) porphyrin [TOBPP]: FT-IR (Nujol, NaCl): 3318 (N-H str., porphyrin), 2929, 2868 (C-H str.,



phenyl), 1605, 1507 (C=C str., phenyl) 1244 (C-N str., porphyrin), 1173 (C-O str., porphyrin) 965 (N-H bend, porphyrin), 800 (C-H bend, porphyrin) cm^{-1} . Mass spectrum (m/z): 902.19 (cal., 903.16). $^1\text{H-NMR}$ (400 MHz, CDCl_3): δ 8.86 (8H, Pyrrole, β -H), 8.10 (8H, Phenyl, o -H), 7.29 (8H, Phenyl, m -H), 4.24 ($-\text{OCH}_2$), 1.98 ($-\text{OCH}_2\text{CH}_2$), 1.29 ($-\text{CH}_2\text{CH}_3$), 0.92 ($-\text{CH}_3$).

2.3 Synthesis of silver(II) porphyrin [Ag-TOBPP]

[Ag-TOBPP] was synthesized by adapting a previous published procedure.¹⁰ The desired purple solid of complex was obtained in 5.1% yield by refluxing TOBPP with excess silver nitrate (AgNO_3) in mixed solvent between DMF and dichloromethane. After refluxing for 5 hours, the reaction mixture was cooled to room temperature. The mixture was kept in the refrigerator overnight after adding distilled water. Finally, the purple crystal was filtrated, washed with cold water, and dried by vacuum filtration. The reaction product was purified by silica gel column chromatography with the mixture of dichloromethane and hexane as eluent to afford [Ag-TOBPP] as purple crystals.

5,10,15,20-*tetrakis*(4-butyloxy) phenyl porphyrinatosilver(II) [Ag-TOBPP]: FT-IR (Nujol, NaCl): 2935, 2857 (C-H str., phenyl), 1605, 1507 (C=C str., phenyl), 1245 (C-N str., porphyrin), 1174 (C-O str., porphyrin), 784 (C-H bend, porphyrin) cm^{-1} . Mass spectrum (m/z): 1009.60 (cal., 1009.03). $^1\text{H-NMR}$ (400 MHz, CDCl_3): [Ag-TOBPP] was unable to identify by this technique due to a paramagnetic character.

2.4 Alcohol sensing application

The alcohol sensing applications of [Ag-TOBPP] film have been tested by using methanol, ethanol vapor samples and e-nose as a detector. The [Ag-TOBPP] film was prepared similarly with previous reports.¹¹⁻¹² The complex was dissolved in dichloromethane at a concentration of 5 mg

mL^{-1} . Then, the solution was dropped onto the cleaned glass slide, before drying using evaporation method. The [Ag-TOBPP] thin film was investigated by a modified UV-Vis spectrophotometer to act as a so-called "electronic nose". It allows the dynamic measurement of the absorption change due to the interaction of silver derivative porphyrins film with flow-in gases. These instruments were supported by the Faculty of Medical Technology, Mahidol University. For gas sensing measurement, the silver derivative porphyrins film was placed inside the chamber to interact with the sample gases. The acquired data can be then analyzed in real-time by in-house software based on the Principle Component Analysis (PCA).

3. Results & Discussion

The free base porphyrin (TOBPP) was synthesized by a slightly modification of Alder-Longo procedure, resulting the purple crystals of TOBPP with 8.4 % yield. Adding silver ion into the center hole position of ligand TOBPP by refluxing in DMF for 5 hours, yielded 5.1 % of [Ag-TOBPP]. Both TOBPP and [Ag-TOBPP] were characterized and data are shown in Table 1. The $^1\text{H-NMR}$ data showed clear identified signals of TOBPP ligand at 8.86 ppm (for Pyrrole), 8.10-7.29 ppm (Phenyl ring), 4.24 ppm (for $-\text{OCH}_2$), 1.98 ppm (for $-\text{OCH}_2\text{CH}_2$), 1.29 ppm (for $-\text{CH}_2\text{CH}_3$) and 0.92 ppm (for $-\text{CH}_3$). However, the $^1\text{H-NMR}$ gives an unsuccessful analysis for [Ag-TOBPP], which was found only a group of broad peaks, due to their paramagnetic property. The mass spectra of porphyrin long chain and silver porphyrin could also confirm the expected structures as shown in Table 1.



Table 1. Percentage yield, mass spectrometric, UV-Visible spectroscopy data and fluorescence spectroscopy data of porphyrins.

Compounds (Molecular Mass)	Yield (%)	Mass (m/z)	UV-Vis absorption (nm)				Fluorescence (nm)		
			S-band	Q-band				Excitation	Emission
				1	2	3	4		
TOBPP (903.16)	8.4	903.7	422	519	556	595	651	530	655
[Ag-TOBPP] (1009.03)	5.1	1009.6	427	543	-	-	-	560	655

The absorption spectra of free base ligand (TOBPP) and complex [Ag-TOBPP] were acquired from 300 to 700 nm in dichloromethane. The strong absorption intensity was related to the highly conjugated π -electron systems. The spectrum of [Ag-TOBPP] shows an extreme intense Soret band at 427 nm with one weaker intensity Q-band at 543 nm. TOBPP shows one Soret band at 422 nm with a set of 4 Q band peaks at 519, 556, 595 and 651 nm (shown in Table 1.), suggesting the metal ion (Ag^{2+}) has effected on the π - π^* electronic transition. The fluorescence spectra of [Ag-TOBPP] and TOBPP were characterized in dichloromethane. Both [Ag-TOBPP] and TOBPP exhibited a similar emission band at 655 nm, when excited at 560 and 530 nm, respectively. (shown in Table 1 and Figure 3)

Furthermore, the alcohol vapors sensing application by using [Ag-TOBPP] film was investigated. The results showed that the [Ag-TOBPP] film coated on glass slide gave a positive signal for methanol and ethanol vapor, which was different from iso-propopropanol sample. From the PCA results, 96.2% of PC1, and 1.8% of PC2 were detected (already account for 98.0% of the information). These results suggest that [Ag-TOBPP] film can be used as an efficient sensing material to discriminate alcohols.

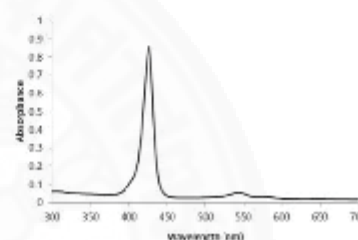


Figure 2. UV-Vis spectra of [Ag-TOBPP] in CH_2Cl_2 .

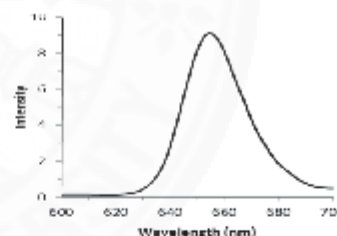


Figure 3. Emission spectrum of [Ag-TOBPP] in CH_2Cl_2

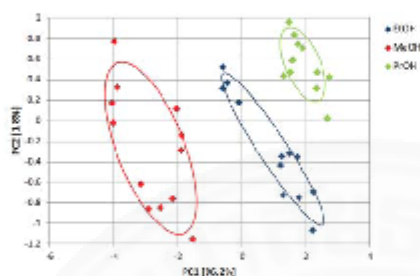


Figure 4. PCA plot of the optical response of the [Ag-TOBPP] thin film to alcohols: methanol, ethanol and iso-propanol.

4. Conclusion

The 5,10,15,20-tetrakis(4-butyloxy)phenyl porphyrinat silver(II) [Ag-TOBPP] was successfully synthesized by using tetrakis(4-butyloxyphenyl)porphyrin ligand and silver nitrate in DMF. The spectroscopic data with a combination of mass spectrometry confirmed the expected [Ag-TOBPP] complex. The result from UV-Vis spectroscopy shows strongly two bands, firstly one intense Soret band at 427 nm, with the second strong intensity weaker Q-band at 543 nm, suggesting the metal ion (Ag^{2+}) has an impact on the π - π^* electronic transition. The fluorescence spectra for both ligand TOBPP and complex [Ag-TOBPP] were found at 655 nm, when excited at 530 and 560 nm, respectively. The clear signal from e-nose for methanol, ethanol and iso-propanol vapor were observed and calculated by using PCA program, suggesting that [Ag-TOBPP] film can be an efficient sensing material to discriminate alcohols.

Acknowledgements

The financial and all experiment equipments were supported by the Department of Chemistry, Faculty of Science and Technology, Thammasat

University and the Faculty of Medical Technology, Mahidol University.

References

1. Abraham, R.J.; Medforth, C.J.; Mansfield, K.E.; Simpson, D.J.; Smith, K.M. *J Chem Soc* 1998, 2, 1365-1369.
2. Huang, G.; Mo, L.-Q.; Cai, J.-L.; Cao, X.; Peng, Y.; Guo, Y.-A.; Wei, S.-J. *Appl Catal B* 2015, 162, 364-371.
3. Castro, K.A.D.F.; Simões, M.M.Q.; Neves, M.G.P.M.S.; Cavaleiro, J.A.S.; Ribeiro, R.R.; Wypych, F.; Nakagaki, S. *Appl Catal A* 2015, 503, 9-19.
4. Alenezi, K.; Tovmasyan, A.; Batinic-Haberle, I.; Benov, L.T. *Photodiagnosis Photodyn Ther* 2017, 17, 154-159.
5. Xu, X.-J.; Xue, Z.; Q, Z.-D.; Hou, A.-X.; Li, C.-H.; Liu, Y. *Thermochimica Acta* 2008, 476, 33-38.
6. Song, F.; Ma, P.; Chen, C.; Jia, J.; Wang, Y.; Zhu, P. *J Colloid Interface Sci* 2016, 474, 51-57.
7. Wang, Y.; Ma, P.; Song, F.; Yao, S.; Chen, C.; Zhu, P. *J Colloid Interface Sci* 2017, 490, 129-136.
8. Maestrin, A.P.J.; Tedesco, A.C.; Neri, C.R.; Gandini, M.E.F.; Serra, O.A.; Iamamoto, Y. *J Braz Chem Soc* 2004, 15, 708-713.
9. Adler, A.D.; Longo, F.R.; Finarelli, J.; Goldmacher, J.; Assour, J. *J Org Chem* 1967, 32, 476.
10. Liao, J.-X.; Zhao, H.-B.; Yang, D.-L.; Chen, L.; Wang, B.-Y. *Acta Cryst E* 2011, E76, m1316.
11. Esteves, C.H.A.; Iglesias, B.A.; Li, R.W.C.; Ogawa, T.; Araki, K.; Gruber, J. *Sensor Actuat B-Chem* 2014, 193, 136-141.
12. Kladsomboon, S.; Kerdcharoen, T. *Anal Chim Acta* 2012, 757, 75-82.

BIOGRAPHY

Name	Miss Monta Malaithong
Date of Birth	September 15, 1992
Educational Attainment	2014: Bachelor of Science in Chemistry, Thammasat University
Scholarship	2016: Scholarship for Talent Student to study graduate program in Faculty of Science and Technology, Thammasat University 2017: The National Research Council of Thailand (NRCT) for supporting “FY2017 Thesis Grant for Master Degree Student” 2017: Thammasat University Research Fund under the TU Research Scholar

Extracurricular activities (Conference)

1. Participate and present poster in topic “Catalyst granules forming from calcium oxide mixed waste glass for biodiesel production” at Pure and Applied Chemistry International Conference 2016 (PACCON2016) (9-11 February 2016)
2. Oral presentation in topic “The application of catalyst granules forming from calcium oxide mixed waste glass for biodiesel production” at Thailand Research Symposium 2016 (20 August 2016)
3. Participate and present poster in topic “The Novel 2-Nitro-Tetrakis(4-Alkoxyphenyl)phenylporphyrinatocopper(II) Complexes: Synthesis, Characterization and It's Bacterial Activity” at the 42nd Congress on Science and Technology of Thailand (STT42), Thailand (30 November - 2 December 2016)
4. Participate and present poster in topic “Synthesis, spectroscopic characterization, crystallographic studies and antibacterial activity of 4-(4-nitrophenoxy) benzaldehyde” at 14th Conference of The Asian Crystallography Association (AsCA 2016), Hanoi (4 – 7 December 2016)

5. Participate and present poster in topic “Gas sensor for alcoholic volatile organic compounds based on silver porphyrin molecular film” at Pure and Applied Chemistry International Conference 2017 (PACCON2017) (2-3 February 2017)

Publications

1. M. Malaithong, S. Boonyuen, A. Prokaew, B. Cherdhirunkorn and C. Santhudkijkarn (2016) Catalyst granules forming from calcium oxide mixed waste glass for biodiesel production. Proceedings of Pure and Applied Chemistry International Conference 2016 (PACCON 2016), Thailand, 9-11 February 2016. pp. 253 – 257.
2. M. Malaithong, S. Boonyeun, T. Prohmsatit, A. Nuchthanom, P. Na-Nakorn, A. Poomkleang (2017) The Novel 2-Nitro-Tetrakis(4-Alkoxyphenyl)phenyl porphyrinato copper(II) Complexes: Synthesis, Characterization and It's Bacterial Activity. Proceedings of the 42nd Congress on Science and Technology of Thailand (STT42), Thailand, 30 November - 2 December 2016. pp. 253–257.
3. M. Malaithong, S. Boonyeun, T. Prohmsatit and S. Kladsomboon (2017) Gas sensor for alcoholic volatile organic compounds based on silver porphyrin molecular film. Proceedings of Pure and Applied Chemistry International Conference 2017 (PACCON 2017), Thailand, 2-3 February 2017. pp. 525 – 529.